The role of the BBSome in *Trypanosoma brucei*

Sakura Yamamoto

Lincoln College

A thesis submitted for the degree of

Master of Science by Research

University of Oxford

Michaelmas Term 2012

Sir William Dunn School of Pathology

Abstract

In humans, 7 genes causing the cilia-related disorder Bardet-Biedl syndrome (BBS) encode proteins that form a complex, named the BBSome. The highly conserved 7 BBSome components facilitate ciliary membrane biogenesis by sorting and transporting specific membrane proteins to the ciliary membrane. The BBSome subunits are also conserved in the protozoan parasite *Trypanosoma brucei*, the causative agent of African sleeping sickness. *T. brucei* has been used as a model organism providing huge insight into basal body/flagella biology; it is therefore a good candidate for further analysis of BBSome function.

Even though it has been suggested that BBSome traffics specific ciliary membrane proteins to the ciliary membrane in mammalian cells, we still do not know whether the function is universal or present in *T. brucei*. In my thesis, I have focused on the most conserved BBSome protein, BBS5, to characterize its localisation and function in flagella formation in *T. brucei.* Through bioinformatics, I identified that BBS5 was predicted to possess a predicted lipid binding domain which is not present in the other BBSome components, and that the diseases causing residues are most conserved in BBS5. Moreover, I generated a cell line in which endogenous BBS5 was tagged with TY-epitope and GFP to assess the localisation, which was found to be in transition zone of the flagellum. In order to investigate the function of BBS5 in the flagellum formation, RNAi mediated knockdown of BBS5 was then performed. Knockdown of BBS5 did not cause any defect in cell morphology and flagellum formation, indicating that BBS5 is not required for flagellum formation in *T. brucei*. This thesis provides the first insight into the localisation of BBS5 in *T. brucei,* and may shed the light on the importance of the transition zone proteins in *T. brucei*, where selection of proteins to enter the flagellum membrane may take place.

Declaration

No portion of the work referred to in this thesis has been submitted in support of an application for another degree or qualification of this or any other university or other institute of learning.

Acknowledgement

First of all, I would like to thank to my supervisor, Professor Keith Gull, who provided me a great environment in which to do a research and giving me an opportunity to work with talented people. I am also extremely grateful to Dr. Eva Gluenz for constant support and spending time with me whenever I needed help. I cannot put into words how much I have learned from you!

Moreover, I am thankful to all past and current Gull lab members by providing me warm support and sharing their scientific experiences. Without all of their support, I don't believe I could achieve my thesis. Particularly, thanks to Nicole, who was like my older sister by giving me a lot of valuable advice. Mike, who was my entertainer and cheerleader that made me laughs. Flavia, for being a good friend and sharing the experience.

I also sincerely want to thank to my boyfriend Ollie, for his unending support, kindness, and encouragement.

Furthermore, I cannot express how appreciative I am to my parents, for their huge love and support.

Finally, Without the Oxford-Kobe scholarship and Heiwa-Nakajima foundation, I was not able to come to Oxford to study. I am greatly thankful to them for providing me the funding.

Table of Content

List of figures and tables

Introduction

Materials and Methods

Results: The role of the BBSome in *Trypanosome brucei*

Abbreviations

aa	Amino acid
ARF	ADP-ribosylation factor
BB	Basal body
BBS	Bardet-Biedl Syndrome
BLAST	Basic Local Alignment Search Tool
bp	Base pairs
bp	Basal plate
CTS	Ciliary targeting sequence
COPI	Coat protein complex
CV	Ciliary vesicle
DAPI	4,6-diamidino-2-phenylindole
ddH2O	Double Distilled Water
DNA	Deoxyribonucleic Acid
dNTP	Deoxynucleotide Triphosphate
DNA	Deoxiribonucleic acid
D1	Dopamine receptor 1
dsRNA	Double Stranded RNA
FAZ	Flagellum attachment zone
GABA	G-protein-coupled receptor for γ-aminobutyric acid
GFP	Green Fluorescent Protein
GPCRs	G protein-coupled receptors
GPI	Glycosylphosphatidylinositol
IFT	Intraflagellar transport
Kb	Kilobases
kDa	KiloDaltons
K	Kinetoplast
LB	Luria Broth
LECA	Last eukaryotic common ancestor
Lov-1	For location of vulva
MCHR1	Melanin-concentrating hormone receptor 1
MDCK	Madin-Darby canine kidney
MKS	Meckel - Gruber syndrome
N	Nucleus
NPHP	Nephronophthisis
ORF	Open Reading Frame
PACRG	Parkin coregulated gene protein
PBS	Phosphate-buffered saline
PCM1	Pericentriolar material 1
PCR	Polymerase chain reaction
PDGFR	Platelet-derived growth factor receptor
PFR	Paraflagellar rod
PH	Pleckstrin homology
PKD-1	Polycystic kidney disease 1
PKD-2	Polycystic kidney disease 2
PM	Plasma membrane
RNAi	RNA interference
RPE	Retinal pigment epithelium
SSTR3	Somatostatin receptor 3
TP	Terminal plate

TPR	Tetratricopeptide repeat
TZ	Transition zone
UTR	Untranslated Region
VSG	Variable Surface Glycoprotein
ZPFM	Zimmerman Post-Fusion Medium

Chapter 1

Introduction

1.1 Introduction to eukaryotic cilia and flagella

Eukaryotic cilia and flagella are microtubule-based organelles projecting from the surface of a wide range of cell types. Eukaryotic flagella and motile cilia are considered to be the same organelle, as they are ultrastructurally identical. However, they have distinct patterns of movement; flagella move with a beating wave-like motion, whereas motile cilia exhibit a power stroke followed by a recovery stroke (Pan et al., 2005). Other differences are also seen between flagella and motile cilia, such as in their length and numbers. Cilia are relatively short and typically present in much greater numbers per cell than flagella. For example, the mammalian spermatozoon bears a single flagellum and the unicellular green alga *Chlamydomonas reinhardtii* possesses two flagella, whereas the unicellular ciliate protozoan *Paramecium tetraurelia* is covered with thousands of cilia.

The basic structures of cilia and flagella are well conserved throughout eukaryotes; these consist of a 9+2 microtubule structure for motile cilia and flagella, and a 9+0 microtubule structure for non-motile cilia. A detailed description of non-motile cilia is given in section 1.3.

A single motile flagellum functions in the propulsion of single cells, such as the swimming of protozoa including *Trypanosoma brucei* and mammalian sperm, is well known. For cilia, they are required for motility but also help in collecting particles of food. However, mammalian cilia can be motile or immotile and can have a variety of cell type specific structures. Cells with motile cilia, such as those of the embryonic node, have a single cilium, whereas the ependymal cells of the adult brain can have multiple cilia, and cells in the bronchial epithelium can have hundreds of cilia (Afzelius, 2004). In contrast to motile cilia, primary cilia (monocilia) are very small, which is about 1-2 µm and project from the cell surface as single immotile organelles (Singla and Reiter, 2006). Primary cilia are found on nearly all cell types in mammals, including the kidney tubules, neurons, and retina (Wheatley et al., 1996) and many are highly adapted to serve specialised sensory functions. The detailed function of primary cilia will be discussed in the next section.

1.1.1 Function of cilia and flagella

The functions of motile cilia in moving fluids and particles over epithelial surfaces and in the cell motility of vertebrate sperm and many protist flagellates (for example, *T. brucei* or *C. reinhardtii*) have been well studied. In addition to their function in motility, cilia with the 9+2 structure also have important sensory functions, which may play a role in regulating motility (Christensen et al., 2007). However, in terms of cilia-mediated signalling, primary cilia have attracted the most attention in recent years. Primary cilia have come to be appreciated for their roles in sensing the environment, such as in seeing, hearing, and smelling. For example, photoreceptor proteins in the vertebrate retina are housed in an elaborate cilium of the 9+0 type, connected to the cell body by a second "connecting" cilium that emerges from the basal body (Rohlich, 1975). Odorant receptors in olfactory epithelial cells are found in tufts of long cilia that project from the olfactory knob (Besse et al., 2009). Sound perception occurs in kinocilia on the hair cells of the ear. Various signals necessary for the normal functioning of human tissues and body development are detected by the primary ciliary membrane, which is enriched with specific receptors and ion channels to the cell body. These include platelet-derived growth factor receptor (PDGFR) α (Christensen et al., 2007), somatostatin receptor 3 (SSTR3), serotonin receptor 5, melanin-concentrating hormone receptor 1 (MCHR1)(Berbari et al., 2008b), and polycystins 1 and 2 (Yoder et al., 2002). The components of the Hedgehog and Wnt signalling pathways, which are necessary for carrying out specific signalling responses during the regulation of cell and tissue homeostasis growth and differentiation, are localised on the ciliary membrane, as well (Christensen et al., 2007; van Reeuwijk et al., 2011). Consequently, primary cilia are now seen as key sensory organelles and started to appreciate its important role in sustaining physiology.

1.1.2 Structures of cilia and flagella

Both cilia and flagella consist of a microtubule-based axoneme covered by a specialised membrane that extends from the cell surface into the extracellular space. The axoneme is a highly ordered structure of 9 peripheral microtubule doublets arranged around a central core that may or may not contain 2 central microtubules (9+2 or 9+0 axoneme, respectively)(Fig. 1.1). In the 9+2 axoneme arrangement, the 9 peripheral microtubule doublets are attached to each other via nexin links, forming a cylinder-like structure that surrounds the central pair consisting of the C1 and C2 microtubules (Lee, 2011). Each of the 9 peripheral doublets is composed of an A microtubule (13 protofilaments) associated with a B microtubule (11 protofilaments)(Nojima et al., 1995). The power for motility is generated by inner and outer dynein arms, which are present in the outer doublets of the microtubules in the axoneme, and radial spokes project from each outer microtubule doublet toward the central pair, regulating the direction of ciliary beating (DiBella and King, 2001; Salathe, 2007). In contrast, non-motile cilia exhibit the 9 peripheral doublets but usually lack the central pair, dynein arms, and radial spokes required for motility (Pazour and Witman, 2003).

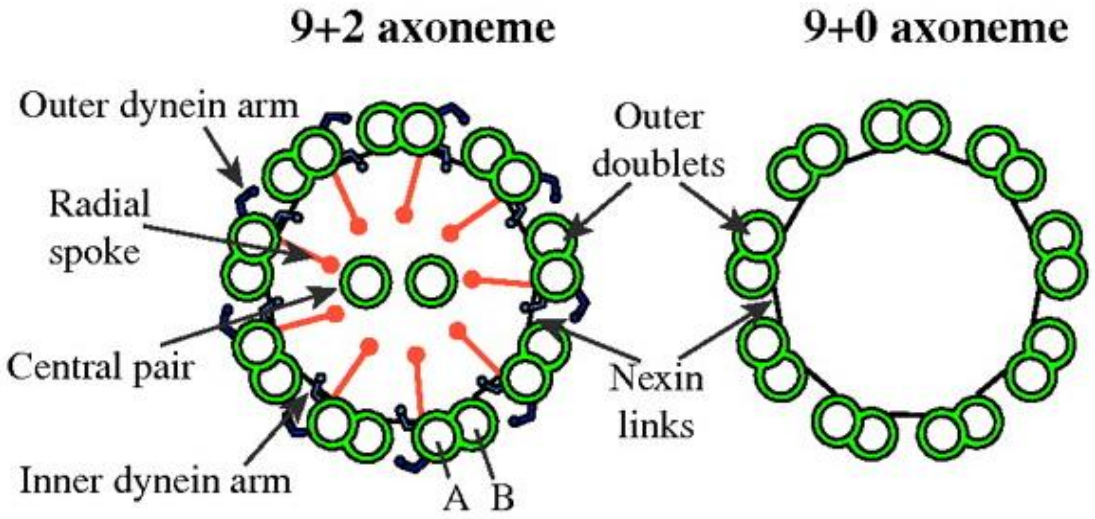

Figure 1.1 **Diagram of motile (left) and immotile (right) ciliary axoneme.** Diagram is adapted from (Dawe, Farr et al. 2007).

The proximal end of the cilium is elongated from the basal body, a barrel-like structure consisting of 9 triplet microtubules; the continuation of the basal body microtubule structures forms the axoneme doublet microtubules. The basal body ends at the terminal plate, where the transition zone originates and extends to the basal plate, where the structures of the central pair of microtubules are nucleated in 9+2 cilia (Fig. 1.2). The transition zone encompasses transition fibres, which are electron dense fibres forming a propeller-like array, and connect the distal end of basal body to the periciliary membrane, yet the composition of these transition fibres are largely unknown. The main body of the transition zone is defined by the presence of multiple rows Y-shaped linkers, which are immediately distal to the transition fibres projecting out from the outer double microtubules, attaching to the ciliary membrane (Gibbons and Grimstone, 1960). These Y-shaped linkers organise and terminate a circumferential intra-membrane structure, called the "ciliary necklace", which is observable in freeze fracture electron microscopy preparations (Gilula and Satir, 1972). The transition zone ends distally with the last row of Y-linkers.

The region of the transition fibres and transition zone is considered to function as a filter for the cilium, regulating the access of ciliary membrane proteins to the axoneme, and is called the "ciliary gate" (Chen et al., 2008; Gilula and Satir, 1972; Reiter et al., 2012) (Fig. 1.2). Over the past few years, various proteins localised in this area have been identified; their dysfunction has caused human ciliopathies, such as Meckel - Gruber syndrome (MKS) and nephronophthisis (NPHP) (Czarnecki and Shah, 2012). The MKS and NPHP proteins are localised in transition zone and form a module, that is necessary for attaching the axoneme of the transition zone to the surrounding ciliary membrane and for establishing the ciliary gate to regulate protein transport into the cilium (Williams et al., 2011). Moreover, a protein called CEP290 is associated with Y-shaped linkers, and impairment of CEP290 causes several ciliopathies, with a range of severity (Rachel et al., 2012). Depletion of *CEP290* caused the detachment of the flagellar membrane from

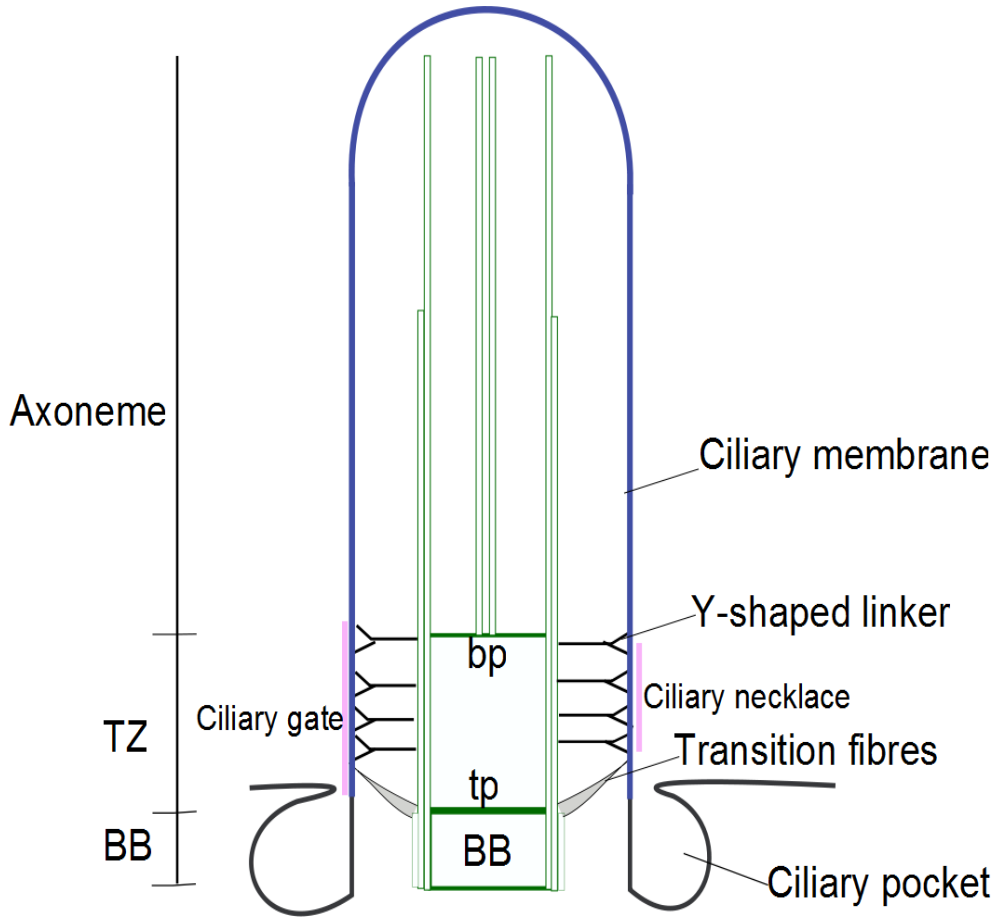

Figure 1.2 **Diagram of the base of a motile cilium**. The basal body (BB) derived from the mother centriole, nucleates the microtubule axoneme of the cilium. At the end of the basal body is the terminal plate (tp) and the transition fibers are radiated from the distal end of the basal body. The transition zone (TZ) is characterized by the existence of Y-linkers, the end of which corresponds to the basal plate (bp). Central microtubules emanate from the basal plate.

the transition zone microtubules, and also results in abnormal levels of protein expression in the isolated flagella in *C. reinhardtii* (Craige et al., 2010). The protein levels of polycystin-2 and BBS4, encoded by genes identified in the human ciliopathies polycystic kidney disease and Bardet-Biedl syndrome respectively, and of other flagellar components were altered in *CEP290* mutant flagella (Craige et al., 2010). These results support the idea that proteins localised in the transition zone are responsible for regulating ciliary membrane protein access into the cilium.

The proximal end of the cilium has a flask shaped membrane pocket, called the ciliary membrane pocket. The protist *T. brucei* also possess similar structure called flagllar pocket, which is in the base of flagellum and both ciliary pocket and flagellar pocket are the only place where clathrin-coated pits and vesicles are found (Hung et al., 2004; Molla-Herman et al., 2010). Although the ciliary membrane appears as a continuum of the cell membrane, it is both structurally and functionally distinct that ciliary membrane retains a different component of lipids and proteins required for cilia-mediated sensing/signalling events (Hu and Nelson, 2011). In order to block the lateral diffusion of membrane proteins from the cells body to the ciliary membrane, a lipid condensed barrier, named diffusion barrier exists at the base of cilium (Musgrave et al., 1986). The ciliary membrane in the necklace zone in Madin-Darby canine kidney (MDCK) cells has a highly condensed lipid composition (Vieira et al., 2006), which supports the idea that a barrier or fence structure is present at the base of cilium in order to separate the ciliary membrane compartment from the plasma membrane.

Cilia are often classified as immotile 9+0 primary cilia or motile 9+2 cilia; however, exceptions to these traditional classifications do occur. For example, renal cilia have a motile 9+0 configuration (Kramer-Zucker et al., 2005), and odorant receptors have been found on the immotile 9+2 sensory cilia of specialised olfactory neurons (Menco, 1994). In addition, nodal cilia, which are localised to the node in gastrulation-stage embryos, are primary cilia because they are solitary organelles that contain a 9+0 microtubule architecture (Nonaka et al., 1998). However, unlike most cilia having a

whip-like back and forth movement, nodal cilia move in a propeller-like fashion (Marszalek et al., 1999; Nonaka et al., 1998). The extent of ciliary architectural diversity is illustrated further by the observation that in some cell types and species, the axoneme contains additional structures (Bastin et al., 1996b). For example, *T. brucei* contains a paraflagellar rod (PFR), which is physically attached to the axoneme, usually at the point where the flagellum exits its flagellar pocket to emerge beyond the cell body, providing a distinctive asymmetry to the flagellar ultra structure. For more information about PFR, see also section 8.1.2.

1.1.3 Ciliogenesis

Ciliogenesis is initiated by the migration of mother centriole to the cell cortex (Fig. 1.3). In the first step, a Golgi-derived vesicle is attached to the distal end of the mother centriole/basal body in mammalian cells (Sorokin, 1962). Subsequently, the vesicle invaginates to generate the ciliary membrane and the ciliary bud is formed. The elongation of the ciliary bud develops into an axoneme, and the proximal end of the constructed axoneme forms the basal body and transition

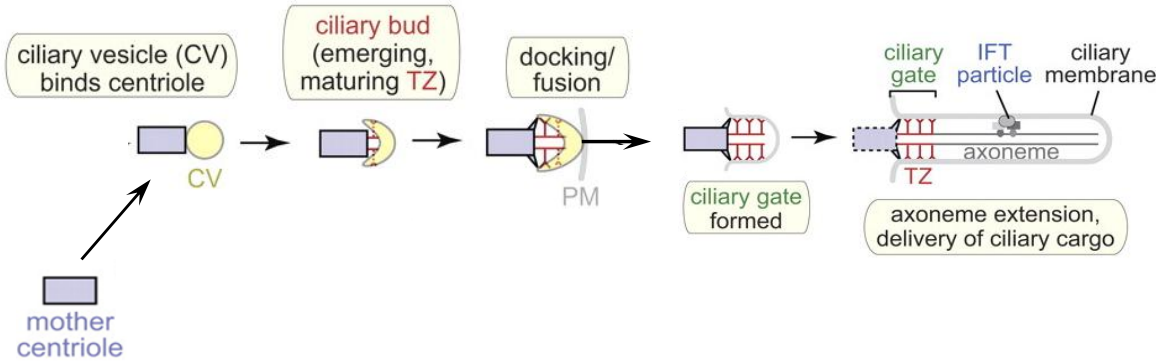

Figure 1.3 **Diagram of early and late ciliogenesis**. The ciliary vesicle (CV) binds to the distal appendage of the mother centriole, and then migrates towards the plasma membrane (PM). Invagination of the CV forms a ciliary bud (likely to be a maturing transition zone (TZ)). The membrane surrounding the axoneme reaches to and fuses with the plasma membrane, followed by formation of a ciliary gate. Once the cilium is extended to the extracellular environment, the axoneme elongation is depending on IFT. Diagrams are adapted from (Williams et al., 2011).

zone (Boisvieux-Ulrich et al., 1989). Acquiring a transition zone during the early process of axoneme and flagellar membrane growth is necessary, because the disruption of several transition zone proteins has been shown to cause defects in centriole migration, membrane docking, and transition zone membrane association in mammalian cells and in *Caenorhabditis elegans* (Williams et al., 2011). The membrane-surrounded axoneme migrates to the cell surface, allowing the fusion of the ciliary membrane with the plasma membrane. At this stage, a cup-like structure is generated at the plasma membrane, which is known as the ciliary gate. The cilium extends to the extracellular environment after the ciliary membrane and the plasma membrane are fused, but the ciliary pocket is maintained at its base. Afterwards, the cilium elongates depending on intraflagellar transport (IFT).

1.1.4 Intraflagellar transport

During ciliogenesis, cilia elongate from the basal body by the addition of new axonemal subunits to the distal tip. As protein synthesis does not occur in cilia, axonemal components, particularly structural and force-generating components, as well as sensory ciliary membrane receptors and associated signalling molecules, are conveyed by intraflagellar IFT along the axonemal doublet microtubules (Kozminski et al., 1993). Direct experimental evidence supports the hypothesis that the IFT machinery transports axoneme components such as the inner dynein arms (Cole et al., 1998) and tubulin subunits (Marshall and Rosenbaum, 2001). IFT was first described in *C. reinhardtii* as the bidirectional movement of particles along the flagellar axoneme (Kozminski et al., 1993). The transport of IFT particles are powered by 2 motors; kinesin-2, which is responsible for the anterograde transport of IFT particles to the distal tip of cilia, and cytoplasmic dynein II (dynein 1b in *C. reinhardtii*), which is responsible for the retrograde transport of IFT particles back to the cell body. The anterograde motor in *C. reinhardtii* is made up of 2 motor subunits, FLA10 and FLA8, and a non-motor subunit called kinesis associated protein (KAP) (Cole et al., 1993;

Wedaman et al., 1996). The retrograde IFT motor possesses heavy chain (HC) and light intermediate chain (LIC) subunits (Perrone et al., 2003; Schafer et al., 2003).

These 2 motors are attached to IFT particles composed of at least 16 distinct proteins that can be separated biochemically into 2 fractions, IFT Complex A (6 proteins) and Complex B (~11 proteins)(Cole et al., 1998; Piperno and Mead, 1997). Complex A consists of IFT144, IFT140, IFT139, IFT122A, IFT122B, and possibly a sixth subunit, IFT43 (Piperno et al., 1998; Rosenbaum and Witman, 2002). Complex B consists of IFT172, IFT88, IFT81, IFT80, IFT74/72, IFT57/55, IFT52, IFT46, IFT27, and IFT20 (Lucker et al., 2005).

The process of assembling these particles occurs at the base of the cilia near the transition fibres (Fig. 1.4). At this point, the IFT particles are transported in an anterograde manner toward the tip of the axoneme by the action of the heterotrimeric kinesin-II motor complex. Activated kinesin-2 is attached to IFT complex A, and axonemal precursors are bound to complex B. When they reach the ciliary tip, the IFT particles and motors are remodelled and their size is reduced; presumably, the cargo is unloaded. Moreover, the kinesin-2 motors become inactivated, whereas dynein 1b motors become active and bind complex A, transporting the IFT particles and their cargos to the ciliary base (Pedersen et al., 2006). Finally, the cargo proteins are unloaded from IFT particles and the IFT particles are recycled (Chen et al., 2008). Thus, IFT particles function as constantly moving molecular trucks on a closed loop. Most of the protein subunits that comprise the IFT motors and particles are strongly conserved in ciliated organisms (Rosenbaum and Witman, 2002). On the other hand, genes encoding IFT homologues are absent from the genomes of non-ciliated organisms, including yeast and higher plants (Cole, 2003).

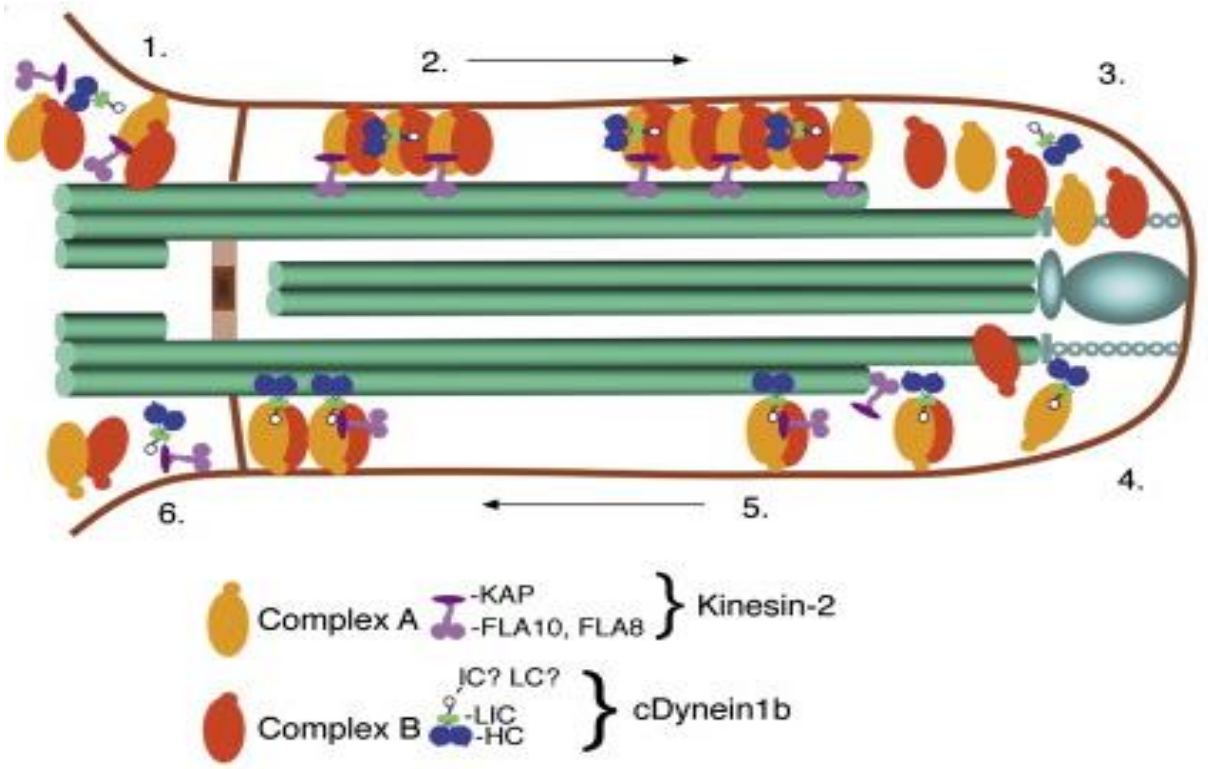

Figure 1.4 **Diagram of flagellum assembly by IFT movement in *Chlamydomonas reinhardtii* .**
1. IFT motors, IFT particles, and associated cargo accumulate in the base of the flagellum prior to entering the axoneme.
2. Assembled IFT particles and cargo complexes are transported to the tip of the flagellum by anterograde kinesin-2 motors.
3. IFT particles are remodelled at the distal tip.
4. IFT particles are rearranged and associate with activated retrograde dynein 1b motors.
5. IFT particles are transported to the base of the flagellum by dynein 1b motors.
6. Proteins are unloaded from IFT particles and recycled.
Diagram is adapted from (Pedersen, Geimer et al. 2006).

1.2 Conserved 9+2 axoneme structure

The cilium is a remarkably well-conserved structure across a broad spectrum of organisms, although a few model organisms lack cilia, such as *Arabidopsis thaliana, Saccharomyces cerevisiae,* and *Dictyostelium discoideum* (Inglis et al., 2006). Given the phyletic distribution of cilia, it is estimated that the last eukaryotic common ancestor (LECA) possessed 9+2 structural cilia and a centriole, with motile and sensory functions (Carvalho-Santos et al., 2011; Hodges et al., 2010). Over the past ten years, proteomic studies, bioinformatics screening, and RNAi analysis across diverse species have identified genes encoding core proteins that are shared among the extended eukaryote families, which are linked to microtubules and centrioles/basal bodies, suggesting that these proteins were present in LECA (Carvalho-Santos et al., 2011; Inglis et al., 2006; Keller et al., 2006; Merchant et al., 2007; Pazour et al., 2005). Some of these core proteins identified in a wide range of eukaryotes are those that have functions specific to ciliary roles. For example, they are associated with the outer and inner dynein arms, and radial spokes (Carvalho-Santos et al., 2011; Satir, 1998). SAS-4, which is required for microtubule attachment to centriolar microtubules is involved in centriole duplication (Kirkham et al., 2003; Leidel and Gonczy, 2003), shows high level of conservation across species (Hodges et al., 2010); the radial spokes protein RSP1 is identified in both human and in *C. reinhardtii* (Yang et al., 2006); and motor proteins, such as dynein subunits that function in generating a flagellar beat force, are widely conserved, as well (Wickstead and Gull, 2007).

Regarding the ancestral sensory function of cilia, cilia were selectively utilised as sensory antennae because higher sensitivity could be achieved by gathering receptor proteins to the ciliary membrane (Jekely and Arendt, 2006). Indeed, specific receptors localised at the ciliary surface are discovered in both protists and in metazoan cilia; for example, the ciliary membrane in *Tetrahymena thermophila* has insulin receptor-like proteins (Christensen et al., 2003); further, polycystin 2, a cation channel defective in human polycystic kidney disease has been identified in *C. reinhardtii* (Pazour et al., 2005), and the G-protein-coupled receptor for γ-aminobutyric acid

(GABA), which regulates synaptic transmission in the human central nervous system is discovered also in *P. tetraurelia* (Ramoino et al., 2003).

A polarised vesicle transport system was initially required for forming specialised membrane protrusions, which later evolved into the IFT machinery (Jekely and Arendt, 2006). Many IFT protein sequences are similar to those of proteins found in the coat protein complex (COPI) and in clathrin coats (Avidor-Reiss et al., 2004). The IFT proteins IFT140, IFT122/OSM-4, and IFT172 structurally resemble COPI and clathrin vesicle coats, sharing several N-terminal WD40 and C-terminal TPR repeats (Jekely and Arendt, 2006). The link between ciliary evolution and IFT can be observed in the wide phyletic distribution of the IFT complex among a broad range of eukaryotes, such as human, *T. brucei, C. elegans,* and *C. reinhardtii.* IFT proteins are absent in organisms that do not possess cilia, such as *Dictyostelium*, *S. cerevisiae,* or *Plasmodium,* which do not need IFT for ciliary assembly (the cytoplasm is used instead)(Briggs et al., 2004; Sinden et al., 1976). The development of IFT along with the axoneme possibly creates a link that segregates the ciliary compartment from the rest of the cytoplasm. Subsequently, further improvement of the IFT trafficking machinery for vesicle fusion has occurred at the base of the cilium. This process might have led to the creation of the diffusion barrier found in the ciliary necklace region in order to regulate the free entry of vesicles into the ciliary lumen. The evolutionally highly conserved protein, septin, is localised in the ciliary necklace; this supports the idea of the early generation of diffusion barriers in the cilia (Hu et al., 2010).

In the present day, we are able to see some flagellar structures that have been modified from the original 9+2 flagellum. Some of these flagellar structures are no longer required and the 9+2 structure has been simplified by the removal of unnecessary apparatus. 9+0 sensory cilia function only in signal sensing and lack the structures necessary for motility (central pair, dyneins, and radial spokes), that are present in 9+2 cilia (Mitchell, 2004). In this type of cilium, the ciliary

membrane and doublet axoneme is retained; additionally, the IFT machinery is still required in order to transport ciliary membrane proteins.

1.3 Ciliary dysfunction and ciliopathy

Defects in ciliary function or ciliogenesis cause genetic disease syndromes, which are termed ciliopathies. Ciliopathies include a variety of abnormalities, such as cystic disease in the kidney, polydactyly, brain malformations, hydrocephalus, blindness, anosmia, obesity, and cognitive deficits. However, the list of disorders categorised as ciliopathies is still expanding. Since cilia are found in nearly all organs and have important roles in physiology, the genetic mutations associated with these syndromes that disrupt ciliary proteins result in a huge variety of pathologies (Christensen et al., 2008; Veland et al., 2009).

Cilia are comprised of different organisational modules, such as the basal body and the dynein arms, to sustain ciliary functions and each organisational module has different functions. Therefore, dysfunction of proteins encoded by genes associated with particular functions can affect a particular subset of ciliary structures or functions, yet leaving other parts intact (Marshall, 2008). A good example of this is a disease called primary ciliary dyskinesia (PCD), which is caused due to immotile cilia in respiratory track affecting mucus clearance. This is caused due to the impairment of genes involved in dynein arms, radial spokes, and central pair. Therefore, defects in these structures lead to dysfunction of motility in cilia, but do not cause any failure in signalling pathways. Another example of a distinct ciliary component that plays a different role is the ciliary membrane. As mentioned previously, the ciliary membrane contains a wide range of receptor proteins and channels, which make the cilium a sensory organelle. Polycystin 1 and polycystin 2 are receptor proteins localised in the membranes of primary cilia in epithelial cells lining the renal tubules and mutation of the corresponding *PKD1* and *PKD2* genes causes polycystic kidney disease

(PKD) (Gunay-Aygun, 2009; Yoder, 2007). These receptors sense flow in the kidney and transmit a calcium-mediated signal to the cell. Polycystin 1 has a large extracellular domain, and it is believed that it serves as an extracellular sensor that responds to the flow of urine in the kidney and subsequently causes the activation of polycystin 2 (Patel and Honore, 2010). Polycystin 2 functions as a Ca^{2+}-permeable cation channel that allows Ca^{2+} to enter the cell (Abou Alaiwi et al., 2009). The resulting inflexed Ca^{2+} changes the intracellular concentration of Ca^{2+}, resulting in gene activation that is involved in tissue maintenance. PKD patients, in whom the PKD proteins are impaired, show no other phenotype, indicating that the PKD proteins are not required for ciliary assembly or other ciliary functions.

Impaired localisation of the receptor proteins to the ciliary membrane leads to failure in detecting and transducing the appropriate signals to the cell body. Therefore, dysfunction of ciliary membrane biogenesis affects ciliary sensory function and also causes disease; the typical example is Bardet-Biedl Syndrome (BBS).

1.4 Bardet-Biedl Syndrome

Bardet-Biedl Syndrome (BBS) is a genetically heterogeneous pleiotropic disorder characterised by a multitude of symptoms whose aetiology lies in primary ciliary disorder, linked to the dysfunction of basal bodies and/or cilia (Ansley et al., 2003). The major clinical phenotypes of BBS are obesity, gonadal abnormalities, retinal degradation, renal abnormalities, polydactyly, and mental retardation (Tobin and Beales, 2007; Ventura et al., 2006). To date, 16 *BBS* genes have been identified, and dysfunction of any of these genes causes the disorder (Waters and Beales, 2011). Identifying genes that are linked to BBS helps to understand the molecular mechanisms and biochemical pathways linked to the BBS phenotype. Despite the tremendous genetic heterogeneity, BBS proteins are found in the basal body, centrosome, and primary cilia (Ansley et

al., 2003; Garcia-Gonzalo et al., 2011; Nachury et al., 2007). The first major finding in revealing the BBS protein function in basal body/cilia was demonstrated using *myc*-epitope tagged BBS8 in mammalian cells; this study revealed the specific localisation of BBS8 in the basal body and centrosome (Ansley et al., 2003). Moreover, immunohistochemical analysis demonstrated that the localisation of BBS8 is restricted to ciliated structures in mice and human tissues, including the connecting cilium in the retina and maturing spermatids (Ansley et al., 2003). Finally, *BBS* gene homologues (*BBS1, 2, 7*, and *8*) were expressed exclusively in ciliated neurons in *C. elegans* (Ansley et al., 2003). These findings underlined the involvement of BBS proteins in the cilia and basal body.

In many cases, proper signalling is tightly coupled to the correct translocation of receptors and down-stream effector molecules that are involved in signal transduction to the cilium. Hence, controlling the trafficking of signal components into the cilium is a critical mechanism for sustaining the proper function of the primary cilium in sensing. Defects in the trafficking of membrane proteins to the ciliary membrane leads to mislocalisation of receptor proteins and ultimately causes ciliary defects, manifested as BBS phenotypes. Among the 16 proteins, 7 proteins (BBS1, BBS2, BBS4, BBS5, BBS7, BBS8, and BBS9) play a key role in maintaining the correct function of cilia and a recent study showed that these 7 BBS proteins form a stable complex, named the BBSome (Nachury et al., 2007). The BBSome is required to transport receptor proteins to the ciliary membrane and to allow cilia to detect extracellular signals by recruiting Rab8 and transport vesicles that contain ciliary membrane proteins to the ciliary membrane (Nachury et al., 2007). Moreover, several receptor proteins and signalling molecules are localised to cilium of hippocampal neurons, and the BBSome is responsible for delivering at least some of the G-protein coupled receptors, such as MCHR1 and the dopamine receptor 1 (D1) (Berbari et al., 2008b; Domire et al., 2011).

1.5 Evolutionally conserved BBSome proteins

Various genes are engaged in ciliary biogenesis and maintenance and their encoded proteins are expressed in cilia, the basal body, or the centrosome. Dysfunction of these proteins causes ciliopathies, as described previously. Interestingly, many of these ciliopathy associated proteins are highly conserved across ciliated eukaryotes. For example, human cystic kidney disease genes, such as *NPHP4*, which is associated with nephronophthisis, and *lov-1* and *pkd-2,* which are linked to polycystic kidney disease, are conserved in *C. elegans* (Hildebrandt et al., 2009). They are expressed in the head and tail of *C. elegans,* and mutations in these genes cause male mating defects (Barr et al., 2001; Wolf et al., 2005). A homologue of polycystin 2 was found in the *C. reinhardtii* flagellar proteome (Pazour et al., 2005). An integral component of the axoneme, parkin coregulated gene protein (PACRG), which was discovered in Parkinson's disease (West et al., 2003) is conserved in *T. brucei*, as well (Broadhead et al., 2006). Importantly, many BBS proteins, particularly the 7 BBSome proteins, BBS1, BBS2, BBS4, BBS5, BBS7, BBS8, and BBS9, are highly conserved across ciliated eukaryotes (Hodges et al., 2010; Nachury et al., 2007), but not in non-ciliated organisms (e.g., *S. cerevisiae, A. thaliana,* and *Schizosaccharomyces pombe*)(Chiang et al., 2004). However, no homologues of these BBSome proteins were identified in the ciliates, *Physcomitrella patens, Plasmodium falciparum, Thalassiosira pseudonana*, and *Batrachochytrium dendrobatidis* (Hodges et al., 2010). These 4 species possess only motile cilia in their gametes or zoospores (Berger et al., 2005; Johnson and Speare, 2003; Merchant et al., 2007; Sinden et al., 1978), indicating that the BBSome is involved not only in gametes or motility, but also in other functions of cilia, such as sensing signals. This idea is supported by the bioinformatics data that all 7 BBSome proteins are conserved in *C. elegans*, which has only sensory cilia (Hodges et al., 2010; Nachury et al., 2007). Notably, *Drosophila melanogaster*, *Giardia lambli,* and *Toxoplasma gondii* have lost certain IFT subunits and have also lost some of the BBSome proteins, while all eukaryotes with a full complement of IFT subunits have retained all 7 BBSome proteins (Nachury

et al., 2007). These data further support the hypothesis that the BBSome is also involved in the sensory functions of cilia, perhaps associated with IFT machinery.

The discovery that a subset of 7 out of the 16 BBS proteins forms a complex has helped in understanding why one or more mutations in different *BBS* genes can cause the consistent BBS phenotype. In addition to the BBSome, a chaperonin complex group was identified comprising BBS6, BBS10, and BBS12, which seems to mediate BBSome assembly (Seo et al., 2010). However, unlike the BBSome proteins, these chaperonin complex proteins are not widely conserved across ciliated eukaryotes, instead limited to vertebrate lineages.

1.6 BBSome function in trafficking of membrane receptor proteins

The BBSome was discovered in an experiment in which a tagged BBS4 protein was precipitated from cultured mammalian retinal pigment epithelium (RPE) cells, and 6 other BBS proteins that interact with BBS4 were identified (Nachury et al., 2007). Specific protein-protein interactions were confirmed by co-immunoprecipitation (Fig. 1.5).

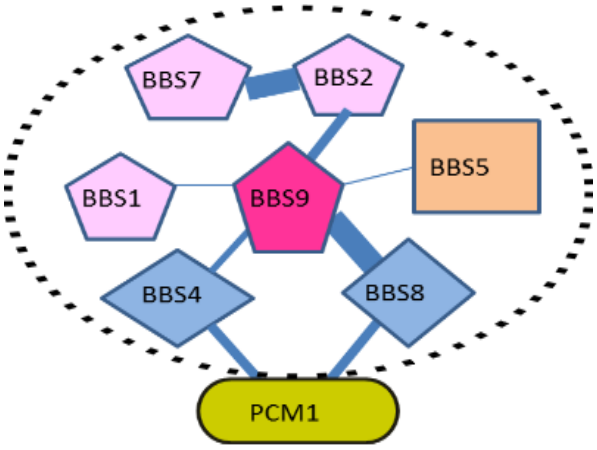

Figure 1.5 **Schematic model of the BBSome.** Thickness of line indicates the strength of each proten interaction. The shape depicts the domain contained in each BBSome protein. BBS1, 2, 7, and 9 have the β-propeller domain, BBS4 and 8 have tetratricopeptide repeats (TPR), and BBS5 has the PH domain. The diagram is adopted from (Nachury et al., 2007) .

Co-fractionation and pull-down experiments suggested that this complex localises to non-membranous centriolar satellites (PCM1) in the cytoplasm as well as the ciliary membrane. This complex functions in the biogenesis of the ciliary membrane through vesicle transport (Nachury et al., 2007), depend on IFT (Lechtreck et al., 2009). The function of the BBSome in the biogenesis of ciliary membranes is explained by its association with Rabin 8, a Rab8 GDP/GTP exchange factor at the basal body (Nachury et al., 2007) (Fig. 1.6). Rab GTPases play a role in mediating the transport, docking, and fusion of carrier vesicles, and Rab8 associates with vesicles after they bud from the Golgi (Emmer et al., 2010). Rabin 8 is necessary for loading GTP to Rab8; it allows the localisation of GTP-Rab8 to cilia and promotes ciliary membrane elongation (Nachury et al., 2007). This implies that through the interaction of the BBSome with Rabin8, the BBSome might potentiate Rabin8 to activate GTP-Rab8 and thereby promote the docking and fusion of vesicles to the ciliary membrane (Nachury et al., 2007). In addition, a study using *C. reinhardtii* also described a role for the BBSome in transporting proteins inside cilia. In this system, mutations in *BBS* genes did not affect flagellum assembly, revealing that the BBSome is not required for IFT stability in *C. reinhardtii*; however, mutations in *BBS1, 4,* and *7* accumulated specific sets of proteins, including putative signalling proteins in the flagellar membrane and matrix (Lechtreck et al., 2009). In addition, *BBS1, 2, 4*, and *6* mutant mice exhibited abnormal accumulation of membrane vesicles at the ciliary tip, implying that this phenotype is probably due to the loss of cargo from the IFT complex. In particular, the BBSome was not able to facilitate the transport of the cargo to the IFT, and therefore the export of the flagellar proteins was prevented (Shah et al., 2008). These studies indicate that the BBSome is not an integral component of the IFT machinery; rather, it functions as an adaptor for IFT and transports receptor proteins.

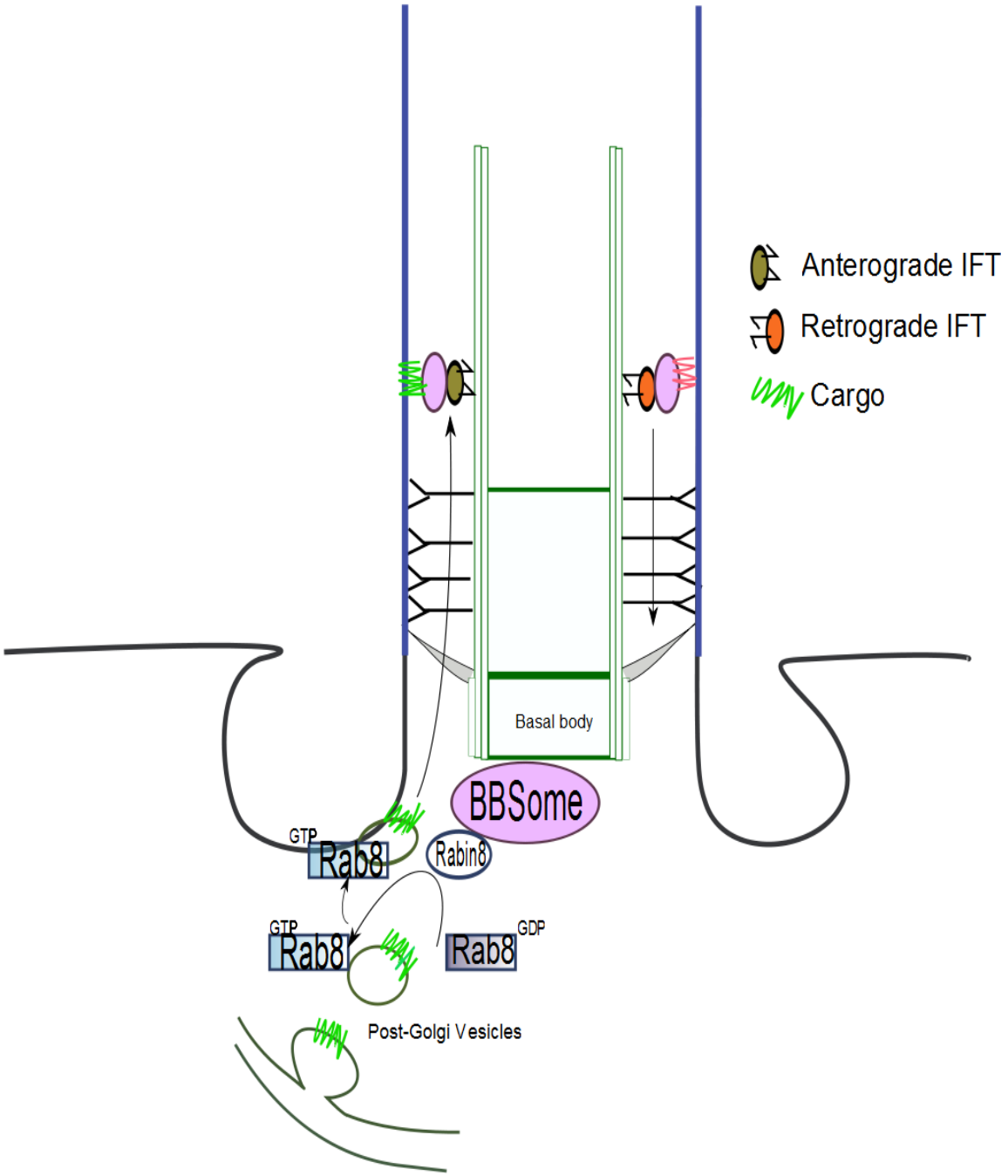

Figure 1.6 **A schematic diagram illustrating vesicle trafficking to the primary cilium by the BBSome.** A vesicle carrying cargo leaves the golgi, destined for the primary cilium via interaction with GTP-Rab8. GTP-Rab8 is produced by GDP-GTP exchange factor Rabin8, catalyzed by the BBSome. Once receptor proteins are directed into the primary cilium, the IFT complexes associate with the BBSome and continuously traffick cargo up and down along the length of the axoneme.

In order to enter the cilia, ciliary membrane proteins have to cross the diffusion barrier that physically and functionally separates the ciliary and plasma membranes, and special machinery is required to facilitate lateral transport between the ciliary and plasma membranes (Berbari et al., 2008a; Nachury et al., 2007). For certain receptor proteins, their targeting signals are precisely recognised by proteins that are responsible for trafficking receptor proteins into the ciliary membrane (Emmer et al., 2010). Therefore, correct identification of the ciliary targeting sequence (CTS) is required for sorting and trafficking receptor proteins to their appropriate locations within the ciliary membrane. Indeed, various CTSs have been identified in proteins linked to ciliopathies. The ciliary G protein-coupled receptors (GPCRs) such as MCHR1, and SSTR3 rely on CTSs to enter cilia (Berbari et al., 2008a). Among the CTSs, the RVxP motif is very well characterised and has been identified in polycystin-2 (Geng et al., 2006) and rhodopsin (Deretic et al., 1998). The small GTPase ADP-ribosylation factor (ARF)4 recognises the RVxP motif in rhodopsin and transports rhodopsin from the Golgi apparatus to the photoreceptor outer segment (Mazelova et al., 2009).

A recent outstanding study demonstrated that the BBSome forms a coat complex together with Arl6 and serves as a sorting machine for ciliary membrane proteins by binding directly to the CTSs of SSTR3 (Fig. 1.7). This function of the BBSome was first suggested by the finding that, the BBSome shares the structure of coat-like structural elements common to COPI, COPII, and clathrin coats, and interacts with the ARF-like GTPase, Arl6 (Jin et al., 2010). Arl6 is exclusively conserved in ciliated organisms (Avidor-Reiss et al., 2004), and its human orthologue Arl6 is encoded by *BBS3* (Fan et al., 2004). The interaction of the BBSome with $Arl6^{GTP}$ was discovered by affinity chromatography using bovine retinal extract; 7 BBSome proteins were captured by $Arl6^{GTP}$ and they co-localised together along the primary cilium in RPE cells (Jin et al., 2010). $Arl6^{GTP}$ is necessary for targeting the BBSome to cilia, as evidenced by the observation that loss of $Arl6^{GTP}$ results in the failure of the BBSome to localise in the cilia (Jin et al., 2010). Moreover, $Arl6^{GTP}$ recruits the BBSome to the basal body, since $Arl6^{GTP}$ is localised at the distal end of the basal body

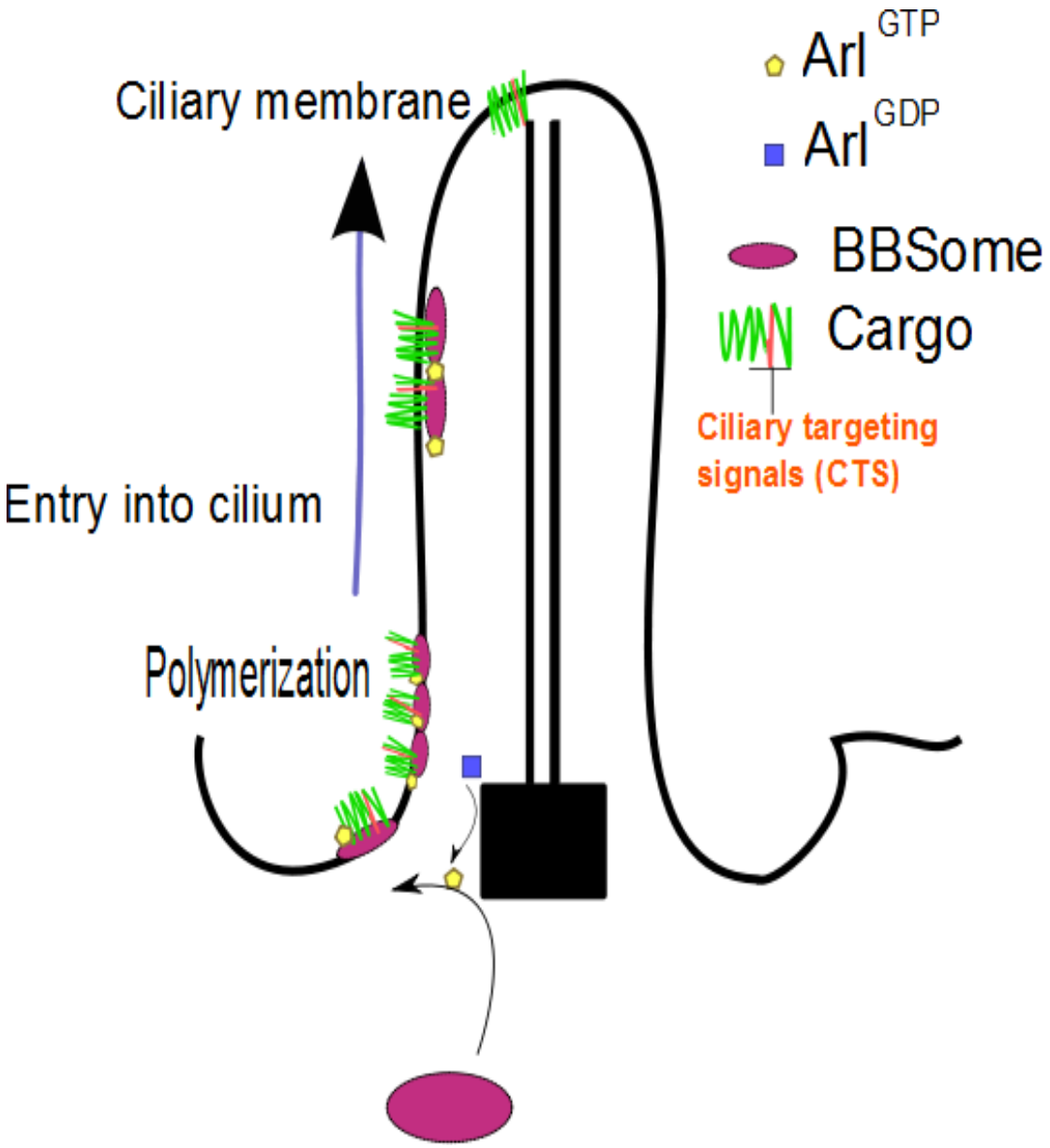

Figure 1.7 **Schematic model of the BBSome function as a coat complex to target ciliary membrane proteins into the ciliary membrane in mammalian cells.** Arl6 localises at the distal end of the basal body and upon GTP binding, Arl6 associates with membranes and recruits the BBSome. Preclustering complex is formed through the recognition of ciliary targeting signals (CTS) of ciliary membrane protein by the BBSome. BBSome/CTS/Arl6^{GTP} polymerizes to form a membrane coat complex on the membrane and target the ciliary membrane protein to the cilia.

in ciliated cells, where vesicles containing cargos are fused to the membrane (Wiens et al., 2010) (Fig. 1.7). Next, $Arl6^{GTP}$ is able to bind to brain lipid derived liposomes and recruits the BBSome to liposomes (Jin et al., 2010). Moreover, the morphological consequences of this interaction were demonstrated by the incubation of the BBSome, $Arl6^{GTP}$ and liposomes, which resulted in the formation of polymerised patches on the surface of liposome (Jin et al., 2010). This suggests that the interaction of the BBSome with $Arl6^{GTP}$ can produce small vesicles that bud from the membrane, which could be characterised as coated vesicles. Finally, directing the SSTR3 to the ciliary membrane was absolutely depending on direct binding of the BBSome to the CTS of SSTR3 ($SSTR3^{i3}$). When $SSTR3^{i3}$ was bound to the plasma membrane protein CD8α to form CD8α- $SSTR3^{i3}$, the targeted movement of CD8α- $SSTR3^{i3}$ to cilia was depended on Arl6 and the BBSome. Mutations in $SSTR3^{i3}$ disrupted the binding of the CD8α- $SSTR3^{i3}$ chimera to the BBSome and prevented the ciliary targeting of CD8α-$SSTR3^{i3}$. These results showed that the BBSome recognises the receptor protein SSTR3, and targets it to cilia. Taken together that the BBSome composition is similar to the structure of the canonical vesicle coat complexes and able to recruit lipids, it has been considered that the BBSome may function as the ciliary membrane protein sorting machinery at the primary cilium.

Knowledge of BBSome function leads to an understanding of the aetiology of BBS; in BBS patients, the BBSome may not be able to traffic organ-or-tissue specific signalling receptor proteins to ciliary membrane; therefore, organ-or-tissue specific signal transduction is disrupted, resulting in BBS pathology. In fact, several G-protein coupled receptors such as MCHR1, SSTR3, and D1 fail to localise to the cilia, in BBS mutants (Berbari et al., 2008b; Domire et al., 2011).

1.7 BBS5 plays a key role in BBSome association with flagellar/ciliary membranes

The ciliary membrane is a specialised domain with a lipid and protein composition, different from the cell body membrane (Rohatgi and Snell, 2010). The BBSome is able to bind to lipid, and the association of the BBSome with lipid is a crucial step in ciliary elongation (Nachury et al., 2007). BBS5, one of the 7 BBSome subunits, mediates BBSome association with lipid. BBS5 is the only protein among the BBSome components that contains a pleckstrin homology (PH) domain and binds to phosphoinositides (Nachury et al., 2007). The PH domain has been identified in diverse eukaryotic proteins, and is involved in various functions, such as cellular signalling, cytoskeletal organisation, regulation of intracellular membrane transport, and modification of membrane phospholipids (Lemmon and Ferguson, 2001; Mayer et al., 1993). Most proteins containing the PH domain function in membrane association (Gibson et al., 1994) and may also function as membrane adaptors, that link host proteins to the membrane surface (Maffucci and Falasca, 2001). The association of the PH domain with the membrane is demonstrated by the binding of the PH domain to phosphoinositides or inositol phosphates. For example, PH domains contained in the pleckstrin protein, and several other proteins bind to lipid vesicles, that contain the phosphoinositide phosphatidylinositol 4,5-bisphosphate (PtdIns-4,5-P_2) (Harlan et al., 1994). In addition, the PH domain can recruit the host protein to membranes by binding phosphorylated forms of phosphatidylinositol. The PH domain contained in the ARF6 nucleotide exchange factor, ARNO, can interact with phosphatidylinositol 3,4,5-trisphosphate, the lipid product of phosphoinoditide 3- kinase activation. Through this interaction, ARNO moves to the plasma membrane from the cytosol (Cullen et al., 2001). Interestingly, BBS5 selectively recognised phosphatidylinositol 3-phosphate on PIP blots and perhaps this interaction is necessary for ciliogenesis, because inhibition of both of BBS5 and 3-phosphoinositides prevented ciliation (Nachury et al., 2007).

Recent studies showed the importance of phosphatidylinositol signalling in human physiology. Defective phosphatidylinositol signalling mediated by 5-phosphatase E, which converts phosphatidylinositol 3,4,5-trisphosphate to phosphatidylinositol 3,4-bisphosphate (PtdIns (3,4)P2), causes instability of primary cilia and leads to multi-organs disorders similar to the BBS phenotype (Bielas et al., 2009; Jacoby et al., 2009). Moreover, In addition to BBS5, the protein tubby can also bind to PtdIns (3,4)P2, and the loss of tubby leads to obesity, retinal degeneration, and hearing impairment, which is highly reminiscent of mice with BBS mutations (Santagata et al., 2001). It is already known that in *C. elegans*, *tubby-1* and *BBS1* are interact genetically and regulate fat deposition (Mak et al., 2006). These findings suggest that the binding of the BBSome to phosphoinositides regulates the transporting of signalling factors involved in weight control.

Remarkably, BBS5 is the most widely conserved protein among BBSome proteins (Hodges et al., 2010; Nachury et al., 2007). Even though some species have lost certain BBSome components, BBS5 is never excluded in these species. For example, BBS5 and BBS8 are present in *Giardia lamblia*, and only BBS5 is present in *Toxoplasma gondii*; the rest of the BBSome proteins are not present in these species (Hodges et al., 2010). This suggests that BBS5 has an essential role in the function of the BBSome. If membrane association is a fundamental function of the BBSome, the lipid binding subunit is indispensable for maintaining BBSome function. Among the 7 BBSome components, BBS5 is the only protein able to bind to lipid; therefore, it was probably conserved selectively during evolution even when the rest of BBSome subunits may have been lost. Studies of BBS5 revealed that it is localised in the basal body in hTERT-RPE cells (Garcia-Gonzalo et al., 2011) and in multiciliated ependymal cells lining the ventricles in the brain (An et al., 2004).

The evolutionarily conserved BBS5, along with other BBSome subunits, is conserved in *T. brucei*, which possesses a single flagellum that performs various essential functions. However, we still do not know whether BBS5 localises at the basal body like other organisms (An et al., 2004) and perform a critical function for the cell, such as flagellum formation. *T. brucei* can therefore be

used as a model organism to characterise the localisation and function of BBS5, whether it is linked to flagellum formation, or not.

1.8 *Trypanosoma brucei*

The protozoan *Trypanosoma brucei* belongs to the order Kinetoplastida, which is defined by the presence of a single condensed mitochondrial DNA called a kinetoplast. *T. brucei* is the causative agent of African sleeping sickness, which kills 50.000 people every year in sub-Saharan Africa, and responsible for Nagana in cattle. There is no protective vaccine against trypanosome infection, and new therapeutic approaches have to be developed because the existing drugs are highly toxic (Brun et al., 2010). *T. brucei* is transmitted to mammalian blood by the bite of a tsetse fly and can undergo various different cell morphological changes associated with its life cycle stage during the transition between its mammalian hosts and vectors (fig. 1.8).

While *T. brucei* proliferate in mammalian blood, they are able to escape from the host immune response by switching antigens on their surface coat, called the variant surface glycoprotein (VSG)(Cross, 1977). *T. brucei* undergoes a complex lifecycle associated with morphological differentiation and changes in cell metabolism according to the insect vector and mammalian host (Vickerman, 1985). *T. brucei* replicate in the bloodstream and tissues in a long slender form, and once the density of the parasites is reaches a critical level, they differentiate into a short stumpy form that is non-proliferative and pre-adapted to transmission into the fly (Vassella et al., 1997). Upon uptake by the tsetse fly, the stumpy form is transported into the midgut of the fly, where they transform into the proliferative procyclic form. In this stage, the composition of the surface coat changes and the cells lose VSG and gain procyclin (Roditi and Liniger, 2002), which is considered to be required for efficient transmission in the fly vector (Acosta-Serrano et al., 2001; Nagamune et al., 2000). In addition, their energy metabolism changes from glycolysis to a mitochondrion-based respiratory system with an elaborate mitochondrial structure

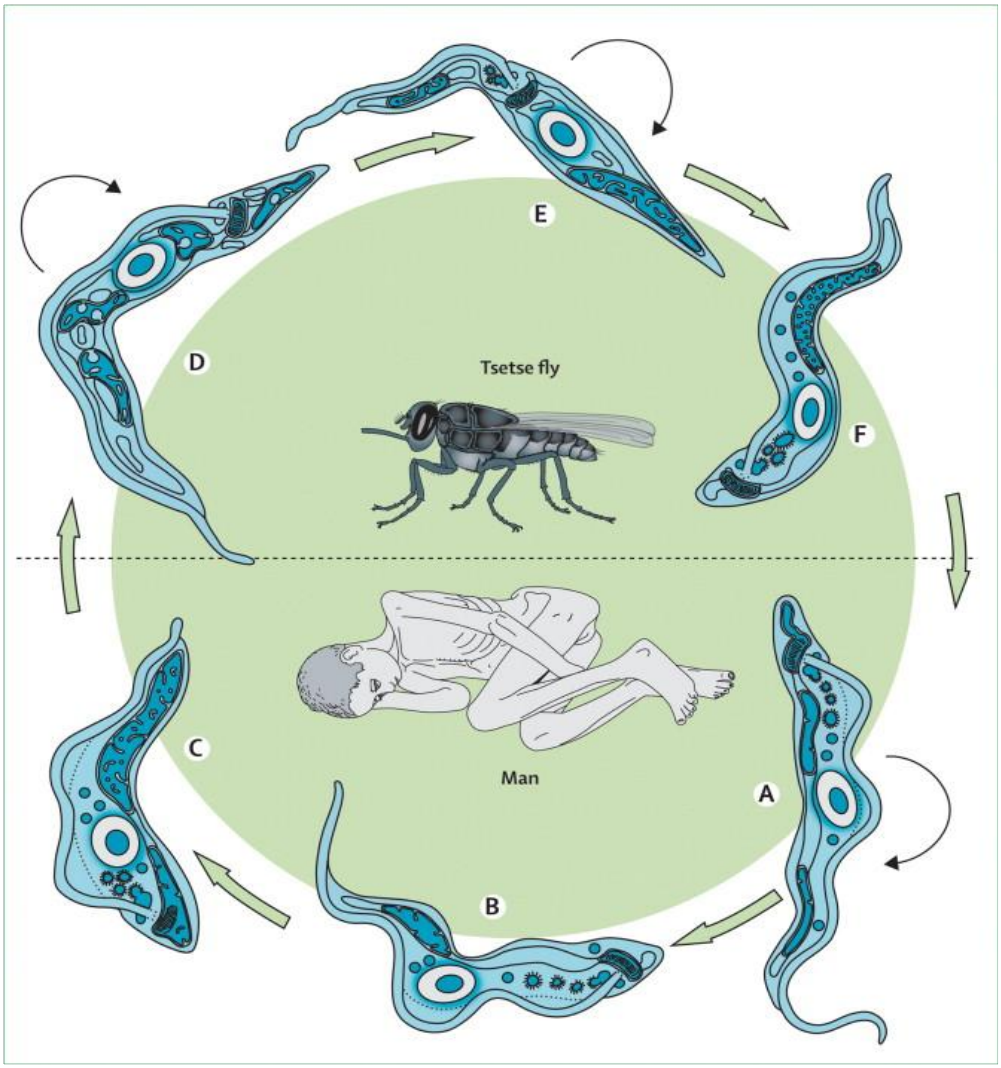

Figure 1.8 **Life cycle of *Trypanosoma brucei*.** Inside the mammalian host, the bloodstream form cell shows a polymorphism with (A) dividing slender form, (B) intermediate form, and (C) stumpy form. In the tsetse fly vector, the bloodstream form cell transforms to (D) dividing procyclic form in the midgut of the fly, then to (E) the migrating epimastigote form, which develops in the salivary glands to (F) the infective metacyclic form, which is injected during the next blood meal into the mammalian host. Diagram is adapted from (Brun et al., 2010)

(Matthews, 2005). Procyclic form trypanosomes proliferate in the midgut and then migrate to the salivary glands. As they are migrating, they begin to elongate and become even thinner and longer when they reach the proventriculus to the salivary glands, they then differentiate to the epimastigote form, which is accompanied by losing procyclin from their cell surface (Sharma et al., 2008). The characteristic of the elongated epimastigote form is that the position of the nucleus is posterior to

the kinetoplast. The epimastigotes attach to the salivary glands with their membrane of the flagellum, then divide and differentiate into the metacyclic form. Metacyclic trypomastigotes gain the VSG coat again and become host-infective. They can evade the host immune system after inoculation of the mammalian host. Primarily, procyclic form *T. brucei* (In fly form) and bloodstream form *T. brucei* (im mammalian host) cells are used in the laboratory.

All forms of *T. brucei* possess a single flagellum that elongates from the basal body, which is attached to the kinetoplast.

1.8.1 Cell biology of the procyclic form *T. brucei*

T. brucei has an elongated shape and polarised microtubule cytoskeleton, which defines the cell shape. The *T. brucei* has a rigid morphology, which is maintained by a highly ordered array of subpellicular microtubules, located beneath the plasma membrane and maintains cell shape even after detergent extraction (Robinson et al., 1995). This array of microtubules is evenly spaced with the minus end polarity facing the anterior side and the plus end facing the posterior side(Angelopoulos, 1970). The study has demonstrated that RNAi knockdown of the calpain-like protein CAP5.5 causes disruption of regularly spaced array of sub-pellicular microtubules and result in cell morphology and cytokinesis defects in *T. brucei* (Olego-Fernandez et al., 2009). The non-dividing procyclic form *T. brucei* contains a single nucleus, kinetoplast, basal body, flagellum, flagellar pocket, and mitochondrion, and these organelles are positioned precisely within the cell (Fig. 1.9 A). The basal body of the flagellum is linked to the kinetoplast, which is a critical

attachment for the accurate segregation of organelles during cell division (Ogbadoyi et al., 2003; Robinson and Gull, 1991).

1.8.2 Flagellum of *T. brucei*

The flagellum is surrounded by its own membrane, and most of its length is attached to the cell body, following a left-handed helical path to the anterior end (Ralston and Hill, 2008). The proximal end of the flagellum contains the nine triplet microtubules, basal body, which is flanked by the pro-basal body, and the transition zone, in which nine double microtubules are continued. The 9+2 microtubule structure only starts from the distal end of the tansition zone, termed the basal plate, in which the central pair of microtubules emerges and is surrounded by nine double microtubules. The *T. brucei* flagellum is comprised of a 9+2 microtubular eukaryotic axoneme with additional structures which make the flagellum of *T. brucei* unique: the flagellum attachment zone (FAZ) and paraflagellar rod (PFR) (Fig. 1.9 B).

The flagellum and cell body membrane are tightly connected by FAZ, made up by FAZ filament and a specialised microtubules quartet (Lacomble et al., 2009; Sherwin and Gull, 1989a; Sherwin and Gull, 1989b).The microtubule quartet originates next to the basal body, is elongated around the flagellar pocket, and then inserts into a subpellicular microtubules array where the FAZ begins to emerge (Lacomble et al., 2009) .

The flagellum of *T. brucei* contains a lattice-like structure, the PFR, which runs alongside the axoneme (Sherwin and Gull, 1989b). The structure of the PFR is restricted to kinetoplastids, euglenoids, and some dinoflagellates (Bastin et al., 1996b; Maga et al., 1999). The main structural PFR proteins are paraflagellar rod protein 1 (PFR1) and paraflagellar rod protein 2 (PFR2), with other minor proteins localised within the scaffold of the PFR. PFR appears to have multiple functions in the *T. brucei* flagellum. The major function is motility because the reduced expression of PFR2 causes paralysed cells that are unable to swim but does not affect the cell growth and morphology of the procyclic form *T. brucei* (Bastin et al., 1999b; Bastin et al., 1998). In addition to

A

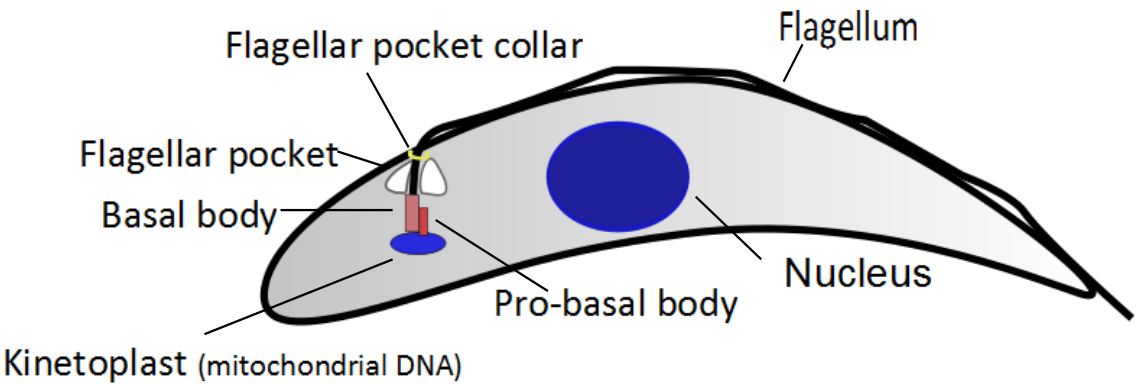

B

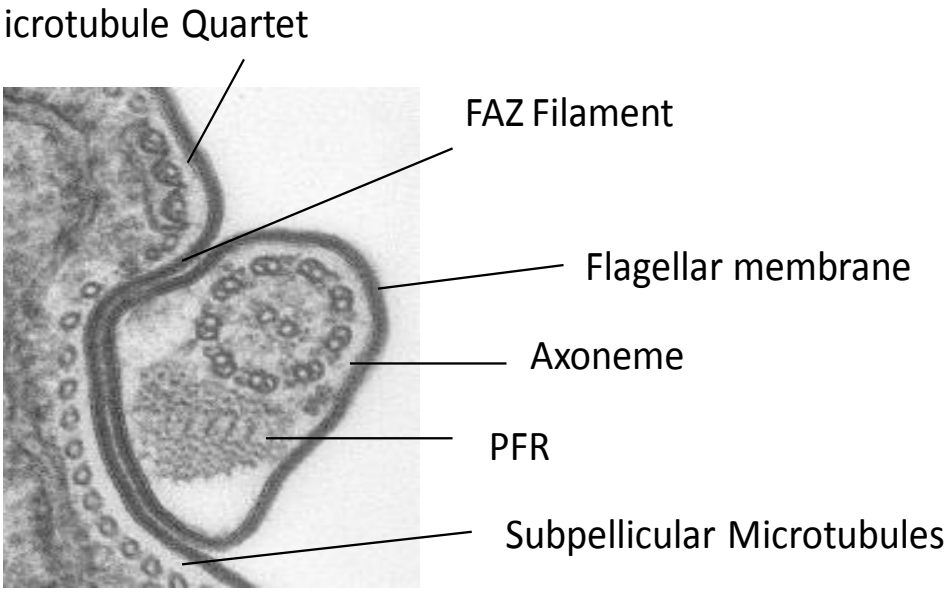

Figure 1.9 (A) **Architecture of *Trypanosoma brucei.*** (B) **Transmission electron micrograph shows a cross-section of the flagellum and PFR.** Image is from Gull lab.

motility, PFR regulates calcium-mediated signalling (Ridgley et al., 2000) and interacts with metabolic enzymes, such as adenylate kinases (Ginger et al., 2005).

1.8.3 The function of the flagellum in *T. brucei*

Various roles can be assigned to the flagellum in trypanosome biology. Beyond the classic motility function, the flagellum involves in cellular morphogenetic event and attachment of the insect's salivary gland, which is critical for parasite's pathogenesis. Lastly, possibly this organelle possess the sensory function for successful developmental transformations within specific hosts.

Motility: The obvious and critical role of the flagellum in *T. brucei* is motility, and various components have been elucidated that facilitate the complex mechanism of flagellar motility. For example, silencing the axoneme component DNAI1, which is an essential component of the outer dynein arms inhibits propulsive waving and causes the absence of forward motility (Branche et al., 2006). However, the level of importance of flagellar motility differs between the procyclic and bloodstream form *T. brucei* that the bloodstream forms is more sensitive to the perturbation of flagellum motility. The ablation of several flagellar proteins, such as PFR2, PACRG-A, and a subunit of the dynein regulatory complex, trypanin caused a flagellar motility defect, but the cells remained viable without any morphological alternations in procyclic form *T. brucei* (Broadhead et al., 2006; Dawe et al., 2005; Hutchings et al., 2002). In contrast, the loss of these proteins caused defects in cytokinesis such that cells become monstrous with multiple nuclei, leading to cell death of bloodstream form *T. brucei* (Bastin et al., 1998; Broadhead et al., 2006; Ralston and Hill, 2006). This result suggested that flagellar motility is essential for the bloodstream form *T .brucei*.

Cell morphogenesis: The cell shape and organelle position of *T. brucei* are remarkably well maintained through cell division. Various observations of RNAi mutated cells revealed an important function of the flagellum in structural inheritance with this organelle dictating cell

morphology. For example, RNAi mutant analysis showed that IFT mutants in *T. brucei* failed to produce a new flagellum, which caused smaller daughter cells and the loss of the normal cell shape (Absalon et al., 2008b; Kohl et al., 2003), indicating that the flagellum controls the cell size. In addition, the elongation of a new flagellum is necessary for the structural integrity of the flagellar pocket. Defects in assembling the new flagellum affect the morphology of the flagellar pocket, suggesting that the elongation of a new flagellum across the flagellar pocket is an essential morphological process for the formation of two flagellar pockets (Absalon et al., 2008a). The flagellum is also required for the correct positioning of the kinetoplalst. Several RNAi studies have revealed that the impairment of flagellum biogenesis or motility caused the mislocalisation of the kinetoplast (Absalon et al., 2007; Branche et al., 2006; Dawe et al., 2005). Since the flagellum and its motility function are critical for the cells, the segregation of the kinetoplast being associated with flagellum formation and function appears beneficial for the cells.

Host cell attachment: In the final stage of maturation to the mammalian infectious bloodstream form, parasite attachment to the salivary gland of the tsetse fly occurs. This attachment is facilitated by the parasite flagellum, which forms extensive outgrowths of the flagellar membrane and cytoskeletal structure that penetrate between the microvilli of the salivary gland epithelium (Vickerman et al., 1988). The flagellum secures the epimastigote attachment, in association with cessation of cell division and elaborate flagella outgrowth (Vickerman, 1969). At this stage, the cell develops into the mammalian infective form, which gains the VSG coat and undergoes further cell development and pathogenesis (Vickerman, 1969). At the end of the developmental transformation, infective metacyclics are released into the salivary gland lumen for mammalian host transmission. The flagellum-mediated salivary gland attachment is, therefore, a critical process for parasite survival and pathogenesis. However, the molecular mechanism of the morphological changes of the cell and signalling that dictate the developmental changes is still largely unknown, and further study is required.

Sensory function: *T. brucei* may detect signals from the host and parasite that can instruct *T. brucei* for its successful developmental transformation. During the life cycle, a dynamic cellular morphological transformation is taking place and the cell changes into a form for adapting to the next environment to which they are to be exposed. Moreover, for the host cell attachment, the flagellum needs to sense the substrate for host cell adhesion. Very little is known about this action and the signals that guide *T. brucei* to achieve the regulation of its life cycle are still a mystery. Several studies using various organisms have shown that a flagellum function is sensing. Calcium signalling plays a role in chemotaxis in the flagellum of mammalian sperm (Eisenbach and Giojalas, 2006), and flagellar cAMP signalling is necessary for fusion and zygote formation in *C. reinhardtii* (Zhang and Snell, 1994). The flagellar membrane of *T. brucei* also contains various proteins that make the flagellar membrane a unique region compared with the rest of the cell body. Few flagellar membrane proteins in *T. brucei* had been identified such as, calcium-binding protein (Godsel and Engman, 1999), receptor adenylate cyclases (ESAG4) (Paindavoine et al., 1992), and calflagin (Emmer et al., 2009). Revealing the ligands for these putative receptors and the roles and downstream effects of these receptors, is an important area of research to gain additional deep insight into flagellum biology.

1.8.4 Flagellar pocket

The flagellar pocket is a specialised membrane domain, forming a flask-shaped invagination of the cell membrane that the proximal end of the flagellum emerges from the cytoplasm. Although it represents up to 5% of the total cell surface, it is the sole site of vesicle endocytosis and exocytosis (Overath and Engstler, 2004), as it is not surrounded by the subpellicular microtubules. The flagellar pocket is a structure for transporting and recycling the glycosylphosphatidylinositol (GPI)-anchored surface proteins such as, procyclin in the procyclic form and VSG in the bloodstream form *T. brucei* (Overath and Engstler, 2004). Endocytosis is mediated by clathrin-coated vesicles bud from the flagellar pocket, transporting nutrients, VSG, and various receptor

proteins (Engstler et al., 2004). However, The rate of endocytosis differs between the procyclic and bloodstream forms, with endocytosis in the bloodstream form to remove and recycle VSG from the cell surface being extremely rapid, finishing within 7 minutes (Grunfelder et al., 2003), indicating the importance of developmental adaptation. Particularly, the bloodstream form parasite contain about 10^7 VSG molecules in their surface and able to turn over the total cell surface of VSG molecules every 12 minutes (Engstler, et al., 2004). This explains the reason of first endocyctosis in bloodtsream form cells, which enables the cells to defence themselves against the host immune response.

Clathrin dependent endocytosis has been shown by knockdown of the clathrin heavy chain that ablation of clathrin heavy chain prohibited endocytosis, resulting in a massively enlarged flagellar pocket in bloodstream form, which is termed the "Big eye"(Allen et al., 2003), and reduced the efficiency of endocyosis in the procyclic form (Hung et al., 2004). In the flagellar pocket, various cell surface receptors are selectively retained, such as transferrin receptor, which is necessary for iron uptake (Mussmann et al., 2004), and cysteine-rich acidic integral membrane protein (CLAM), which is responsible for signal sorting so that they are exporting from endoplasmic reticulum to the flagellar pocket (Qiao et al., 2006).

The architecture of the flagellar pocket is firmly maintained by electron dense annules called flagellar pocket collar at the neck of the flagellar pocket, which demarcates the boundary of the flagellar pocket membrane and cell membrane; a protein named BILBO1 has been identified as a component of the flagellar pocket collar (Bonhivers et al., 2008). In the region immediately after the flagellum exits from the flagellar pocket, a specific membrane domain is observed, known as the flagellar pocket neck region (Henley et al., 1978). Endocytosis is occurs in the entire flagellar pocket region, but the only site where the clathrin is not taken is the specialised microtubules quartet originating next to the basal body that runs around the flagellar pocket, and the neck region (Gadelha et al., 2009).

1.8.4 *T. brucei* as a model organism

As well as being a harmful pathogen, *T. brucei* has been used as an excellent model organism for basal body/flagellum biology. *T. brucei* can be easily propagated in culture medium with a relatively rapid doubling time, which is approximately 6 hours for the bloodstream form and 8 hours for the procyclic form, and it takes only about 10 days to gain clonal transfectants. The cells contain a flagellum throughout the cell cycle; when the new flagellum starts to elongate, the old flagellum is not disassembled. Therefore, we can compare the new and old flagella in the same cell (Bastin et al., 1999a). Moreover, the greatest advantage in using *T. brucei* as a model organism is the feasibility of reverse genetic analysis to determine the function of proteins, including the inducible expression of RNAi for gene knockdown, targeted gene knockout, and inducible expression (Clayton, 1999; Morris et al., 2002), and the straightforward endogenous loci tagging technique (Kelly et al., 2007). The 9+2 flagellar axoneme is evolutionally conserved and recent proteomic and genomic studies have revealed highly conserved human ciliopathies genes in *T. brucei* (Baron et al., 2007; Broadhead et al., 2006; Hodges et al., 2010), which enable us to conduct tractable reverse genetics to investigate the function of flagellar proteins. In some cases, the genes identified in human ciliary diseases showed bona fide flagellum function in *T. brucei*. For example, the dysfunction of *hydin* cause hydrocephaus in humans, due to the impairment of the epithelial cilia in brain ventricles; this gene is also conserved in *T. brucei* (Broadhead et al., 2006; Smith, 2007). The RNAi approach using *T. brucei* has identified the function of hydin as regulating the position of the central pair of microtubules, which may underlie the flagellar motility (Dawe et al., 2007). Therefore, *T. brucei* is a powerful experimental model for dissecting eukaryotic cilia/flagella biology to unveil the cellular mechanism of ciliopathy.

1.9 Aim of the study

The aim of this study is to determine the function of the BBSome in *T. brucei*, particularly with respect to flagellum formation. Numerous studies have shown a link between the BBSome and cilia, with the BBSome being necessary for ciliary function via delivering ciliary membrane proteins to the ciliary membrane. More precisely, the BBSome is responsible for making cilia as sensory antennae by recognising and transporting ciliary receptor proteins from the cell body to the ciliary membrane, by passing the ciliary diffusion barrier. Since the7 BBSome proteins have been evolutionally conserved, the function of the BBSome is considered essential for cell survival. Previous studies have demonstrated that the loss of the BBSome proteins perturbs protein localisation and leads to the loss of ciliary function, without affecting ciliary assembly (Lechtreck et al., 2009; Mykytyn et al., 2004; Reed et al., 2011). However, what will happen to *T. brucei* if the BBSome is knocked-down? In *T. brucei,* the single flagellum plays various vital roles in cell survival, not only in cell motility. Given that the BBSome is widely conserved in ciliated eukaryotes, including *T. brucei*, we predict that the BBSome plays a critical role in *T. brucei* linked to flagellum formation and/or function. The knockdown of BBSome subunits may show us a phenotype that may reveal the role of the BBSome within the *T. brucei* flagellum formation.

Among the 7 BBSome proteins, I have focused on BBS5 since it is more conserved than other BBSome subunits, possibly because the ability in lipid association may crucial for sustaining the BBSome function.

The aim of my study is to determine the localisation of BBS5 in *T. brucei*, particularly whether BBS5 also localises in basal body, which was shown in other studies. Next, perform RNAi knockdown of BBS5 to investigate the function of BBS5 through analysis of the resulting phenotype, particularly whether the ablation of BBS5 affects the flagellum formation and lead to defect in cell survival and cell morphology. Finally, because the 7 BBSome proteins have been hypothesised to interact with each other in the cell, I examined whether *T. brucei* BBS5 requires other BBSome subunits for its expression and localisation. I aimed to characterise the highly

conserved BBS5, which the mutation causes human ciliopathy BBS, in *T. brucei* to reveal further the pathogenicity of BBS and investigate the requirement of BBS5 in flagellum formation of *T. brucei.*

Chapter 2

Materials and Methods

2.1 Cell lines and culture of trypanosomes

Procyclic form *Trypanosoma brucei* cells were cultured at 28°C in SDM-79 medium supplemented with 10% fetal bovine serum [Gibco] (Brun and Jenni, 1977). Bloodstream form *T. brucei* cells were cultured in HMI-9 medium supplemented with 15% fetal bovine serum using vented-cap flasks at 37°C in 5% CO_2 (Hirumi and Hirumi, 1989). In order to maintain mid log phase growth (procyclic form: $1x10^5$ - $2x10^7$ cells/ml, bloodstream form: $1x10^3$ to $1x10^6$ cells/ml), cells were diluted as necessary. Cell density was measured by a Casy-counter [Schärfe systems GmbH]. Procyclic form *T. brucei* were frozen in a freezing medium which contains 7.5% Glycerol and 92.5% procyclic form culture medium. Bloodstream form *T. brucei* were frozen in a freezing medium, which contains 10% Glycerol and 90% bloodstream forms culture medium. Cells were stored in liquid nitrogen and defrosted at 1:10 dilution in pre-warmed medium.

The parental cell lines used were as follows:

Procyclic form *T. brucei*:

SMOX P9 (TREU-927 expressing T7-RNA polymerase and tetracycline repressor from a single plasmid insert) (Poon et al., 2012).

Bloodstream form *T. brucei*:

S16 (Lister-427 expressing T7 RNA polymerase and tetracycline repressor from a single plasmid insert).

90-13 (Lister-427 expressing T7 RNA polymerase and tetracycline repressor from double plasmid inserts) (Wirtz et al., 1999).

SMOX B4 (Lister-427 expressing T7-RNA polymerase and tetracycline repressor from a single plasmid insert) (Poon et al., 2012)

2.2 Molecular Biology

2.2.1 Plasmid strategy

In my thesis, I used three types of strategies to study the proteins of interest. Endogenous locus tagging, RNAi induction, and inducible over expression. Different plasmids were used to achieve these three projects.

Endogenous locus tagging to single allele:

To generate TY::GFP fused proteins for investigating protein's localisations, TY-epitope and green fluorescent protein (GFP) were tagged endogenously in N-terminal of proteins. 390 to 440 base pairs of the 5'-end of the targeted open reading frame (ORF) and 250 to 300 base pairs of the 3'-end of the 5' UTR were amplified by PCR. The PCR fragment of ORF was digested with XbaI and NotI and 5'UTR was digested with NotI and BamHI. Restriction enzyme digested ORF and 5'UTR were ligated into the pEnT6B vector for endogenous tagging; between the XbaI and BamHI restriction sites (Kelly et al., 2007) (Fig. 2.1)(Table 2.1).

Endogenous locus tagging to double alleles:

The pEnT6B vector which already contained 5'UTR and ORF of gene of interest and pEnT5-TY-CFP-TY vector were utilised. The target cassette consisted of TY-epitope, GFP, target ORF, and 3'UTR nucleotide sequence present between HindIII and BamHI in modified pEnT6B vector was digested with HindIII and BamHI and ligated to pEnT5-TY-CFP-TY vector. The TY-cerulean-TY region in pEnT5-TY-CFP-TY vector was removed by HindIII and BamHI prior to ligation and replacement of target cassette construct was carried out (Fig. 2.2).

RNAi induction:

For generating RNAi plasmid constructs, 300-400 base pairs of the target ORF were amplified by PCR from genomic DNA of *T. brucei* and inserted between XbaI and HindIII sites of the p2T7-177

A

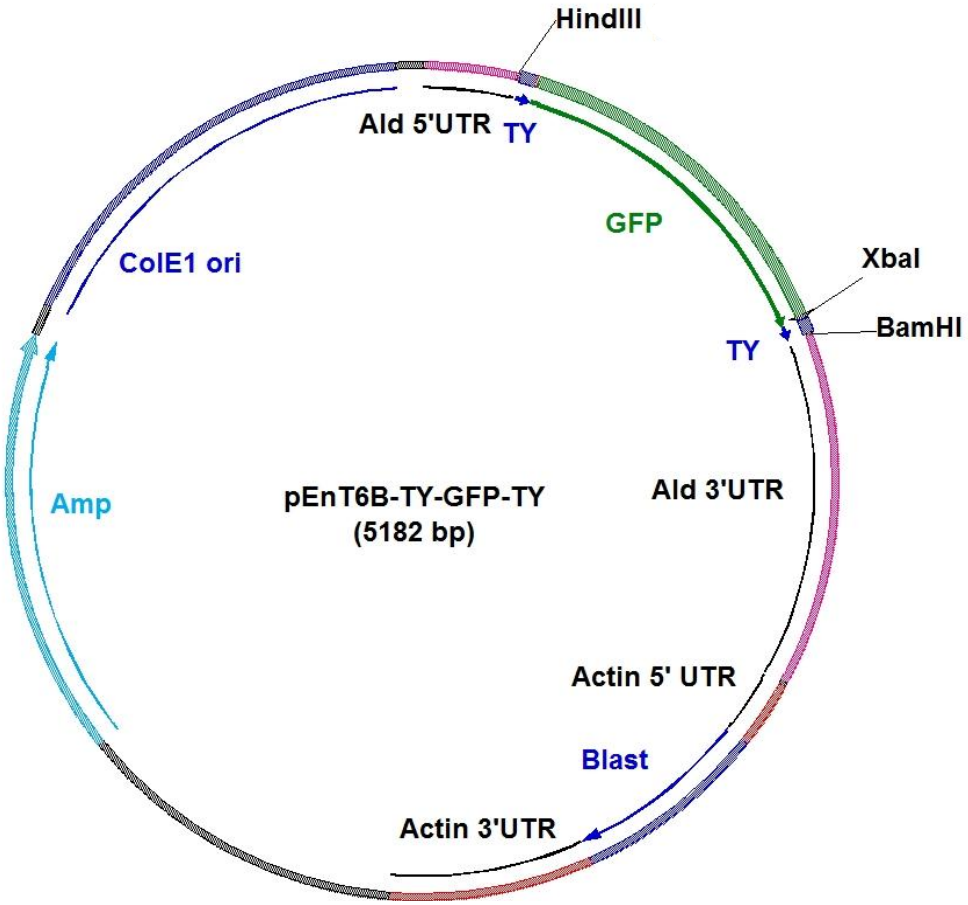

B

Table 2.1 **The generated vectors in my thesis for endogenous locus tagging using pEnt6B-TY-GFP-TY vector.**

Vector Name	Parental Vector	Insert 1	Restriction enzymes	Insert 2	Restriction enzymes
pEnT6B-TY-GFP-BBS5	pEnT6B-TY-GFP-TY	Tb927.1.4140 5'UTR (654-991)	NotI BamHI	Tb927.1.4140 ORF (4-389)	XbaI NotI
pEnT6B-TY-GFP-BBS8		Tb11.01.4290 5'UTR (647-1003)		Tb927.1.4140 ORF (4-447)	
pEnT6B-TY-GFP-BBS9		Tb11.01.6070 5'UTR (629-996)		Tb11.01.6070 ORF (4-427)	

Figure 2.1 **pEnT6B-TY-GFP-TY vector for endogenous locus tagging.** (A) Plasmid map of pEnT6B-TY-GFP-TY vector (Kelly et al., 2007) utilised for endogenous tagging of BBS5, BBS8, and BBS9. In order to modify the 5' end of the allele, the gene cassette consisted of 390-440 bp of ORF right after the start codon and 250 to 300 bp of 3' end of 5'UTR was inserted between XbaI and BamHI. ORF fragments contained XbaI and NotI, and 5'UTR fragment contained NotI and BamHI. This vector contains blasticide resistance gene for selection. (B) Inserts and restriction enzymes for generating pEnT6B vectors for endogenous locus tagging of BBS5, BBS8, and BBS9.

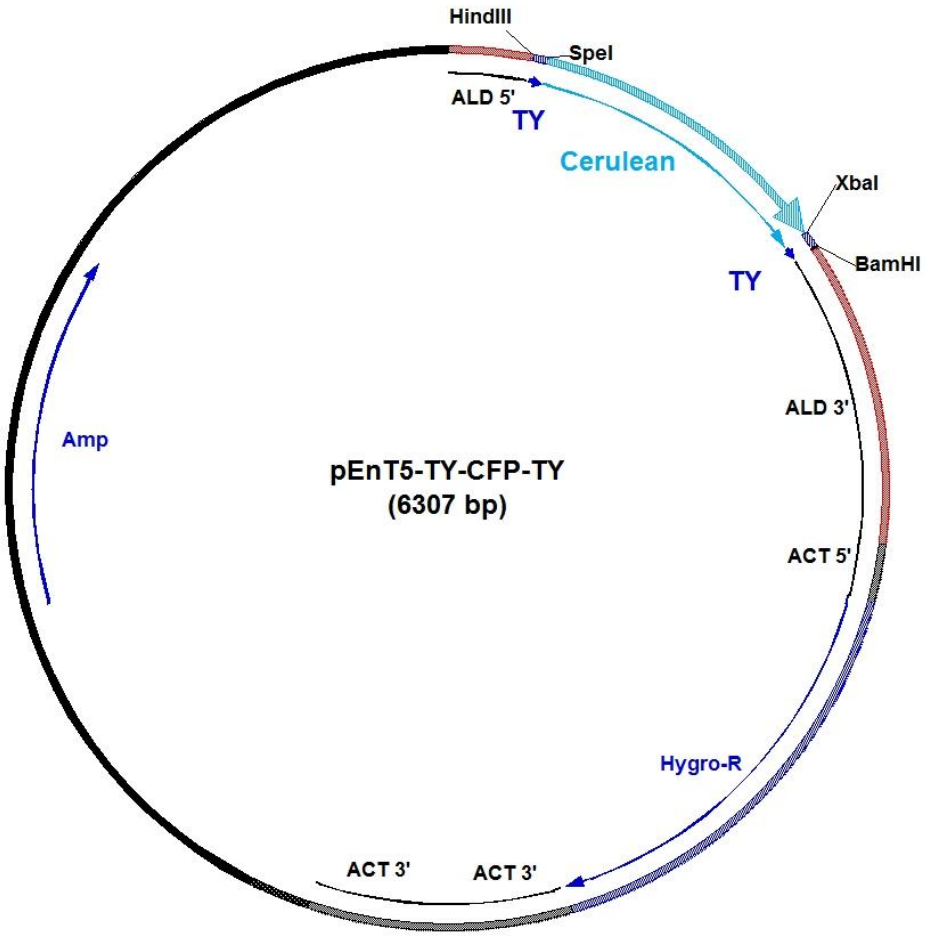

Figure 2.2 **pEnT5-TY-CFP-TY vector for double BBS5 allele tagging**. Plasmid map of pEnT5-TY-CFP-TY vector utilised for tagging the both endogenous alleles of BBS5 to express TY::GFP::BBS5. The target cassette consisted of TY-GFP-ORF-5'UTR which positions between HindIII and BamHI in the modified pEnT6B vector was inserted to HindIII and BamHI region of pEnT5-TY-CFP-TY vector to replace TY-Cerulean-TY. The vector contains hygromycine resistance gene for selection.

vector (Wickstead et al., 2002) (Fig. 2.3)(Table 2.2). The target sequence is flanked by opposing T7 promoters for producing dsRNA of the target in the p2T7-177 vector.

Ectopic expression of C-terminally tagged protein:

For ectopic expression of TY-epitope tagged proteins, the full-length ORF of genes of interests were inserted in frame with the TY- reading frame between the XbaI site and the HindIII site into the pDEX777 vector (Kelly et al., 2007) (Fig. 2.4)(Table 2.3).

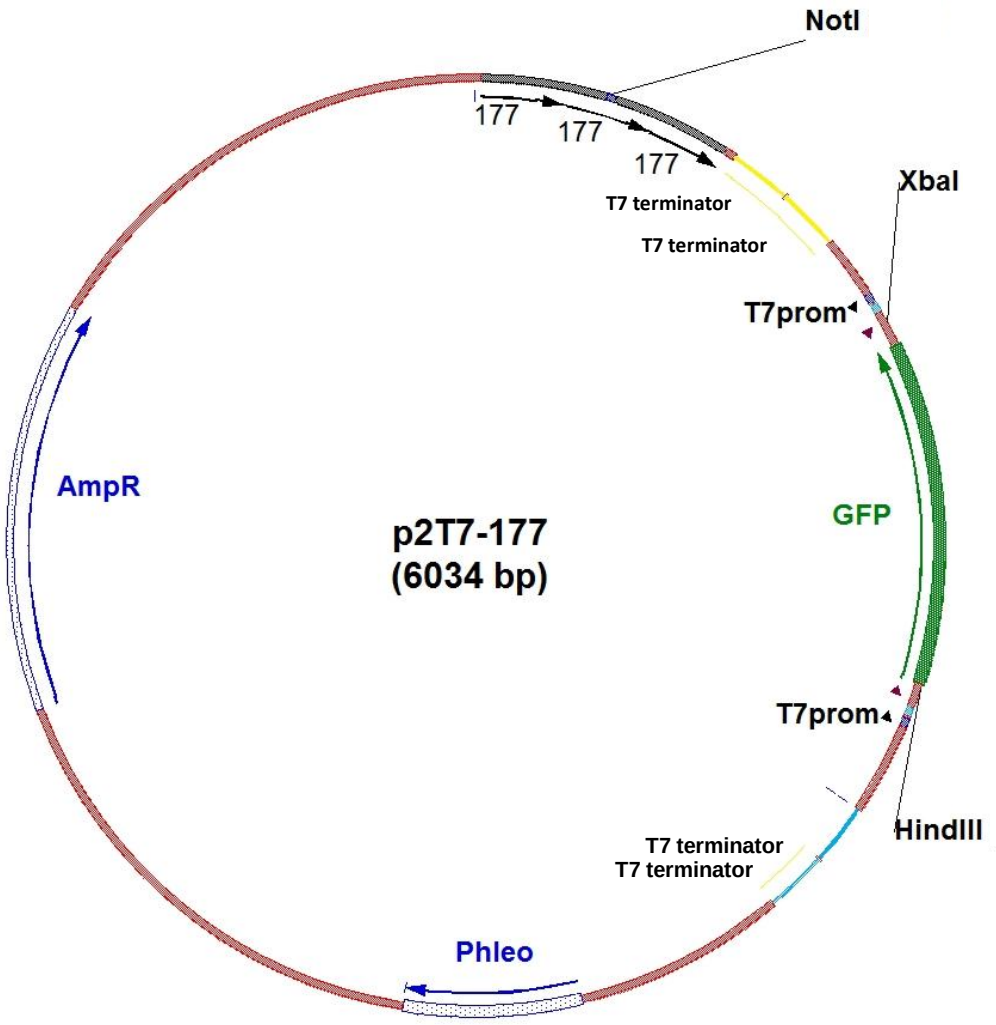

Figure 2.3 **p2T7-177 vector for RNAi induction against mRNA**. Plasmid map of p2T7-177 vector utilised for RNAi induction against BBS1, BBS2, BBS4, BBS5, BBS7, BBS8, and BBS9. 300-400 bp of target ORF was replaced to the GFP region, flanked by two opposing T7 promoters. NotI linearization enables the plasmid to integrate to 177 mini-chromosome repeat. The vector contains phleomycine resistance gene for selection.

Table 2.2 **The generated vectors in my thesis for knockdown the BBSome subunits using p2T7-177 vector.**

Vector name	Parental vector	Insert	Restriction enzyme
p2T7-177-BBS1	p2T7-177	Tb09.211.2080	XbaI & HindIII
p2T7-177-BBS2		Tb927.6.2020	
p2T7-177-BBS4		Tb927.10.6830	
p2T7-177-BBS5		Tb927.1.4140	
p2T7-177-BBS7		Tb927.3.3640	
p2T7-177-BBS8		Tb11.01.4290	
p2T7-177-BBS9		Tb11.01.6070	

A

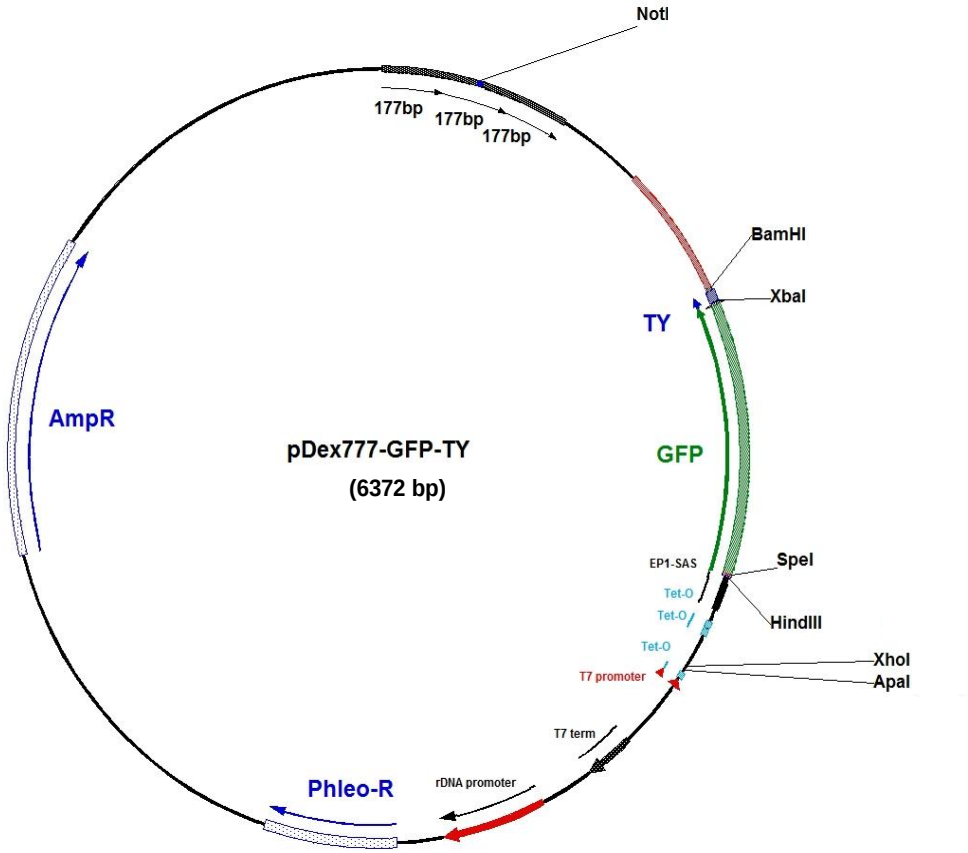

B

Table 2.3 **The generated vectors in my thesis for ectopic expression using pDex777-GFP-TY vector.**

Vector Name	Parental Vector	Insert	Restriction enzymes
pDex777-BBS5-TY	pDex777-GFP-TY	Tb927.1.4140	XbaI HindIII
pDex777-BBS8-TY		Tb11.01.4290	

Figure 2.4 pDex777-GFP-TY vector for ectopic expression. (A) Plasmid map of ectopic expression of C-terminally tagged BBS5::TY and BBS8::TY. Full length of BBS5 and BBS8 ORF were inserted between XbaI and HindIII to exclude GFP. Under the regulation of tet operators, T7 RNA-polymerase promoter initiates transcription. NotI linearization enables the plasmid to integrate to 177 mini-chromosome repeat. The vector contains phleomycine resistance gene for selection. (B) Inserts and restriction enzymes for generating pDex777 vectors for ectopic expression of BBS5 and BBS8.

2.2.2 Polymerase chain reaction

Primers for PCR were designed using Primer3 software (http://frodo.wi.mit.edu/primer3/). Since the restriction sites were added to 5' end of primer, 2-3 random nucleotides were added to 5' end of every primer to increase digestion effectiveness. The PCR reaction was performed in 50 µl total volume with genomic DNA isolated from *T. brucei*, appropriate amount of PCR buffer, 0.2 mM of each dNTPs (dATP, dCTP, dGTP and dTTP), 1µM of each primer, 0.5µl of polymerase (Roche Expand High Fidelity PCR system), and the appropriate amount of ddH2O in order to make up to the 50µl volume. PCR was performed by using a Perkin Elmer GeneAmp 2400 PCR machine. The thermal cycling conditions were 3 minutes at 94 °C followed by 30 cycles of 30 seconds at 94 °C, 30 seconds at 55 °C and 1 minute at 72 °C. The amplified PCR products were examined by agarose gel electrophoresis.

Table 2.4 **Primers for amplifying the gene of interest.**
Restriction sites are added to 5' end of each primer in addition to 2 to 3 nucleotides.
(F: Forward, R: Reverse) aagctt=HindIII; tctaga=XbaI; gcggccgc=NotI; ggatcc=BamHI

Purpose	Primer sequence	
Endogenous BBS5 tagging	BBS5 ORF	F: gggtctagaCCAGCTGGTGGTGACACG
		R: tttgcggccgcGTCCTCACTTGGATG
	BBS5 5'UTR	F: aaagcggccgcGCTGTTTACCGTCC
		R: aaaggatccGTTGTACACACAGGCCGG
Endogenous BBS8 tagging	BBS8 ORF	F: gggtctagaGGTGTCCGTGCCATTACTTTG
		R: tttgcggccgcCGCAGTTGCATTCGATGG
	BBS8 5'UTR	F: aaagcggccgcGCTGTTTACCGTCC
		R: aaaggatccCAGTGCACTTAGTTCTCAC
Endogenous BBS9 tagging	BBS9 ORF	F: gggtctagaGGATCCCTATTCAAGCTACGTG
		R: tttgcggccgcCATGTCCCTCCAAGGACG
	BBS9 5'UTR	F: ttt gcggccgcGCCTGCATAAGGGTAAGTG

		R: aaaggatccGCGCTATTATAACAGCG
BBS5 ectopic expression	F: gagaagcttATGCCAGCTGGTGGTGACAC	
	R: attctagaCACGACATTCCACAAATCCTGCAA	
BBS8 ectopic expression	F: ttaagcttATGGGTGTCCGTGCCATTA	
	R: aatctagaGGCCGCAAGTATTTTTCGA	
BBS1 RNAi induction	F: gctctagaGGTAGGAATCATGCCGAAAA	
	R: cgaagcttACGGAAACATCGACCTCATC	
BBS2 RNAi induction	F: gctctagaTACACTCGTT TGC GGACTTG	
	R: ccaagcttCAGC TTCCGCTATGTCATCA	
BBS4 RNAi induction	F: gctctagaTTTGTTCGTAAAGGGGTTGC	
	R: ccaagcttGCCACACCAAACTCTCCATT	
BBS5 RNAi induction	F: ggtctagaAGGCACTTCGCATAACTGCT	
	R: ttaagcttGCCAAACTCGGTATCCTGAA	
BBS7 RNAi induction	F: gctctagaCTGACTCGAAGGAGGAGGTG	
	R: cgaagcttGGTGGAGGAAACAGCCAATA	
BBS8 RNAi induction	F: aatctagaCAGCACCAACGTAGAAGCAA	
	R: ggaagcttGCTGCGTTGTAAAGGGACTC	
BBS9 RNAi induction	F: aatctagaCCGTTAGGTGAGGATGCAAT	
	R: gcaagcttCCCGGTGTGATGC TCTCTAT	

2.2.3 Agarose gel electrophoresis

DNA samples were separated in gels containing 0.7 to 1.5% Agarose/TAE (40 mM Tris, 20 mM acetic acid, 10 mM EDTA), in addition to 0.2 µg/ml ethidium bromide, applying 100 V.

2.2.4 Ligation for plasmid generation

The amplified PCR fragments were purified using the QIAquick PCR Purification Kit (Qiagen) and restriction enzyme digestion was performed according to manufacturer's instruction (Roche). Vectors after the restriction enzyme digests were purified using QIAquick gel extraction kit, (QIAGEN). Prior to ligations, vectors were dephosphorylated using Alkaline Phosphatase (Roche) by incubation at 37°C for 30 minutes to prevent self-ligation. Vector and insert fragments were ligated using 1:3 ratio of plasmid vector versus insert fragment molecules. The ligation reaction was carried out by adding T4 DNA ligase (Roche) and incubating at room temperature for 4 hours.

2.2.5 Bacterial transformation

For transformation, *Escherichia coli* XL1-blue (Stratagene) strain was used. 100µl of competent cells were incubated on ice for 20 minutes with 10 µl of the ligation reaction, subjected to heat shock at 42 °C for 1 minute, then placed back on ice at least for 2 minutes. Cells were spread onto LB-agar plate containing 100 µg/ml ampicillin and incubated at 37 °C overnight.

2.2.6 Plasmid isolation

For isolation and amplification of the derived plasmid, single colonies from LB plates were selected and incubated overnight in 3ml of LB culture medium (Sigma) with 100 µg/ml ampicillin at 37°C with shaking. 1.5 ml of bacterial culture was used for small scale plasmid isolation, purified by a silica membrane column (QIAprep Spin Miniprep kit - QIAGEN). After confirmation of presence of DNA insertion by restriction enzyme digestion and agalose gel electrophoresis, large scale preparation was performed for plasmid isolation by culturing 150 ml bacterial culture at 37 °C overnight. Plasmid was isolated and purified by using an anion exchange column (HiSpeed Plasmid Midi kit, QIAGEN) and eluted with 500µl ddH_2O. Plasmids were examined using restriction enzymes and if presence of expected insert DNA was confirmed, they were sequences and used

for transfection.

2.3 Transfection of *Trypanosoma brucei*

10 µg of plasmid DNA was used per transfection. The plasmid DNA was linearized by NotI digestion and purified by ethanol precipitation.

Transfection of procyclic form *T. brucei* : $3x10^7$ cells were used for transfection and they were centrifuged at 800g for 10 minutes and washed 2 times with 10ml of Zimmerman Post Fusion Medium (ZPFM) (132 mM NaCl, 8 mM KCl, 8 mM Na_2HPO_4, 1.5 mM $Mg[CH_3COO]_2$, 90 µM $Ca[CH_3COO]_2$). Following washing with ZPFM, cells were suspended in 500µl of ZPFM and transferred to 4mm electroporation cuvettes. 10 µg of linearized plasmid DNA was added to cells, and then cells were electroporated by applying 3x 100 ms square pulses, twice in the interval of 1.5kV at 200 ms. Cells were transferred into 10 ml pre-warmed medium and selective drug was added after 16 hours in the medium. Cells were diluted to 1/400 by limiting dilution and 200 µl of culture medium containing selection drug was aliquot to each well in 96 well plate. Approximately after 7 to 11 days after adding the drug, drug resistance clones were recovered and they were transferred to larger volume of medium for further growing.

Transfection of bloodstream form *T. brucei*: $5x10^7$ cells were used for transfection and cells were centrifuged at 800g for 10 minutes and washed 2 times with 10 ml of pre-warmed ZPFM containing 50 mM glucose. Cells were resuspended in 500 µl of ZPFM and transferred into the 4 mm electroporation cuvettes. 10 µg of linearized plasmid DNA was added to cells and cells were electroporated by applying 3x 100 ms square pulses, once in the interval of 1.5 kV at 200 ms. Cells were transferred to pre-warmed 25 ml culture medium and aliquot to 1 ml per 1 well in 24 well plate, and cultured overnight (~16 hours). After 16 hours transfection, 1ml of 37°C pre-warmed medium containing double concentrated selection drug was added to each well. Approximately 4

to 6 days after adding the selection drug, drug resistance clones were recovered and they were transferred to larger volume of medium for further growing.

The drugs which were used and their concentration are as follows:

Table 2.5

Drug for selection	Final concentration (Procyclic form *T. brucei*)	Final concentration (Bloodstream form *T. brucei*)
Hygromycin	50 µg/ml	5 µg/ml
Blasticidin	10 µg/ml	5 µg/ml
Puromycin	1 µg/ml	0.1 µg/ml
Phleomycin	5 µg/ml	2.5 µg/ml

2.4 RNAi induction and/or ectopic expression

Procyclic form *T. brucei* was diluted to $1x10^6$ cells/ml and bloodstream form *T. brucei* was diluted to $1x10^5$ cells/ml. RNAi induction and ectopic expressions were carried by addition of 1µg/ml doxycycline to the culture medium.

2.5 Immunofluorescence microscopy

T. brucei were washed twice with PBS, and then resuspended to a final concentration of 8×10^6 to 2×10^7 cells/ml. Cells were settled on slides (glutaraldehyde-derivatised slide for bloodstream form *T. brucei*) for 5 to 10 minutes. Cells were fixed with 4 % formaldehyde for 10 minutes. Slides were washed with PBS 3 times for 10 minutes, and then permeabilized for 5 minutes with 0.1% NP-40 in PBS. Cells were blocked in 1% milk in PBS for 5 minutes at room temperature and incubated with the primary antibody for 1 hour at room temperature in a humid chamber. Slides were washed with PBS 3 times 10 minutes and incubated with fluorescence conjugated secondary antibody for 1 hour at room temperature. After washing 3 times 10 minutes with PBS, 100 µg/ml

DAPI (4',6-diamidino-2-phenylindole) was applied to slides for 5 minutes following by another wash in PBS. Slides were mounted in mounting medium (1% DAPCO, 50% glycerol, 50 mM sodium phosphate, pH 8.0). Leica DM5500B was used for fluoresence microscopes. All images were processed and analyzed by ImageJ (http://rsbweb.nih.gov/ij).

Table 2.6

Primary antibody	**Dilution**
Anti- GFP rabbit polyclonal antibody (Invitrogen) (A11122)	1:200
BB2 (Bastin et al., 1996a)	1:10
YL1/2 (Kilmartin et al., 1982)	1:50
Rabbit pre-immune serum (Raised in Gull lab)	Neat
Secondary antibody	**Dilution**
Swine Anti-rabbit IgG, FITC (DAKO)(F0205)	1:50
Goat Anti-rat IgG, TRITC (Jackson Immunogen Research)(112-025-003)	1:50
Goat Anti-rabbit IgG, TRITC (Jackson Immunogen Research)(112-025-167)	1:500
Rabbit Anti-mouse IgG, TRITC (Jackson Immunogen Research)(315-025-003)	1:50

2.6 Protein Biochemistry

2.6.1 Preparation of cell extracts

For whole cell extracts, $5x10^7$ cells were centrifuged at 500g for 10 minutes, washed with PBS, then resuspended in 100µl of 90 °C laemmli buffer (2% SDS, 10% glycerol, 400 mM β-mercaptoethanol, 0.002% bromphenol blue, 50 mM Tris-HCl pH 6.8) to give a final concentration of $5x10^5$cells/µl. Mixture of cells and laemmli buffer were incubated for 5 minutes at 90°C, and then they were cooled down on ice.

2.6.2 SDS electrophoresis

Cell lysates from $5x10^6$ cells were separated by SDS-PAGE in mini gels 0.75 millimetres (mm) thick and 6 cm long (BioRad). The gels were made of 10% of acrylamide resolving gels, which were made with 10% acrylamide from 30% acrylamide stock (BioRad), 150 mM Tris-Cl pH 8.8, 0.1% SDS, 0.1% ammonium persulfate and 0.04% *N*,*N*,*N*′,*N*′-Tetramethylethylenediamine) in ddH_2O. In addition, 5% acrylamide stacking gel were prepared with 5% acrylamide from a 30% acrylamide stock (BioRad), 125 mM Tris-Cl pH 6.8, 0.1% SDS, 0.1% ammonium persulfate and 0.001% *N*,*N*,*N*′,*N*′-Tetramethylethylenediamine. Gels were run in running buffer (25mM Tris, 250mM glycine, 0.1% w/v SDS at pH 8.3) at 30 mA per gel for about and 1 hour. For visualising proteins, gels were stained with Brilliand Blue R (Sigma) for 10 minutes and treated with destain solution (10% acetic acid, 50% methanol, 40% distilled water) for 30 minutes.

2.6.3 Western blotting

Proteins were transferred onto nitrocellulose membranes (Whatman) in transfer buffer (25 mM Tris-Cl, 192 mM glycine, 20% methanol) for 14 h with a constant current of 120 mA. After membrane transfer, the membrane was stained with Ponceau-S stain (0.1% Ponceau S in 5% acetic acid) for 5 minutes. The membrane was blocked in 5% skim milk in TBST (10 mM Tris HCl pH7.4, 140 mM NaCl, 0.05% Tween-20) for 20 minutes at room temperature. Primary antibody, BB2 which detect the TY-epitope (Bastin et al., 1996a) was diluted in 1:100 in 5% milk in TBST and the membrane was incubated for 1 h at room temperature. The membrane was then washed three times for 10 minutes in TBST. Rabbit anti-mouse horseradish peroxidase-conjugated secondary antibody (Sigma Aldrich, A9044) was diluted in 1:10000 in 5% milk in TBST and the membrane was incubated for 1 h at room temperature. The membrane was washed three times for 10 minutes in TBST, treated with enhanced chemiluminescence reagent ECL [Elmer-Perkins according to the manufacturer's instructions. The membrane was exposed to Kodak biomax MR film (Anachem) for 5-30 minutes and developed in a processor, Kodak M35-M X-OMAT.

Chapter 3

Results

The role of the BBSome in *Trypanosoma brucei*

3.1 BBSome proteins are widely conserved across ciliated eukaryotes

Various studies have already shown that the highly conserved homologues of BBSome subunits are found in ciliated eukaryotes (Hodges et al., 2010; Li et al., 2004; Nachuryet al., 2007). In order to see their level of conservation more in detail, particularly to determine how well they are conserved among the ciliated organisms, I performed bioinformatic analysis of 7 BBSome proteins (BBS1, BBS2, BBS4, BBS5, BBS7, BBS8, and BBS9). Selected organisms for sequence comparison were common model organisms that build a classical cilium/flagellum, which are *Homo sapiens, Chlamydomonas reinhardtii*, *Paramecium tetraurelia, Trypanosoma brucei,* and *Caenorhabditis elegans. C. elegans* was selected since it produces only sensory cilia and therefore, it is useful to assess the function of BBSome proteins involving in sensory function. ID numbers of BBSome proteins within a putative homologue cluster were gained from published data (Hodges et al., 2010) http://jcs.biologists.org/content/suppl/2010/04/18/123.9.1407.DC1/064873TableS3.pdf. The putative homologue sequences in each organism were searched using the ID numbers by available genomic sequence databases from JGI v3.1 (*C. reinhardtii*), GeneDB (*T. brucei*), ParameciumDB (*P. tetraurelia*), UniProt (*H. sapiens)*, and Wormbase (*C. elegans*). The identified amino acid sequences were aligned by ClustalX and their conservation was examined to evaluate whether phylogenetic data could support the function of BBSome proteins in cilia and flagellar function.

Addtionally, the homology between *T. brucei* and *H. sapines* amino acid sequences were verified by reciprocal best BLAST hit approach and sequence alighnment using Clustal Omega, and predict whether the BBSome proteins perform a critical function in *T. brucei,* or not.

The domains contained in individual BBSome proteins in *H. sapiens, C. reinhardtii*, *P. tetraurelia, T. brucei,* and *C. elegans* were also determined by using the Interpro protein domain analysis tool

http://www.ebi.ac.uk/interpro/ and assessed whether the identified domains were shared with the homologue of BBSome proteins in each organism, or not.

Finally, numerous published data identified mutations in 7 BBSome genes from BBS patients (Badano et al., 2003; Chen et al., 2011; Fauser et al., 2003; Hjortshoj et al., 2008; Katsanis et al., 2002; Mykytyn et al., 2004; Mykytyn et al., 2003; Mykytyn et al., 2002). Many of the mutations identified in *BBS1*, *BBS2*, *BBS4*, *BBS5*, *BBS7*, *BBS8*, and *BBS9* were either frameshift or missense mutations, and all BBSome genes have nonsense mutations. Using these published data, I looked at which residues are mutated in their BBSome proteins. Consequently, I evaluated the critical residues for each BBSome component's function by assessing how well the amino acid sequence residues affected by missense, frameshift, or nonsense mutations are conserved across the species. This helps us to identify the crucial residues for each BBSome protein's function and speculate the pathogenic potential of each mutation.

3.1.1 Bioinformatic analysis of BBS1

The *T. brucei* orthologue of BBS1 (Tb09.211.2080) encodes a protein of 609 amino acids, with a predicted molecular weight of 67.1kDa and a predicted isoelectric point of pH 8.1.

An amino acid comparison of BBS1 homologues showed their identities and similarities throughout sequences (Fig. 3.1). A 10aa insert was seen in *T. brucei* between positions 490 and 500. BLAST analysis revealed that the amino acid sequences of *H. sapiens* and *T. brucei* were 31% identical and 51% similar, suggesting that *T. brucei* BBS1 is conserved (Fig. 3.2).

To investigate the domain structure of BBS1, the amino acid sequences of all organisms were scanned using the Interpro protein domain database. *T. brucei* and *C. reinhardtii* were found to contain WD-40 repeat domains in their N-termini and middle sections of the amino acid sequences (Fig. 3.3). WD-40 repeat domains are short (approximately 40 amino acids) motifs and

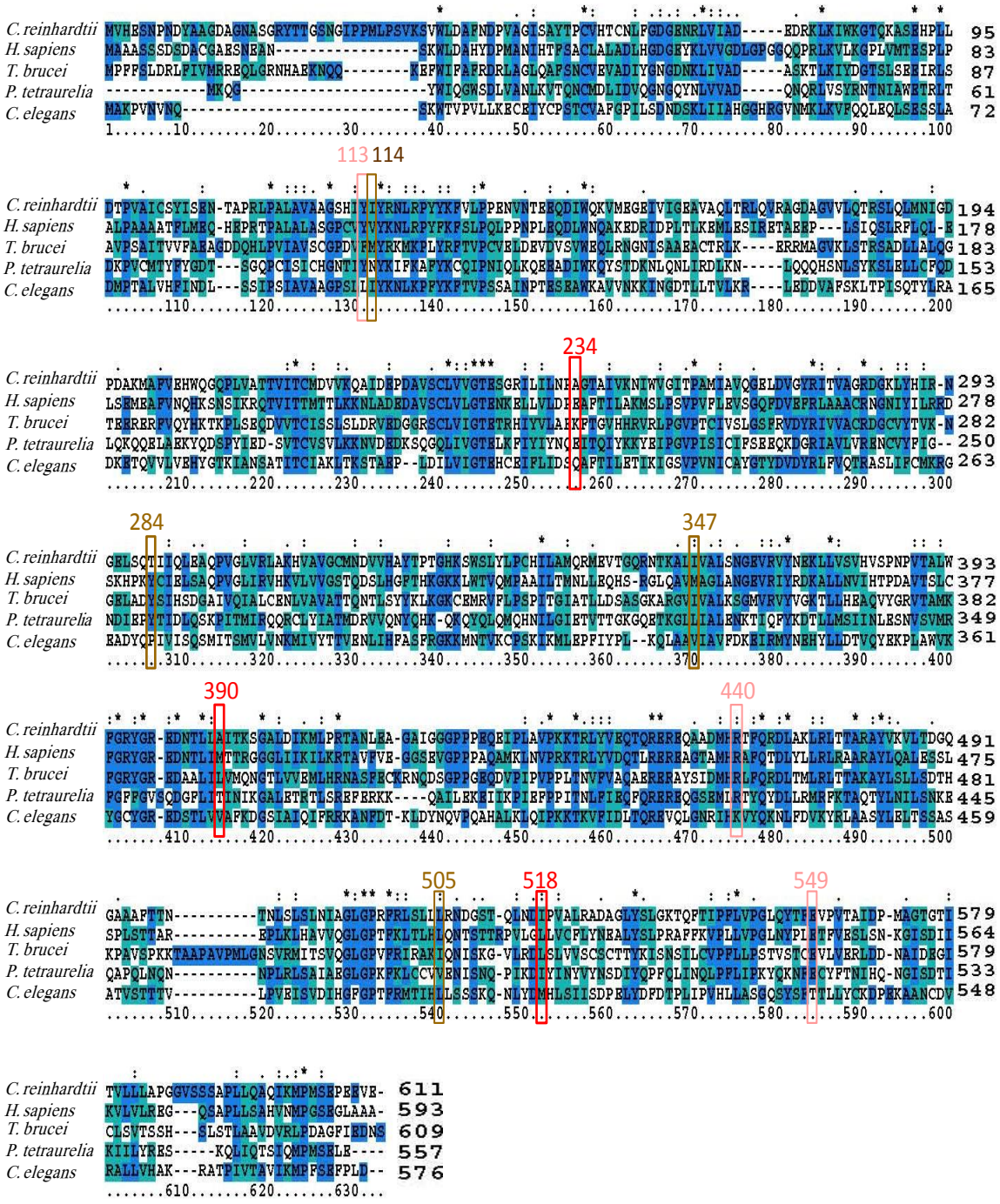

Figure 3.1 **Bioinformatic analysis of *T. brucei* BBS1**. Amino acid sequence alignment of *T. brucei* BBS1 (Tb09.211.2080) with gene of products from *H. sapiens* (OTTHUMP00000064288), *C. reinhardtii* (132537), *P. tetraurelia* (GSPATP00033252001), and *C. elegans* (CE25181). Identical residues are highlighted in blue colour and similar residues are highlighted in light blue colour. Asterisks (*) indicate identical amino acids, while colons (:) and periods (.) represent conserved amino acids. The numbers of amino acid residues are shown on the right and the positions are shown along the bottom. Alignment was generated with clustalx. Amino acid sequence conservation around residues by missense, nonsense, and frameshift mutations identified in BBS patients are also shown. Red squares around residues indicate the positions of the missense mutations: E234K, M390R, and L518P. Pink squares around residues indicate the positions of nonsense mutations: Y113X, R440X, and R549X. Brown squares around residues the positions of frameshift mutations: V114fsX150, Y284fsX288, M347fsX373, and L505fsX556.

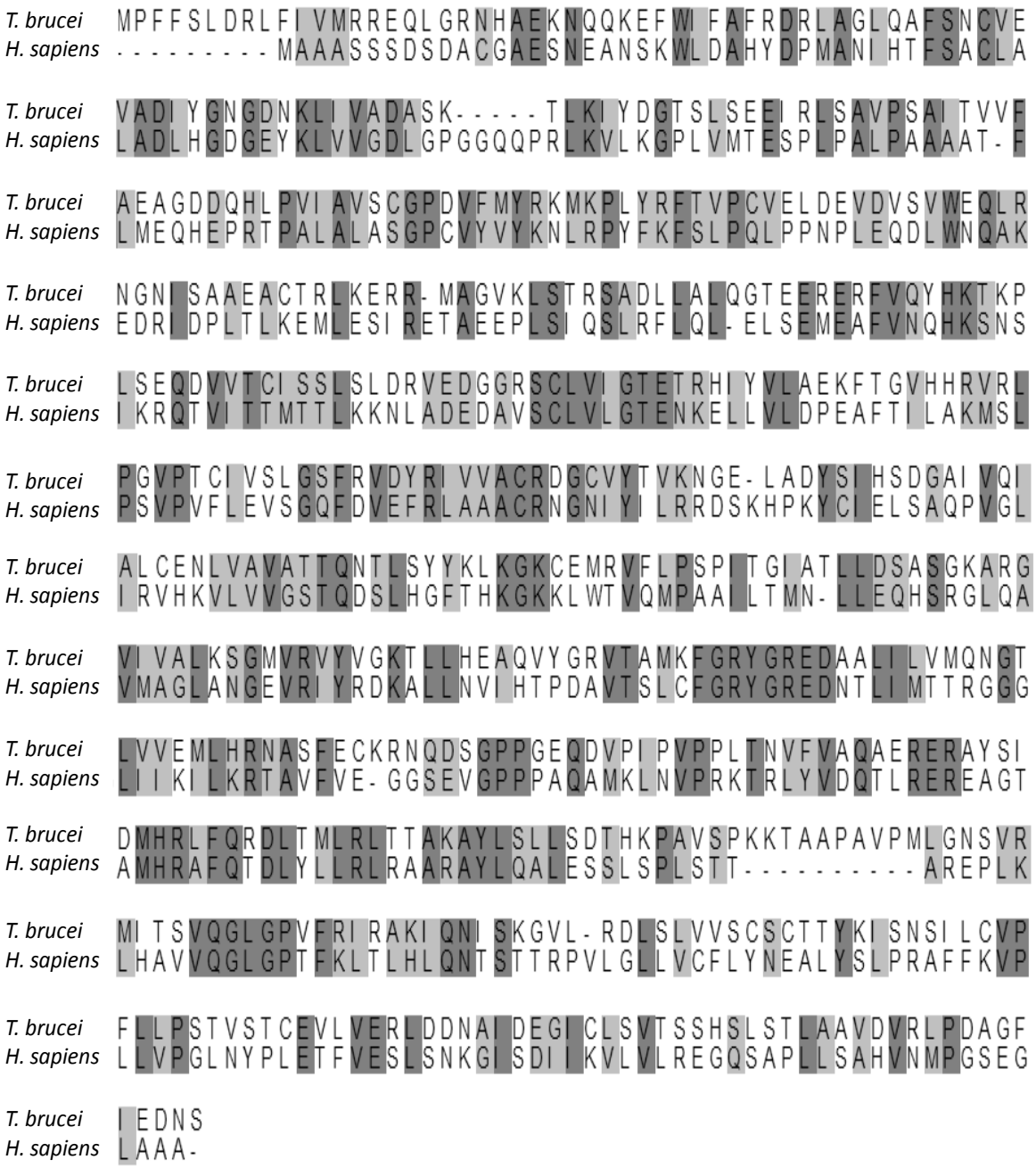

Figure 3.2 **Amino acid sequence alignment of *H. sapiens* and *T. brucei* BBS1.**
The alignment was created in Clustal Omega, and is shown with black background when the residues are identical and in gray when they are similar.

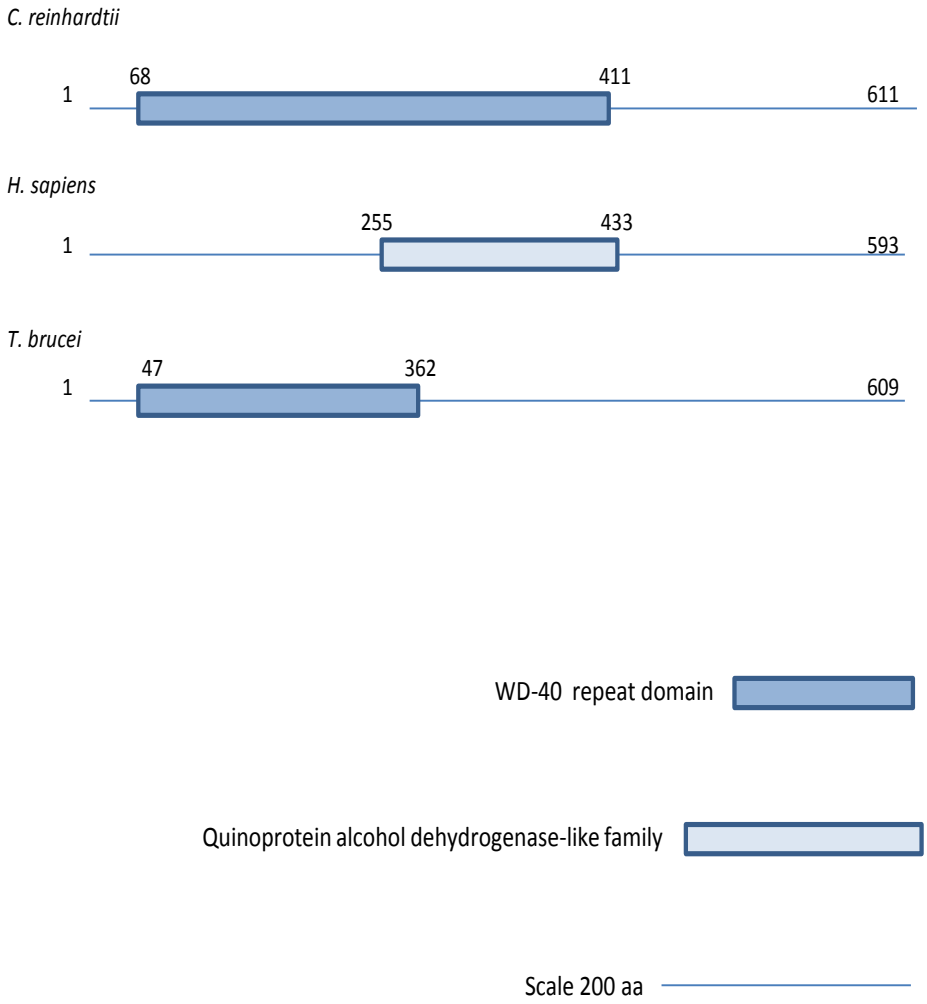

Figure 3.3 **Predicted domain structure of BBS1 in *C. reinhardtii, H. sapiens,* and *T. brucei*.** Diagrams show that BBS1 in *C. reinhardtii* and *T. brucei* contain WD-40 repeat domain near their N-termini, and *H. sapiens* contains Quinoprotein alcohol dehydrogenase-like family in its middle. Both WD-40 repeat domain and Quinoprotein alcohol dehydrogenase form an eight-bladed β-propeller structure. Dark blue box is depicted as WD-40 repeat domain; light blue box is depicted as Quinoprotein alcohol dehydrogenase-like family. The number indicates the residue of amino acid defines the localisation of domain in each organism. The numbers of the first and the last amino acid residues are shown at the left and right end, respectively. The amino acid sequences were scanned by Interpro to identify their domains. Domains of *C. elegans* and *P. tetraurelia* were not identified.

form 4 to 16 repeat units that fold into a four to eight-bladed β-propeller structure (Xu and Min, 2011). This is one of the most abundant protein domains found in eukaryotes (Xu and Min, 2011). Proteins containing WD-40 repeat domains are implicated in a variety of functions ranging from signal transduction, cell cycle control, vesicle trafficking, cytoskeletal assembly, and apoptosis. The proteins possessing WD-40 repeat domains act as platforms for the assembly of protein complexes, or mediate protein-protein interactions. The amino acid sequence of *H. sapiens* was found to contain a Quinoprotein alcohol dehydrogenase-like family in the middle of its sequence, with a position that is partially overlapping with the WD-40 repeat domain in *C. reinhardtii* (Fig. 3.3). Quinoprotein alcohol dehydrogenases are a protein family identified in methylotrophic or autotrophic bacteria, involved in catabolic pathways so that the bacteria grow by producing carbon and energy. Likewise the WD-40 domain, the quinoprotein contains an eight-bladed β-propeller motif (Oubrie et al., 2002). Domains of *P. tetraurelia* and *C. elegans* were not identified.

Evaluation of mutated residues across the species revealed that the level of conservation in residues affected by the missense mutations p.Glu234Lys, p.Met390Arg, and p.Leu518Pro (Mykytyn et al., 2003) is not very high (Fig. 3.1). The residue affected by the nonsense mutation p.Tyr113X showed a low level of conservation, but p.Glu549X and p.Arg440X (Mykytyn et al., 2003) exhibited minimal-conservation except *C. elegans*. The residues affected by the frameshift mutations p.Val114fsX15, p.Tyr284fsX288, and p.Met347fsX373 (Mykytyn et al., 2003) showed a low level of interspecies conservation.

3.1.2 Bioinformatic analysis of BBS2

The *T. brucei* orthologue of BBS2 (Tb927.6.2020) encodes a protein of 736 amino acids, with a predicted molecular weight of 80.1kDa and a predicted isoelectric point of pH 4.8 The amino acid comparison of BBS2 showed that *C. reinhardtii* BBS2 has a much shorter sequence than others (Fig. 3.4). In order to certify whether *C. reinhardtii* BBS2 is conserved, I performed reciprocal BLAST of *H. sapins* BBS2 with *C. reinhardtii* BBS2, which demonstrated 45% identity and 70% similarity

between them. This suggests that even though the length of sequence is truncated, which is possibly due to the evolution, the *C. reinhadtii* BBS2 is still conserved. Furthermore, the BLAST analysis showed that *T. brucei* BBS2 is 32% identical and 52% similar to the *H. sapiens* BBS2 protein, showing their identity and similarity throughout the sequences (Fig 3.5). The domain analysis of each organism revealed that the homologues of *P. tetraurelia, T. brucei*, and *H. Sapiens* BBB2 contain a WD-40 repeat domain near their N-terminal region and the position of WD-40 repeat domain in their sequences is shared between them (Fig. 3.6). *C. elegans* BBS2 contains two C2 domains in its C-terminus. In fact, the C- terminus of the BBS2 amino acid sequence in *C. elegans* shows less similarity with other organisms, which is indicated by large gaps positioned at residue 219 in *C. elegans*, which is within the first C2 domain. The C2 domain is approximately 130 residues long and a large number of proteins contain this domain (Brose et al., 1995). Proteins containing a C2 domain are able to bind to phospholipids, either calcium-dependently or -independently, and play a role in signal transduction or membrane trafficking (Nalefski and Falke, 1996). The finding that *C. elegans* BBS2 contains C2 domain, suggesting the possibility that the function of BBS2 has not evolutionally conserved. The domain of *C. reinhardtii* was not identified.

Evaluation of mutated residues across the species revealed that the residues affected by the missense mutations p.Asp104Ala and p.Gly139Val are highly conserved (Fig. 3.4). In addition, p. Arg315Trp showed its conservation across the species, except for *C. elegans* (Katsanis et al., 2001). However, the residues affected by in p.Val75Gly (Nishimura et al., 2001), p.Thr560Ile, and p.Arg634Pro (Katsanis et al., 2001) revealed their non-conservative substitution. In addition, the residues affected by the nonsense mutations p.Arg275X (Katsanis et al., 2001) and p.R413X (Fauser et al., 2003), and residues altered in the frameshift mutations p.Cys210fsX246 and p.Val158fsX200 (Katsanis et al., 2001) demonstrated their low level of conservation across the

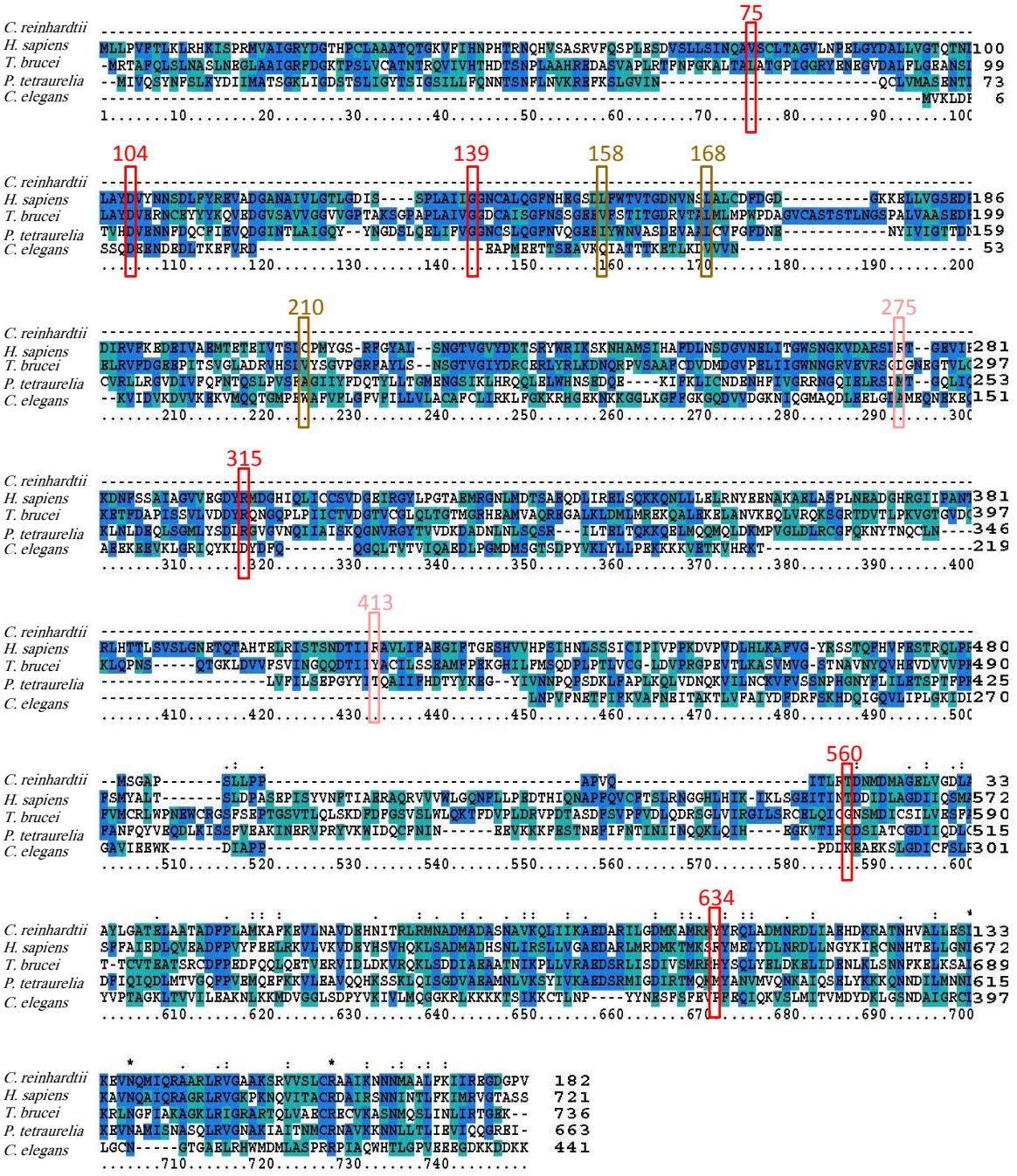

Figure 3.4 **Bioinformatic analysis of *T. brucei* BBS2**. Amino acid sequence alignment of *T. brucei* BBS2 (Tb927.6.2020) with gene of products from *H. sapiens* (OTTHUMP00000080176), *C. reinhardtii* (126758), *P. tetraurelia* (GSPATP00000964001) and *C. elegans* (CE04433). Identical residues are highlighted in blue colour and similar residues are highlighted in light blue colour. Asterisks (*) indicate identical amino acids, while colons (:) and periods (.) represent conserved amino acids. The numbers of amino acid residues are shown on the right and the positions are shown along the bottom. Alignment was generated with clustalx. Amino acid sequence conservation around residues by missense, nonsense, and frameshift mutations identified in BBS patients are also shown. Red squares around residues indicate the positions of the missense mutations: V75G, D104A, G139V, R315W, T560I, and R634P. Pink squares around residues indicate the positions of nonsense mutations: R275X and R413X. Brown squares around residues the positions of frameshift mutations: V158fsX200, L168fsX170, and Y210fsX246.

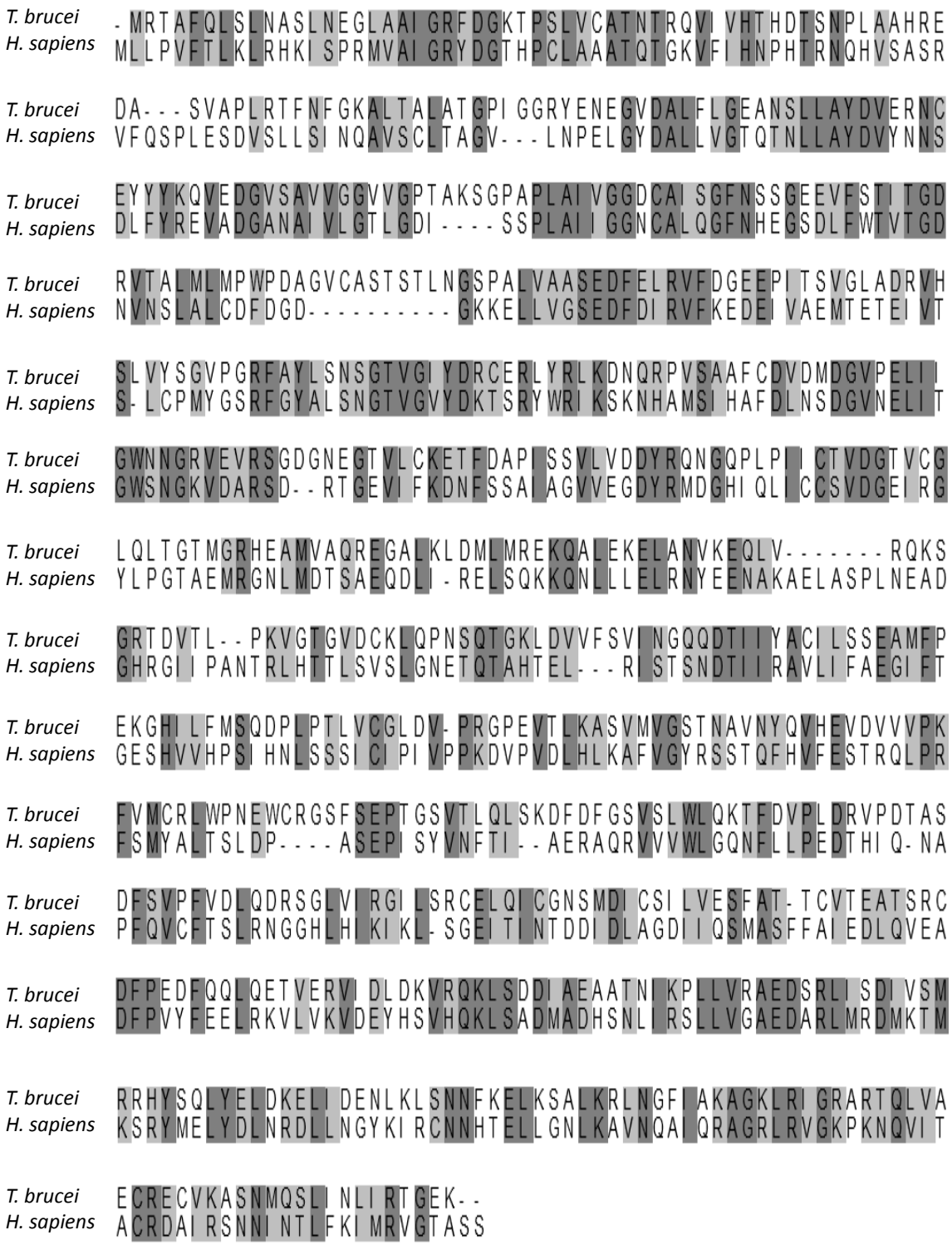

Figure 3.5 **Amino acid sequence alignment of *H. sapiens* and *T. brucei* BBS2.**
The alignment was created in Clustal Omega and is shown with black background when the residues are identical and in gray when they are similar.

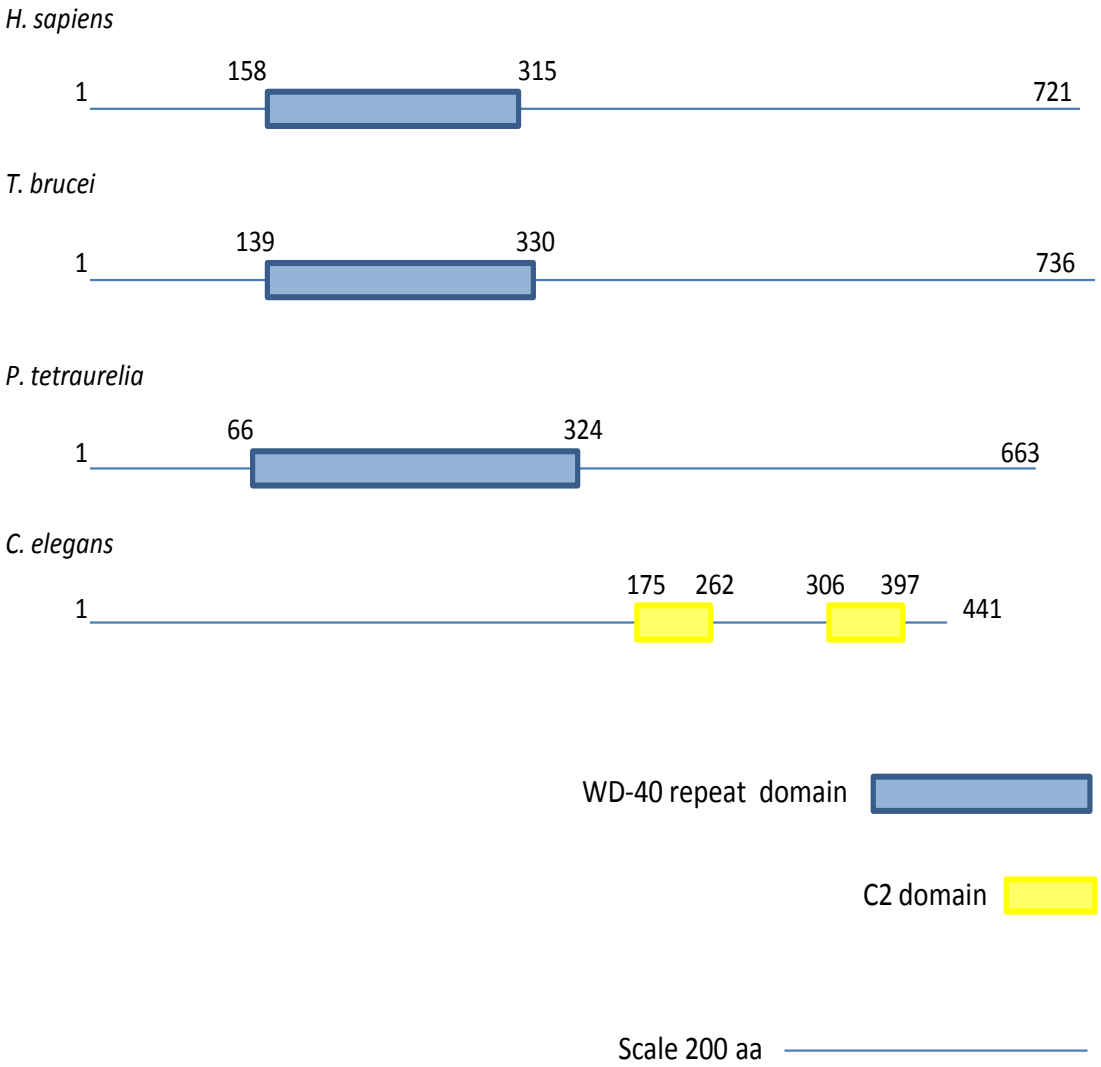

Figure 3.6 **Predicted domain structure of BBS2 in *H. sapiens, T. brucei, P. tetraurelia,* and *C. elegans*.** Diagrams show that BBS2 in *H. sapiens, T. brucei,* and *P. tetraurelia* contain WD-40 repeat domain near their N-termini. *C. elegans* contains C2 domain in its C-terminus. Dark blue box is depicted as WD-40 repeat domain, yellow box is depicted as C2 domain. The number indicates the residue of amino acid defines the localisation of domains in each organism. The numbers of the first and the last amino acid residues are shown at the left and right end, respectively. The amino acid sequences were scanned by Interpro to identify their domains. Domain of *C. reinhardtii* was not identified.

species (Fig. 3.4). The residues affected by the frameshift mutation p.Leu168fsX170 showed interspecies conservation, except in *C. elegans* (Katsanis et al., 2001).

3.1.3 Bioinformatic analysis of BBS4

The *T. brucei* orthologue of BBS4 (Tb927.10.6830) encodes a protein of 466 amino acids, with a predicted molecular weight of 51.8kDa and a predicted isoelectric point of pH 8.95.

Comparison of BBS4 homologous showed their high level of identity and similarity across the organisms. All species show 6 to 20aa gaps in their N-termini and only *H. sapiens* BBS4 shows a non-conservative region in its C-terminus (Fig. 3.7), which is about 90aa long.

In order to compare how well the BBS4 orthologue is conserved between *H. sapiens* and *T. brucei*, BLAST analysis was performed and showed 40% identity and 64% similarity between them, and their alignments showed the homology between the sequences (Fig. 3. 8).

BBS4 amino acid sequences in all organisms were scanned using the Interpro domain database to identify their domains. All organisms contained as many as six to eight tandem tetratricopeptide repeats (TPR) and their entire sequences were consisted of TPR flanked by small N and C-terminal regions (Fig. 3.9). This is consistent with the finding that the most conserved region across the organisms does not include amino acid sequences positioned between 1 and 80 residues in the N-termini and between 430 and 560 in the C-termini. TPR are composed of degenerated stretches of 34 amino acids that fold into helix-turn-helix structures and often occur as single or multiple triplet arrays. The proteins possessing TPRs mediate protein-protein interactions by cradling a specific linear peptide sequence (D'Andrea and Regan, 2003). Evaluation of mutated residues across the species revealed that the residue affected by the missense mutation p.Ala364Glu (Katsanis et al., 2002) is conserved across the species, except in *P. tetraurelia* (Fig. 3.7). The residues affected in the mutations p.Asn165His, p.Arg295Pro, and p.Leu327Pro (Katsanis et al., 2002) showed their non-conservative substitution (Fig. 3.7).

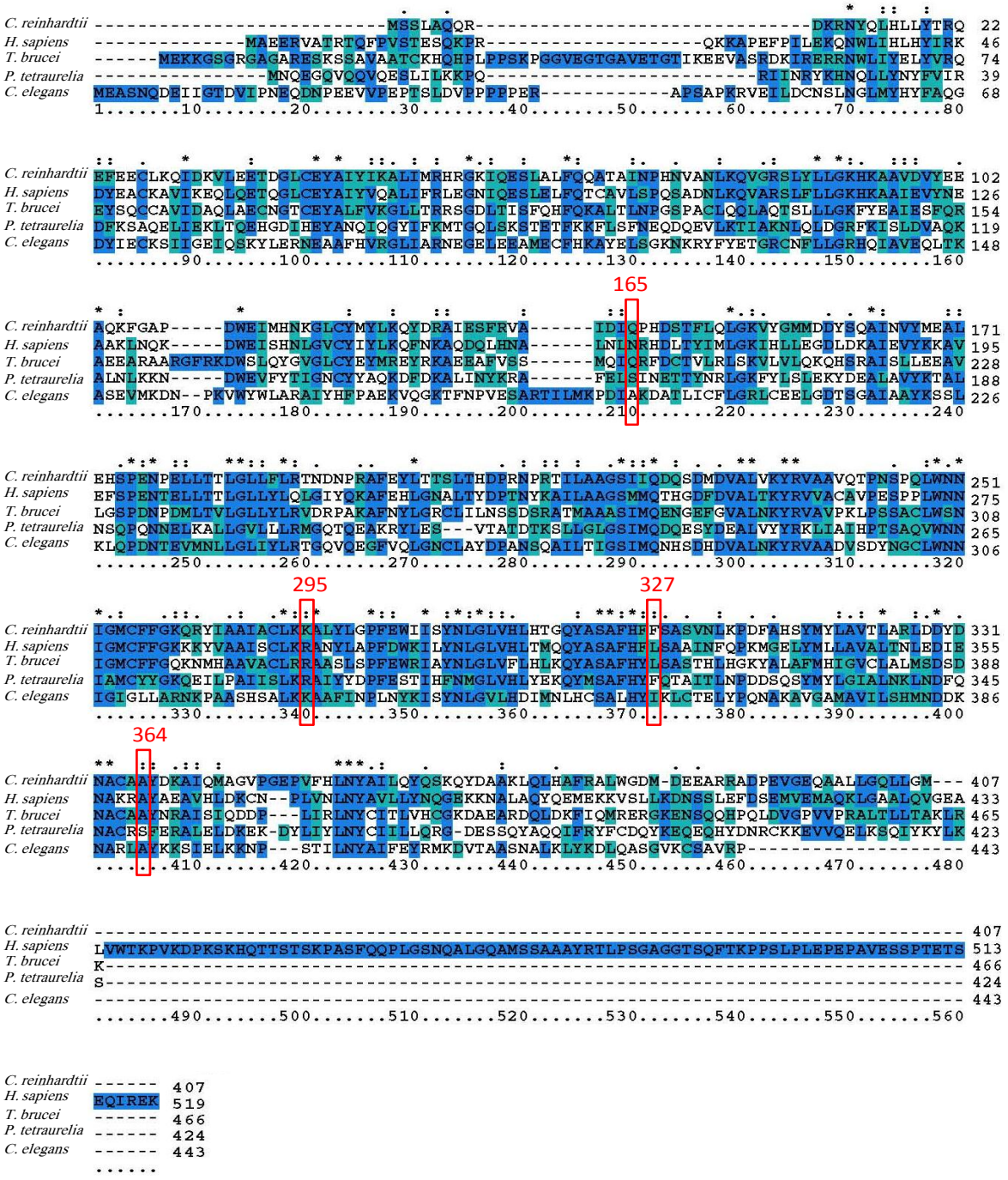

Figure 3.7 **Bioinformatic analysis of *T. brucei* BBS4**. Amino acid sequence alignment of *T. brucei* BBS4 (Tb927.10.6830) with gene of products from *H. sapiens* (OTTHUMP00000175949), *C. reinhardtii* (129948), *P. tetraurelia* (GSPATP00005292001), and *C. elegans* (CE37774). Identical residues are highlighted in blue colour and similar residues are highlighted in light blue colour. Asterisks (*) indicate identical amino acids, while colons (:) and periods (.) represent conserved amino acids. The numbers of amino acid residues are shown on the right and the positions are shown on the bottom. Alignment was generated with clustalx. Amino acid sequence conservation around residues by missense mutation identified in BBS patients was are also shown. Red squares around residues indicate the positions of the missense mutations: A364E, R295P, N165H, and L327P.

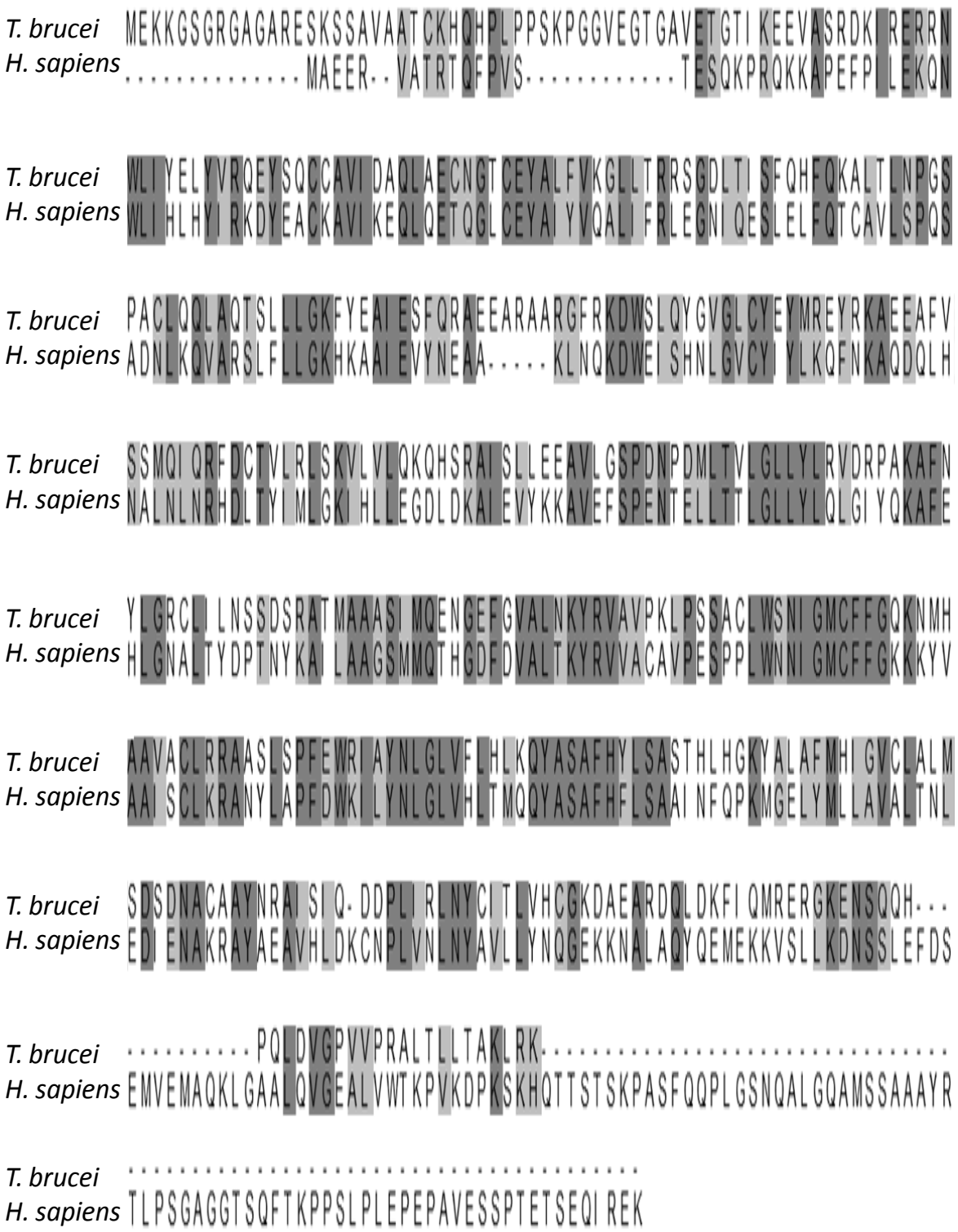

Figure 3.8 **Amino acid sequence alignment of *H. sapiens* and *T. brucei* BBS4.**
The alignment was created in Clustal Omega and is shown with black background when the residues are identical and in gray when they are similar.

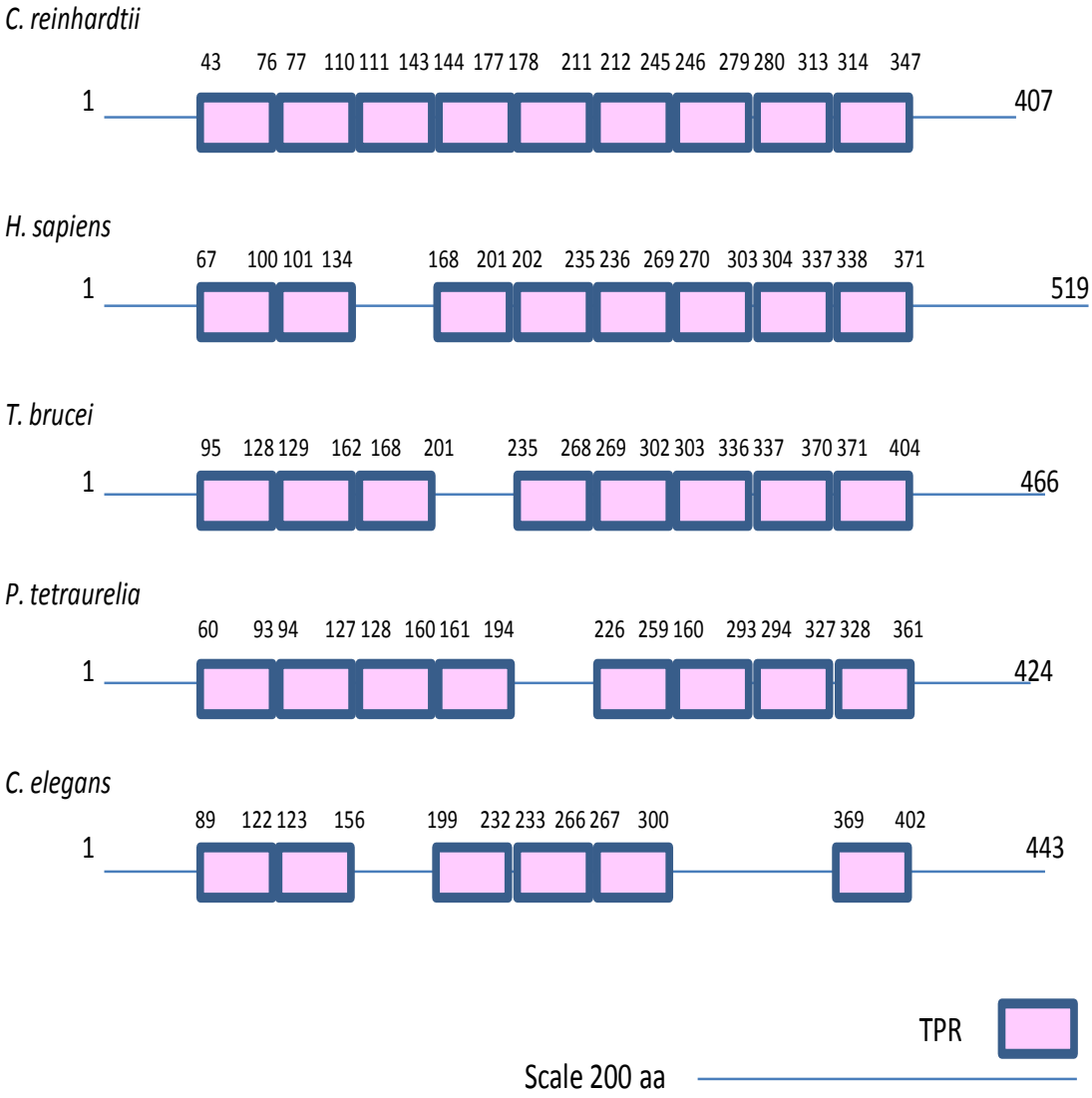

Figure 3.9 **Predicted domain structure of BBS4 in *C. reinhardtii*, *H. sapiens*, *T. brucei*, *P. tetraurelia*, and *C. elegans*.** Diagrams show that BBS4 in all organisms given above are consists of multiple tetratricopeptide repeat (TPR) flanked by small N and C-terminal regions. The number indicates the residue of amino acid sequences defines the localisation of TPR in each organism. TPR repeat is depicted as a pink box. The number indicates the residue of amino acid defines the localisation of domains in each organism. The numbers of the first and the last amino acid residues are shown at the left and right end, respectively. The amino acid sequences were scanned by Interpro to identify their domains.

3.1.4 Bioinformatic analysis of BBS5

The *T. brucei* orthologue of BBS5 (Tb927.1.4140) encodes a protein of 369 amino acids, with a predicted molecular weight of 41.0kDa and a predicted isoelectric point of pH 7.59.

BBS5 is widely conserved across the organisms stated above, and the amino acid comparison of BBS5 showed a relatively high level of identity and similarity throughout the sequences (Fig. 3.10). In addition, the BLAST analysis showed that *T. brucei* BBS5 is 40% identical and 61% similar to the predicted *H. sapiens* BBS5, likewise, the amino acid sequences alignment exhibited their homology (Fig. 3.11)

Analysis of the protein domain architecture showed that all organisms of BBS5 amino acid sequences possess DUF1448, the domain annotated with “Domain of unknown function”. (Fig. 3.12). DUF1448 family consists of several eukaryotic proteins of approximately 375 residues in length, and DUF1448 is included in the PH domain family. The PH domain consists of seven β-strands forming two antiparallel, terminating β-sheets, followed by an amphipathic alpha-helix (Timm et al., 1994). The PH domain can be found in various intracellular proteins with multiple functions, such as in intracellular signalling or cytoskeleton formation (Mayer et al., 1993). Notably, the PH domain has an ability to bind to phosphatidylinositol within biological membranes and directing proteins to different membranes.

The evaluation of mutated residues revealed that they are highly conserved across the species (Fig. 3.10). The residues affected by the missense mutations p.Gly72Ser (Hjortshoj et al., 2008) and p.Asn184Ser (An et al., 2004), and the residue affected by the nonsense mutation p.Trp59X (An et al., 2004) are significantly well conserved across species, suggesting that these residues have been critical for sustaining the BBS5 function. The residue affected by the missense mutation p.Leu50Arg (Chen et al., 2011) is conserved across all species, except for *C. elegans,* and p.Thr183Ala (Hjortshoj et al., 2008) is conserved across the species except for *C. reinhardtii.* The missense mutation p.Arg207His (An et al., 2004) and nonsense mutation p. Leu142X

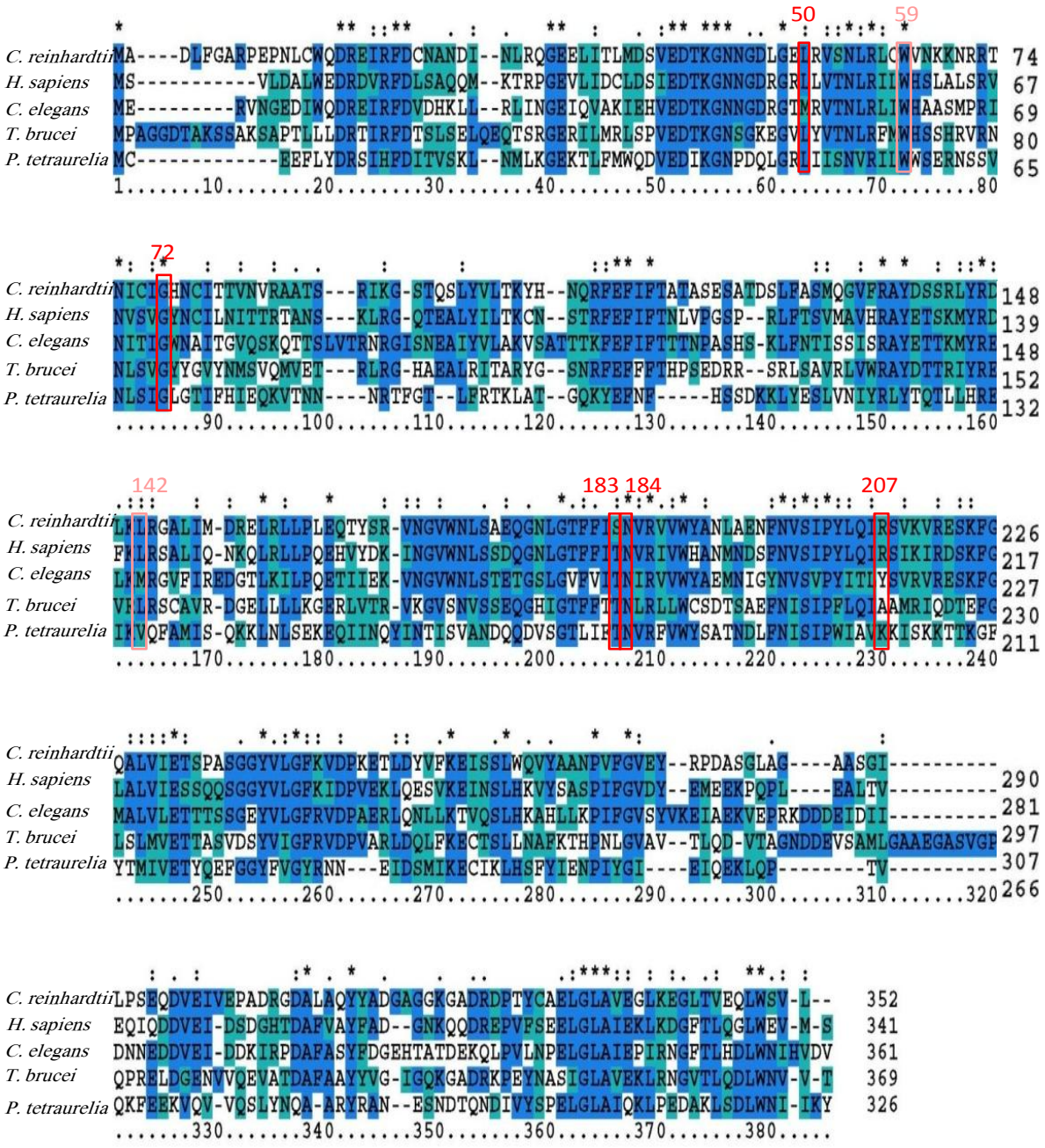

Figure 3.10 **Bioinformatic analysis of *T. brucei* BBS5**. Amino acid sequence alignment of *T. brucei* BBS5 (Tb927.1.4140) with gene of products from *H. sapiens* (OTTHUMP0000016362), *C. reinhardtii* (129948), *P. tetraurelia* (GSPATP00036912001), and *C. elegans* (CE01042). Identical residues are highlighted in blue colour and similar residues are highlighted in light blue colour. Asterisks (*) indicate identical amino acids, while colons (:) and periods (.) represent conserved amino acids. The numbers of amino acid residues are shown on the right and the positions are shown on the bottom. Alignment was generated with clustalx. Amino acid sequence conservation around residues by missense and nonsense mutations identified in BBS patients are also shown. Red squares around residues indicate the positions of the missense mutations: L50R, G72S, T183A, N184S, and R207H. Pink squares around residues indicate the positions of nonsense mutations: W59X and L142X.

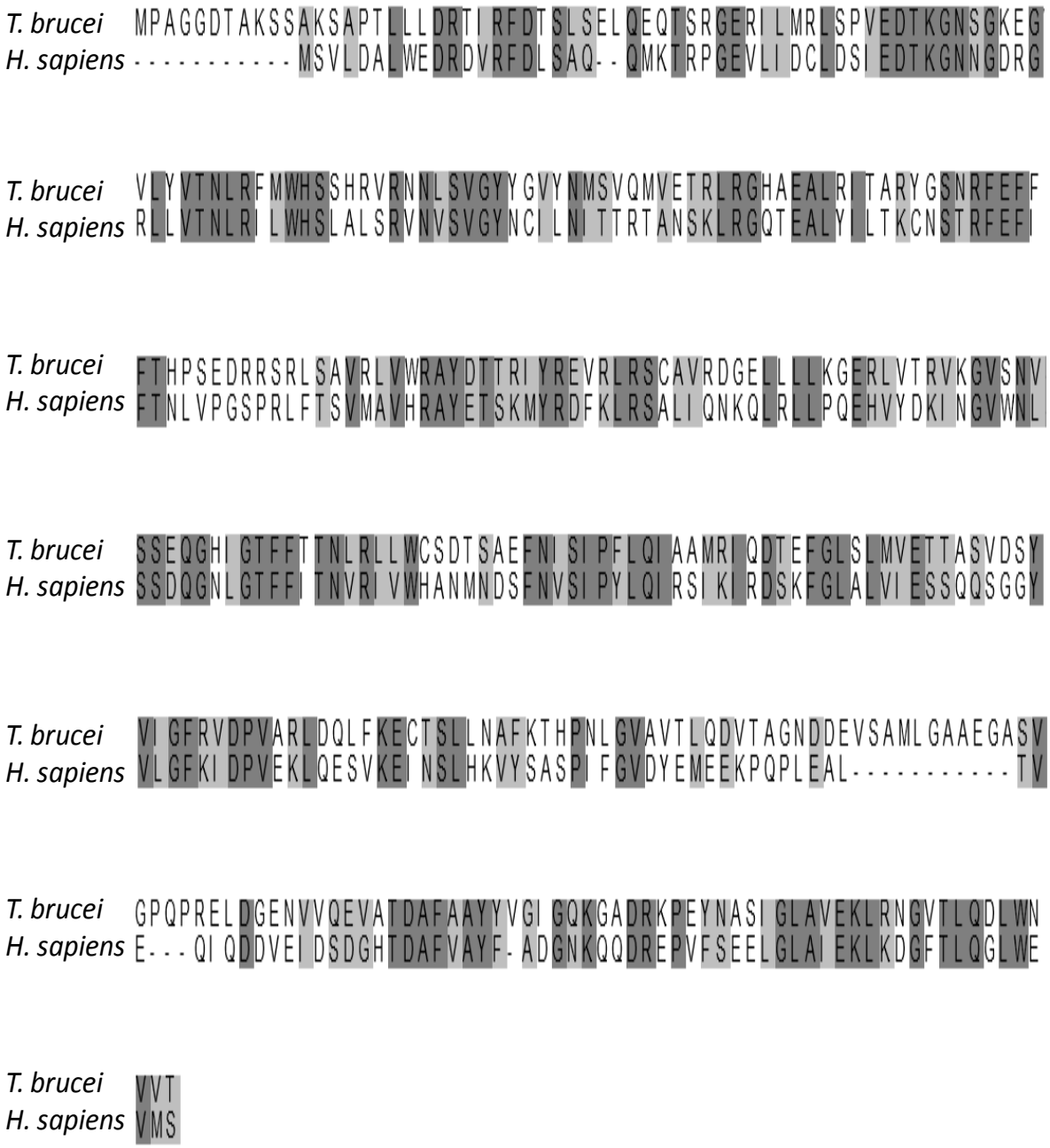

Figure 3.11 **Amino acid sequence alignment of *H. sapiens* and *T. brucei* BBS5.**
The alignment was created in Clustal Omega and is shown with black background when the residues are identical and in gray when they are similar.

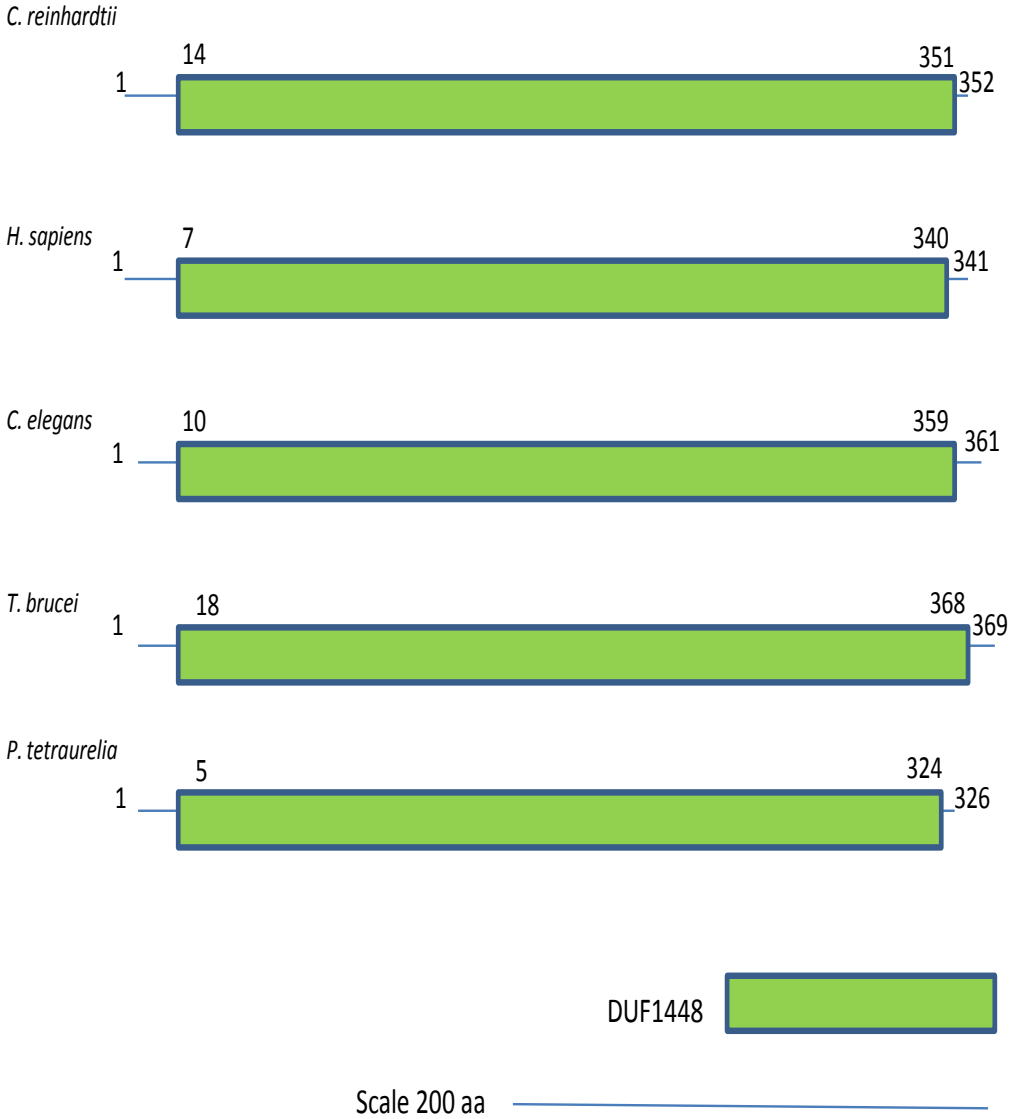

Figure 3.12 **Predicted domain structure of BBS5 in *C. reinhardtii, H. sapiens, C. elegans, T. brucei,* and *P. tetraurelia*.** Diagrams show that BBS5 in all organisms given above contain DUF1448. DUF1448 is annotated with the protein of unknown function, but belongs to a PH-domain family. The number indicates the residue of amino acid defines the localisation of DUF1448 in each organism. The numbers of the first and the last amino acid residues are shown at the left and right end, respectively. The amino acid sequences were scanned by Interpro to identify their domains.

(Hjortshoj et al., 2008) showed their non-conservative substitution. The mutation of highly conserved residues might affect the structure of the BBS5 protein. Consequently, it resulted in prohibitting the association of BBS5 with lipids, which might have caused diseases in the species used in this study.

3.1.5 Bioinformatic analysis of BBS7

The *T. brucei* orthologue of BBS7 is encoded by Tb927.3.3640. It encodes a protein of 751 amino acids with a predicted molecular weight of 82.5kDa and a predicted isoelectric point of pH 4.99.

Amino acid comparison of each organism showed that BBS7 is widely conserved across organisms and shows high identity and similarity throughout the sequences (Fig. 3.13). The amino acid comparison of BBS7 between *H. sapiens* and *T. brucei* showed that they have homology to each other, and the BLAST analysis identified their identities and similarities of 21% and 45%, respectively (Fig. 3.14). Amino acid sequence alignment also showed several short lengths of insertions or gaps in the sequences.

To investigate the domain structure of *T. brucei* BBS7, I scanned the protein sequence using the Interpro protein domain database. *H. sapiens, P. tetraurelia, C. reinhardtii,* and *T. brucei* contain WD-40 repeat domains close to the N-termini and *C. elegans* has two Quinoprotein alcohol dehydrogenase-like families near its N-terminus, showing that the distribution pattern of their domains within the sequence is similar (Fig. 3.15).

Evaluation of mutated residues revealed that the residues affected by the missense mutations p.Lys211Ile and p.His323Arg, and the frameshift mutation p.Lys237fsX60, are not conserved across species (Fig. 3.13).

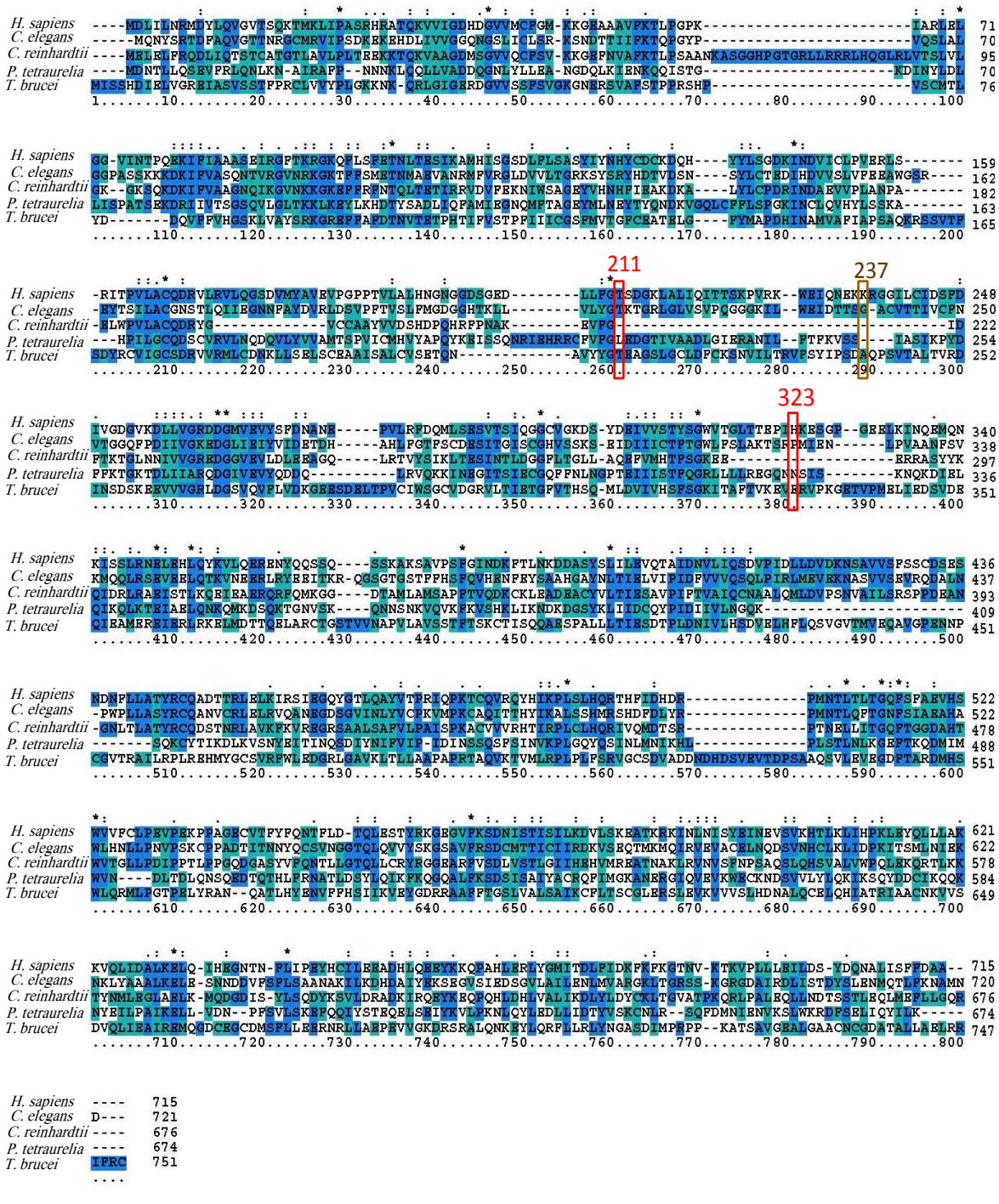

Figure 3.13 **Bioinformatic analysis of *T. brucei* BBS7.** Amino acid sequence alignment of *T. brucei* BBS7 (Tb927.3.3640) with gene of products from *H. sapiens* (NP_060660.2), *C. reinhardtii* (190054), *P. tetraurelia* (GSPATP00026091001), and *C. elegans* (CE23024). Identical residues are highlighted in blue colour and similar residues are highlighted in light blue colour. Asterisks (*) indicate identical amino acids, while colons (:) and periods (.) represent conserved amino acids. The numbers of amino acid residues are shown on the right and the positions are shown on the bottom. Alignment was generated with clustalx. Amino acid sequence conservation around residues by missense and frameshift mutations identified in BBS patients are also shown. Red squares around residues indicate the positions of the missense mutations: T211I and H323R. Brown squares around residues the positions of frameshift mutations: K237fsX60.

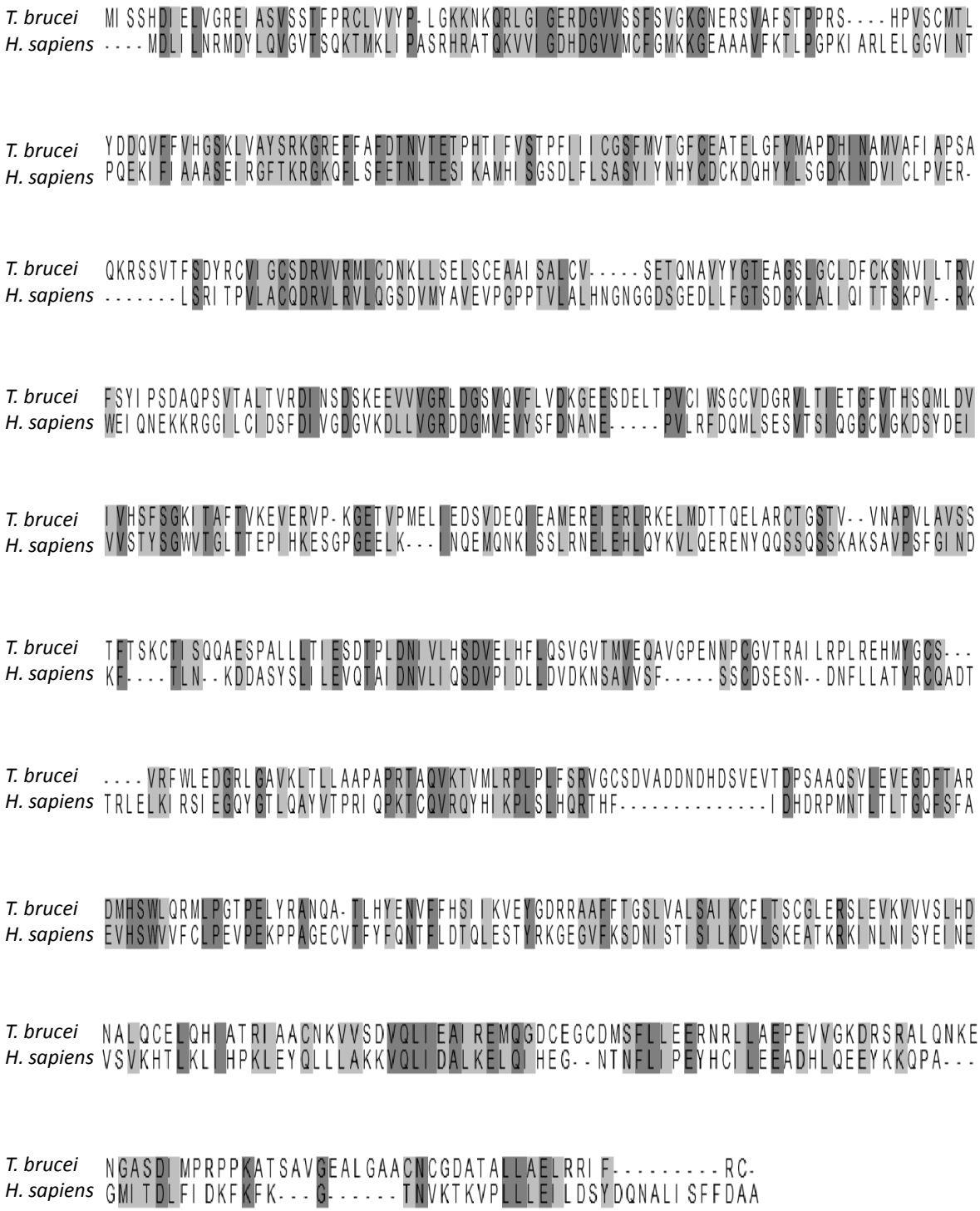

Figure 3.14 **Amino acid sequence alignment of *H. sapiens* and *T. brucei* BBS7.**
The alignment was created in Clustal Omega and is shown with black background when the residues are identical and in gray when they are similar.

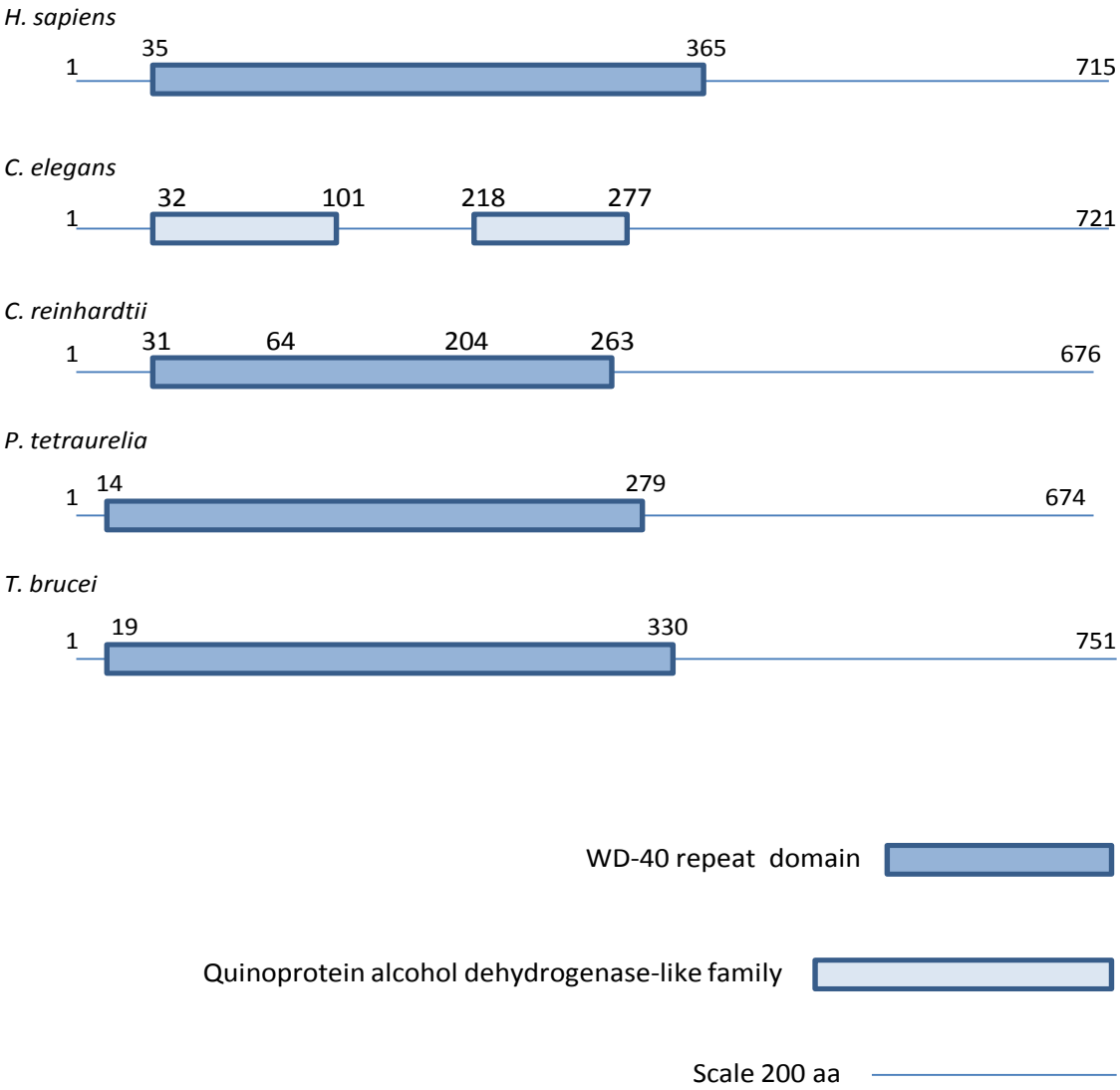

Figure 3.15 **Predicted domain structure of BBS7 in *H. sapiens, C. elegans, C. reinhardtii, P. tetraurelia,* and *T. brucei.*** Diagrams show that BBS7 in *H. sapiens, P. tetraurelia, C. reinhardtii,* and *T. brucei* contain WD-40 repeat domain near their N-termini *C. elegans* has two Quinoprotein alcohol dehydrogenase-like family near its N-terminus. Both WD-40 repeat domain and Quinoprotein alcohol dehydrogenase from an eight-bladed β-propeller structure. Dark blue box is depicted as WD-40repeat domain, light blue box is depicted as Quinoprotein alcohol dehydrogenase-like family. The number indicates the residue of amino acid defines the localisation of domains in each organism. The numbers of the first and the last amino acid residues are shown at the left and right end, respectively. The amino acid sequences were scanned by Interpro to identify their domains.

3.1.6 Bioinformatic analysis of BBS8

The *T. brucei* orthologue of BBS8 (Tb11.01.4290) encodes a protein of 568 amino acids with a predicted molecular weight of 62.6kDa and a predicted isoelectric point of pH 6.56.

The amino acid sequence comparison of BBS8 with the organisms given above showed that the whole amino acid sequences are relatively identical and similar to each other; however, the highest level of homology was seen in the C-termini compare to N-termini (Fig. 3.16).

Comparison of BBS8 in *T. brucei* and *H. sapiens* showed that they are 37% identical and 58% similar to each other; likewise, the amino acid sequence comparison demonstrated their sequence similarity (Fig. 3.17). The remarkable inserts seen in the amino acid sequence alignment of *T. brucei* involve the amino acid residues from 78 to 92 and 98 to 104, with *H. sapiens* showing an insertion between residues 197 and 222. The high level of identity and similarity between the amino acid sequences at the C-terminal region support the identified domains of each organism, that all BBS8 proteins contain six to seven TPR towards their C- terminal regions (Fig. 3.18).

The evaluation of mutated residues revealed that the residue affected by the missense mutation p.Phe337Leu (Chen et al., 2011) is conserved across the species, except for *C. elegans* (Fig. 3.16). Moreover, the position of Phe337 in *H. sapiens* lies in the predicted 5th TPR repeat, which is also conserved across the species, since all other species also contain TPR in that region (Fig. 3.18). This suggests that Phe337 is an essential residue and that the alteration of this residue might cause the phenotype. However, the residues affected by the missense mutations p.Lys95Arg and p.Met135Ile (Chen et al., 2011) showed a low level of evolutionary conservation.

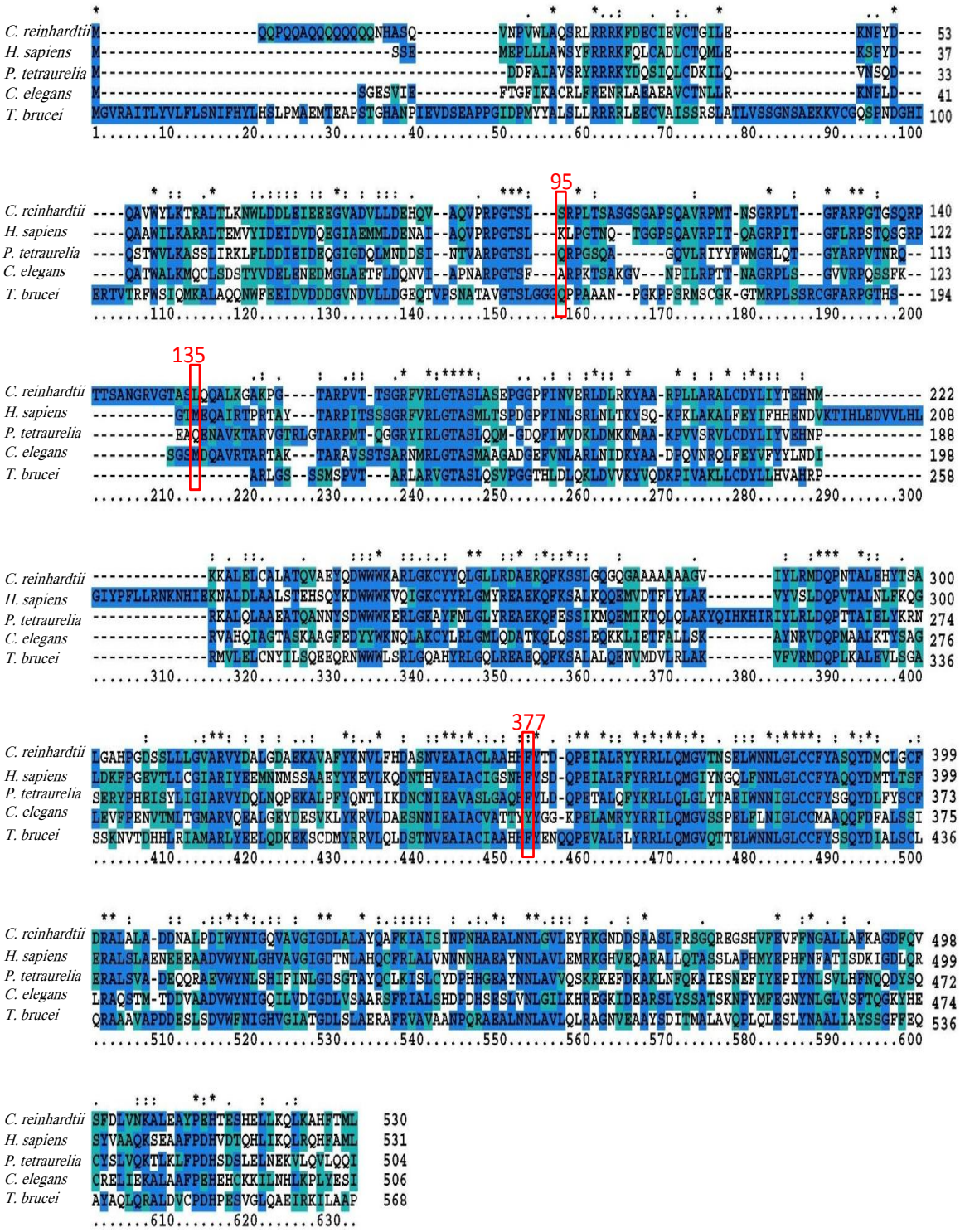

Figure 3.16 **Bioinformatic analysis of *T. brucei* BBS8**. Amino acid sequence alignment of *T. brucei* BBS8 (Tb11.01.4290) with gene of products from *H. sapiens* (OTTHUMP00000028245), *C. reinhardtii* (140113), *P. tetraurelia* (GSPATP00028481001), and *C. elegans* (CE31071). Identical residues are highlighted in blue colour and similar residues are highlighted in light blue colour. Asterisks (*) indicate identical amino acids, while colons (:) and periods (.) represent conserved amino acids. The numbers of amino acid residues are shown on the right and the positions are shown on the bottom. Alignment was generated with clustalx. Amino acid sequence conservation around residues by missense mutations identified in BBS patients is also shown. Red squares around residues indicate the positions of the missense mutations: K95R, M135I, and F337L.

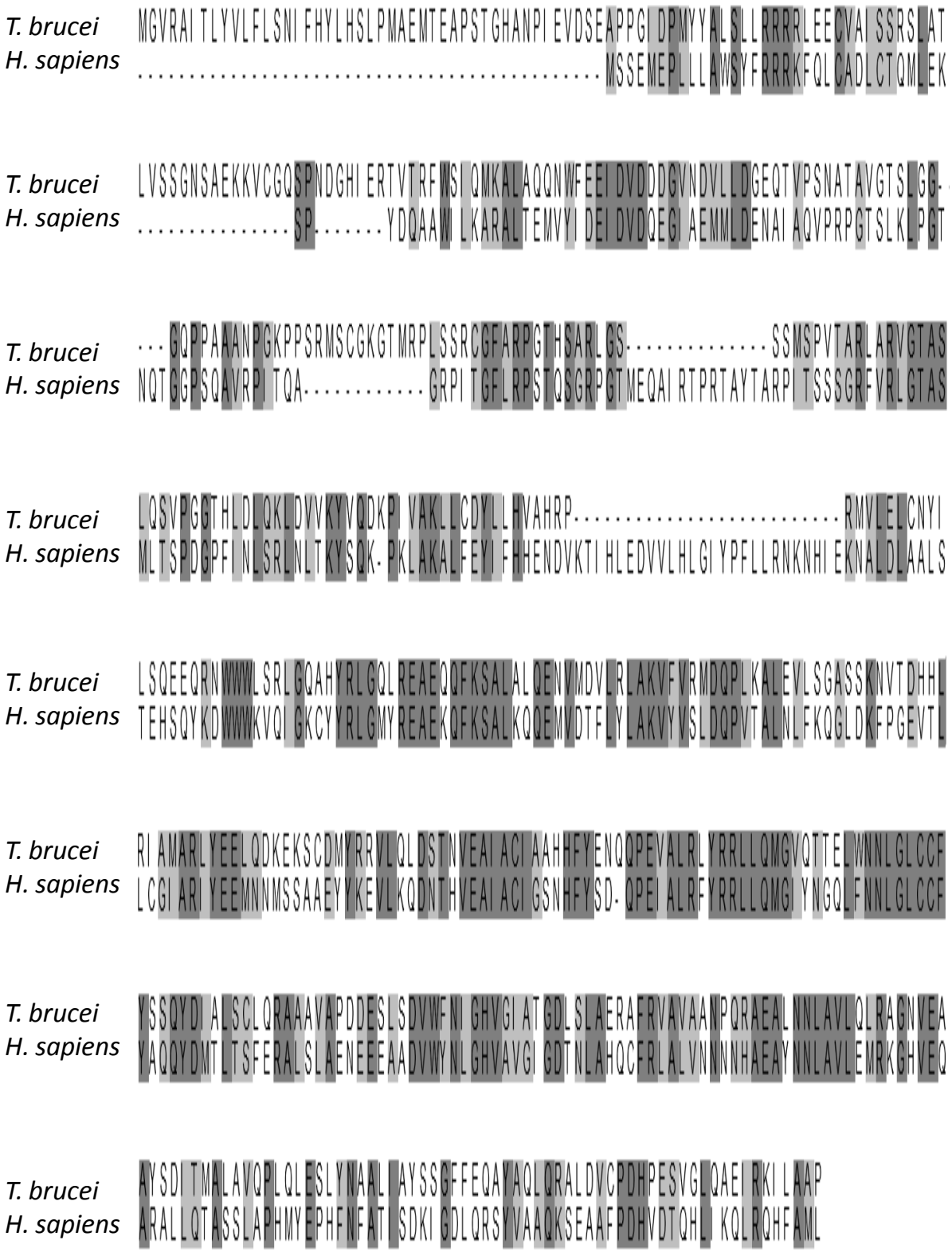

Figure 3.17 **Amino acid sequence alignment of *H. sapiens* and *T. brucei* BBS8.**
The alignment was created in Clustal Omega and is shown with black background when the residues are identical and in gray when they are similar.

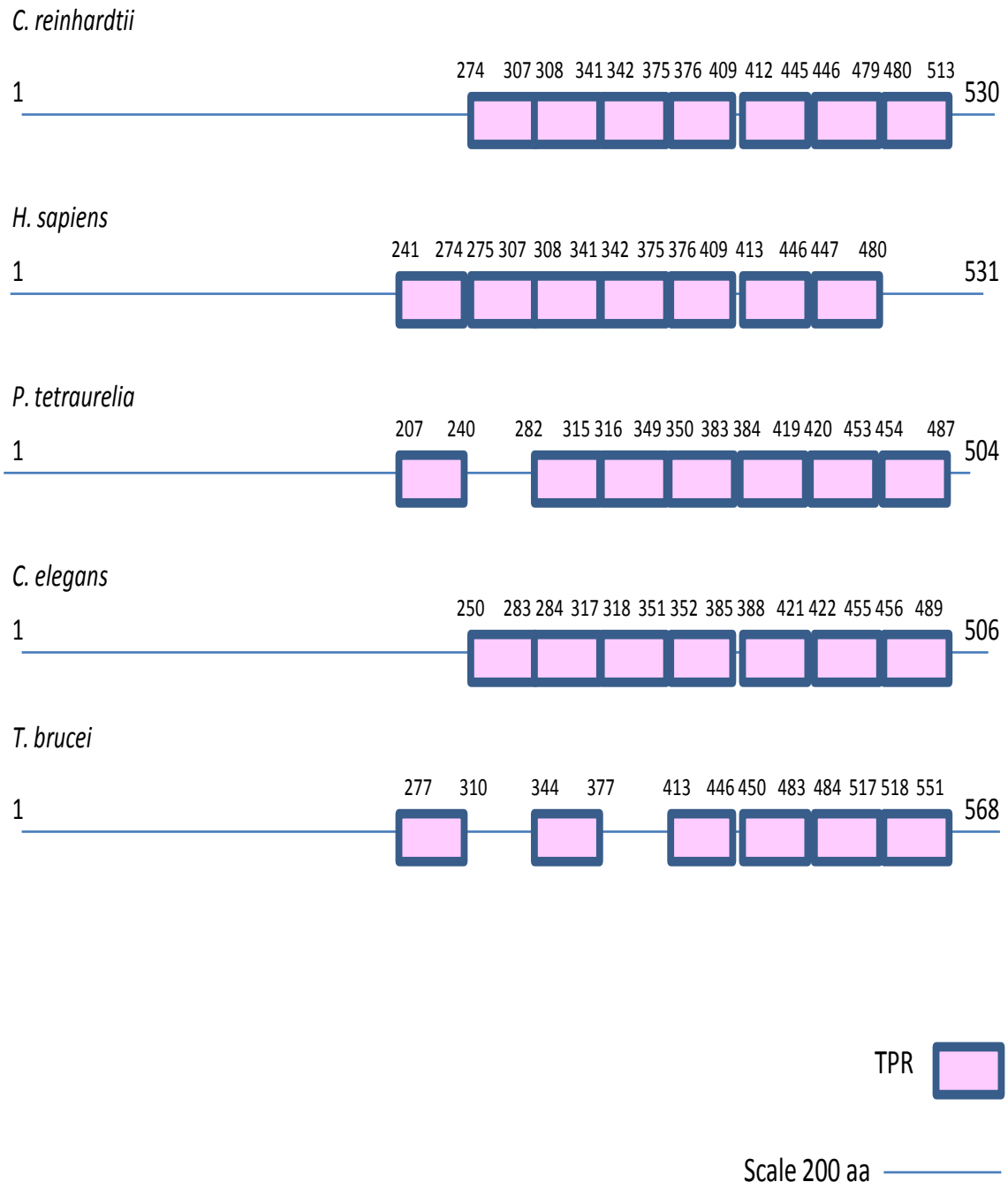

Figure 3.18 **Predicted domain structure of BBS8 in *C. reinhardtii, H. sapiens, P. tetraurelia, C. elegans,* and *T. brucei.*** Diagrams show that BBS8 in all organisms given above contain multiple tetratricopeptide repeat (TPR) in their C terminal regions. TPR repeat is depicted as a pink box. The number indicates the residue of amino acid defines the localisation of TPR in each organism.The numbers of the first and the last amino acid residues are shown at the left and right end, respectively. The amino acid sequences were scanned by Interpro to identify their domains.

3.1.7 Bioinformatic analysis of BBS9

The *T. brucei* orthologue of BBS9 is encoded by Tb11.01.6070. It encodes a protein of 836 amino acids with a predicted molecular weight of 92.3kDa and a predicted isoelectric point of pH 5.39. The amino acid sequence comparison of BBS9 showed the most sequence identities and similarities in the N-terminal region; however, the sequence of *C. reinhardtii* is very short compare to others (Fig. 3.19). The reciprocal BLAST of *H. sapiens* BBS9 with *C. reinhardtii* showed that they are 36% identical and 46% similar. This suggests that *C. reinhardtii* BBS9 has still an evolutionary relationship between *H. sapiens*, yet its C-terminus has truncated through the evolution. Furthermore, the BLAST analysis showed that *H. sapiens* BBS9 is 32% identical to *T. brucei* BBS9 and the similarity is 49%, also the alighnment of both amino acid sequences demontrated their similalities (Fig. 3.20). The domain was identified only in *P. tetraurelia* and *C. elegans,* demonstrating that they have a WD-40 repeat domain in their N-termini, which shows the most conservation (Fig. 3.21).

The evaluation of mutated residues revealed that the residue affected by the missense mutation p.Gly141Arg is conserved across the species, except for *C. elegans* (Fig. 3.19). The residue affected by the nonsense mutation p.Arg598X is highly conserved across the species, suggesting that the mutation was evolutionally conserved. However, the residues affected by p.Gln132His and p.Gln355X showed a low level of inter-species conservation (Fig. 3.19).

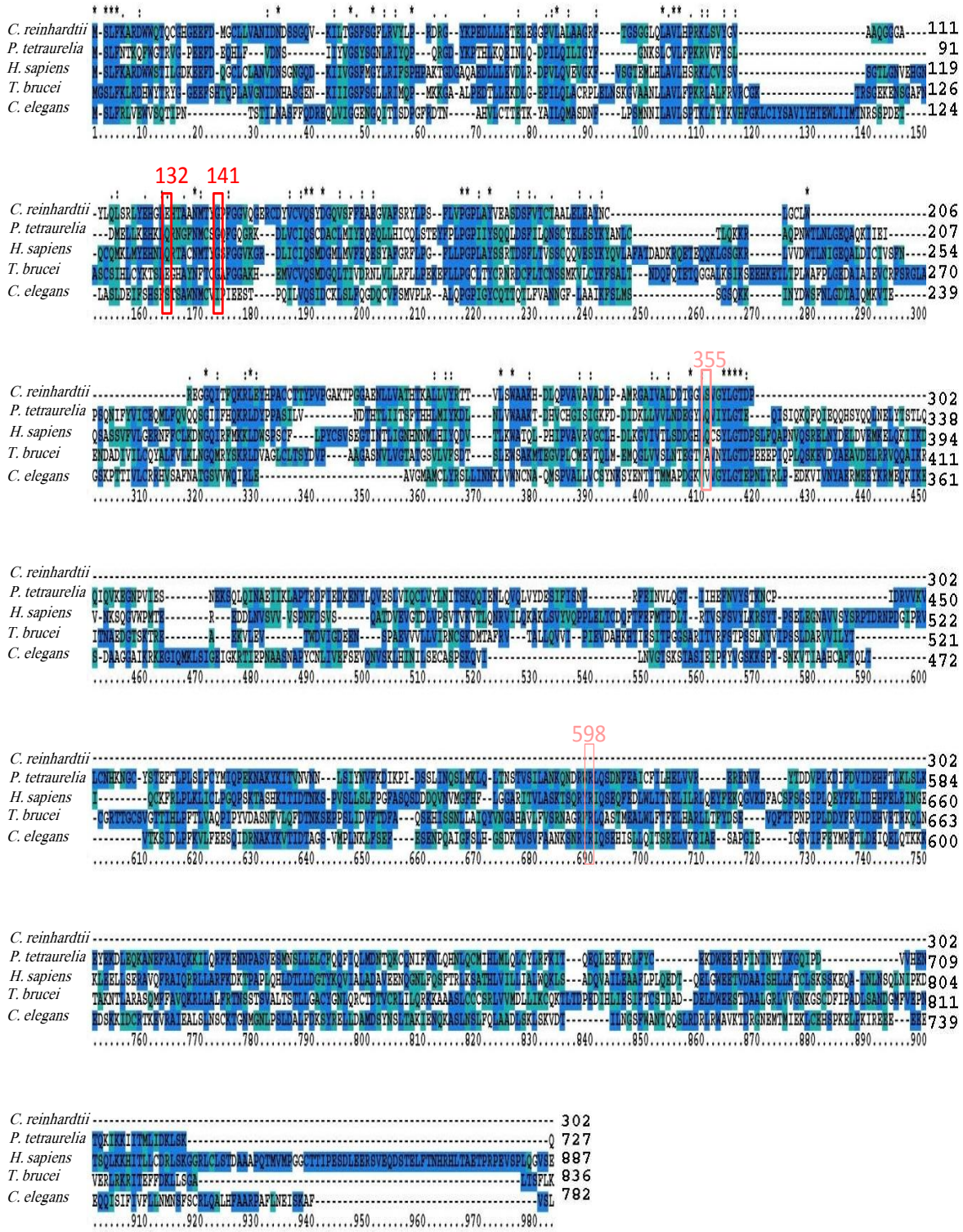

Figure 3.19 **Bioinformatic analysis of BBS9.** Amino acid sequence alignment of *T. brucei* BBS9 (Tb11.01.6070) with gene of products from *H. sapiens* (NP_940820.1), *C. reinhardtii* (101137), *P. tetraurelia* (GSPATP00027545001), and *C. elegans* (CE32166). Identical residues are highlighted in blue colour and similar residues are highlighted in light blue colour. Asterisks (*) indicate identical amino acids, while colons (:) and periods (.) represent conserved amino acids. The numbers of amino acid residues are shown on the right and the positions are shown on the bottom. Alignment was generated with clustalx. Amino acid sequence conservation around residues by missense and nonsense mutations identified in BBS patients is also shown. Red squares around residues indicate the positions of the missense mutations: Q132H and G141R. Pink squares around residues indicate the positions of nonsense mutations: Q355X and R598X.

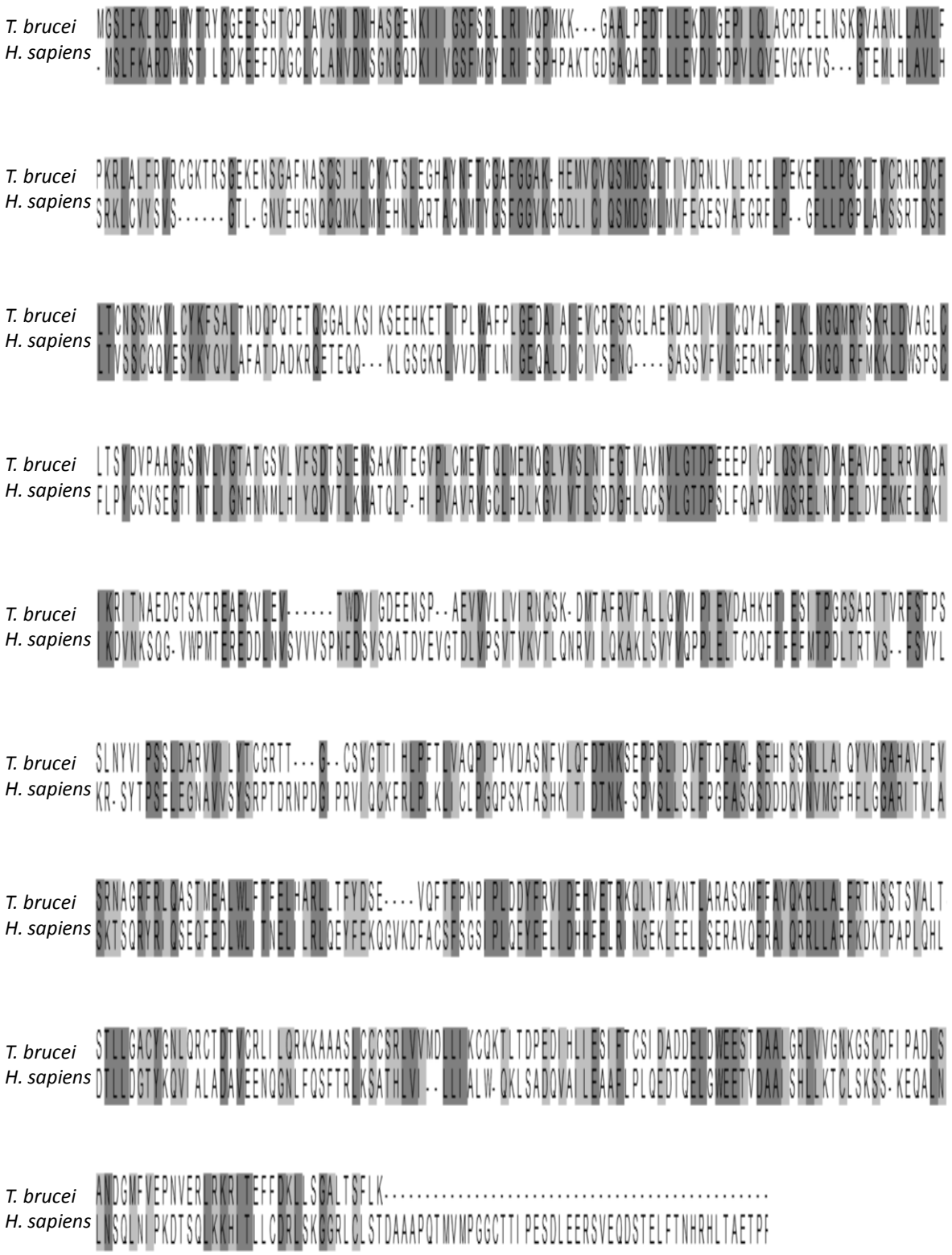

Figure 3.20 **Amino acid sequence alignment of *H. sapiens* and *T. brucei* BBS9.**
The alignment was created in Clustal Omega and is shown with black background when the residues are identical and in gray when they are similar.

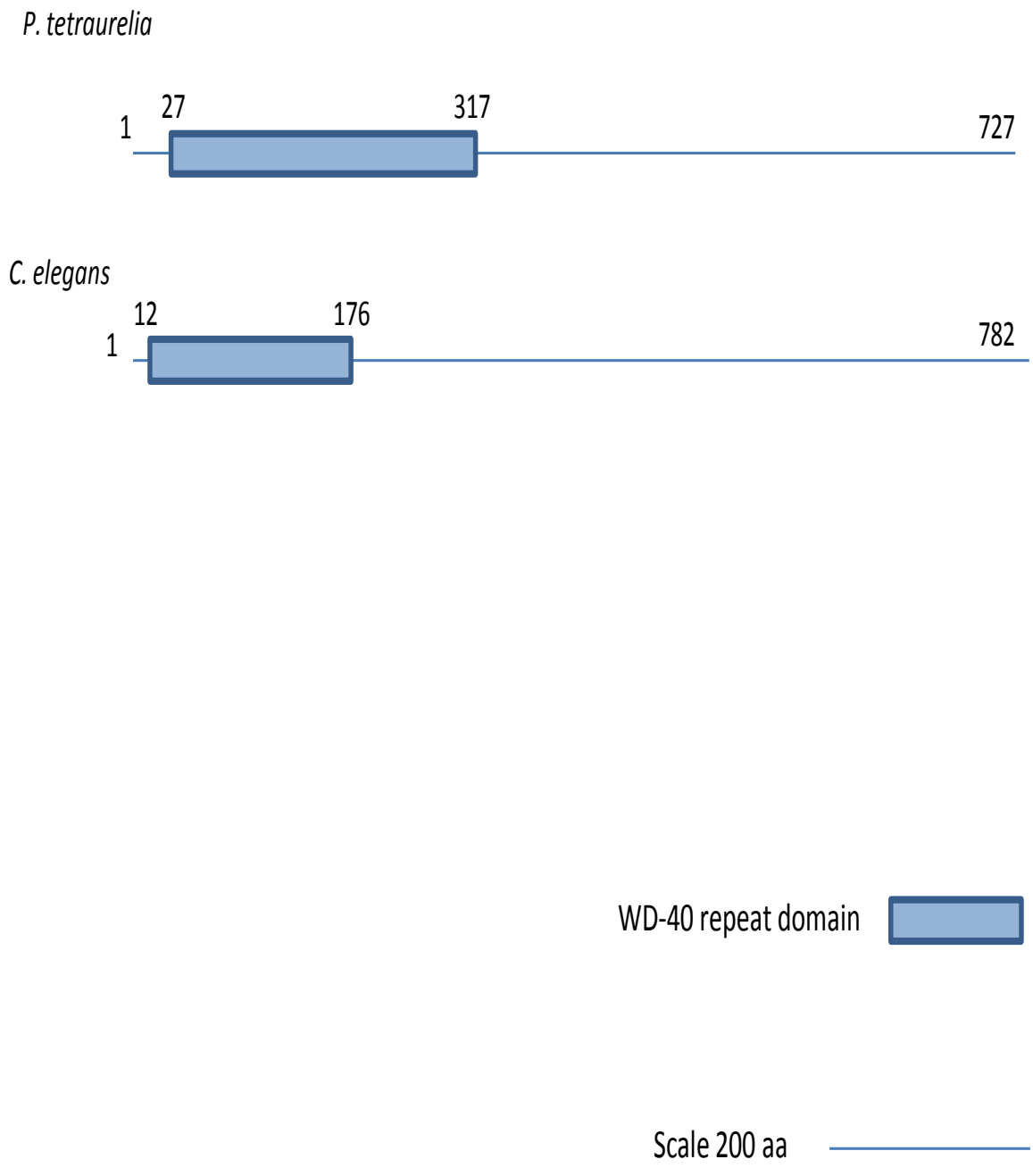

Figure 3.21 **Predicted domain structure of BBS9 in *P. tetraurelia* and *C. elegans*.** Diagrams show that BBS9 in *P. tetraurelia* and *C. elegans* contain WD-40 repeat domain near their N-termini. Dark blue box is depicted as WD-40 repeat domain.The number indicates the residue of amino acid defines the localisation of domains in each organism. The numbers of the first and the last amino acid residues are shown at the left and right end, respectively. The amino acid sequences were scanned by Interpro to identify their domains. The domain of *H. sapiens, C. reinhardtii,* and *T. brucei* were not identified.

In summary, this bioinformatic analysis of individual BBSome subunits demonstrated that ciliated eukaryotes have homologous sequences for BBSome components, which supports the finding that BBSome has a specific function in ciliary function (Hodges et al., 2010). Furthermore, even lower single-cell ciliated organism, *T. brucei* has highly homologous sequences to BBSome proteins. The BLAST analysis and amino acid sequence alighnment confirmed that human BBSome proteins are all conserved in *T. brucei.* The bioinformatics results support the hypothesis that BBSome is required for ciliary function, which possibly includes sensory functions, since the conservation was observed in *C. elegans*, as well. However, in terms of *C. elegans* BBS2, it may possess a different function from other *C. elegans* BBSome components, as only the *C. elegans* BBS2 contained C2 domain. Even though I selected the amino acid sequences of BBSome components in *C. elegans* with the aim of predicting BBSome involvement in sensory function, this finding may imply in different way. Possibly, *C. elegans* BBS2 has a role in ciliary biogenesis, or having both functions in ciliary sensory and structure, which suggests that *C. elegans* BBS2 may not has a shared function with other BBSome subunits.

Domain analysis of each organism demonstrated that most organisms of BBS1, BBS2, BBS7, and BBS9 proteins share WD-40 repeat domains which are folded into a β-propeller structure in their N-termini, except for *C. elegans* BBS2. Moreover, the domain identified in BBS1, BBS2, BBS7, and BBS9 were seen in their N-terminal regions, suggesting that function of these proteins may similar to each other. Among the orthologues of BBSome proteins in ciliated organisms used in this test, *H. sapiens* BBS1 and *C. elegans* BBS7 contain quinoprotein alcohol dehydrogenase, which is also folded into a β-propeller structure. Nevertheless, it is still possible that these proteins have gained other functions or lost ancestral functions through the evolution. Moreover, all orthologues of BBS4 and BBS8 share multiple TPRs in their amino acid sequences. The similarity between the amino acid sequences of BBS4 and BBS8 was not surprising since BBS8 was identified via a shared homology with BBS4 (Ansley et al., 2003). Among 7 BBSome proteins, only BBS5 does not share a

domain with other BBSome proteins that is consisted of a DUF1448, suggesting that BBS5 does not share the same function as other BBSome proteins.

The analysis of residues affected by mutations identified by BBS patients revealed that the most highly conserved amino acid residues were identified in BBS5 amino acid sequences. Trp59, Gly72, and Asn184 were all conserved in *H. sapiens, C. reinhardtii*, *P. tetraurelia, T. brucei,* and *C. elegans,* suggesting the importance of these three residues for the function of BBS5, which is predicted in lipid binding.

To analyse the BBSome in *T. brucei* further, I selected three BBSome proteins; BBS5, BBS8, and BBS9 for following reasons:

BBS5: BBS5 is highly conserved across ciliated eukaryotes and has a predicted PH domain which is not shared with other BBSome proteins. The ability of BBS5 for lipid binding might be crucial for the cell and therefore BBS5 might be the most conserved of the BBSome proteins. The function of BBS5 might be critical for *T. brucei*, as well. Considering that the function of the BBSome is transporting receptor proteins to ciliary membranes, BBS5 is possibly associated with flagellar formation through flagellum membrane biogenesis in *T. brucei*.

BBS8: BBS8 is required for the normal localisation/motility of the IFT in *C. elegan*s (Blacque et al., 2004). A study showed the association of BBSome proteins with IFT (Lechtreck et al., 2009), suggesting that the BBSome acts as a cargo of IFT. Revealing the function of BBS8 may lead us to understand whether the BBSome is also associated with IFT in *T. brucei,* or not. Since the IFT is playing an important role for flagellar assembly in *T. brucei*, it is interesting to find out whether the IFT machinery actually requires BBS8.

BBS9: The conserved domain of BBS9 in *T. brucei* and *H. sapiens* were not identified, and the characteristics of BBS9 in ciliary function/formation have not been well studied compared to

other BBSome proteins. However, BBS9 is the BBSome protein which interacts the most with other BBSome proteins, suggested that BBS9 may be a central subunit of the BBSome (Nachury et al., 2007). Therefore, BBS9 may be responsible for other BBSome proteins function in *T. brucei*, and revealing the function of BBS9 in *T. brucei* might identify how BBS9 supports other BBSome proteins function and localisation in this organism.

3.2 Localisation of BBS5

To determine the localisation of BBS5, BBS8, and BBS9 in procyclic form *Trypanosoma brucei*, I generated SMOX P9-based cell lines in which one copy of BBS5, BBS8, and BBS9 of the two endogenous alleles were modified to express TY::GFP::BBS5, TY::GFP::BBS8, and TY::GFP::BBS9, respectively. The pEnT6B vector was used for endogenous locus tagging; the N-termini of BBS5, BBS8, and BBS9 were tagged with a TY epitope and green fluorescent protein (GFP) for immune detection (see chapter2, plasmid strategy). The resulting cell lines were named BBS5/TY::GFP::BBS5, BBS8/TY::GFP::BBS8, and BBS9/TY::GFP::BBS9.

3.2.1 Confirmation of TY::GFP::BBS5 protein expression

To assess the protein expression of TY::GFP::BBS5, TY::GFP::BBS8, and TY::GFP::BBS9 in the cells, I performed western blot analysis of whole cell extracts from each cell line using an anti-TY epitope antibody, BB2. Subpellicular Associated Protein-Procyclic (SAP-P) endogenously tagged with a TY epitope and yellow fluorescent protein (YFP) at the C-terminus, SAP-P::YFP::TY, was used as a positive control due to its robust expression. This cell line expressing SAP-P::YFP::TY was derived from Neil Portman from the Gull lab, University of Oxford. The parental cell line, SMOX P9, which did not contain the TY epitope or GFP was used as a negative control. As expected, western blot analysis revealed strong expression of SAP-P::TY::YFP and no protein expression in the negative control, SMOX P9 was seen (Fig. 3.22 A). The BBS5/TY::GFP::BBS5 band was detected slightly

below the 75 kDa marker, which corresponds to the expected size of TY::GFP::BBS5, 70 kDa. However, the protein expression level of TY::GFP::BBS5 was not high compared to the band intensity of SAP-P::TY::YFP. BBS8/TY::GFP::BBS8 and BBS9/TY::GFP::BBS9 expression at the expected sizes of 91 kDa and 121 kDa, respectively, were not detected. Ponceau staining demonstrated that equal protein amounts of each cell lysate were loaded onto the gel (Fig. 3.22 B). In addition, western blot analysis demonstrated high protein expression levels of the positive control and no expression of the negative control, indicating that appropriate blotting was conducted. These results indicate that TY::GFP::BBS8 and TY::GFP::BBS9 were either not expressed or the levels expressed were below the limit of detection of the western blot analysis.

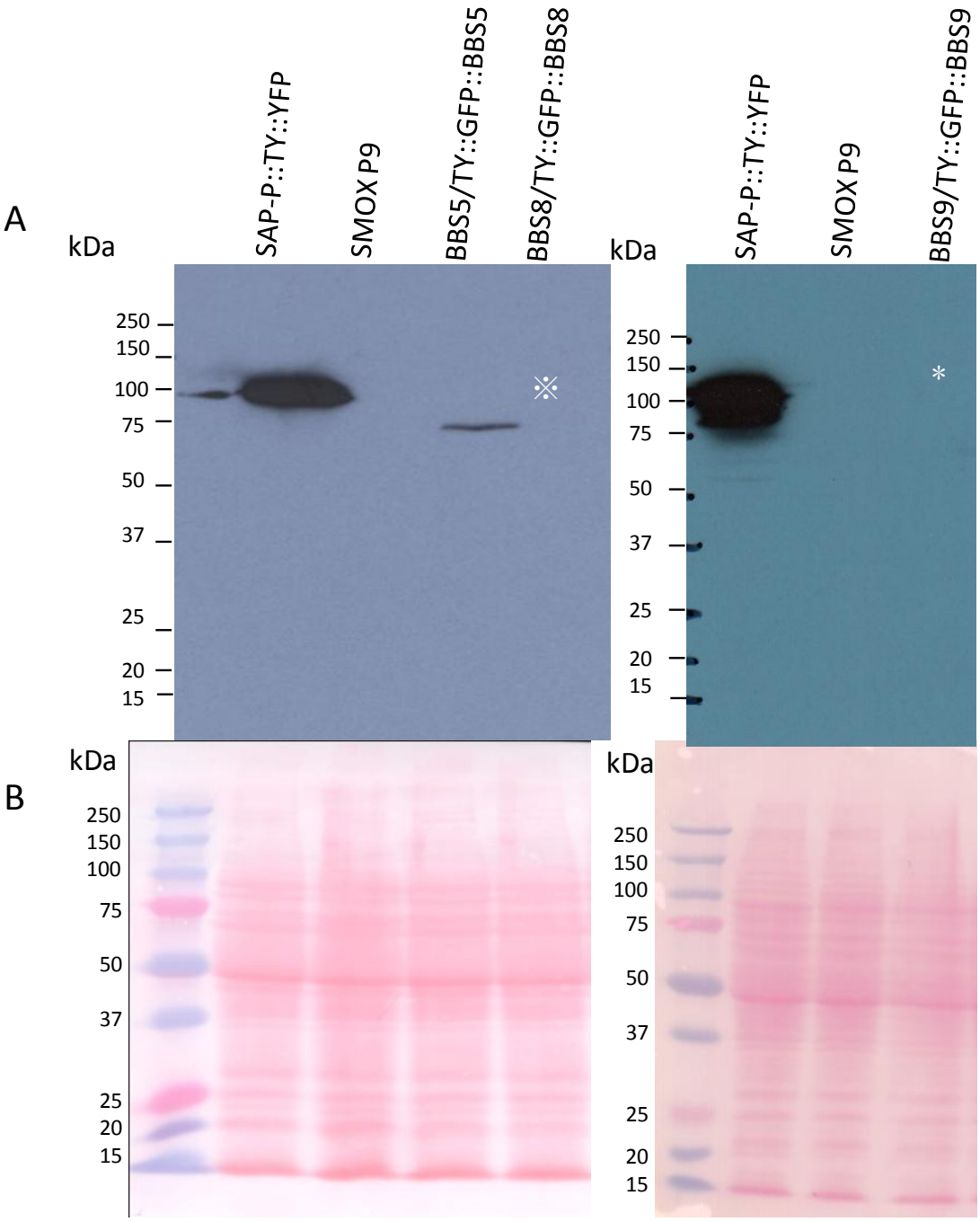

Figure 3.22 **Expression profile of TY::GFP::BBS5, TY::GFP::BBS8, and TY::GFP::BBS9 detected by western blot.** Western blot of whole cell extracts of procyclic form cells of BBS5/TY::GFP::BBS5, BBS8/TY::GFP::BBS8, and BBS9/TY::GFP::BBS9. (A) Western blot analysis using anti-TY epitope antibody, BB2 confirmed the protein expression of TY::GFP::BBS5 in the expected size; 70 kDa. However, the protein expression of TY::GFP::BBS8 and TY::GFP::BBS9 were not detected. (※ indicates the expected position of TY::GFP::BBS8 at 91 kDa. * indicates the expected position of TY::GFP::BBS9 at 121 kDa). TY::YFP tagged Subpellicular Associated Protein-Procyclic, SAP-P::TY::YFP was used as a positive control of blotting provided by Neil Portman (Gull lab). SMOX P9 was used as a negative control of blotting. Loaded per lane: $5x10^6$ cells. (B) Loading control for the western blot analysis was provided by ponceau staining.

3.2.2 TY::GFP::BBS5 is localised above the transition fibres

To determine the localisation of TY::GFP::BBS5, I examined the native GFP signal of the TY::GFP::BBS5 fusion protein by microscopy, but was unable to detect GFP signal. Likewise, TY::GFP::BBS5 was not detected by the TY-epitope using the anti-TY-epitope antibody, BB2. As an alternative approach, I fixed the cells and immunolabelled them with a polyclonal anti-GFP antibody and stained with DAPI to detect the nucleus and kinetoplast. Microscopic examination revealed that TY::GFP::BBS5 was localised at the flagellar pocket, specifically at the base of the flagellar pocket throughout the cell cycle (Fig. 3.23). When the Phase/DAPI and Phase/DAPI/anti-GFP images were compared, I found that TY::GFP::BBS5 was localised to the base of the flagellar pocket where the proximal end of the flagellum is emerged. This suggests that TY::GFP::BBS5 may localise to the distal end of the basal body or the base of the transition zone of the flagellum. No signal was detected in the parental cell line, SMOX P9, indicating that the signal detected in the BBS5/TY::GFP::BBS5 cells was expressed from TY::GFP::BBS5.

To further investigate the localisation of TY::GFP::BBS5 in the proximal end of the flagellum region, cells were stained with a mature basal body marker, YL1/2 and polyclonal anti-GFP antibody. The YL1/2 antibody recognizes tyrosinated α-tubulin, which localises to the posterior end of the subpellicular microtubule cytoskeleton and transition fibres, which is the radiated fibres at the distal end of the basal body (Stephan et al., 2007). Co-staining with YL1/2 and anti-GFP antibody revealed that TY::GFP::BBS5 did not overlap with YL1/2, but localised to the distal end of YL1/2 with a small gap (Fig. 3.24).

Upon microscopic examination, I found that the distribution pattern of TY::GFP::BBS5, which includes the number and localisation of TY::GFP::BBS5, differs between cells in different cell cycle stages. To determine how the localisation pattern of TY::GFP::BBS5 changed with cell cycle progression, I counted the foci of TY::GFP::BBS5 in each cell cycle stage and examined their localisation.

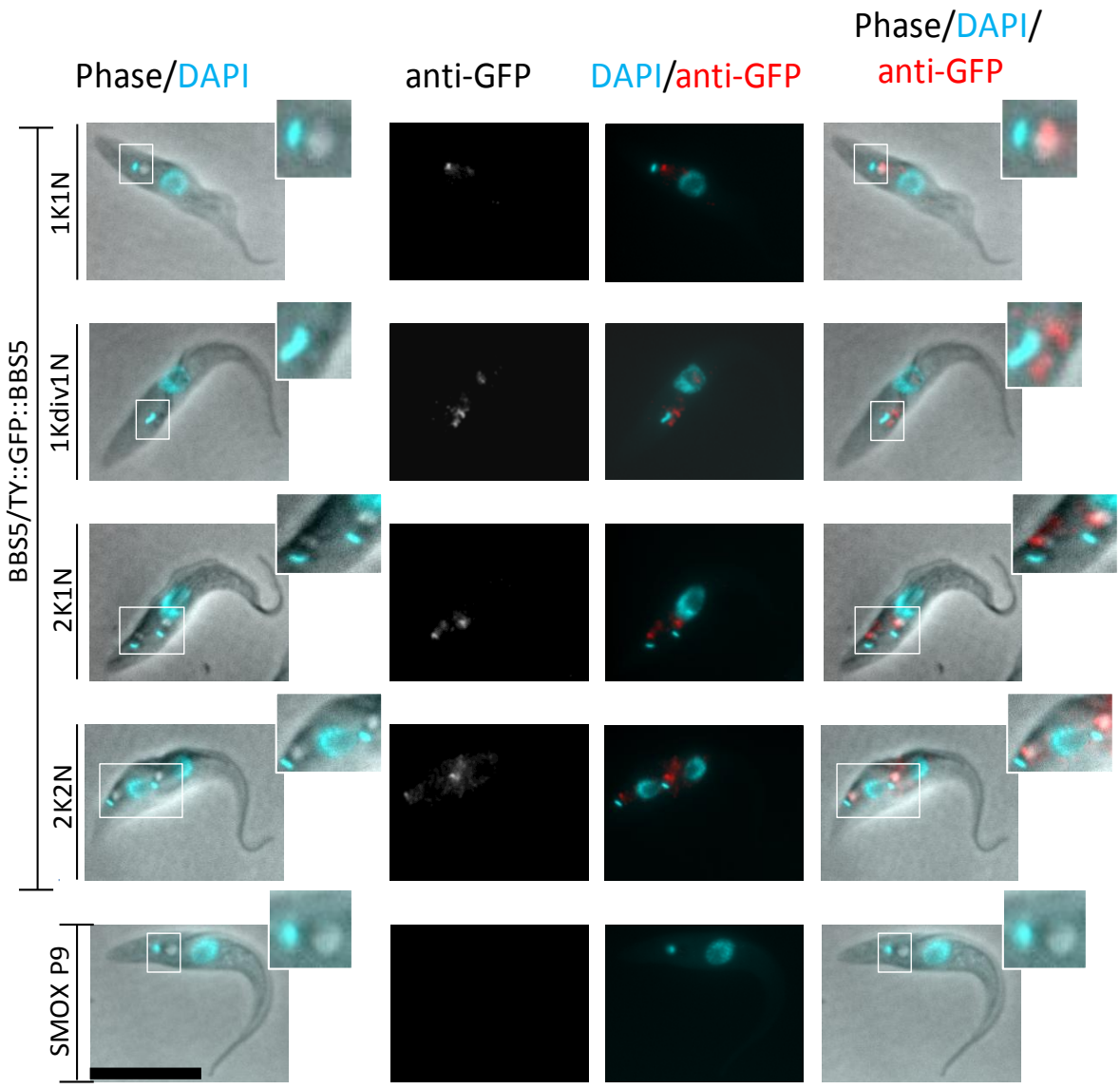

Figure 3.23 **Localisation of TY::GFP::BBS5 throughout the cell cycle: TY::GFP::BBS5 localises at the base of flagellar pocket where the flagellum emerges.** *T. brucei* BBS5 N-terminally tagged with TY::GFP, TY::GFP::BBS5 was expressed from the endogenous BBS5 locus in procyclic forms. TY::GFP::BBS5 localised at the base of the flagellar pocket where the proximal end of flagellum is emerging. The negative control, the parental cell line (SMOX P9) showed no signal. Cells were fixed in formaldehyde and DNA was labelled with DAPI (blue) and TY::GFP::BBS5 was immunolabelled with anti-GFP antibody (red). The magnified views of the areas indicated by the white boxes in the Phase/DAPI images show the flagellar pocket and kinetoplast. The magnified views of the phase/DAPI/anti-GFP images show the localisation of TY::GFP::BBS5 at the base of the flagellar pocket, also at the proximal end of the flagellum. The images were aligned according to the cell cycle progression. Scale bar: 10 µm.

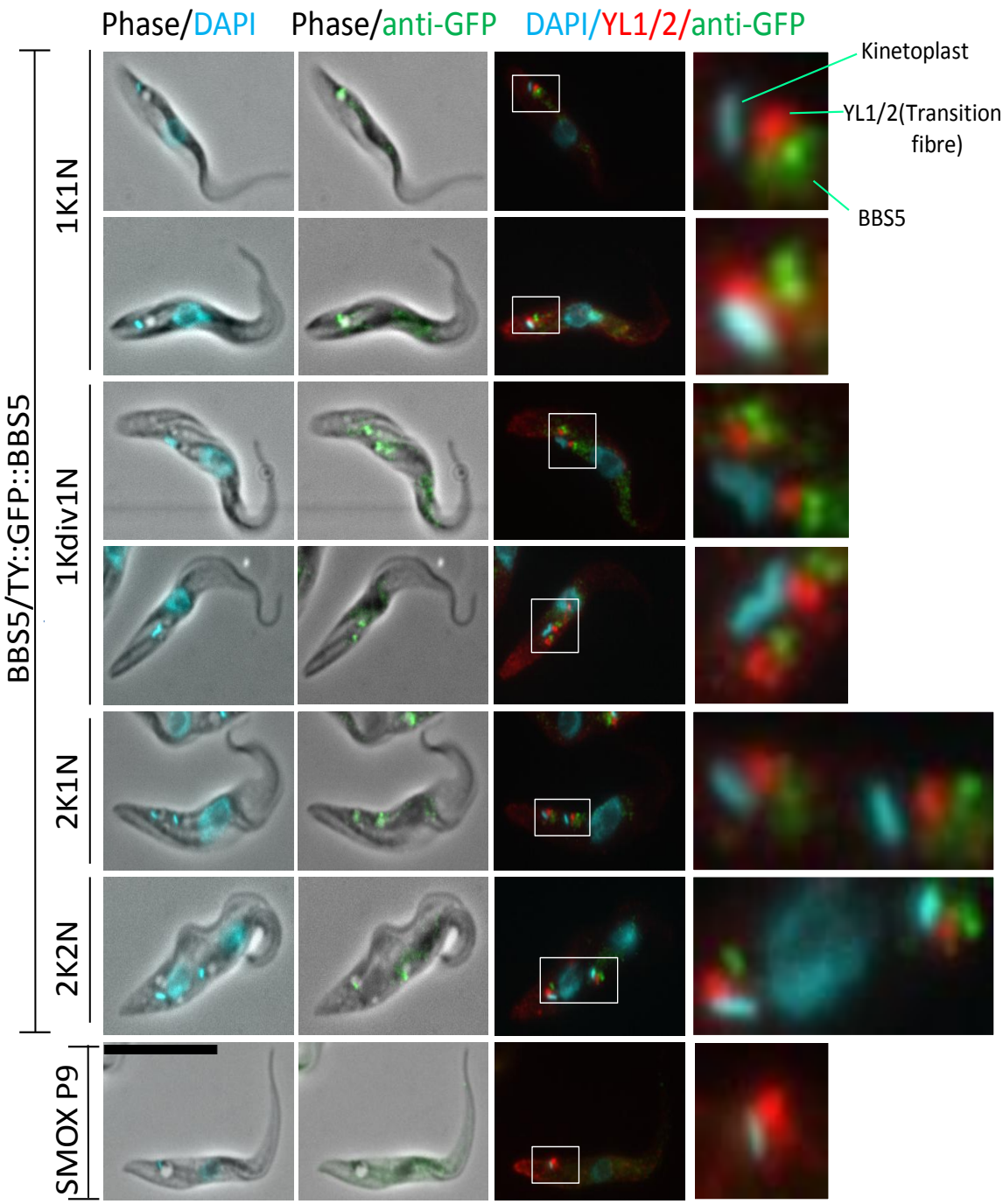

Figure 3.24 **Double-labelling of BBS5/TY::GFP::BBS5 cells with anti-GFP antibody and YL1/2.** TY::GFP::BBS5 localised to the distal end of the YL1/2 region, which labels transition fibres radiating from the mature basal body.BBS5/TY::GFP::BBS5 cells were fixed in formaldehyde and immunolabelled with anti-GFP antibody (green) and with YL1/2 (red). DNA was labelled with DAPI (blue). The magnified view of the area indicated by the white box in the merged image shows the kinetoplast-basal body region. The images were aligned according to the cell cycle progression. Scale bar: 10 µm.

Most 1K1N cells appeared to have a single focus of TY::GFP::BBS5, but in 1Kdiv1N cells, where the kinetoplast is still connected but elongated, most TY::GFP::BBS5 foci appeared to have duplicated (Table 3.1) (Fig. 3.25). In the 1Kdiv1N cells, the pro-basal body has already begun the maturation process and initiated new flagellum elongation; therefore, the cell starts to possess two flagella. In the late cell cycle stage, cells possess two flagella and showing two TY::GFP::BBS5 foci. The duplication of TY::GFP::BBS5 foci with cell cycle progression supports the hypothesis that TY::GFP::BBS5 is localised to the base of the flagellum because the foci correspond to the number of flagellum in the cells of each cell cycle stage. Though the number of TY::GFP::BBS5 foci changed with cell cycle progression, the position of TY::GFP::BBS5 was consistent, which was at the base of the flagellar pocket and the proximal end of the flagellum.

In conclusion, microscopic analysis revealed that TY::GFP::BBS5 did not co-localise with the basal body, but rather localised above YL1/2. In addition, the number of TY::GFP::BBS5 foci corresponded to the number of flagella in the cells. These findings suggest that BBS5 is localised to the base of the transition zone, which is above the transition fibres.

3.2.3 Tagging TY::GFP to the second BBS5 allele did not alter TY::GFP::BBS5 protein level

In addition to BBS5/TY::GFP::BBS5, I generated a cell line, TY::GFP::BBS5/TY::GFP::BBS5, in which both endogenous BBS5 alleles were modified to express TY::GFP::BBS5. PCR was conducted to confirm correct integration of the targeting constructs and absence of the wild-type BBS5 allele in TY::GFP::BBS5/TY::GFP::BBS5 cells. The primers GFP F and BBS5 R amplified a 482 bp fragment, indicating that the 3’ end of GFP is conjugated to the 5′ end of the BBS5 ORF (Fig 3.26 A, B). The primers 5′UTR F and BBS5 R amplified a 642 bp fragment, indicating that the 3′ end of the 5′UTR

Table 3.1. Number of TY::GFP::BBS5 foci throughout cell cycle. The count of TY::GFP::BBS5 foci throughout the cell cycle showed that 1K1N cells possessing a single kinetoplast and flagellum, have mostly a single TY::GFP::BBS5 focus. However, the focus duplicates from 1Kdiv1N cells when the kinetoplast is physically connected but the new flagellum starts to grow. 2K1N and 2K2N cells show duplicated foci of TY::GFP::BBS5.

	Number of TY::GFP::BBS5 foci			
	0	1	2	Total
1K1N	5	75	0	80
1K div 1N	0	9	40	49
2K1N	0	0	21	21
2K2N	0	0	18	18
Total	5	84	79	168

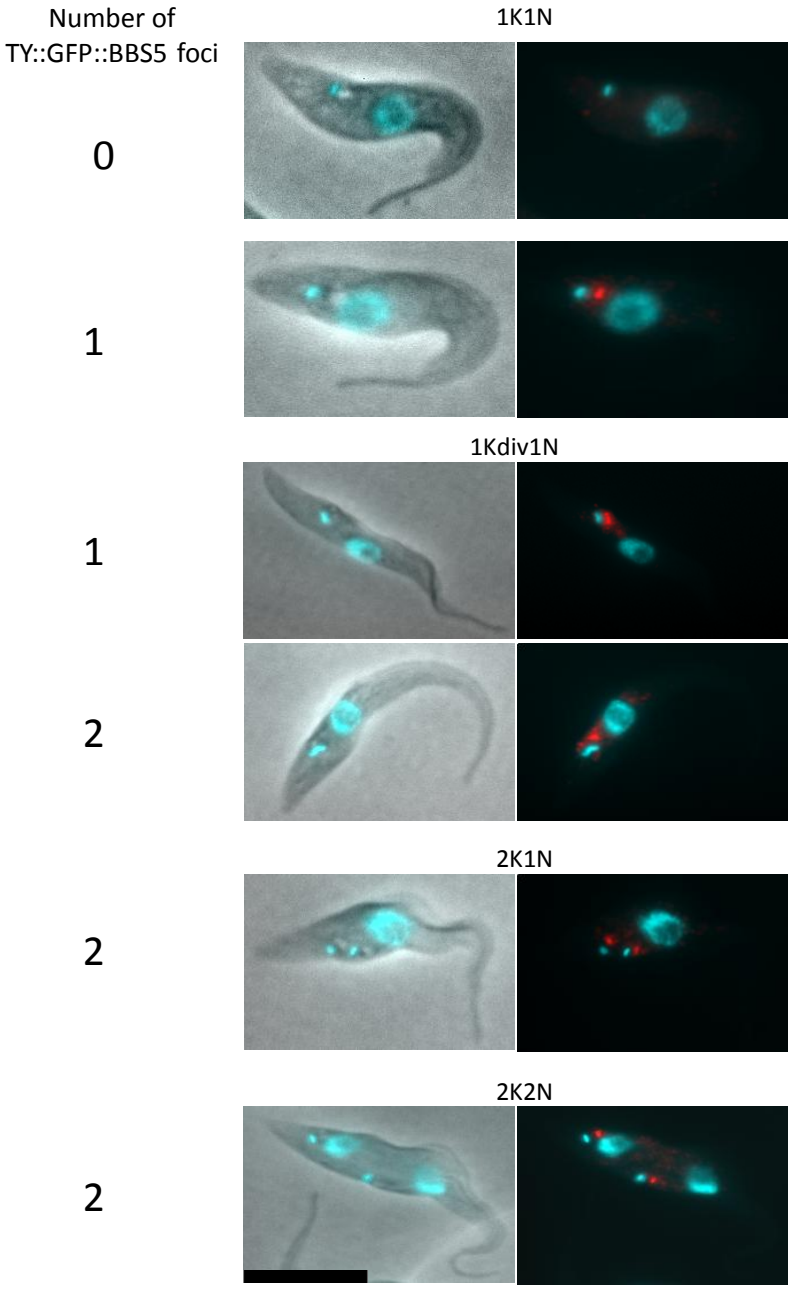

Figure 3.25 **The number and localisation of TY::GFP::BBS5 foci throughout cell cycle.** Left images: phase/DAPI, Right images: DAPI/anti-GFP. 1K1N cells showing none or single TY::GFP::BBS5 and 1Kdiv1N cells showing single or duplicated TY::GFP::BBS5 foci. In later cell cycle stage, 2K1N cells and 2K2N cells show duplicated TY::GFP::BBS5 foci. Cells were fixed in formaldehyde and DNA was labelled with DAPI (blue) and TY::GFP::BBS5 was immunolabelled with anti-GFP antibody (red). The images were aligned according to the cell cycle progression. Scale bar: 10 μm

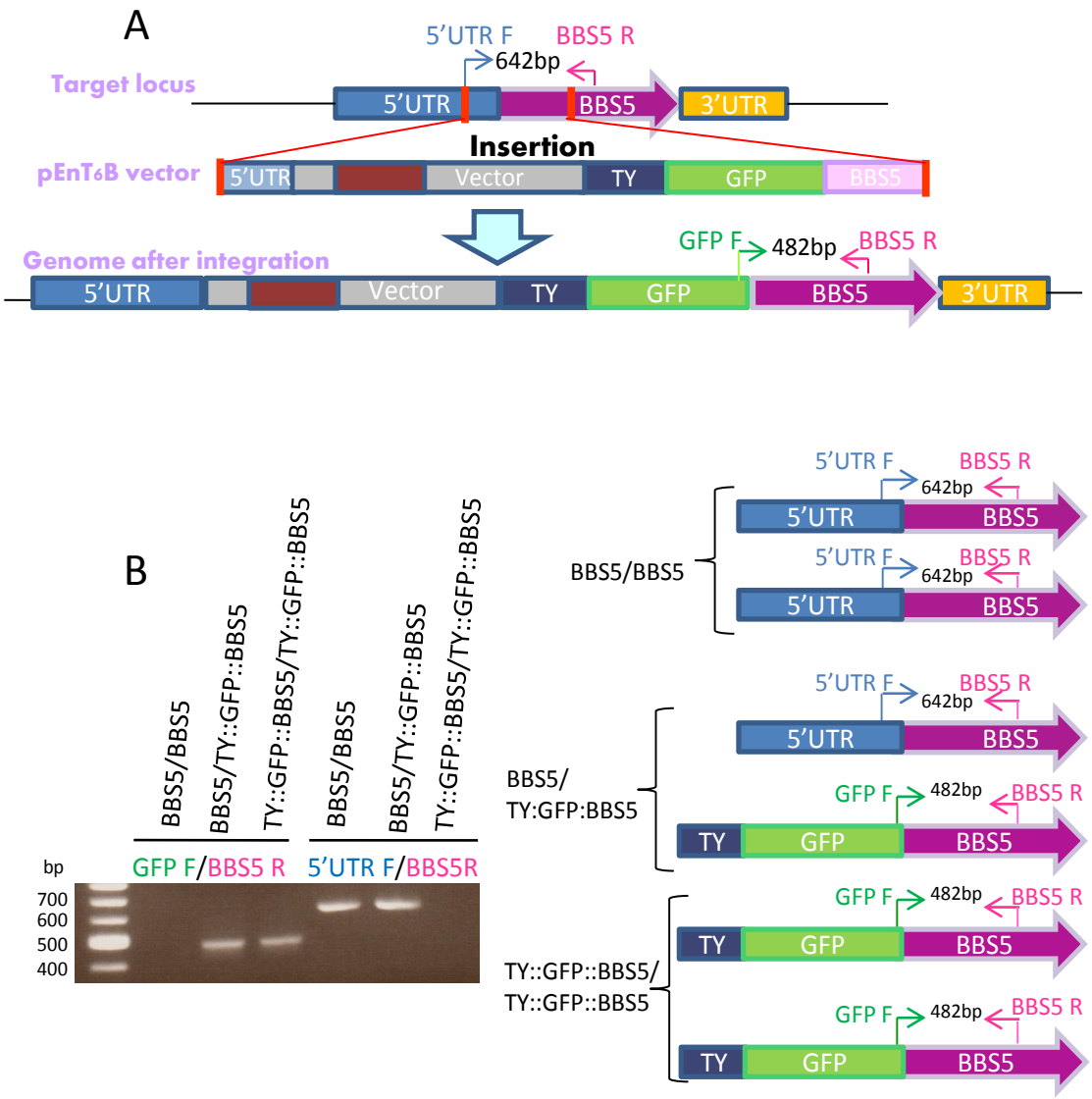

Figure 3.26 **Examination of genomic DNA of wild type (BBS5/BBS5), cells with a single BBS5 replaced by TY::GFP (BBS5/TY::GFP::BBS5), and cells with both BBS5 replaced by TY::GFP (TY::GFP::BBS5/TY::GFP::BBS5) using PCR.** (A) Diagram showing the mechanism of endogenous BBS5 locus tagging with TY::GFP using pEnt6B vector. The primers 5'UTR F and BBS5 R amplify 642bp which verifies that 3' end 5'UTR is positioned next to the 5' end of BBS5. The primers GFP F and BBS5 R amplify 482bp, which verifies that the 3' end of GFP sequence is positioned next to the 5' end of BBS5. (B) Left panel: PCR products using the template from genomic DNA. Expected size of PCR products from primers 5'UTR F and BBS5 R is 642bp and primers GFP F and BBS5 R is 482bp. The PCR confirmed the correct integration of TY::GFP with BBS5. TY::GFP::BBS5/TY::GFP::BBS5 has no wild type allele left. Right panel: Maps of wild type BBS5 allele (BBS5/BBS5). Single BBS5 allele modified to express TY::GFP::BBS5 (BBS5/TY::GFP::BBS5). Double BBS5 alleles modified to express TY::GFP::BBS5 (TY::GFP::BBS5/TY::GFP::BBS5).

is positioned next to the 5' end of BBS5 (Fig 3. 26 A, B). PCR confirmed that TY::GFP::BBS5/TY::GFP::BBS5 cells contained only the modified, and not the wild-type BBS5 allele, whereas the BBS5/TY::GFP::BBS5 cells contained one modified and one wild-type BBS5 allele (Fig. 3.26 B). Western blot analysis of whole cell extracts using the anti-TY epitope antibody, BB2, demonstrated that TY::GFP::BBS5 was expressed in TY::GFP::BBS5/TY::GFP::BBS5 cells, but the amount of TY::GFP::BBS5 did not increase compared to BBS5/TY::GFP::BBS5 cells (Fig. 3.27). Consistent with the western blot result, the microscopic analysis of TY::GFP::BBS5/TY::GFP::BBS5 cells showed no native GFP signal and no signal was detected by the TY-epitope antibody, BB2. TY::GFP::BBS5 detection using an anti-GFP antibody revealed the same TY::GFP::BBS5 localisation pattern and signal strength as observed in BBS5/TY::GFP::BBS5 cells. TY::GFP::BBS5/TY::GFP::BBS5 cells appeared morphologically normal, in that they were indistinguishable from wild-type or single allele tagged cell lineBBS5/TY::GFP::BBS5 cells, and grew normally without any defect. Yet, we cannot still conclude that TY::GFP::BBS5 is functional and able to compensate the wild-type BBS5, as the TY::GFP tagged BBS5; TY::GFP::BBS5 was not detected.

3.2.4 TY::GFP::BBS5 is expressed very low in the bloodstream form *T. brucei*

The localisation of BBS5 in the bloodstream form *T. brucei* was determined using the same approach as was used for tagging the procyclic forms; one allele of BBS5 was modified to express TY::GFP::BBS5. The sequence of TY::GFP was inserted to the upstream of BBS5, so that TY::GFP would tagged at the N-terminal of BBS5 in the parental cell lines SMOX B4 (Poon et al., 2012) and S16 (Wirtz et al., 1999), designated SMOX B4-BBS5/TY::GFP::BBS5 and S16-BBS5/TY::GFP::BBS5, respectively. Western blot analysis of whole cell extracts from each of these cell lines using the anti-TY epitope antibody, BB2, showed very low levels of TY::GFP::BBS5 expression in the bloodstream form *T. brucei* (Fig. 3.28).

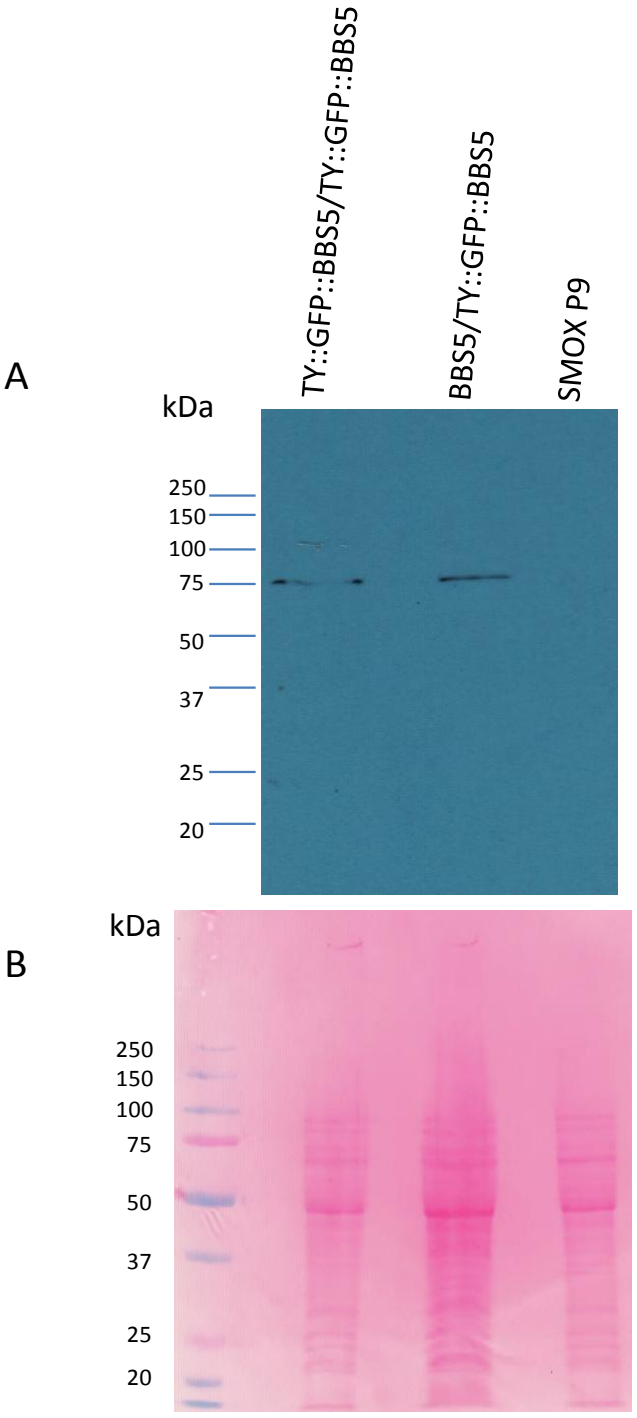

Figure 3.27 **Comparison of protein expression of TY::GFP::BBS5 in TY::GFP::BBS5/TY::GFP::BBS5 and BBS5/TY::GFP::BBS5 by western blot.** (A) Western blot of whole cell extracts of TY::GFP::BBS5/TY::GFP::BBS5 and BBS5/TY::GFP::BBS5 cells, using anti-TY epitope antibody, BB2 showed that the expression level of TY::GFP::BBS5 did not increase in TY::GFP::BBS5/TY::GFP::BBS5 cells. SMOX P9 was used as a negative control of blotting. Loaded per lane: $5x10^6$ cells. (B) Loading control for the western blot analysis was provided by ponceau staining.

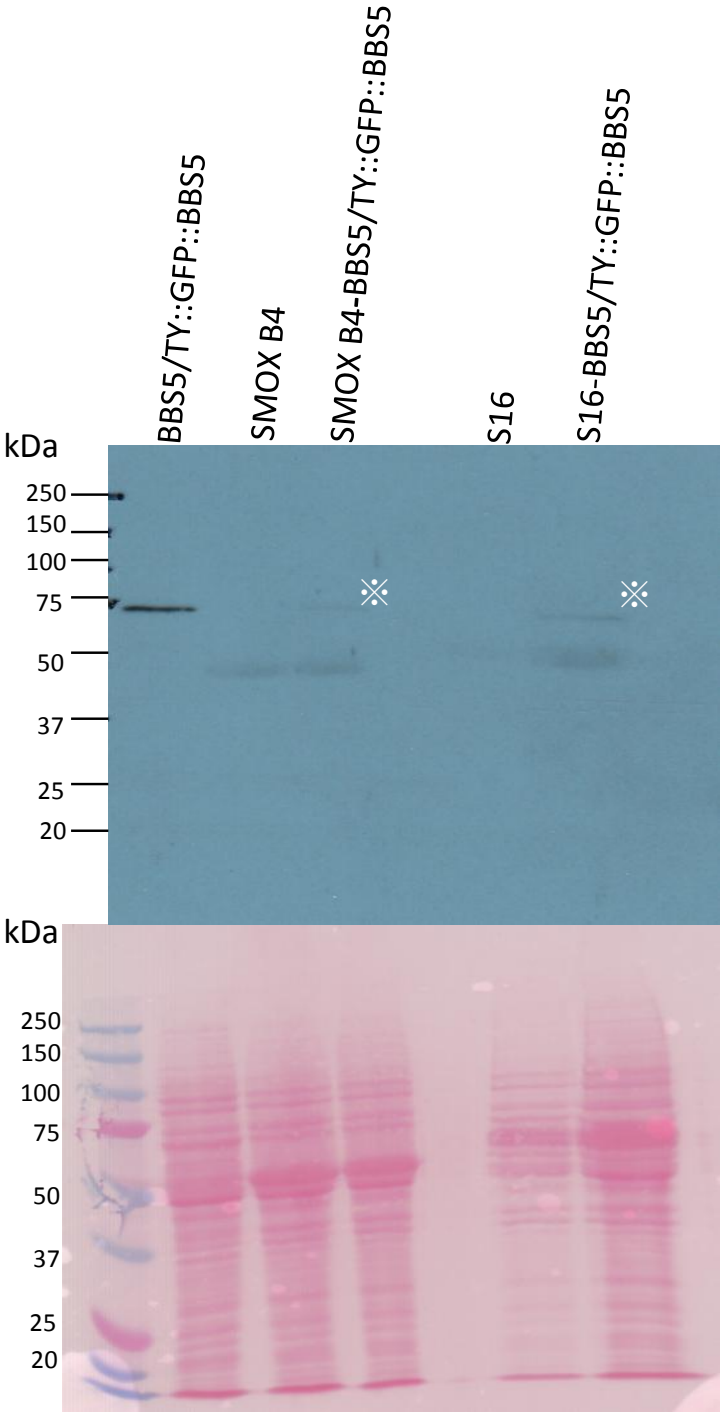

Figure 3.28 **Detection of BBS5 in bloodstream form *T. brucei* by western blot.** One copy of BBS5 was tagged with TY::GFP in bloodstream form *T. brucei*, SMOX B4 and S16 to generate cell lines in which TY::GFP::BBS5 is expressed (SMOX B4-BBS5/TY::GFP::BBS5 and S16-BBS5/TY::GFP::BBS5, respectively). (A) Western blot of whole cell extracts of cell lines given above using anti-TY epitope antibody, BB2 showed very weak expression of TY::GFP::BBS5 in bloodstream form *T. brucei.* ※ indicates the position SMOX B4-BBS5/TY::GFP::BBS5 and S16-BBS5/TY::GFP::BBS5 at the size of 70 kDa. BBS5/TY::GFP::BBS5 was used as a positive control of blotting. SMOX B4 and S16 were used as a negative control of blotting. Loaded per lane: $5x10^6$ cells. (B) Loading control for the western blot analysis was provided by ponceau staining.

In summary, I was able to confirm that the protein of TY::GFP::BBS5 is expressed in the procyclic form *T. brucei*. However, the protein expression level of TY::GFP::BBS5 in procyclic form *T. brucei* was not very high, which was able to be determined by the positive control of blotting. In terms of TY::GFP::BBS5 expression in the bloodstream form *T. brucei,* only very small level of TY::GFP::BBS5 was expressed in the cell. Additionally, protein expression of TY::GFP tagged fusion proteins; TY::GFP::BBS8 and TY::GFP::BBS9 were not detected, likely because these fusion proteins were not expressed in the procyclic form *T. brucei.*

Quantitation of TY::GFP::BBS5 foci and microscopic examination of BBS5/TY::GFP::BBS5 revealed that the number of TY::GFP::BBS5 foci changed according to cell cycle progression. In the early cell cycle stage in 1K1N cells, a single TY::GFP::BBS5 focus was observed at the proximal end of a single flagellum. However, 1Kdiv1N cells began to possess two flagella and the focus of TY::GFP::BBS5 also increased to two. Together with the microscopic analysis demonstrating that TY::GFP::BBS5 was localised to the distal end of the YL1/2 signal, which recognizes transition fibres, BBS5 may localise to the base of the transition zone of the flagellum where it is surrounded by a flagellar pocket.

3.3 RNAi ablation of BBS5 in procyclic form *T. brucei* caused a slight growth defect, but cellular morphology appeared normal

In order to examine whether BBS5 is essential for flagellum formation in procyclic form *T. brucei*, the expression of BBS5 was ablated by doxycycline-inducible RNAi based on the BBS5/TY::GFP::BBS5 strain. The TY::GFP::BBS5 tagged cell line, BBS5/TY::GFP::BBS5, was used since the localisation and protein expression of TY::GFP::BBS5 was confirmed in section 3.2. The RNAi will target BBS5 mRNA so that the TY::GFP::BBS5 would be ablated and the reduction of TY::GFP::BBS5 would be visualised directly by western blot using anti TY-epitope antibody, BB2. Through the analysis of the BBS5 knocked-down phenotype, the function of BBS5 would be

revealed, and whether it is required for flagellum biogenesis would be identified. In order to knockdown BBS5, vector p2T7-177 (Wickstead et al., 2002) was utilised, whereby approximately 200bp of BBS5 sequence would be inserted into mini-chromosomes of *T. brucei*. The BBS5 fragment was to be positioned between two doxycycline-inducible opposing promoters so that complementary RNA could be produced and hybridise to produce dsRNA. The p2T7-177-BBS5 vector was constructed and transfected into BBS5/TY::GFP::BBS5 to generate cell line; BBS5 RNAi -BBS5/TY::GFP::BBS5.

In order to induce RNAi, the cells were diluted to a density of $1x10^6$/ml every 24 hours and 1µg/ml of doxycycline was added to new culture medium each time. At the same time, whole cell lysates of RNAi-induced cells were isolated and the expression level of TY::GFP::BBS5 was evaluated by western blot. Western blot analysis using the anti-TY epitope antibody, BB2, showed that the RNAi construct was effective in reducing the amount of BBS5 protein in the doxycycline-inducible cell line by 24 hours post induction (Fig. 3.29 A). However, low levels of protein remained detectable at 24 and 48 hours post RNAi induction and the level of TY::GFP::BBS5 protein increased again at 72 hours post induction. Ponceau staining of the membrane showed that the cell lysates isolated at 72 hours post RNAi induction contained the same amount of protein as for the earlier time points (Fig. 3.29 B). Therefore, the increase of TY::GFP::BBS5 at 72 hours post-RNAi induction could be due to the emergence of escaped mutants which are resistant to doxycycline induction. This is an occasional feature of RNAi induction of *T. brucei* (Frearson et al., 2007; Price et al., 2012). The protein level detected at 96 hours post-RNAi induction was low due to a smaller amount of loaded cell lysate, which is observable from ponceau staining (Fig. 3.29 B).

In order to test whether the knockdown of BBS5 caused defect on cell growth, RNAi induced and non-induced cells were compared with regard to their cell growth every 24 hours over 96 hours. As a control, the parental cell line BBS5/TY::GFP::BBS5, which did not contain p2T7-177-BBS5, was cultured with and without the addition of doxycycline. Ablation of BBS5 caused a slight growth defect in the RNAi induced cells, which grew slower than non-induced cells (Fig. 3.29 C).

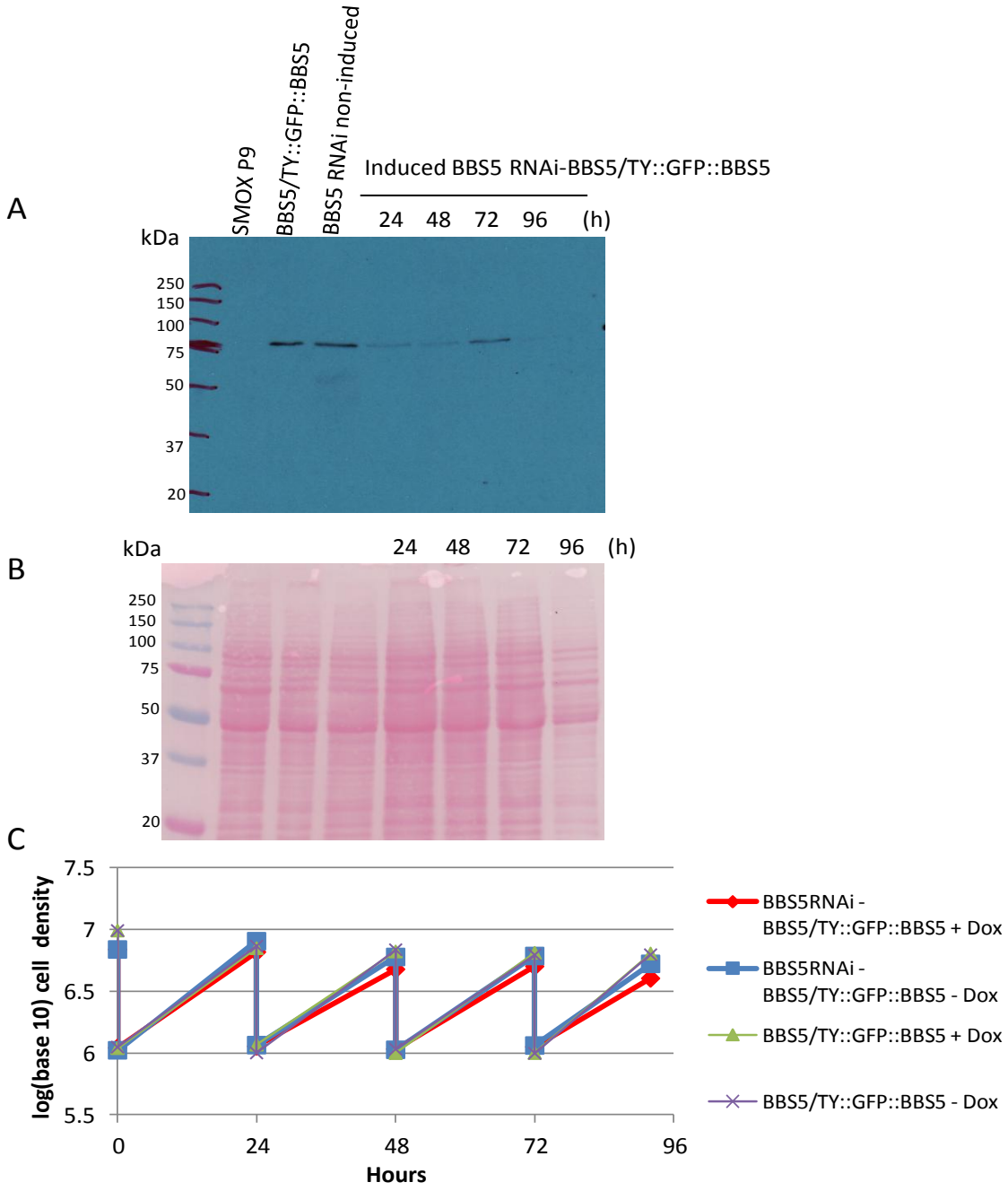

Figure 3.29 **Knockdown of BBS5 was able to reduce the expression level of TY::GFP::BBS5 and ablation of BBS5 caused a slight growth defect on population growth.** (A) RNAi was induced against BBS5 in BBS5 RNAi-BBS5/TY::GFP::BBS5 cells. Cell lysates were isolated every 24 hours over 96 hours and expression levels of TY::GFP::BBS5 were assessed by western blot analysis using anti TY-epitope antibody, BB2. The parental cell line BBS5/TY::GFP::BBS5 was used as a positive control and SMOX P9 cell line was used as a negative control for expression of TY::GFP::BBS5. Loaded per lane: $5x10^6$ cells. (B) Loading control for the western blot analysis was provided by ponceau staining. (C) Cell population growth of RNAi induced (+ Dox) and non-induced (- Dox) cells were measured every 24 hours over 96 hours. RNAi induction caused a slight defect to the cell growth. The parental cell line, BBS5/TY::GFP::BBS5, was used as a control and did not show any defect in cell growth by adding doxycycline.

Next, according to western blot analysis, the level of TY::GFP::BBS5 was most reduced at 48 hours post-RNAi induction. In order to discern whether the reduction of TY::GFP::BBS5 affected the cellular morphology, particularly in flagellum formation, the cells at 48 hours post-RNAi induction were fixed, labelled with DAPI and immunolabelled with an anti-GFP antibody for microscopic analysis. Microscopic examination showed a reduction of TY::GFP::BBS5 detected by polyclonal anti-GFP antibody across the cell population (Fig. 3.30). However, the cell morphology looked normal, and they were indistinguishable from the non-induced cells. Moreover, RNAi induced cells in each cell cycle stage were compared to non-induced cells to assess whether they possessed flagellum and whether new flagellum was assembled in later cell cycle stages, or not. Microscopic analysis showed that RNAi induced cells were able to form flagellum normally, that all cells in every cell cycle stage built flagellum in RNAi induced cells and that they looked indistinguishable from non-induced cells (Fig. 3.31 A).

Cell cycle progression followed by BBS5 RNAi induction was examined by cell count for cells in each cell cycle stage (1K1N, 2K1N, and 2K2N). A number of studies in *T. brucei* showed that the flagellum is involved in cell cycle regulation (Absalon et al., 2007; Kohl et al., 2003) and flagella motility is essential for cytokinesis (Ralston et al., 2006). Therefore, identifying the number of cells in each cell cycle stage (1K1N, 2K1N, and 2K2N) is a reliable indicator to show whether cytokinesis is affected due to flagellum dysfunction, or not. The cell count in each cell cycle stage was performed by counting the kinetoplast and nucleus of every cell. Kinetoplast and nucleus counts showed that ablation of BBS5 did not affect the cell cycle progression; even zoid (1K0N) or monster cells (cells with multiple nuclei, kinetoplasts, and flagella), which are the resultant phenotype due to cytokinesis defects did not emerge (Fig. 3.31 B).

Lastly, since the predicted function of the BBSome is biogenesis of the flagellar membrane by transporting membrane proteins, I tested whether knockdown of BBS5 caused a defect in populating flagellar membrane proteins in procyclic form *T. brucei*. The ideal test to evaluate the defect of flagellar membrane localisation due to the knockdown of BBS5 is using an antibody

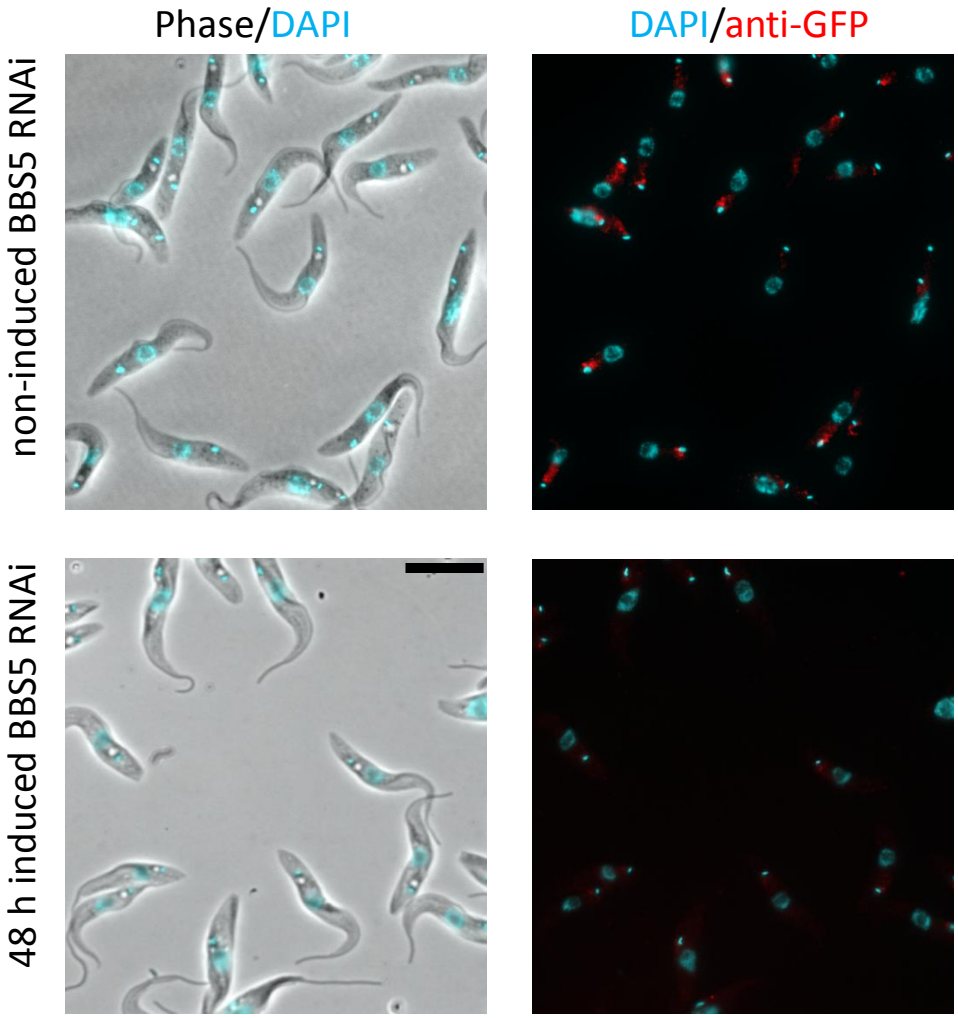

Figure 3.30 **Induced BBS5 RNAi cells appeared morphologically normal**. After 48 hours of RNAi induction, induced BBS5 RNAi and non-induced BBS5/TY::GFP::BBS5 cells were fixed with formaldehyde and DNA was labelled with DAPI (blue) and TY::GFP::BBS5 was immunolabelled with anti-GFP antibody (red). Induced BBS5 RNAi cells showed a reduction of TY::GFP::BBS5 across the cell population, however, they were able to produce a flagellum normally and cell morphology was not affected. Scale bar: 10 µm.

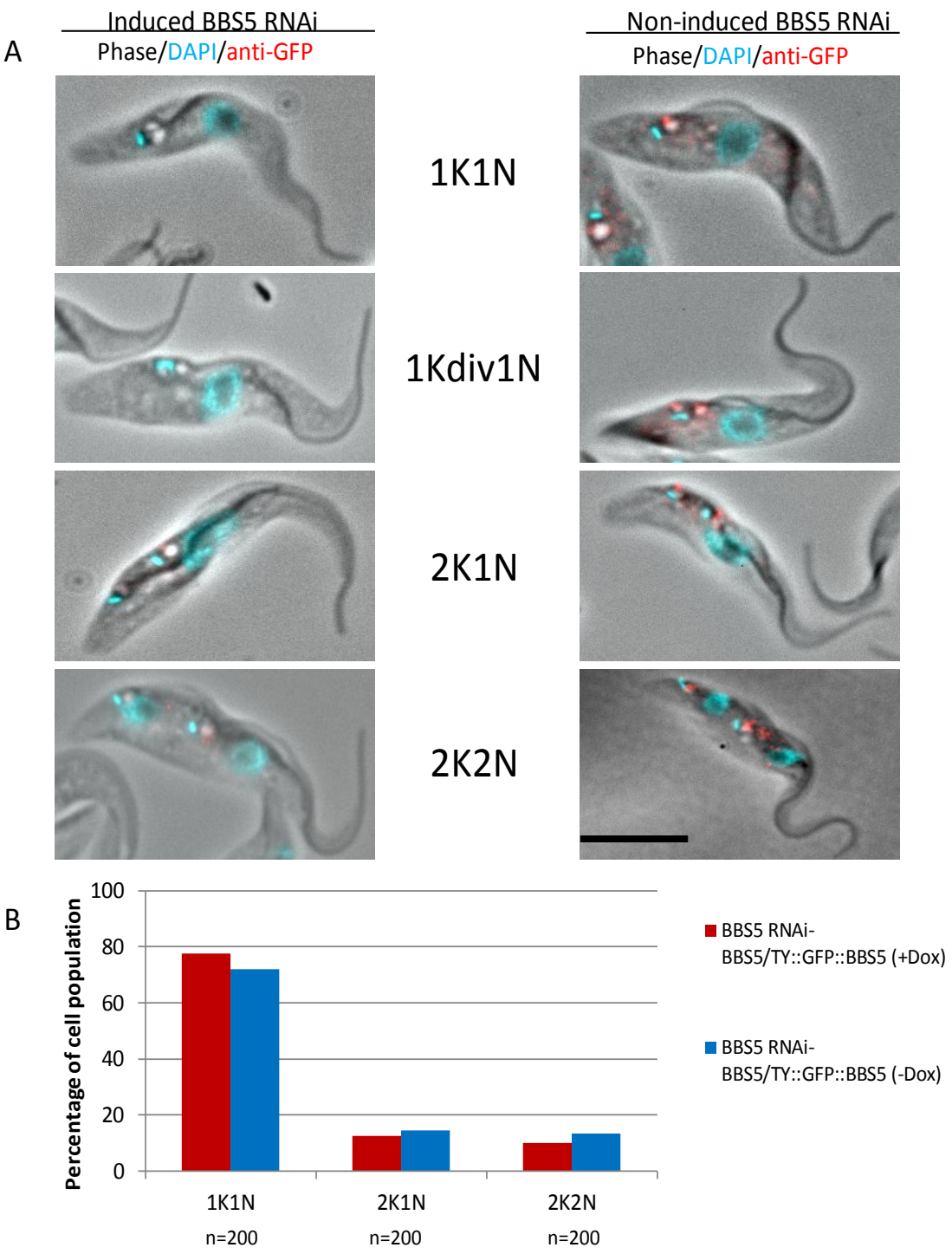

Figure 3.31 **Induced BBS5 RNAi cells possess flagellum in each stage of the cell cycle.** (A) After 48 hours of RNAi induction, induced BBS5 RNAi and non-induced BBS5/TY::GFP::BBS5 cells were fixed with formaldehyde, labelled with DAPI (blue) and anti-GFP antibody (red). Induced BBS5 RNAi cells were able to build flagellum in each cell cycle stage and the morphology was indistinguishable with non-induced cells. The images were aligned according to the cell cycle progression. Scale bar: 10 µm. (B) Kinetoplasts (=K) and nuclei (=N) counts of induced BBS5 RNAi (+Dox) and non-induced (-Dox) BBS5/TY::GFP::BBS5 cells after 48 hours of RNAi induction demonstrated no defect in cytokinesis in BBS5 RNAi induced cells.

which recognises particular flagellar membrane proteins. However, there are not many available antibodies against flagellar membrane proteins and, therefore, it resulted in the limitation of testing the localisation profile of flagellar membrane proteins in *T. brucei*. As a substitution of an antibody detecting the flagellar membrane proteins, a rabbit pre-immune serum was used for staining the flagellar membrane after knockdown of BBS5. The rabbit pre-immune serum was raised in the Gull lab in the past and visualised in the cytoplasm and nucleus, as well as the flagellar membrane. It is not known what the rabbit pre-immune serum detects exactly; however, we could utilise it to assess whether the rabbit pre-immune serum could still visualise the flagellar membrane of BBS5-ablated cells, and assess whether the knockdown of BBS5 causes a defect in populating the flagellar membrane proteins by comparing the staining pattern with non-induced cells. 48 hours after of RNAi induction, cells were fixed with 2% formaldehyde and stained with DAPI and rabbit pre-immune serum. Microscopic examination showed that the rabbit pre-immune serum stained the flagellar membrane of induced BBS5 RNAi cells and showed no significant difference in the flagellar membrane staining pattern compared to non-induced cells (Fig. 3.32). This finding suggests that ablation of BBS5 did not alter the flagellar membrane composition in a way that was still able to be stained by the rabbit pre-immune serum in induced BBS5 RNAi cells.

In summary, the knockdown of BBS5 in procyclic form *T. brucei* reduced the protein levels of TY::GFP::BBS5 and a slight growth defect was detected. Nevertheless, no discernible defect in cell morphology and flagellum formation was noted, suggesting that BBS5 is not critical for flagellum formation.

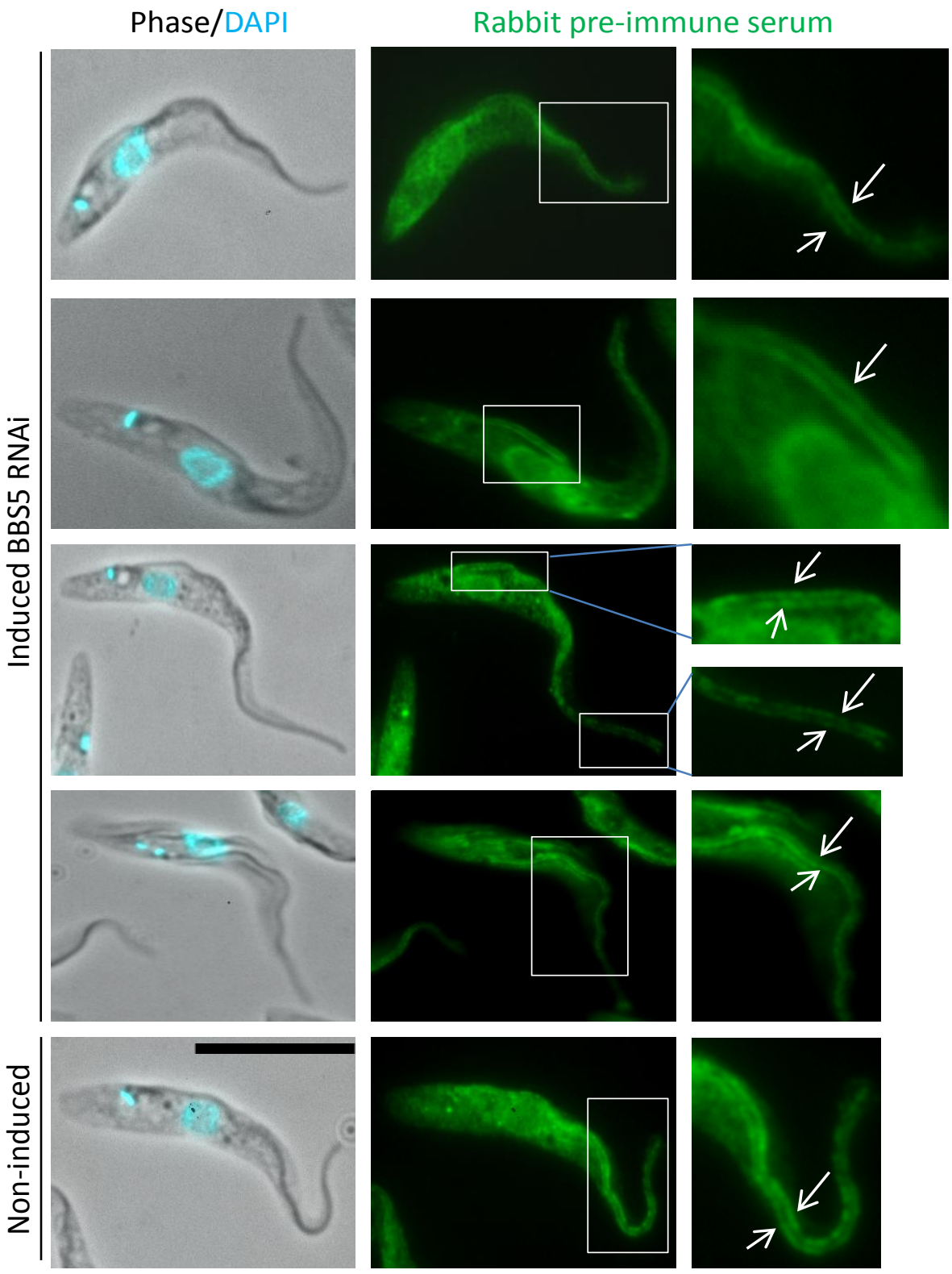

Figure 3.32 **Rabbit pre-immune serum staining for displaying the flagellar membrane in induced BBS5 RNAi and non-induced BBS5/TY::GFP::BBS5 cells.** No difference in the flagellar membrane staining pattern was observed in induced BBS5 RNAi cells compared to non-induced cells. Cells were fixed with formaldehyde and labelled with DAPI (blue) and immunolabelled with rabbit pre-immune serum (green) after 48 hours of induction. Magnified view of the area indicated by the white box shows the flagellar membrane stained by rabbit pre-immune serum. Arrows are showing the flagellar membrane stained by rabbit pre-immune serum. Scale bar: 10 µm.

3.4 RNAi ablation of BBS1 and BBS5 in bloodstream form *T. brucei* caused a slight defect in cellular morphology.

The function of BBS5 was also investigated by disrupting the expression of BBS5 in bloodstream form *T. brucei* using inducible RNAi to test whether the ablation of BBS5 caused any defect in flagellum building or function. For the induction of RNAi in the bloodstream form *T. brucei*, the same approach was used as for the procyclic form (see section 3.3). Two different parental cell lines were used for BBS5 knockdown in this test; 90-13 (Wirtz et al., 1999) and S16 (Wirtz et al., 1999), which both express the T7 RNA polymerase and the tetracycline repressor protein. I transfected p2T7-177-BBS5 vector, which was used for generating a BBS5 RNAi inducible cell line in the procyclic form *T. brucei,* into the bloodstream form 90-13 cell line (Wirtz et al., 1999) to generate the cell line, named 90-13-BBS5 RNAi. The two clones of BBS5 RNAi inducible S16 cell lines, S16-BBS5RNAi-A and S16-BBS5RNAi-B, were derived by Dr. Jack Sunter (Gull lab). In addition, I also received two BBS1 RNAi inducible cell lines in S16: S16-BBS1RNAi-A and S16-BBS1RNAi-B, from Dr. Jack Sunter, which has also been generated previously. For generating S16-BBS5RNAi-A, B and S16-BBS1RNAi-A, B, the p2T7-177 vector, which contained the entire ORF of BBS1 and BBS5 fragments, were transfected into S16. In the S16-BBS5RNAi-A, B and S16-BBS1RNAi-A, B, the glycosylphosphatidylinositol-specific phospholipase C (GPI-PLC) was endogenously tagged with eYFP at the C-terminal. This was done to test whether the knockdown of BBS1 and BBS5 would affect the localisation of GPI-PLC in flagellar membranes in S16 bloodstream forms. However, the knockdown of BBS1 and BBS5 did not cause any defect in GPI-PLC signalling, as the signal remained in the flagellar membrane (Jack Sunter. unpublished data).

In order to assess whether the ablation of BBS5 caused a growth defect in the bloodstream form cell lines, I induced RNAi by adding doxycycline and monitored cell growth for 72 hours. Knockdown of BBS5 in 90-13-BBS5 RNAi and S16-BBS5RNAi-A, B showed a slight growth defect (Fig. 3.33 A, B). These phenotypes were similar to that which was observed in BBS5 RNAi induced

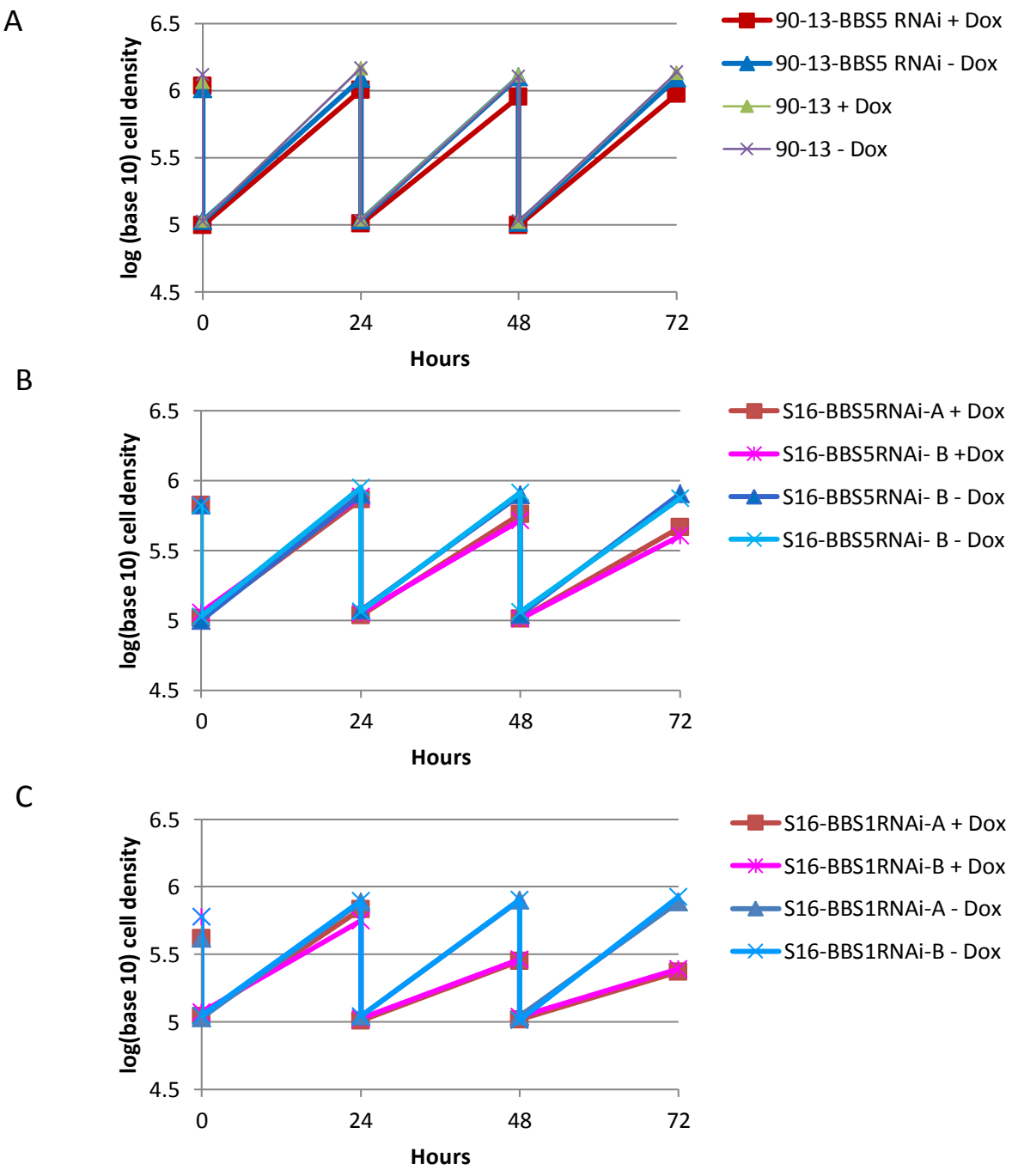

Figure 3.33 **RNAi mediated ablation of BBS1 and BBS5 in the bloodstream form *T. brucei.*** RNA inducible cell lines were cultured with (+) and without (-) doxycycline and cultured for 72 hours. Cells were counted and diluted every 24 hours. (A) 90-13-BBS5 RNAi induced cells showed a slight growth defect. The parental cell line 90-13 was used as a control and did not show any defect in cell growth by adding doxycycline. (B) S16-BBS5 RNAi induced cells showed a slight growth defect. (C) S16-BBS1 RNAi induced cells showed a more severe effect on cell growth than that of BBS5 ablated cells.

cells in the procyclic form *T. brucei* (Fig. 3.29 C). However, the knockdown of BBS1 in S16-BBS1RNAi-A, B showed a stronger growth defect than RNAi induced S16-BBS5RNAi-A, B (Fig. 3.33 C). To test whether the RNAi induced cells were able to progress through the cell cycle normally, RNAi induced S16-BBS1RNAi-A, B and S16-BBS5RNAi-A, B were stained with DAPI. Subsequently, kinetoplasts and nuclei were counted every 24 hours after the RNAi induction. Kinetoplasts and nuclei counts revealed no defects with regard to progression through the cell cycle in RNAi induced cells, yet a minor accumulation of monster cells with abnormal kinetoplasts and nucleus configurations were increased with time progression in BBS1 RNAi induced cells (Fig. 3.34 A). Since the growth defect was more severe in RNAi induced S16-BBS1RNAi-A and -B, an increased number of the monster cells might affect the cell population. The S16-BBS5RNAi-A and -B showed normal cell cycle progression with only a minor accumulation (<5%) of monster cells (Fig. 3.34 B).

From 48 hours post RNAi induction, a small population of cells in both clones of RNAi induced S16-BBS1RNAi and S16-BBS5RNAi began to show slight morphological differences compared to non-induced cells, as a few cells had a pointed posterior tip. In order to see the RNAi induced cell more in detail, RNAi induced S16-BBS1RNAi and S16-BBS5RNAi cells were fixed with formaldehyde and stained with DAPI. The microscopic analysis showed that most cells looked normal after RNAi induction; however, a few cells were seen with pointed posterior tips (Fig. 3.35, 36). In addition, a small proportion of cells had an enlarged flagellar pocket (Fig. 3.36). All of the cells in RNAi induced S16-BBS1RNAi and S16-BBS5RNAi had normal flagellum, and even the cells with pointed posterior tip and enlarged flagellar pocket showed that they were able to build flagellum (Fig. 3.36). However, I did not make a clarification and characterisation of cells which possessed the pointed posterior tip. Even though few of the RNAi induced cells demonstrated that their posterior tips were abnormally pointed, there was a slight difference between these cells, in that some had extremely elongated pointed tips, but others showed posteriors that were just as pointed. It was not clear how much the length of posterior had altered after RNAi induction,

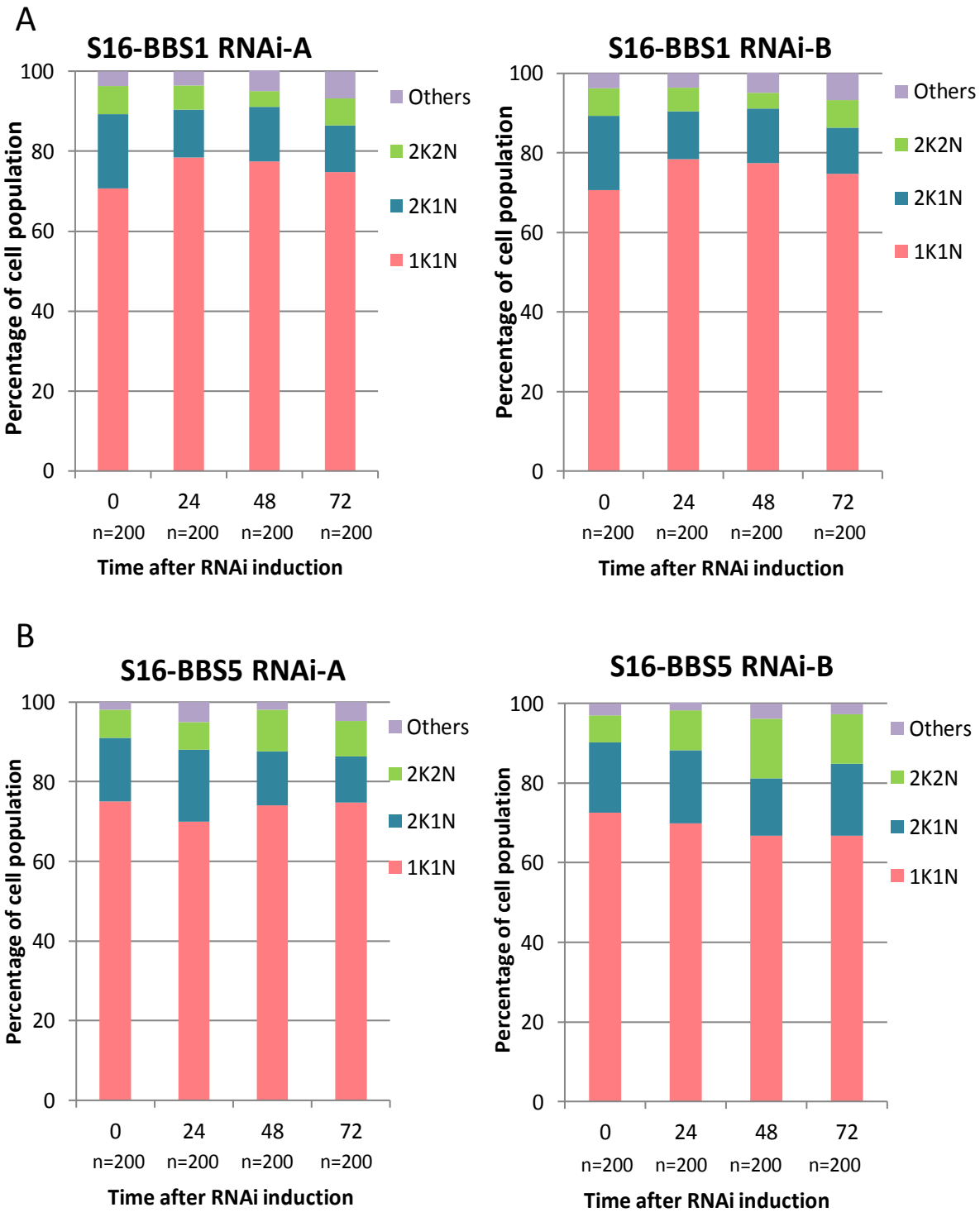

Figure 3.34 **Quantification of cells with different numbers of kinetoplasts and nuclei.** DAPI stained cells were examined visually using fluorescence microscopy and the numbers of 1K1N, 1K2N, 2K2N cells were determined as percentage of a total population at several time points after RNAi induction. Kinetoplasts (=K) and nuclei (=N). (A) Kinetoplasts and nuclei counts of RNAi induced S16-BBS1 RNAi-A and-B revealed no defect in cell cycle progression. (B) Kinetoplasts and nuclei counts of RNAi induced S16-BBS5 RNAi-A and-B revealed no defect in cell cycle progression. "Others" indicate cells with multiple kinetoplasts and nuclei.

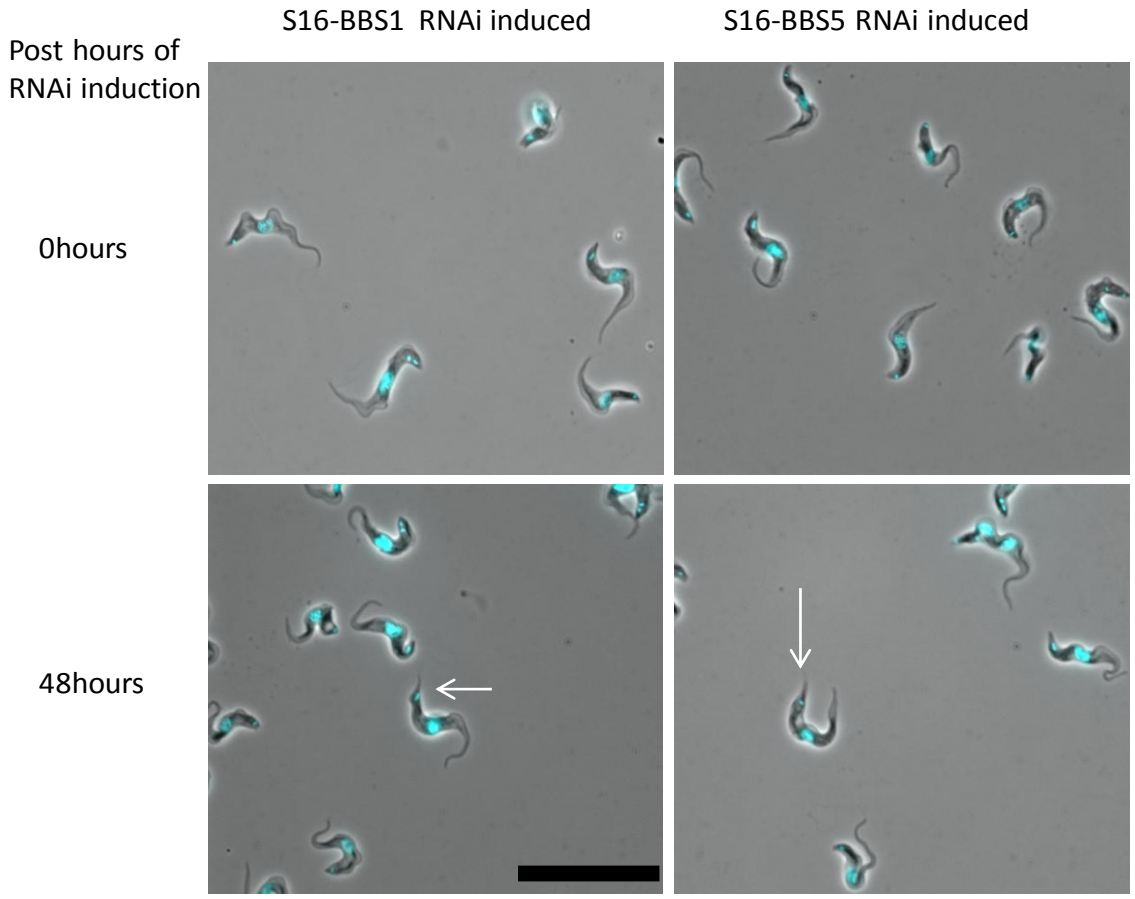

Figure 3.35 **RNAi against BBS1 and BBS5 in bloodstream form *T. brucei* caused morphological change.** Fluorescence microscopy analysis of BBS1 and BBS5 RNAi induced and non-induced cells in S16 showed the emergence of a small population of induced cells which possessed a pointed posterior tip (Pointed posterior tip is indicated with a white arrow). RNAi induced and non-induced cells were fixed with formaldehyde and DNA was labelled with DAPI (blue). Scale bar:10 µm.

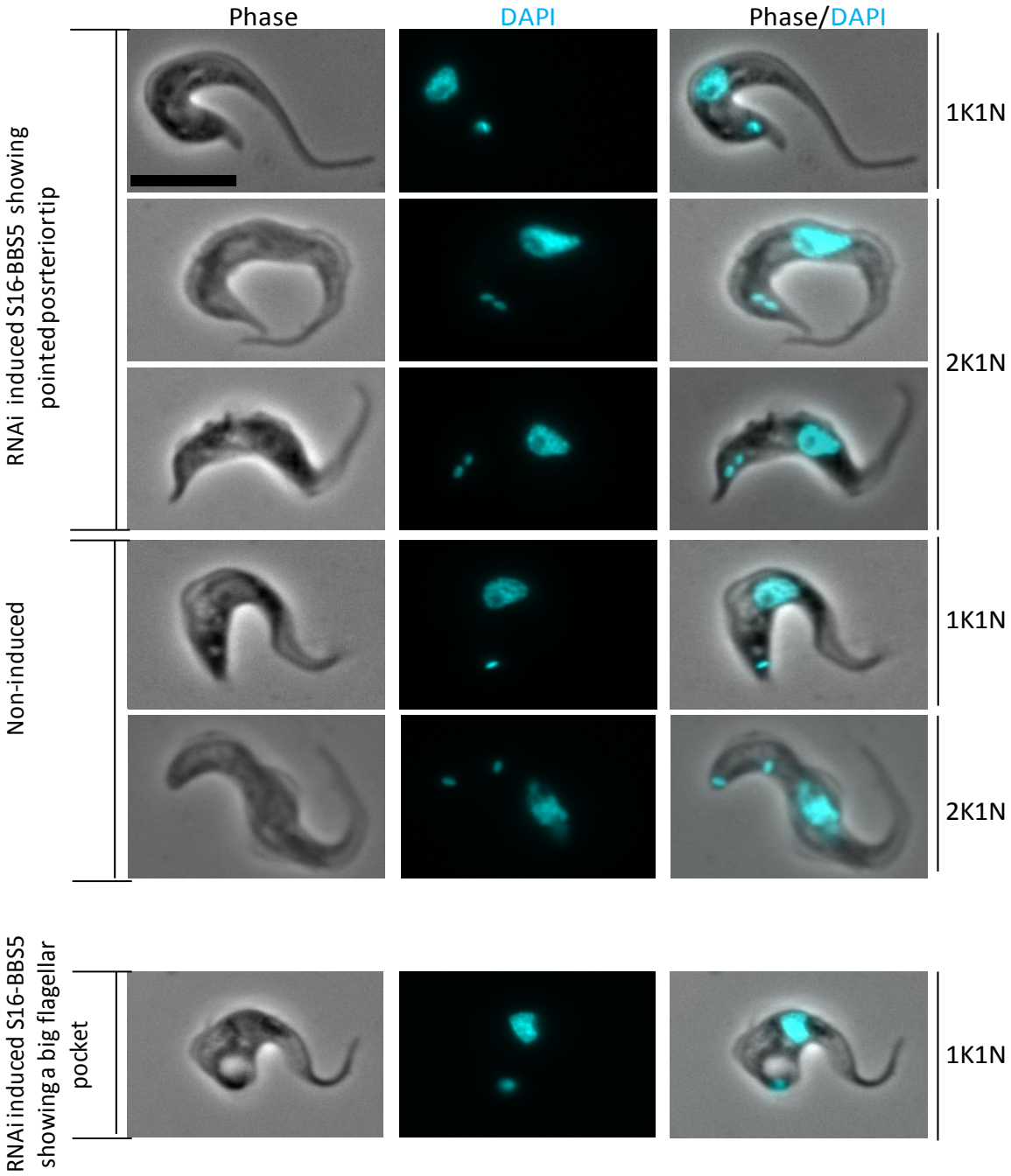

Figure 3.36 **Knockdown of BBS5 caused morphological change.** Fluorescence microscopy analysis of BBS5 RNAi induced and non-induced in S16-BBS5 RNAi cells at 48 hours post induction showed that small population of cells have pointed posterior tip and enlarged flagellar pocket. DNA was labelled with DAPI (blue). Scale bar:10 µm.

hence, the distance between the kinetoplast and the posterior tip needed to be measured and the length of the posterior pole should be compared between the RNAi induced and non-induced cells. Since I did not measure the length between the kinetoplast and posterior tip, I categorised the cells showing a posterior tip according to their appearance.

To evaluate the proportion of pointed posterior cells and enlarged flagellar pocket-containing cells in RNAi induced S16-BBS1 RNAi and S16-BBS5 RNAi cells, the cells were counted and the percentage of normal cells, cells with pointed posterior tips, swollen flagellar pocket-containing cells, and monster cells were clarified. 500 cells of each cell line were counted after 48 hours of RNAi induction since the small number of cell morphological alterations started to appear at 48 hours post RNAi induction. Most cells (<85%) in RNAi induced S16-BBS1RNAi and S16-BBS5RNAi looked normal, a minor population (<12%) of cells had a pointed posterior tip, and even fewer cells (<3%) showed an enlarged flagellar pocket (Fig. 3.37 A). Even though the proportion of cells possessing pointed posterior tips were not significant, this phenotype might be specific to the cell cycle stage and hinder the proper progression of cells with the pointed posterior pole through the cell cycle. Therefore, among the 500 cells, I counted only the cells with pointed posterior tip and determined whether the phenotype was cell cycle specific, or not. The pointed posterior cells count revealed that the phenotype was most often observed in 1K1N cells, and getting fewer in later cell cycle stages (Fig. 3.37 B). This configuration pattern of cells with pointed posterior cells demonstrated their similarity to the normal cell cytokinesis, which also show that 1K1N cells consist of most of the cell population and fewer populations of 2K1N and 2K2N cells. Therefore, even within the pointed posterior cells, cell cycle progression was not affected.

The cell shape of *T. brucei* is defined by the microtubule cytoskeleton, and the morphological changes in the posterior tip in RNAi induced S16-BBS1RNAi and S16-BBS5RNAi cells may be due to the elongation of microtubules. In order to test whether the pointed posterior tip is due to the excessive elongation of microtubules, RNAi induced S16-BBS1RNAi and S16-BBS5RNAi cells were

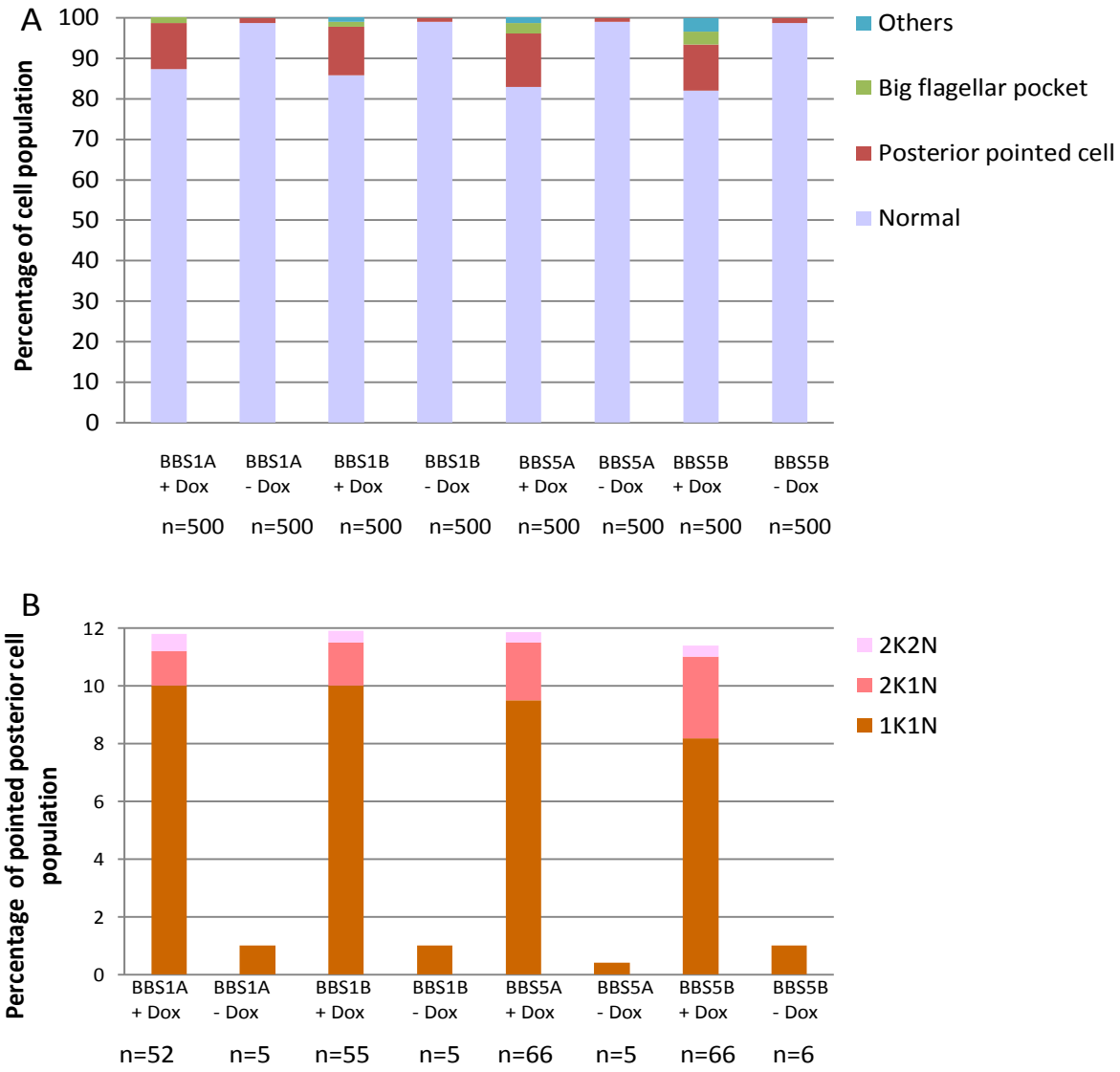

Figure 3.37 **RNAi mediated ablation of BBS1 and BBS5 resulted in slight morphological defects in bloodstream form *T. brucei*.** 2 clones of S16-BBS1 and S16-BBS5 RNAi inducible cell lines were cultured with (+) and without (-) doxycycline. (A) 500 cells of each cell line were counted and categorized after 48 hours of RNAi induction. The ratio of identified phenotypes in BBS1 and BBS5 RNAi induced and non-induced cells showed most cells (<85%) looked normal, but a small proportion of cells (<12%) showed posterior tips were pointed and even fewer cells (<3%) showed enlarged flagellar pockets. “Others” indicate cells with multiple kinetoplasts and nuclei. (B) Only the posterior pointed cells were counted and it was verified whether the phenotype is cell cycle stage specific, or not. The posterior pointed cells are not specific to a particular cell cycle stage and appeared to have normal kinetoplast and nucleus configurations.

stained with an antibody: YL1/2. YL1/2 recognises tyrosinated alpha-tubulin present in newly formed microtubules, such as basal bodies, the posterior tip of the cell, and growing flagellum (Kilmartin et al., 1982). YL1/2 is able to stain the posterior tip of the procyclic form *T. brucei* to visualise microtubule extension in its posterior tip (Matthews et al., 1995). Therefore, YL1/2 was utilised in this test to examine whether YL1/2 would visualise actively elongated microtubules at the pointed posterior pole in RNAi induced cells. Microscopic analysis of BBS1 and BBS5 ablated cells exhibited a YL1/2 signal in their basal bodies, which was also observed in the non-induced cells (Fig. 3.38). According to the YL1/2 signal appearance in RNAi non-induced cells, the YL1/2 recognised only the basal body, while the newly assembled flagellum and posterior poles were not stained. The cells with pointed posterior tips in RNAi induced S16-BBS1RNAi and S16-BBS5 exhibited no strong staining pattern of YL1/2 in their pointed posterior tip, with a signal intensity of YL1/2 that was the same compared to non-induced cells; however it cannot be concluded that microtubules were not extensively elongated in their pointed posterior tips since the non-induced cells also did not show any staining of YL1/2 in the posterior tip.

As for the procyclic form *T. brucei* (see section 3.3), RNAi induced S16-BBS1RNAi and S16-BBS5RNAi were stained with rabbit pre-immune serum 48 hours after RNAi induction in order to examine whether the ablation of BBS1 and BBS5 caused any defect in populating flagellar membrane proteins in flagellar membrane in bloodstream form *T. brucei.* Microscopic analysis showed that the rabbit pre-immune serum could stain the flagellar membrane in RNAi induced S16-BBS1RNAi and S16-BBS5RNAi cells, and no significant difference was noted in their flagellar membrane staining pattern compared to non-induced cells (Fig. 3.39). The flagellar membrane of BBS1 and BBS5 RNAi induced cells looked normal and no particular defect was observed.

In summary, the knockdown of BBS5 in bloodstream form *T. brucei* showed that the ablation of BBS5 caused a slight growth defect that was similar to the procyclic form *T. brucei*, but

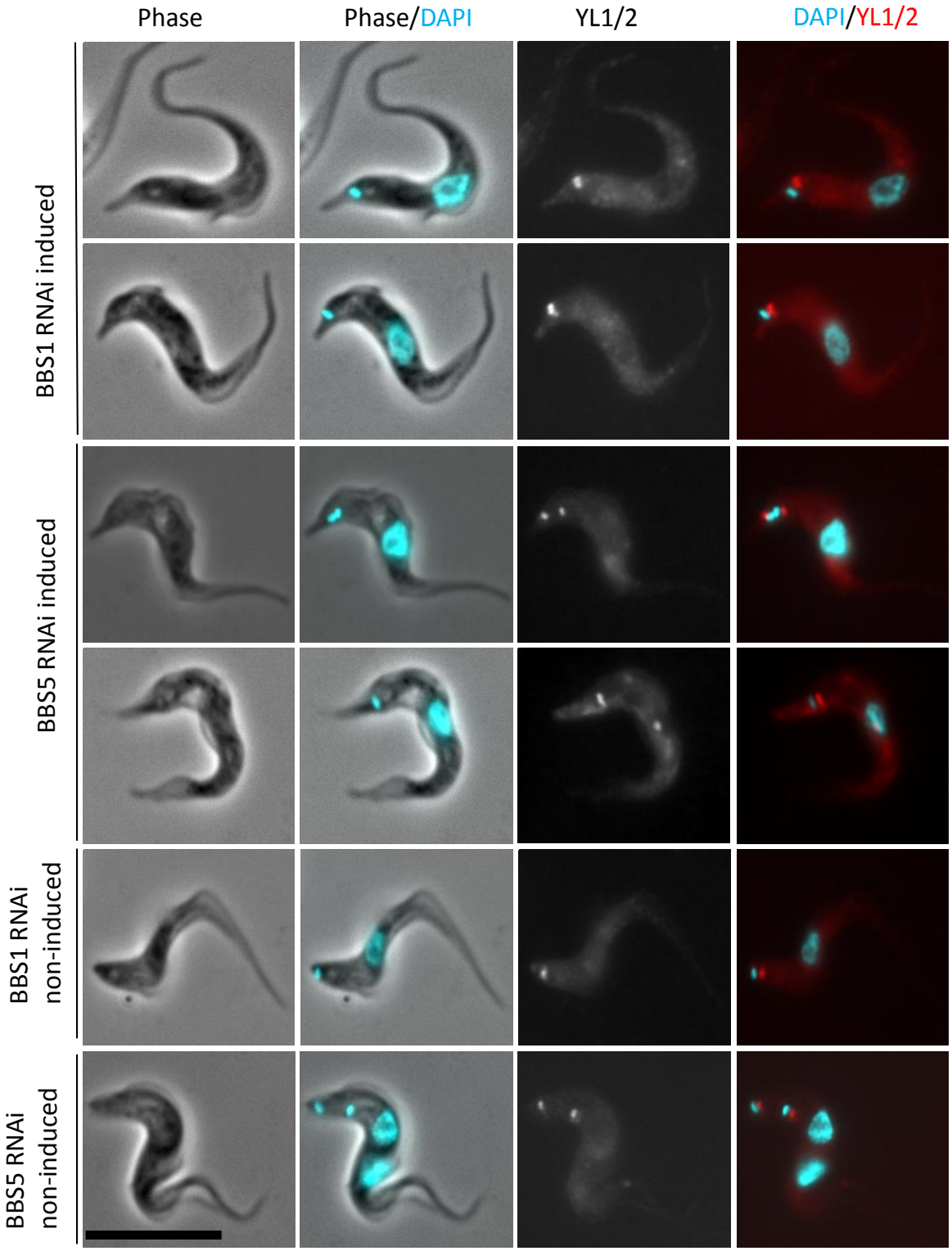

Figure 3.38 **Microscopic images of RNAi induced S16-BBS1RNAi and S16-BBS5RNAi cells following YL1/2 staining.** No strong signal of YL1/2 was observed at the posterior tip of BBS1 and BBS5 RNAi induced cells. BBS1 and BBS5 RNAi induced cell lines at 48 hours post induction were fixed with formaldehyde and labelled with YL1/2 antibody (red) for detecting tyrosinated arpha tubulin, and DAPI (blue). Scale bar:10 µm.

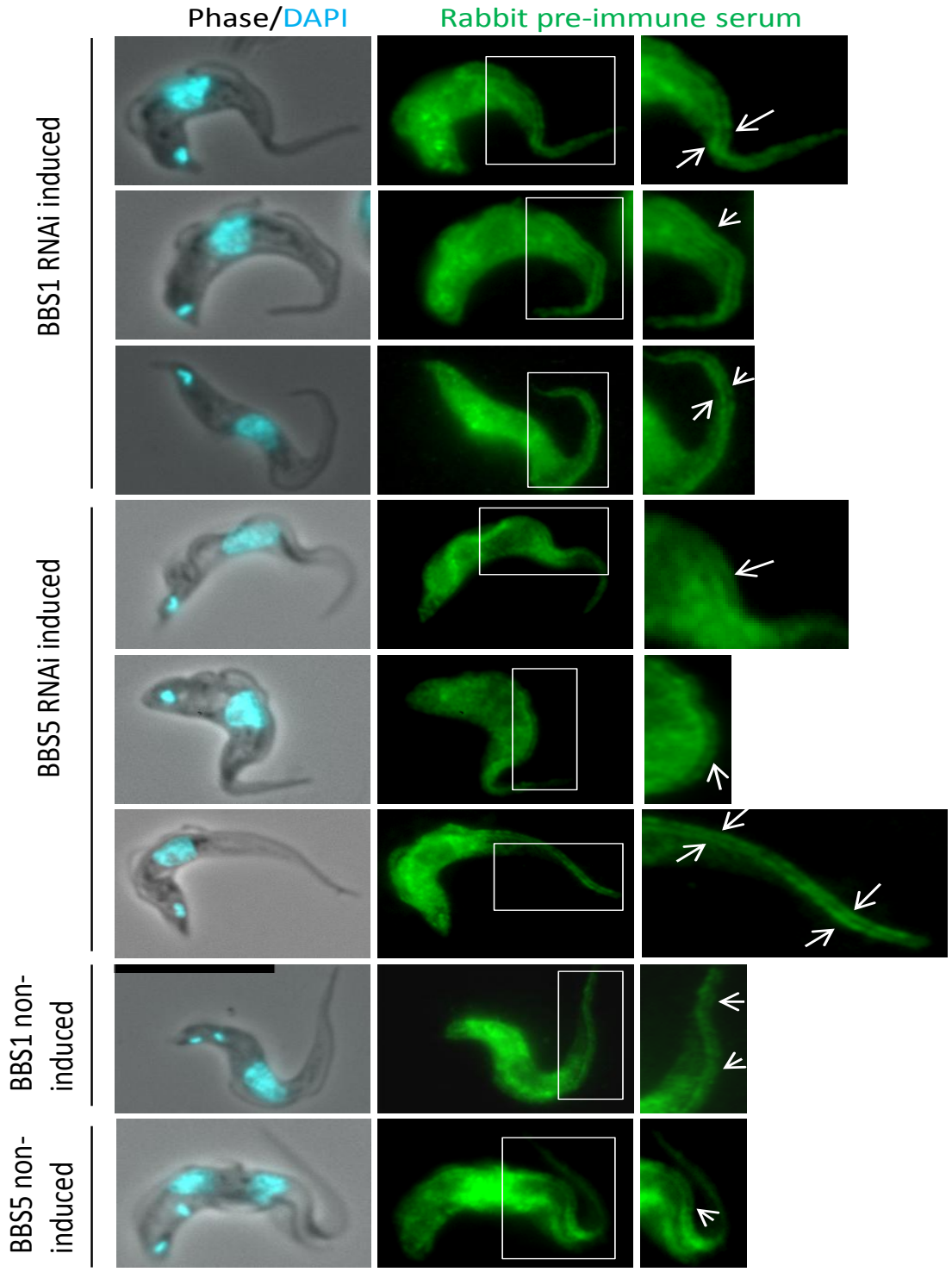

Figure 3.39 **Rabbit pre-immune serum staining for displaying the flagellar membrane in BBS1 and BBS5 RNAi induced cells in bloodstream form *T. brucei*.** BBS1 and BBS5 RNAi induced and non-induced cells were fixed with formaldehyde and labeled with DAPI (blue) and immunolabelled with rabbit pre-immune serum (green) at 48 hours post RNAi induction. RNAi induced cells showed no difference in their flagellar membrane staining pattern compared to non-induced cells. The magnified view of the area indicated by the white box shows the flagellar membrane stained by rabbit pre-immune serum. Arrows are showing the flagellar membrane stained by rabbit pre-immune serum. Scale bar: 10 µm.

knockdown of BBS1 caused a more severe population growth defect. The both RNAi induced S16-BBS1RNAi and S16-BBS5RNAi showed that knockdown of BBS1 and BBS5 did not affect the cell cycle regulation and that flagella were able to grow normally. Moreover, the ablation of BBS1 and BBS5 in bloodstream forms did not affect populating the flagellar membrane protein and cells were able to visualise their flagellar membrane, the same as for non-induced cells. Taken together, these results suggest that BBS1 and BBS5 are not critical for flagellum formation in the bloodstream form *T. brucei*.

3.5 Over-expression of BBS5 and BBS8 in a procyclic form *T. brucei* did not cause defects of growth and cell morphology.

To discover the subcellular localisation of BBS5 and BBS8 in the procyclic form *T. brucei* and to test whether high expression levels produce a cellular phenotype, BBS5 and BBS8 were over-expressed. For inducible over-expression, a pDEX-777 vector was used and the entire sequences of BBS5 and BBS8 were fused to TY tag without GFP tag. In this test, GFP was not tagged to the BBS proteins since one of the considerable reasons of weak protein expression of endogenously-tagged TY::GFP::BBS5 and undetectable TY::GFP::BBS8 protein might be due to tagging the GFP to BBS5 and BBS8, as GFP might hinder their protein expressions. Moreover, BBS9 was not able to be used for this experiment since the ORF of BBS9 contained a HindIII site, which exists also in the pDEX-777 vector and is used for joining the insert and vector. Using the pDEX-777 vector, I generated cell lines with BBS5 and BBS8 over-expressed with C-terminal TY-tagged in the parental cell line, SMOX P9, named BBS5::TY and BBS8::TY.

BBS5::TY and BBS8::TY were cultured with and without doxycycline and whole cell extracts were taken 24 hours after induction. Western blot analysis was performed in order to discern whether the protein expression had increased post induction. Western blotting using an anti-TY epitope

antibody, BB2, confirmed that the protein expression of BBS5::TY and BBS8::TY had increased after doxycycline induction, which was obvious from the comparison of endogenously-tagged proteins, BBS5/TY::GFP::BBS5 and BBS8/TY::GFP::BBS8 (Fig. 3.40). Since the levels of BBS5::TY and BBS8::TY tested by western blot appeared high, the growth and morphology of cells expressing ectopic BBS5::TY and BBS8::TY were assessed to confirm whether inducible expression of BBS5::TY and BBS8::TY might be producing any effects. The growth rate of cells expressing BBS5::TY and BBS8::TY in the presence and absence of doxycycline was monitored over 96 hours. The morphology of induced cells was also tested to detect any morphological differences compared to non-induced cells. Both BBS5::TY- and BBS8::TY-induced cells did not show any cell growth defect, as they were able to grow at the same rate as non-induced cells and parental cell line (Fig. 3.41 A, B). Moreover, induced BBS5::TY and BBS8::TY showed normal morphology, in that they were indistinguishable from non-induced cells, and all cells in each cell cycle stage were able to build flagellum (Fig. 3.42).

In order to discern the precise subcellular localisation of BBS5::TY and BBS8::TY, cells were fixed and immunolabelled with the anti-TY antibody, BB2, after 24 hours of induction and they were examined by fluorescence microscopy. At 24 hours post-induction, the induced BBS5::TY and BBS8::TY showed a strong signal throughout the cell, unlike the endogenously tagged TY::GFP::BBS5 showing its localisation at the base of flagellar pocket. Therefore, the exact subcellular localisation of TY::BBS5 and TY::BBS8 were not able to determine in the ectopically expressed cell lines, that nearly half of the cells (62% of induced BBS5::TY (n=85) and 60% of induced BBS8::TY (n=93)) showed saturated signals all over the cells, and the rest of the cells showed weaker signals, but still covered all of the cells. The western blot analysis showed a high expression level of BBS5::TY and BBS8::TY at 24 hours post induction; therefore, the protein expression might have started to increase at a very early stage after induction. Consequently, doxycycline-induced and non-induced BBS5::TY and BBS8::TY cells were fixed after 1 hour of induction and their localisations were examined by fluorescence microscopy. Nevertheless, 52%

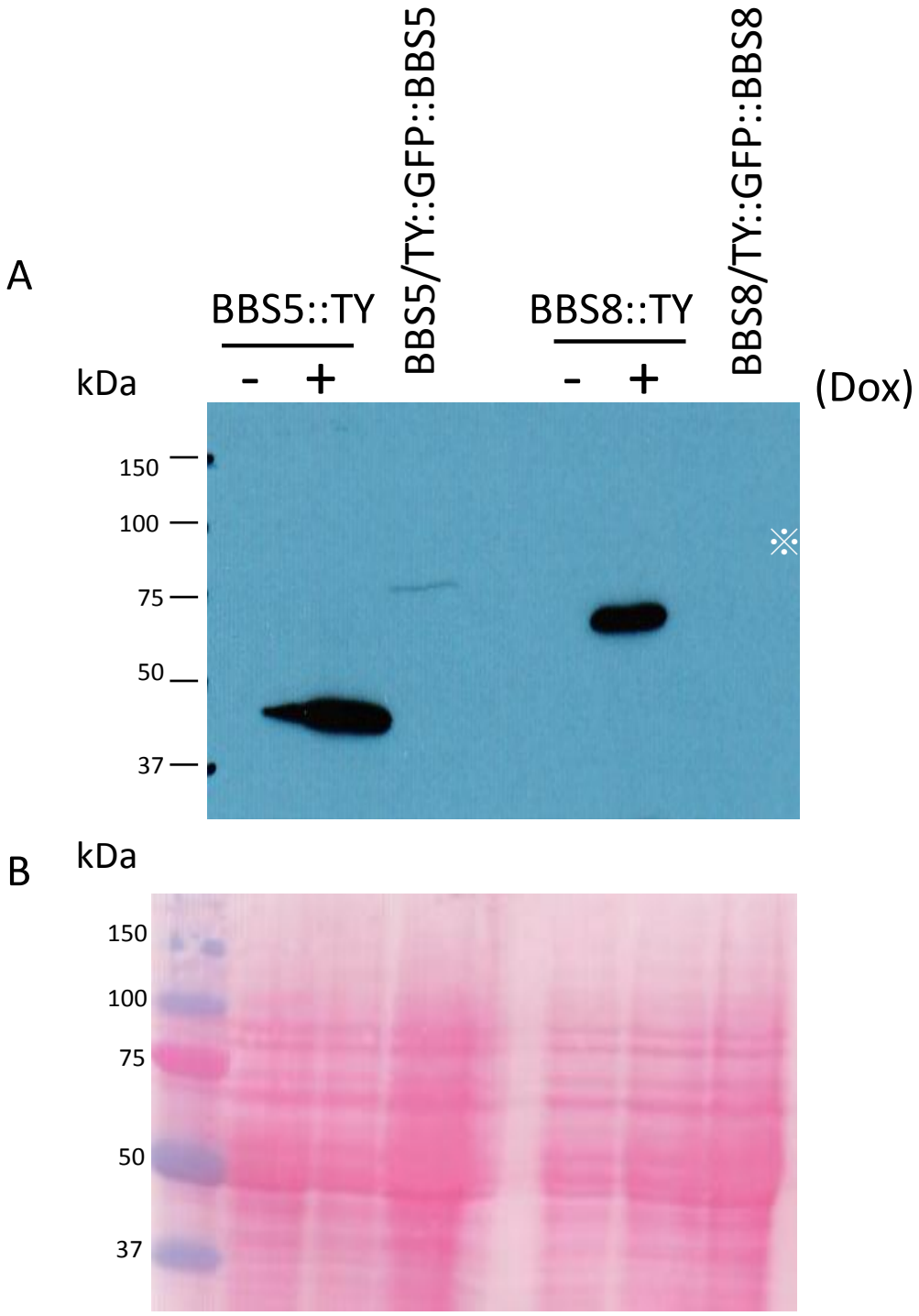

Figure 3.40 **Expression of BBS5::TY and BBS8::TY was increased at 24 hours post doxycycline induction.** Doxycycline inducible cell lines of BBS5::TY and BBS8::TY were cultured with (+) and without (-) doxycycline and whole cell lysates were isolated at 24 hours post induction for western blot analysis. In order to compare the level of protein after the induction, cell lysates of endogenously tagged cell line BBS5/TY::GFP::BBS5 and BBS8/TY::GFP::BBS8 were loaded, as well. (A) Western blot analysis using anti-TY epitope antibody, BB2 showing increased protein expression of BBS5::TY and BBS8::TY compared to endogenously tagged TY::GFP::BBS5 and TY::GFP::BBS8. Expected size of BBS5::TY is 43 kDa and BBS8::TY is 64 kDa. Expected size of Ty::GFP::BBS5 is 70 kDa and Ty::GFP::BBS8 is 91 kDa. (※ indicates the expected position of TY::GFP::BBS8 at the size of 91 kDa). (B) Loading control for the western blot analysis was provided by ponceau staining.

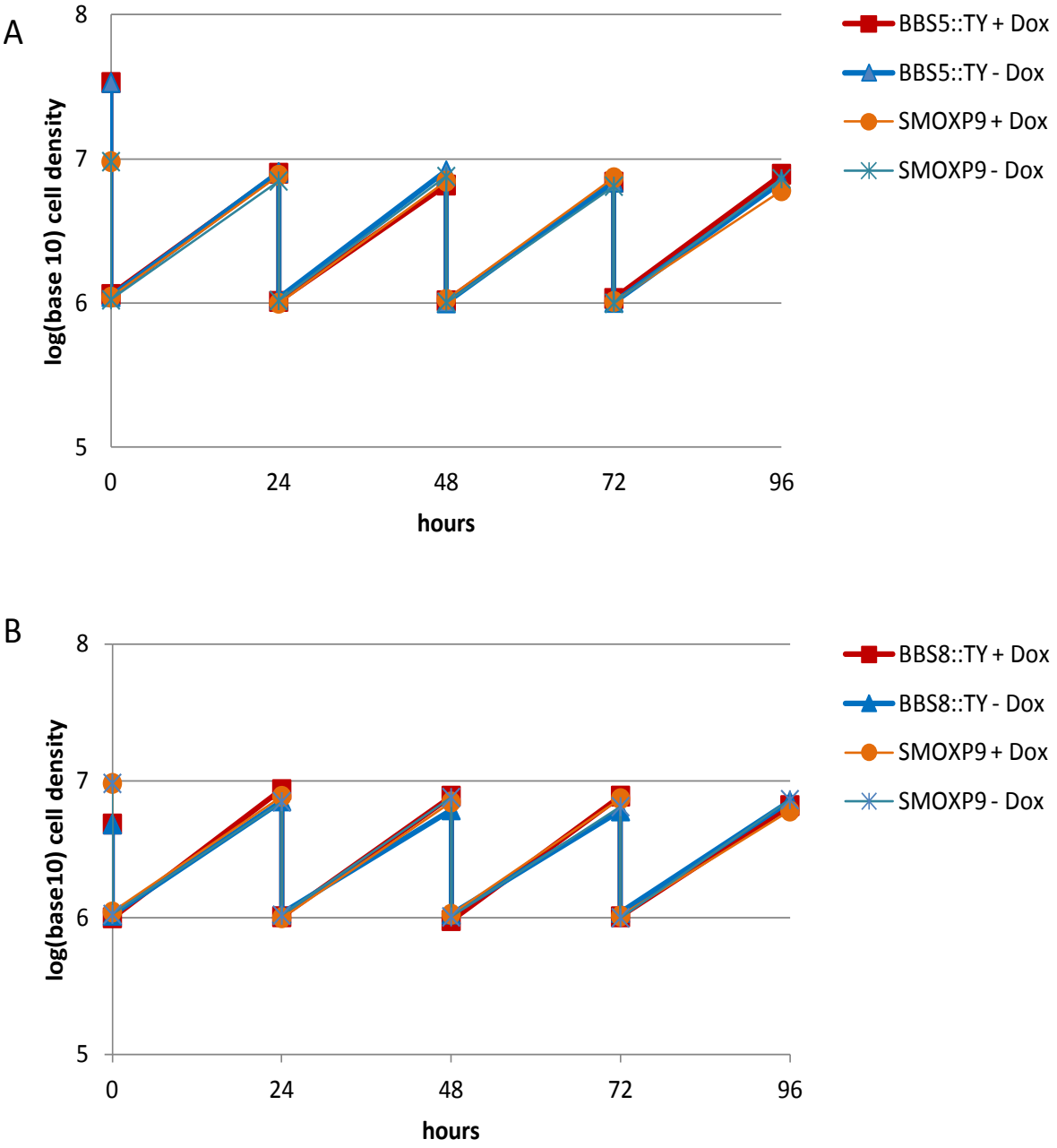

Figure 3.41 **Induction of BBS5::TY and BBS8::TY expression did not affect growth of procyclic form *T. brucei*.** Procyclic form cells possessing inducible BBS5::TY and BBS8::TY vectors were grown with (+Dox) or without (-Dox) doxycycline for 96 hours. Cells were counted every 24 hours and diluted to 1x 10^6 cells/ml. (A) No difference in cell growth was observed between induced and non-induced BBS5::TY cells. (B) No difference in cell growth was observed between induced and non-induced BBS8::TY cells. The parental cell line, SMOX P9, was used as a control and did not show any defect in cell growth by adding doxycycline.

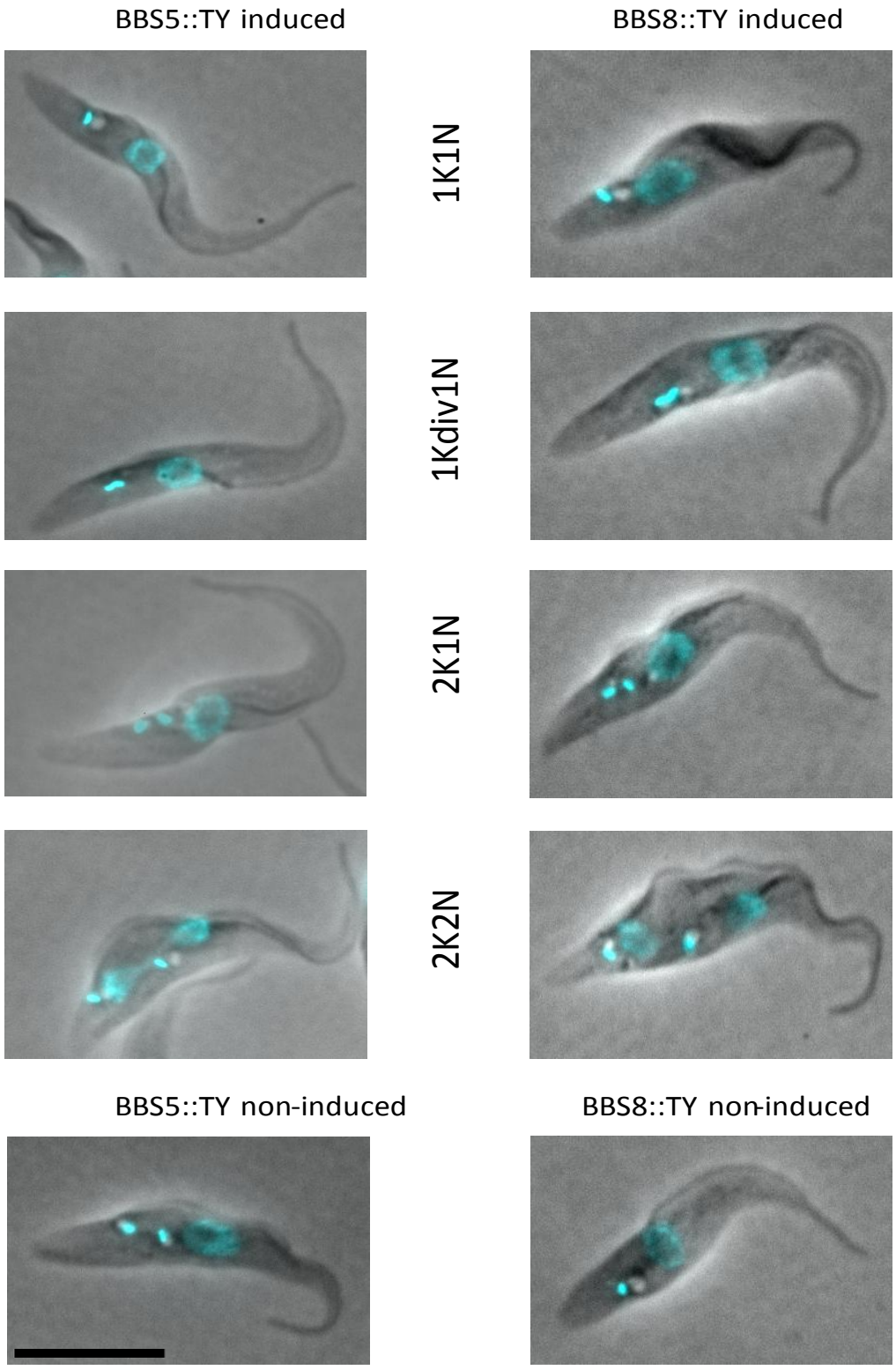

Figure 3.42 **Over-expression of BBS5::TY and BBS8::TY did not affect the cellular morphology.** BBS5::TY and BBS8::TY were induced for 24 hours, fixed, and labelled with DAPI for staining nucleus and kinetoplast (blue). Cells in every cycle stage were able to build flagellum and they were indistinguishable with non-induced cells. BBS5::TY and BBS8::TY cells are aligned in the order of cell cycle progression. Scale bar:10 μm.

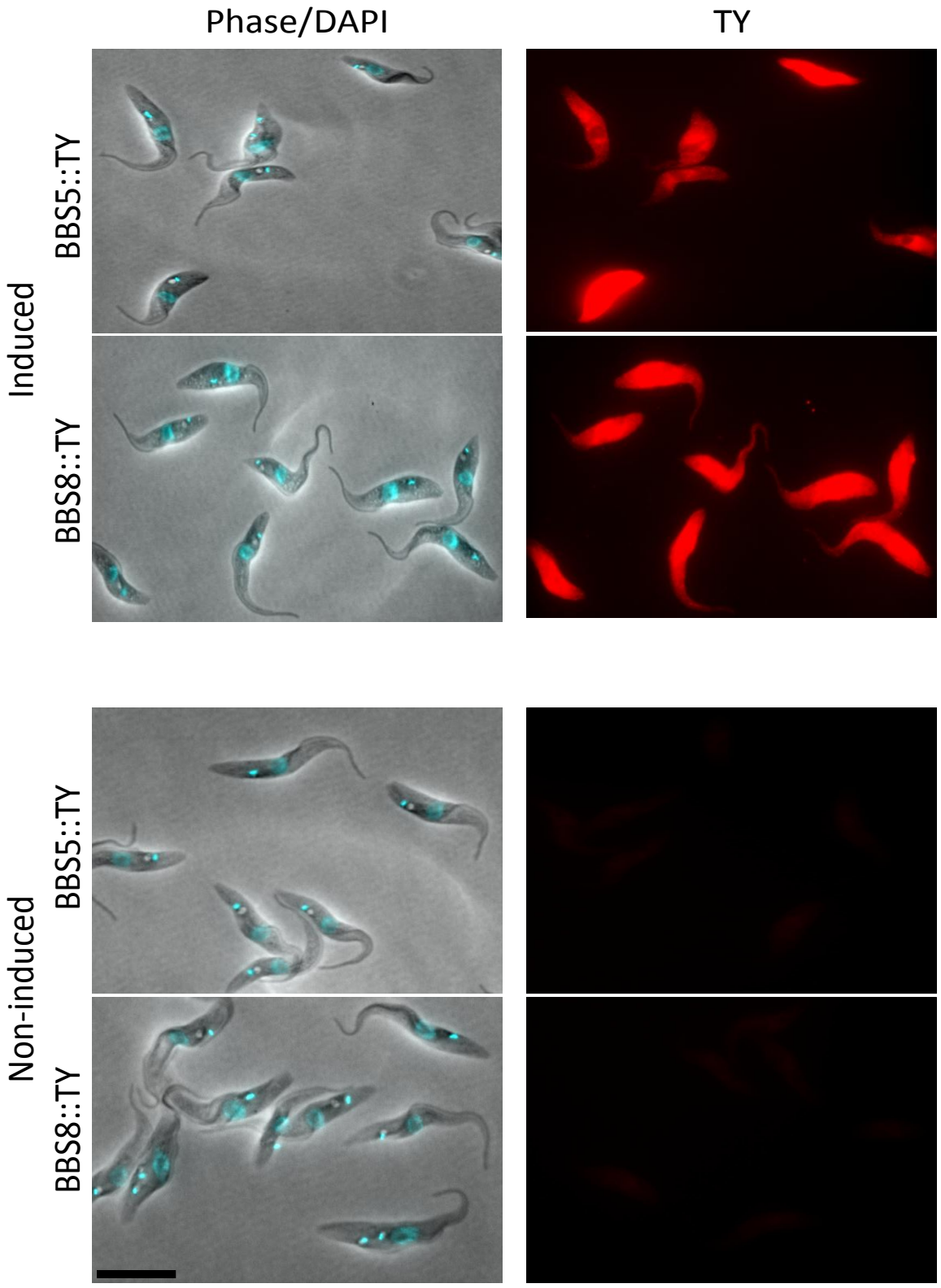

Figure 3.43 **Induction of BBS5::TY and BBS8::TY showed strong signal expression of BBS5::TY and BBS8::TY throughout the cells.** After 24 hours of induction, induced and non-induced BBS5::TY cell line and BBS8::TY cell line were, fixed, and labelled with DAPI (blue) and an anti-TY antibody, BB2. Induced cells showed strong signal that covers the whole cell. The non-induced cells showed no signal of BBS5::TY and BBS8::TY. Scale bar:10 µm.

of induced BBS5::TY (n=86) and 47% of BBS8::TY (n= 88) showed saturated signals all over the cells, and rest of the cells had less intense signals, yet the entire cells were covered with signals (Fig 3. 43). Consistent to the strong expression of BBS5::TY and BBS8::TY confirmed by the western blot, the BBS5::TY and BBS8::TY were over-expressed and therefore, they were possibly not able to localise to the correct localisation in the cell. In this test, a high level of protein expression was observed at 24 hours post induction, but how quickly the protein was produced was not measured. Therefore, the time course of protein expression had to be performed to measure the speed of induction by western blot, and then estimate the appropriate induction time for assessing the localisation of BBS5::TY and BBS8::TY. Furthermore, doxycycline had to be titrated for optimising dilutions to discern the most effective concentration for BBS5::TY and BBS8::TY induction.

3.6 Knockdown of BBSome subunits to find the interdependence of BBS5 and BBSome subunits

Previous studies showed that several BBSome subunits are essential for specific BBSome protein's ciliary localisation in *C. elegans, C. reinhardtii*, and Human retinal pigment epithelial cells (hTERT-RPE1 cells) (Lechtreck et al., 2009; Ou et al., 2007; Seo et al., 2011). However, it is not clear which BBSome subunits are essential for BBS5 localisation and expression in *T. brucei;* also the interdependency of BBSome subunits in *T. brucei* is not known. In order to address this issue, I knocked-down all 7 BBSome subunits (BBS1, BBS2, BBS4, BBS7, BBS8, and BBS9) individually based on the cell lines where endogenous BBS5 is tagged with TY::GFP, BBS5/TY::GFP::BBS5 cell line, in order to test whether ablation of individual BBSome proteins affected the protein expression and localisation of TY::GFP::BBS5. As a control, BBS5 was also knocked-down in BBS5/TY::GFP::BBS5. In order to knockdown each BBSome subunit, approximately 200bp of each BBSome subunit' ORFs were inserted into p2T7-177 vector. The p2T7-177 vectors containing BBS1,

BBS2, BBS4, BBS7, BBS8, and BBS9 were transfected into BBS5/TY::GFP::BBS5, and 2 independent clones were isolated. The generated clonal cell lines are named as follows: BBS1^{RNAi} -BBS5/TY::GFP::BBS5-B6 and -F7; BBS2^{RNAi} -BBS5/TY::GFP::BBS5-3D and -6H; BBS4^{RNAi} -BBS5/TY::GFP::BBS5-A and -B; BBS7^{RNAi} -BBS5/TY::GFP::BBS5-A and -B; BBS8^{RNAi} -BBS5/TY::GFP::BBS5-2D and -6A; and BBS9^{RNAi}/TY::GFP::BBS5-7A and -4D. In section 3.3, western blot analysis showed that the amount of TY::GFP::BBS5 was most reduced at 48 hours post-induction. Therefore, cell cultures of RNAi inducible cell lines of each BBSome subunit were cultured with and without doxycycline and whole cell lysates were isolated at 48 hours post-RNAiinduction. In order to discern whether the knockdown of individual BBSome subunits affected the protein expression of TY::GFP::BBS5, western blot analysis was carried out. Western blot analysis using an anti-TY antibody, BB2, demonstrated that the level of TY::GFP::BBS5 in RNAi induced BBS5/TY::GFP::BBS5 was decreased compared to non-induced cells at 48 hours post-RNAi induction (Fig. 3.44). Therefore, this confirmed that the doxycycline was able to induce RNAi and amount of TY::GFP::BBS5 was reduced in the BBS5/TY::GFP::BBS5 cell line. However, expression of TY::GFP::BBS5 was not affected in any of the BBSome proteins ablated cells, as the expression of TY::GFP::BBS5 was intact in BBS1, BBS2, BBS4, BBS7, BBS8, and BBS9 RNAi induced cells (Fig. 3.44, 45). BBS2 RNAi induced cell showed weak protein expression of TY::GFP::BBS5 compared to non-induced cells, yet this was due to the low amount of cell lysate that was loaded which could be seen via the ponceau staining (Fig. 3.44 B). Next, to examine whether knockdown of each BBSome subunit affected the cell growth, individual BBSome subunit RNAi inducible cell lines were diluted to $1x10^5$/ml and cells were cultured in the presence and absence of doxycycline. The population growth rate was monitored for 120 hours without dilution, as was the parental cell line, BBS5/TY::GFP::BBS5. RNAi induction of BBSome subunits did not affect the population growth rate, as all RNAi induced cells were able to grow at the same rate as non-induced cells and were able to grow such that they reached a high cell density (Fig. 3. 46, 47).

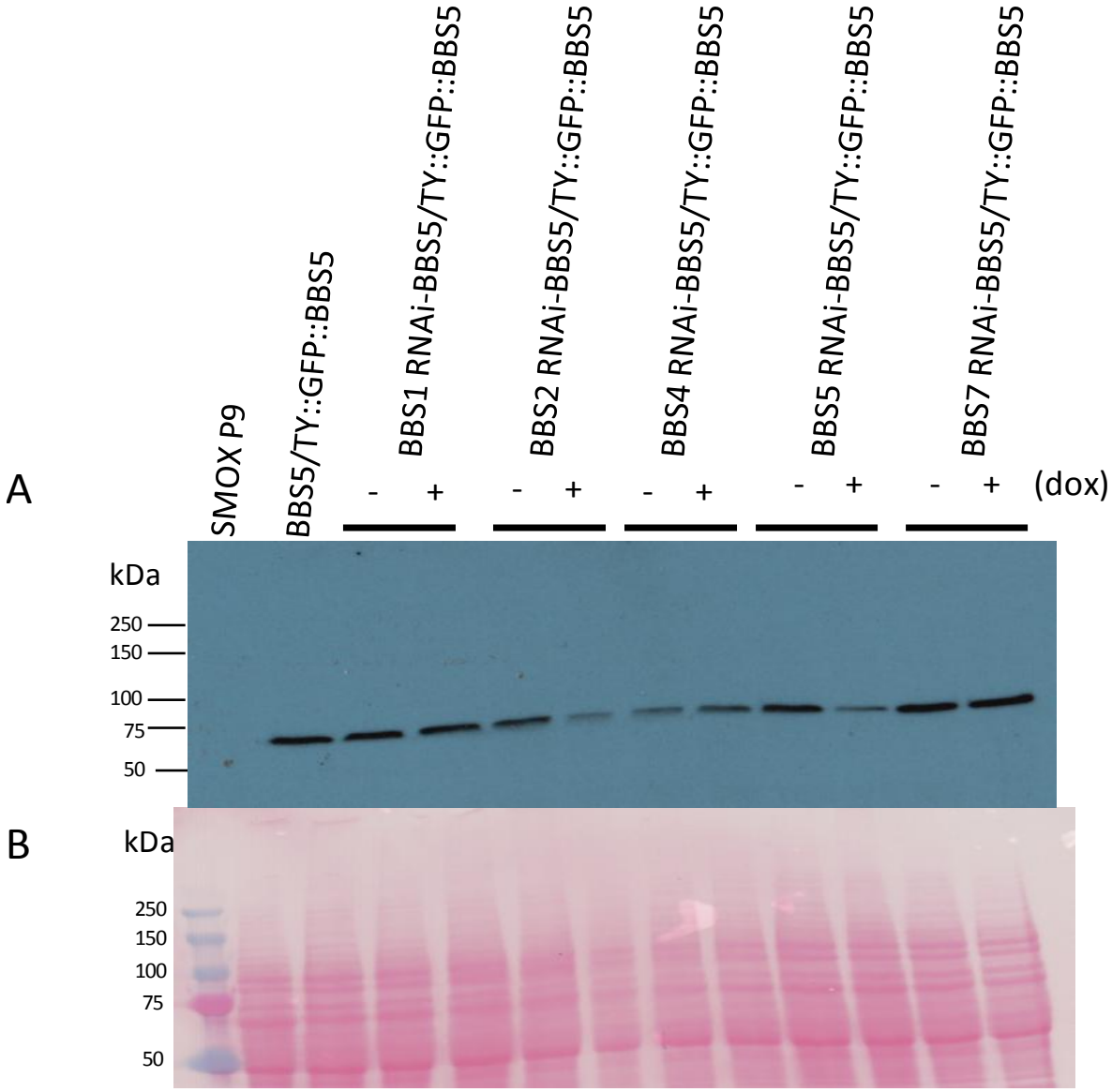

Figure 3.44 **Knockdown of each individual BBSome component did not affect the TY::GFP::BBS5 expression in procyclic form *T. brucei*.** BBS5/TY::GFP::BBS5 containing RNAi inducible vectors for BBS1, BBS2, BBS4, BBS5, and BBS7 knockdown individually were cultured with (+) and without (-) doxycycline and whole cell lystates were taken at 48 hours post induction. (A) Western blot analysis using anti-TY antibody, BB2 showed reduced protein expression of TY::GFP::BBS5 in RNAi induced BBS5 RNAi in BBS5/TY::GFP::BBS5 cells. However, expression level of TY::GFP::BBS5 remained the same in BBS1, BBS2, BBS4, and BBS7 ablated cells. BBS5/TY::GFP::BBS5 was used as a positive control and SMOX P9 was used as a negative control of blotting. All bands were not positioned at the same height since the cell lysates were not run straight, which is visible in ponceau staining. Loaded per lane: $5x10^6$ cells/lane. (B) Loading control for the western blot analysis was provided by ponceau staining.

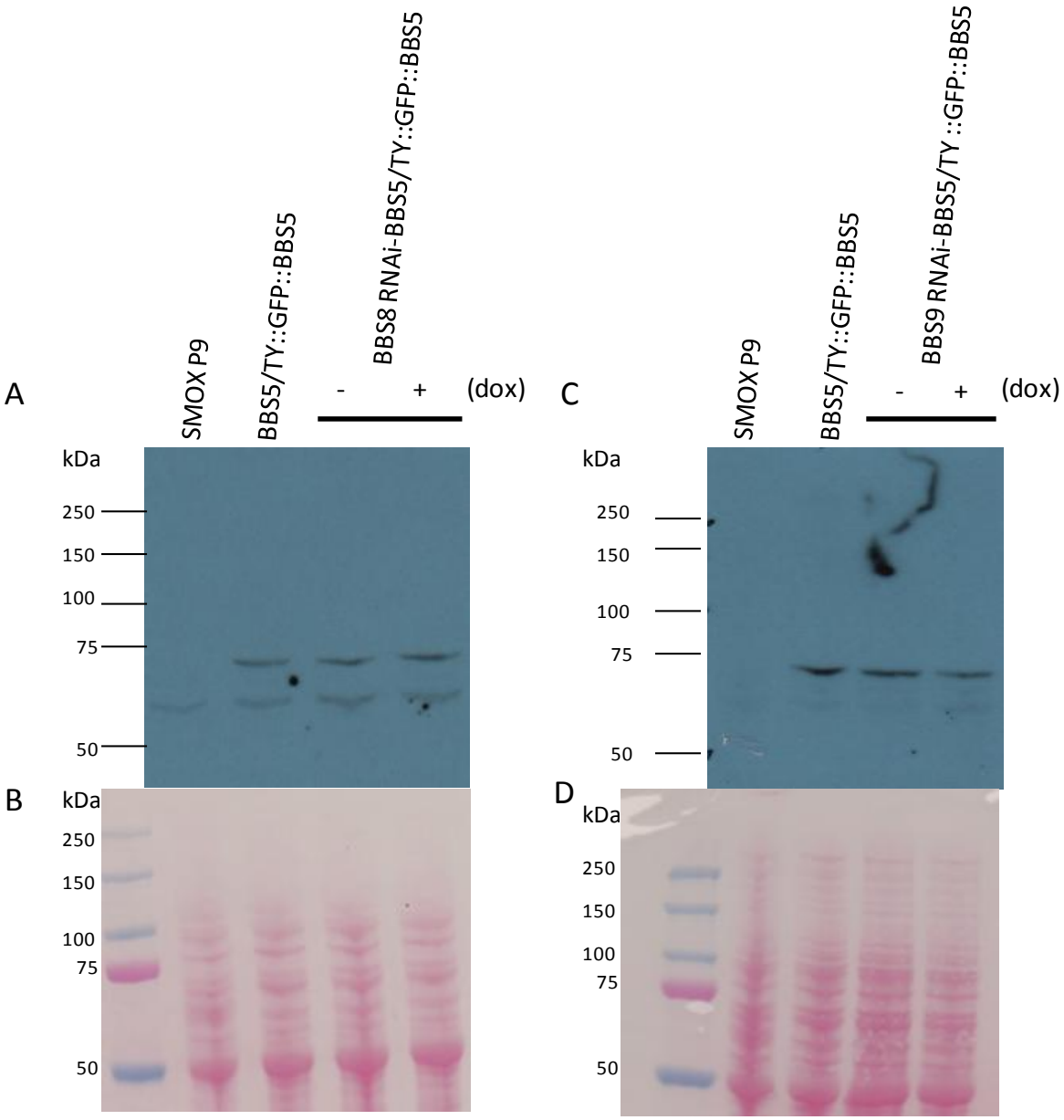

Figure 3.45 **Knockdown of BBS8 and BBS9 did not affect the TY::GFP::BBS5 expression in procyclic form *T. brucei*.** BBS5/TY::GFP::BBS5 containing RNAi inducible vectors for BBS8 and BBS9 knockdown individually were cultured with (+) and without (-) doxycycline and whole cell lystaes were taken at 48 hours post induction. The effect of BBS8 and BBS9 knock down to TY::GFP::BBS5 was evaluated by western blot using anti-TY antibody, BB2. (A) The expression level of TY::GFP::BBS5 was not affected in BBS8 RNAi induced cells. (C) The expression level of TY::GFP::BBS5 was not affected in BBS9 RNAi induced cells. BBS5/TY::GFP::BBS5 was used as a positive control and SMOX P9 was used as a negative control of blotting. Loaded per lane: $5x10^6$ cells/lane. (B, D) Loading control for the western blot analysis was provided by ponceau staining.

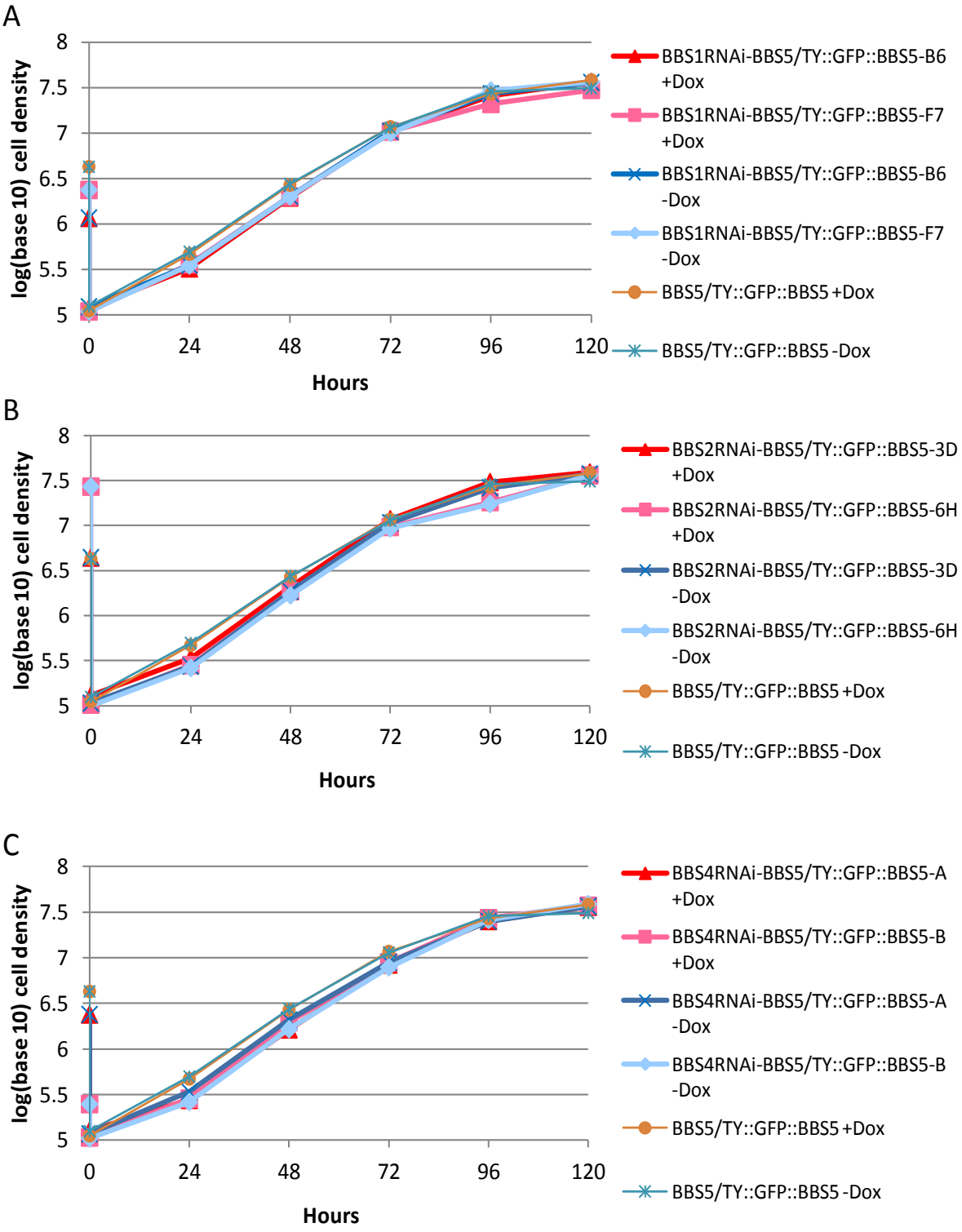

Figure 3.46 **RNAi of BBS1, BBS2, and BBS4 in BBS5/TY::GFP::BBS5 did not affect the population growth.** BBS5/TY::GFP::BBS5 cells containing BBS1, BBS2, and BBS4 RNAi inducible vectors were cultured with (+) and without (-) doxycycline for 120 hours without dilution, as well as parental cell line BBS5/TY::GFP::BBS5. Growth curves show the effect of RNAi on BBS1 (A), BBS2 (B), and BBS4 (C) in BBS5/TY::GFP::BBS5 cells. Ablation of BBS1, BBS2, and BBS4 over BBS5/TY::GFP::BBS5 did not cause a change in the population growth rate. BBS5/TY::GFP::BBS5 did not show any defect in cell growth by adding doxycycline.

A

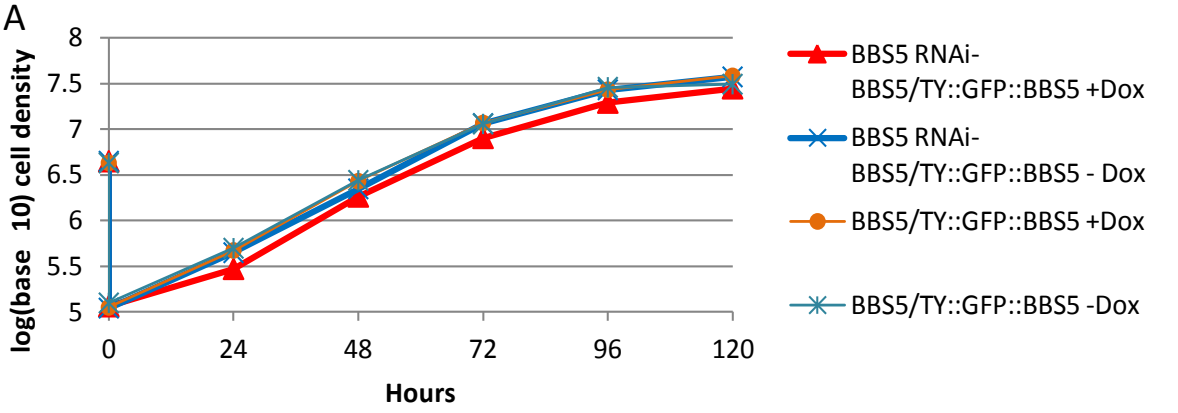
log(base 10) cell density
8
7.5
7
6.5
6
5.5
5
0
24
48
72
96
120
Hours
BBS5 RNAi-BBS5/TY::GFP::BBS5 +Dox
BBS5 RNAi-BBS5/TY::GFP::BBS5 - Dox
BBS5/TY::GFP::BBS5 +Dox
BBS5/TY::GFP::BBS5 -Dox

B

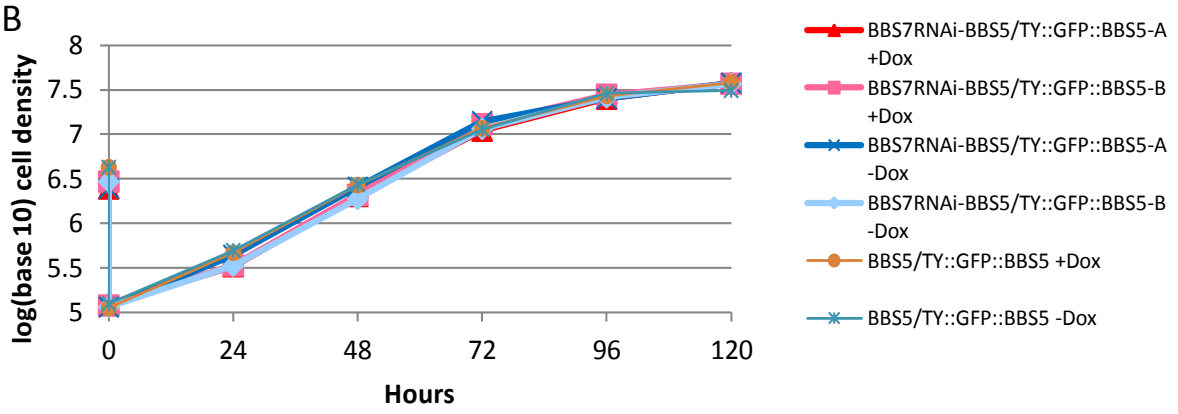
log(base 10) cell density
8
7.5
7
6.5
6
5.5
5
0
24
48
72
96
120
Hours
BBS7RNAi-BBS5/TY::GFP::BBS5-A +Dox
BBS7RNAi-BBS5/TY::GFP::BBS5-B +Dox
BBS7RNAi-BBS5/TY::GFP::BBS5-A -Dox
BBS7RNAi-BBS5/TY::GFP::BBS5-B -Dox
BBS5/TY::GFP::BBS5 +Dox
BBS5/TY::GFP::BBS5 -Dox

C

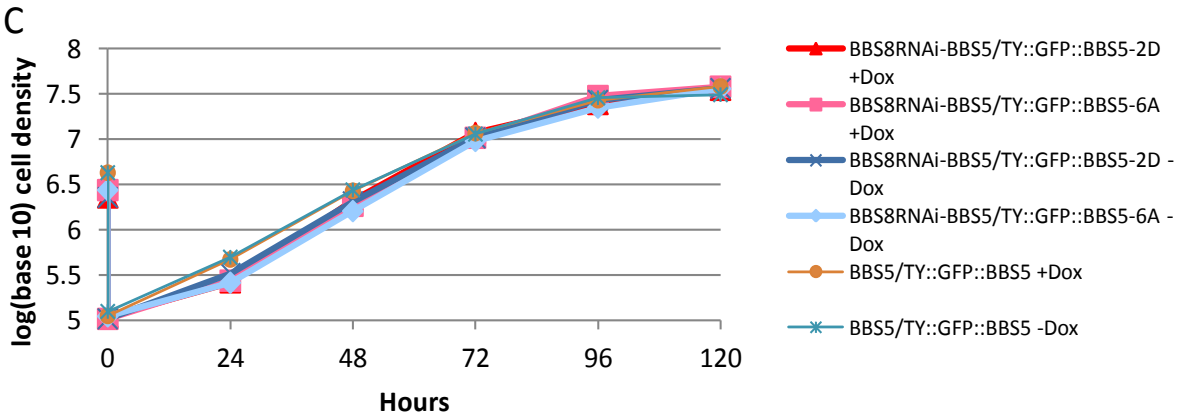
log(base 10) cell density
8
7.5
7
6.5
6
5.5
5
0
24
48
72
96
120
Hours
BBS8RNAi-BBS5/TY::GFP::BBS5-2D +Dox
BBS8RNAi-BBS5/TY::GFP::BBS5-6A +Dox
BBS8RNAi-BBS5/TY::GFP::BBS5-2D -Dox
BBS8RNAi-BBS5/TY::GFP::BBS5-6A -Dox
BBS5/TY::GFP::BBS5 +Dox
BBS5/TY::GFP::BBS5 -Dox

D

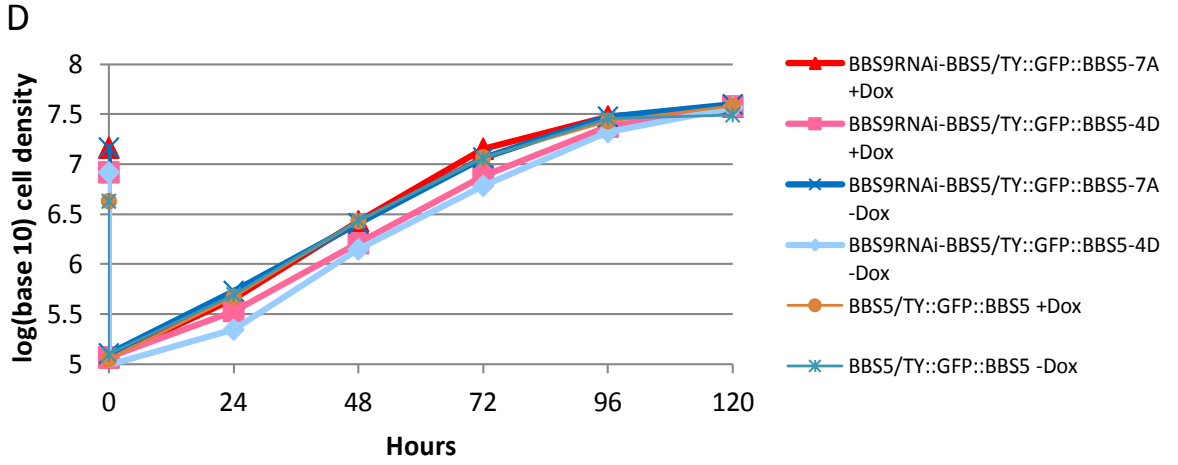
log(base 10) cell density
8
7.5
7
6.5
6
5.5
5
0
24
48
72
96
120
Hours
BBS9RNAi-BBS5/TY::GFP::BBS5-7A +Dox
BBS9RNAi-BBS5/TY::GFP::BBS5-4D +Dox
BBS9RNAi-BBS5/TY::GFP::BBS5-7A -Dox
BBS9RNAi-BBS5/TY::GFP::BBS5-4D -Dox
BBS5/TY::GFP::BBS5 +Dox
BBS5/TY::GFP::BBS5 -Dox

Figure 3.47 **RNAi of BBS7, BBS8, and BBS9 in BBS5/TY::GFP::BBS5 did not affect the population growth.** BBS5/TY::GFP::BBS5 cells containing BBS7, BBS8, and BBS9 RNAi inducible vectors were cultured with (+) and without (-) doxycycline for 120 hours without dilution, as well as parental cell line BBS5/TY::GFP::BBS5. Growth curve showing the effect of RNAi on BBS7 (B), BBS8 (C), and BBS9 (D) in BBS5/TY::GFP::BBS5 cells. As a control, BBS5RNAi-BBS5/TY::GFP::BBS5 cell line was cultured with (+) and without (-) doxycycline (A). Ablation of BBS7, BBS8, and BBS9 over BBS5/TY::GFP::BBS5 did not cause a change in the population growth rate. Ablation of BBS5 in BBS5/TY::GFP::BBS5 showed slight growth defect.

The BBSome is a protein complex involving 7 BBS proteins. Nachury et al. demonstrated that BBSome proteins interact with each other, particularly BBS9 interacts with BBS1, BBS2, BBS4, BBS5, and BBS8 suggesting that BBS9 is a central organising subunit of the BBSome (Nachury et al., 2007). In addition, Zhang et al. also showed that BBS5 is a peripheral subunit of the BBSome and BBS9 is only an interacting component (Zhang et al., 2012). Therefore, among the BBSome proteins, BBS9 is considered as one of the best candidates which associate with BBS5. RNAi was induced in BBS9^{RNAi}-BBS5/TY::GFP::BBS5 cell line and the localisation of TY::GFP::BBS5 was examined to test whether knockdown of BBS9 affected the cellular localisation of BBS5. After 48 hours of RNAi induction, BBS9 RNAi induced and non-induced cells were fixed and labelled with DAPI and immunolabelled with an anti-GFP antibody. Microscopic examination showed that BBS9 RNAi induced cells looked morphologically normal and no significant difference was observed compared to non-induced cells. Furthermore, as shown by western blot, the signal of TY::GFP::BBS5 did not decrease in RNAi induced cells. The localisation pattern of TY::GFP::BBS5 in RNAi induced BBS9^{RNAi}-BBS5/TY::GFP::BBS5 cells showed that the position of TY::GFP::BBS5 was not affected and appeared the same as in non-induced cells (Fig. 3.48). In 1K1N cells, BBS9 RNAi induced cells showed a single TY::GFP::BBS5 focus localised at the base of flagellum emerging from the flagellar pocket, and non-induced cell also showed that TY::GFP::BBS5 was at the base of the flagellum. When the kinetoplast is elongated at the end of a 1K1N cell, the TY::GFP::BBS5 localisation pattern in both RNAi induced and non-induced cells showed that the foci of TY::GFP::BBS5 is duplicated. 2K1N and 2K2N cells in both RNAi induced and non-induced cells showed two TY::GFP::BBS5 localising at the proximal end of flagella. All cells in each cell cycle stage possessed flagellum and the emergence of a new flagellum was seen in 2K1N and 2K2N cells.

In summary, knockdown of each BBSome subunit did not affect the protein expression of TY::GFP::BBS5, and the absence of single BBSome subunits did not affect the TY::GFP::BBS5 expression. Moreover, the BBS5/TY::GFP::BBS5 cells were able to grow normally after RNAi

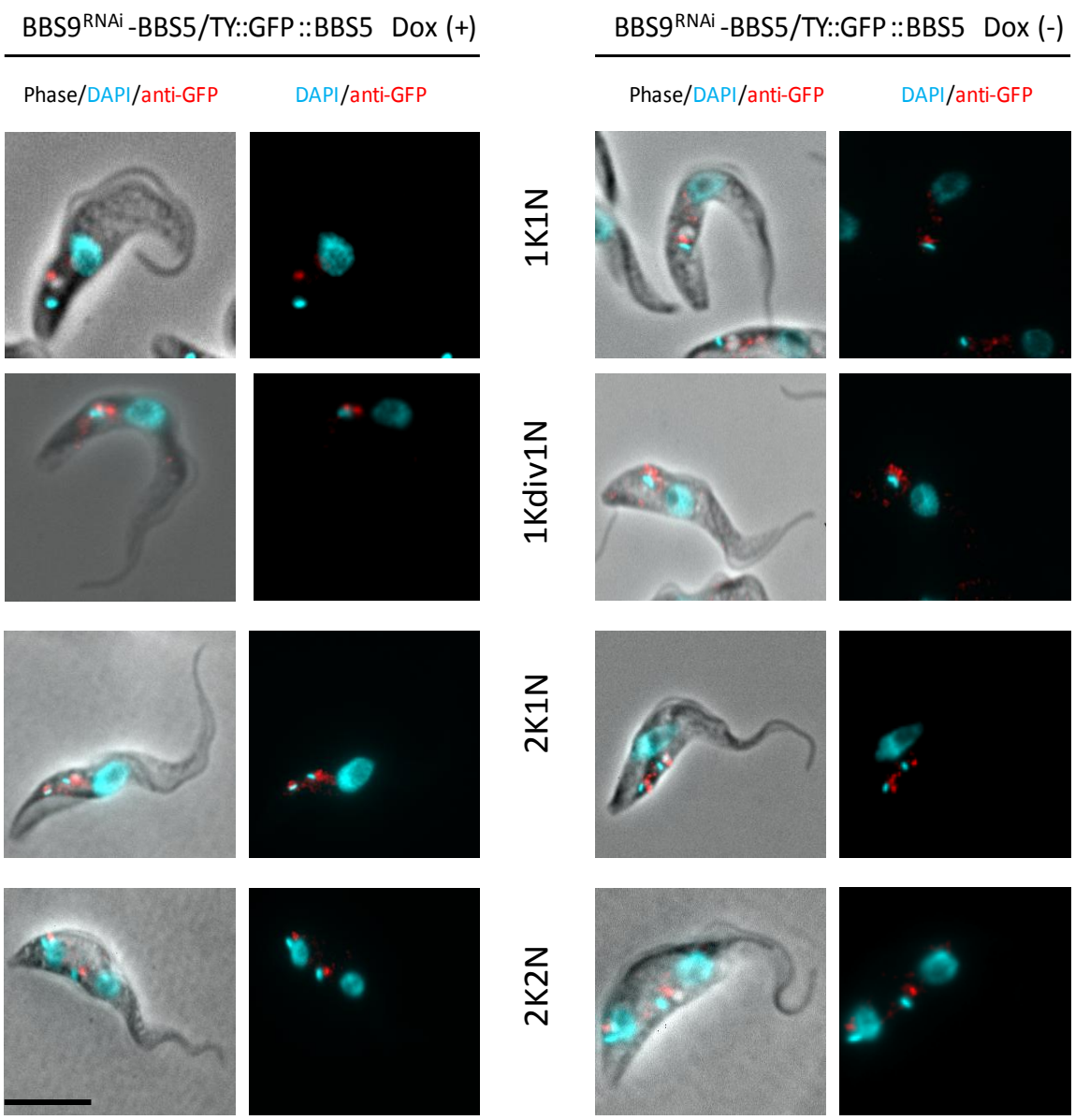

Figure 3.48 **Knockdown of BBS9 in BBS5/TY::GFP::BBS5 did not affect the localisation of TY::GFP::BBS5 and cellular morphology**. BBS5/TY::GFP::BBS5 containing the BBS9 RNAi inducible vector was cultured with (+) and without (-) doxycycline. At 48 hours post RNAi induction, cells were fixed and stained with DAPI (blue) and anti-GFP antibody (red) to determine the localisation of TY::GFP::BBS5 had been affected. The position of TY::GFP::BBS5 remained the same and no significant difference was seen in RNAi induced cells compared to non-induced cells. Cellular morphology was indistinguishable with non-induced cells and all cells in each cell cycle stage possessed flagellum. Images of cells were aligned in the order of cell cycle progression. Scale bar:10 µm.

TY::GFP::BBS5 in doxycycline added BBS5RNAi-BBS5/TY::GFP::BBS5, thereby implying that doxycycline was able to induce RNAi in the cells. Nevertheless, the effect of RNAi on each BBSome subunit was not measured and therefore we cannot conclude that BBS5 is not associated with other BBSome proteins. If the reduced level of BBSome subunits was confirmed, including BBS9, then it could be estimated that BBS5 functions independently and is able to localise at the transition zone.

Chapter 4

Discussion

4. Discussion

In my thesis, I characterised BBS5, which is the one of the components of the BBSome to address its localisation and function in flagellum formation in *T. brucei*. This work represents the first analysis of BBS5 function and localisation in *T. brucei.*

BBS5 is more frequently conserved among ciliated eukaryotes than other BBSome subunits (Hodges et al., 2010; Nachury et al., 2007), and its lipid binding capability has been demonstrated in mammalian cells (Nachury et al., 2007). In this thesis, I showed that *T. brucei* BBS5 has a predicted membrane binding domain and BBS5 is localises to the transition zone at the base of the flagellum in the procyclic form *T. brucei.* However, the BBS5 knockdown did not cause any defect in flagellum formation or cell morphology, suggesting that BBS5 function is not required for flagellum assembly in *T. brucei*.

4.1 The BBSome is evolutionally conserved across ciliated eukaryotic organisms

The conservation of each BBSome component (BBS1, BBS2, BBS4, BBS5, BBS7, BBS8, and BBS9) among ciliated eukaryotes was assessed by a comparison of the relevant amino acid sequences between selected ciliated eukaryotes. The BBSome components are highly conserved among ciliated eukaryotes, and they contain domains that reflect their potential functions. With the exception of *T. brucei* BBS9, the domains of all of the BBSome proteins have been characterised: the *T. brucei* orthologues BBS1, BBS2, and BBS7 contain WD-40 repeat domains, which form a β-propeller domain; BBS4 and BBS8 contain multiple TPR repeats; and BBS5 mostly consists of a DUF1448 that belongs to the PH domain family. According to the domain analysis presented in my thesis, it is feasible that BBS1, BBS2, and BBS7 form a core/scaffold of the BBSome and recruit other BBSome proteins, such as BBS4 and BBS8, which also possess protein-protein interaction

capability, to promote the assembly of the complex. BBS5 may not be required for BBSome assembly, but it may be critical for linking the BBSome to the membrane.

The disease causing residues in the BBS5 amino acid sequence have been remarkably well conserved across the ciliated eukaryotes. Previous studies have revealed that BBS5 is more conserved than other BBSome subunits (Hodges et al., 2010; Nachury et al., 2007); together with my findings, this observation suggests that the BBS5 interaction with lipids is essential for the BBSome function. It is assumed that the BBSome is required for ciliary membrane biogenesis by trafficking specific receptor proteins to the ciliary membrane, and the conservation of BBS5 allows the BBSome to associate with the cell membrane and mediate the signal detection necessary for sustaining the physiology of the cell.

4.2 BBS5 localisation to the transition zone

This study provides the first clue that BBS5 is localised at the transition zone of procyclic form *T. brucei*. A short evolutionarily conserved subcompartment, transition zone, is localised within the flagellar pocket and the site which the central pair of microtubules elongate from the basal plate. Moreover, the flagellar membrane initiates from this region. The localisaiton of BBS5 to the transition zone was further confirmed by co-staining the cells with the YL1/2 antibody, which recognises the transition fibres radiating from the distal end of the basal body (Stephan et al., 2007).

The structure of the proximal end of the flagellum begins with the basal body. The basal body, which is formed by microtubule triplets, is positioned at the extreme proximal end of the flagellum, and the transition fibres radiate out from the distal end of the basal body. At the end of the basal body, the transition zone begins and the triplets become to doublet microtubules. Because TY::GFP::BBS5 was localised above YL1/2 with a small gap, it is plausible that BBS5 is localised to the transition zone within the flagellar pocket.

A recent study revealed that three critical structures exist between the basal body and flagellum, which help to differentiate the flagellar membrane from the flagellar pocket. They are, the transition fibres, the external collarette, and the radial fibres (Lacomble et al., 2009). As described above, the transition fibres are pinwheel-like structures that connect the distal end of the basal body with the flagellar membrane at the base of the flagellar pocket (Lacomble et al., 2009; Reiter et al., 2012). The collarette is positioned in the flagellar membrane of the flagellar pocket lumen, which surrounds the flagellum at the proximal end of the transition zone (Lacomble et al., 2009). The structure of the collarette is well organised, that is similar to the nine microtubule doublets; the nine regularly positioned double tubule-like units are connected to one-another, making a necklace-like structure that surrounds the flagellum (Lacomble et al., 2009). The radial fibres lie within the flagellar membrane of the basal body and the transition zone region that physically separate the flagellum from the cytoplasm (Lacomble et al., 2009). Because the exact localisation and structure of BBS5, i.e., whether the feature is similar to the collarette or radial fibres is unclear, immuno-gold labelling will be useful to pinpoint the localisation of BBS5 at the base of the flagellum.

Because BBS5 is predicted to have the capacity for lipid binding in mammalian cells and BBS5 is located at the proximal end of the flagellum in *T. brucei*, it is tempting to speculate that BBS5 is localised to the flagellar membrane surrounding the flagellum at the transition zone. In particular, *T. brucei* BBS5 contains a DUF1448, a member of the PH domain family that is able to bind to lipids. Moreover, a lipid dense structure, called the diffusion barrier is present at the proximal base of the cilium, which is the transition zone region with its accessory structures for creating a boundary of the ciliary membrane and plasma membrane in mammalian cells (Hu et al., 2010; Vieira et al., 2006). This diffusion barrier prevents the free entry of vesicles to the ciliary membrane; hence vesicles accumulate at the base of the cilium and fuse with the periciliary membrane. In *T. brucei*, such a fusion with the membrane occurs at the flagellar pocket (Rohatgi

and Snell, 2010), and therefore, it is possible that BBS5 is localised to the flagellar membrane of the flagellar pocket lumen and that the BBSome is involved in the sorting the carrier vesicles. However, whether BBS5 is truly associated with the membrane structure in *T. brucei* remains unclear.

To answer this question, testing the localisation of BBS5 in the isolated flagellum can show whether BBS5 is linked to the flagellar membrane of the proximal end of the flagellum in *T. brucei*. Detergent extraction and salt extraction remove the cell membrane and matrix but do not disrupt the insoluble flagellum, including kinetoplast, basal body, and axoneme (Broadhead et al., 2006; Robinson and Gull, 1991; Schlaeppi et al., 1989). The loss of BBS5 in isolated flagellum would thus indicate that BBS5 is associated with the membrane. Western blot analysis of BBS5/TY::GFP::BBS5 cell extracts containing the membrane fractions would also indicate whether BBS5 is a membrane component.

Another critical question to be addressed is whether BBS5 is associated with IFT particles, or not. To date, no studies have shown that BBS5 co-localises with IFT particles. However, another BBSome component, BBS4 moves along the axoneme by IFT in *C. reinhardtii* (Lechtreck et al., 2009), and BBS8 is required for the normal localisation of IFT proteins in *C. elegans* (Blacque et al., 2004). Moreover, transition fibres act as docking sites for the IFT particles, and numerous IFT proteins have been found in this region in *C. reinhardtii* and *T brucei* (Absalon et al., 2008b; Cole et al., 1998; Deane et al., 2001; Rosenbaum and Witman, 2002). Therefore, there is a possibility that BBS5 may associate with IFT particles at the base of flagellum before the BBSome is transported to the flagellum by the IFT machinery. The IFT machinery in *T. brucei* has been well studied, and the IFT particles proteins IFT20, IFT52, and IFT172 have been shown to localise to the basal body and the proximal end of the flagellum (Absalon et al., 2008b). Therefore, it is feasible to compare the localisation of BBS5 with these IFT particles in *T. brucei.* More importantly, the association of the BBSome with IFT proteins has been studied in *C. reinhardtii,* in which it was demonstrated that the BBSome acts as a cargo and is transported via IFT (Lechtreck et al., 2009).

Analyses of the interactions between IFT particles and BBS5 would provide the hint at whether they co-localise at the base of the flagella and whether IFT particles interact with the BBSome in *T. brucei,* or not.

Even though previous studies showed that BBS5 localises to the basal body in *C. elegans* and mammalian cells (An et al., 2004), the detection of BBS5 at the transition zone region was not surprising. According to the model, the BBSome is recruited to the basal body and enters the cilium by crossing the ciliary diffusion barrier, which is defined by the transition fibres and transition zone. Because BBS5 localises to the transition zone, it is presumed that the BBSome is not blocked by the diffusion barrier and is, rather be a part of the transition zone proteins module for restricting the entry of vesicles; and BBS5 may be required for anchoring the BBSome to the flagellar membrane at the transition zone region. Interestingly, a growing number proteins that are implicated in ciliopathies, such as Joubert syndrome (JBTS), nephronophthisis (NPHP), Senior-Loken syndrome (SLSN), and Meckel syndrome (MKS) have been identified as being situated at the transition zone (Garcia-Gonzalo et al., 2011; Jauregui et al., 2008; Mollet et al., 2005; Otto et al., 2005; Otto et al., 2003; Sang et al., 2011; Williams et al., 2011). The *C. elegans* protiens MKS1, MKS3, MKS5, MKS6, NPHP1, and NPHP4, and Tctn1, Tctn3, and Septin2 in mammalian cells are located at the transition zone of the ciliary base and function as “gate keepers” (Garcia-Gonzalo et al., 2011; Hu et al., 2010; Williams et al., 2011). Patients with ciliopathies involving these proteins have phenotypes similar to those of BBS patients, manifest common features, and occasionally overlap genetically. Mutations of the *MKS1* or *MKS6* genes cause BBS (Leitch et al., 2008), suggesting that there is a minimum genetic interaction between these genes and that they may share a common cellular process. Although, a physical interaction between the BBSome and the transition zone proteins has not been reported to date, it is possible that MKS, NPHP, and the BBSome are all localised at the transition zone as entities involved in restricting the access of ciliary membrane proteins into the cilium. Further research is required to verify whether these diverse groups of proteins function at the transition zone to keep some proteins outside of the

cilium while allowing others entry. Some transition zone proteins, such as MKS3, MKS6, and NPHP3, are conserved in *T. brucei* (Hodges et al., 2010); therefore, we will be able to compare their localisations with that of BBS5 to assess the possibility that BBS5 is co-localised with transition zone proteins.

It has been difficult to characterise BBS5 in *T. brucei* because it is expressed at a low level. The expression of TY::GFP::BBS5 was not very strong, and neither native GFP nor the TY-epitope antibody, BB2 could detect TY::GFP::BBS5 in cells. Another possible reason for the weak TY::GFP::BBS5 expression is that tagging BBS5 with GFP may have disrupted the function of BBS5, thus, GFP tagging may not be the best approach for investigating the localisation of BBS5. Since the TY-epitope antibody was able to detect TY::GFP::BBS5 in a western blot, and ectopically expressed BBS5::TY was strongly expressed, tagging BBS5 with the TY-epitope only may a better approach.

4.3 Loss of BBS5 in *T. brucei*

To elucidate the function of the BBSome, various model organisms have been used by analyzing the phenotypes produced by the loss of BBSome protein function. An increasing number of studies have shown that disrupting any of the BBSome genes produced a similar pathology, depending on the tissue, and that signalling pathways were perturbed due to the failure of receptor protein localisation to the ciliary membrane (Abd-El-Barr et al., 2007; Jin et al., 2010; Mykytyn et al., 2004; Nishimura et al.,2004). Both motile and immotile cilia are able to form without the BBSome, yet the signalling function was impaired, suggesting that the BBSome has no direct role in cilium/flagellum formation. A defect in rhodopsin transport in *BBS* mutated mice causes the degeneration of photoreceptor cells (Kulaga et al., 2004). Moreover, Lechtreck et al., showed that the dysfunction of BBSome genes did not affect the length of flagella but caused the abnormal accumulation of several signalling-related proteins in the flagella, indicating that the

BBSome is involved in exporting excessive specific signaling proteins from the flagellum to the cell body (Lechtreck et al., 2009).

In my thesis, I examined the function of BBS5 in flagellum formation in *T. brucei* using a well-established RNAi system to disrupt BBS5 by introducing dsRNA. The RNAi against BBS5 was induced in procyclic form cells that BBS5 was tagged with TY::GFP and bloodstream form cells. Both the procyclic and bloodstream forms remained viable after BBS5 knockdown and also remained able to assemble a flagellum, suggesting that BBS5 is not critical for flagellum formation. Nevertheless, several issues remain to be addressed to confirm that BBS5 is not essential for flagellum formation in *T. brucei*.

First, western blotting showed that TY::GFP::BBS5 was still detectable after BBS5 knockdown, indicating that BBS5 was not completely removed from the procyclic form cells after the knockdown. Hence, there is a possibility that some BBS5 function was retained, allowing the cells to form a flagellum. Furthermore, it is unclear whether the knockdown of BBS5 had subtle effects of flagellum formation. A slight effect on flagellum formation due to the partial loss of BBS5, might have been responsible for the slower growth rate of the RNAi induced cells. A recent report indicates that Arl6, which is encoded by *BBS3*, is distributed in punctuate throughout the cell body and that the knockdown of Arl6 does not cause any defect in *T. brucei* cell growth, cell morphology, and motility (Price et al., 2012). However, the measurement of the PFR length shows that Arl6 knockdown reduces the flagellum length (Price et al., 2012). Although Arl6 does not interact with BBS5, it is possible that the knockdown of BBS5 also affected the length of the flagellum. Therefore, the measurement of flagellum length, along with cell size and motility, will provide more insight into the role of BBS5 in flagellum biogenesis.

Nevertheless, the BBS5 reduced cells were able to assemble flagella, showing that wild-type levels of BBS5 is not critical for this process. Additionally, BBS5 may also be expressed at a low level. The

western blotting results demonstrated that TY::GFP::BBS5 was expressed at very low levels in the procyclic forms and it was hardly expressed in the bloodstream forms. Consequently, RNAi may not be able to achieve a level of knockdown that is sufficient to produce a phenotype.

Elongation of the posterior poles, a phenotype that was not directly linked to flagellum assembly, was observed in the RNAi induced bloodstream form *T. brucei*. A similar phenotype was reported in procyclic form *T. brucei* which extended microtubules caused abnormally elongated posterior pole, named "Nozzle" (Hendriks and Matthews, 2005). The ablation of cell cycle protein CYC2 caused the nozzle phenotype in procyclic forms and caused accumulation of cells in the 1K1N stage; 100% of 1K1N cells show a nozzle phenotype after 96 hours of RNAi induction (Hammarton et al., 2004). However, a pointed posterior tip was only observed in approximately 12% of BBS1 and BBS5 RNAi induced bloodstream form cells and no accumulation of 1K1N cells was observed. Considering that RNAi induced BBS1 and BBS5 cells had no defects in cell cycle progression and that the populations of pointed posterior cells were not very large, this may a represent minor phenotype of BBS1 and BBS5 RNAi induction.

Unlike the cilia/flagella in other eukaryotic organisms, the sensory function of the flagellum in *T. brucei* is mostly unknown. However, considering the fact that *T. brucei* has a complex life cycle, the flagellum may possess an environmental-sensing ability that activates or inactivates a specific differentiation programme for the next developmental transformation. Moreover, the flagellar membrane is able to detect particular substrates in the host tissues for attachment. Specific membrane proteins might be transported to the flagellum membrane to enable and mediate this adhesion. We know that proteins receiving signals do exist on the surface of *T. brucei*: the short stumpy bloodstream form has exposed carboxylate transporters on their surface that are involved in the differentiation of the procyclic forms (Dean et al., 2009). It is possible that the flagellar membrane requires receptor proteins to detect signals for differentiation, and the BBSome may

be activated only in a specific form of *T. brucei* to transport receptor proteins to facilitate their sensory function. Although numerous proteins that are required for flagellar motility have been identified and characterised in *T. brucei*, signal-detecting flagellar membrane proteins in *T. brucei* are not well known. To date, several calcium-binding proteins have been identified in trypanosome flagella, indicating that a Ca^{2+} signalling pathway is present in *T. brucei* (Godsel and Engman, 1999; Ridgley et al., 2000; Wu et al., 1992). However, the signalling ligands and their downstream effects remain largely unexplored. Further studies in this area will help to elucidate the function of the BBSome in *T. brucei.*

4.4 Interdependency between BBS5 and BBSome subunits

The 7 BBSome subunits (BBS1, BBS2, BBS4, BBS5, BBS7, BBS8, and BBS9) have interdependent functions, but the intensities of their interactions vary (Seo et al., 2011; Zhang et al., 2012). In this thesis, the 7 BBSome components were assumed to form a BBSome complex, and the requirement of BBSome subunits for TY::GFP::BBS5 localisation in the transition zone and protein expression were examined. In addition, the growth rates of individual BBSome gene disrupted cells were measured.

I showed that the knockdown of 6 BBSome subunits (BBS1, BBS2, BBS4, BBS7, BBS8, and BBS9) did not affect the expression of TY::GFP::BBS5 and that the knockdown of BBS9 did not alter the localisation of TY::GFP::BBS5. This finding was not surprising because, with the exception of BBS5, the BBSome proteins possess specific protein-protein interaction domains, suggesting that BBS5 may interact less strongly with other BBSome subunits. Moreover, Seo., et al indicated that BBS5 is not closely associated with other BBSome subunits by examining the requirement of the BBSome subunits for BBSome assembly by analysing BBSome assembly status in the absence of each BBSome gene (Seo et al., 2011). Individual BBSome genes were disrupted in hTERT-RPE1 cells, and the cells were separated by 10-40% sucrose gradient centrifugation (Seo et al., 2011).

They demonstrated that BBS1, BBS2, BBS7, and BBS9 are strongly required for BBSome assembly and that BBS4 and BBS8 are moderately required. Conversely, the disruption of BBS5 does not cause BBSome disassembly, indicating that BBS5 is not required for the interactions among other BBSome components (Seo et al., 2011).

Additional assays are required to confirm that BBS5 does not depend on other BBSome subunits for its localisation and expression in *T. brucei*. First, qRT-PCR should be performed to verify the efficient knockdown of each BBSome gene after RNAi induction. Recently, RNAi target sequencing (RIT-seq) was performed to individually knockdown each gene in the *T. brucei* genome and assess the effects of each gene's knockdown on cells' loss of fitness (Alsford et al., 2011). According to the RIT-seq data base, the knockdowns of BBS2, BBS4, and BBS8 result in loss of fitness in procyclic form *T. brucei*, but knockdown of the remaining BBSome genes do not confer any defects in their fitness (Alsford et al., 2011). In my studies, none of the BBSome gene knocked-down cells showed any fitness defects, and the cells were able to grow normally, suggesting that there is a possibility that the knockdown was imperfect and that a sufficient growth phenotype was not produced.

Moreover, it is possible that some BBSome proteins are replacing other BBSome protein whose gene was knocked-down. Particularly, BBS1, BBS2, and BBS7 may able to cover the function of BBS9 when the RNAi was induced against BBS9, since they are interacting to each other (Seo et al., 2011). Hence, the double or triple knockdown of BBSome genes may enhance the effects of the knockdown and enable the identification of the level of interdependency of BBS5 with other BBSome subunits, which cannot be observed in the context of individual gene knockdowns.

Finally, even though we assume that the 7 BBSome proteins form a complex in *T. brucei*, this hypothesis has not been tested directly. In *C. reinhardtii*, several BBS proteins (BBS1, 5, 7, and 8) were identified by the affinity purification of a BBS4 extracted flagellar membrane-plus-matrix fraction, demonstrating that the BBS proteins do, indeed, form a complex (Lechtreck et al., 2009).

Nevertheless, it is still uncertain whether all 7 BBSome components are present in *T. brucei* and forming a complex; therefore, the existence and contents of the BBSome protein complex should to be confirmed.

4.5 A possible mechanism of ciliogenesis involving the BBSome

Based on the finding that the MKS and NPHP proteins localise to the transition zone and are required for the attachment of the ciliary membrane to the basal body and transition zone in *C. elegans* (Williams et al., 2011), a new theory of ciliogenesis has been proposed, recently (Williams et al., 2011). Early ciliogenesis is dependent on the MKS and NPHP proteins, and late ciliogenesis is depending on not only MKS and NPHP, but also the BBSome and IFT. Williams., et al revealed that basal body and transition zone membrane docking and transition zone formation occur in early ciliogenesis, before axoneme growth depends on IFT (Williams et al., 2011). The early stage of ciliogenesis is described in detail in chapter 1.3, that the transition zone develops during the early step of ciliogenesis. After the ciliary vesicle attaches to the distal appendage of the mother centriole, the basal body/ciliary vesicle module fuses with the plasma membrane and the matured transition zone forms ciliary gate. Late ciliogenesis depends on IFT for the extension of the axoneme, and the BBSome for generating cilia as sensory antennae. However, MKS and NPHP proteins are still required in late ciliogenesis to control the entry of vesicles into the cilia. In my study, BBS5 was detected at the transition zone, suggesting that BBS5 and the MKS and NPHP proteins form a gate together at the base of the flagellum, which is necessary for maintaining the specialisation of the flagellar compartment. It is also possible that BBS5 is responsible for allowing the BBSome to be able to localise at basal body/transition zone region to be attached to the flagellar membrane. Although the single knockdown of MKS5, MKS6, and NPHP4 did not affect cilium formation, double mutations caused the basal body and transition zone to disconnect from the membrane and destabilised the cilia in *C. elegans* (Williams et al., 2011). The double knockdown of transition zone genes and with BBS5 in *T. brucei* may provide insights into the

mechanisms by which BBS5 associates with the flagellar membrane around the transition zone in *T. brucei.*

Chapter 5

References

Abou Alaiwi, W.A., S.T. Lo, and S.M. Nauli. 2009. Primary Cilia: Highly Sophisticated Biological Sensors. *Sensors-Basel*. 9:7003-7020.

Absalon, S., T. Blisnick, M. Bonhivers, L. Kohl, N. Cayet, G. Toutirais, J. Buisson, D. Robinson, and P. Bastin. 2008a. Flagellum elongation is required for correct structure, orientation and function of the flagellar pocket in Trypanosoma brucei. *Journal of Cell Science*. 121:3704-3716.

Absalon, S., T. Blisnick, L. Kohl, G. Toutirais, G. Dore, D. Julkowska, A. Tavenet, and P. Bastin. 2008b. Intraflagellar transport and functional analysis of genes required for flagellum formation in trypanosomes. *Mol Biol Cell*. 19:929-944.

Absalon, S., L. Kohl, C. Branche, T. Blisnick, G. Toutirais, F. Rusconi, J. Cosson, M. Bonhivers, D. Robinson, and P. Bastin. 2007. Basal body positioning is controlled by flagellum formation in Trypanosoma brucei. *PLoS One*. 2:e437.

Acosta-Serrano, A., E. Vassella, M. Liniger, C.K. Renggli, R. Brun, I. Roditi, and P.T. Englund. 2001. The surface coat of procyclic Trypanosoma brucei: Programmed expression and proteolytic cleavage of procyclin in the tsetse fly. *P Natl Acad Sci USA*. 98:1513-1518.

Afzelius, B.A. 2004. Cilia-related diseases. *J Pathol*. 204:470-477.

Allen, C.L., D. Goulding, and M.C. Field. 2003. Clathrin-mediated endocytosis is essential in Trypanosoma brucei. *EMBO J*. 22:4991-5002.

Alsford, S., D.J. Turner, S.O. Obado, A. Sanchez-Flores, L. Glover, M. Berriman, C. Hertz-Fowler, and D. Horn. 2011. High-throughput phenotyping using parallel sequencing of RNA interference targets in the African trypanosome. *Genome Res*. 21:915-924.

An, J.Y., Z.M. Fan, Z.H. Zhuang, Y.R. Qin, S.S. Gao, J.L. Li, and L.D. Wang. 2004. Proteomic analysis of blood level of proteins before and after operation in patients with esophageal squamous cell carcinoma at high-incidence area in Henan Province. *World J Gastroenterol*. 10:3365-3368.

Angelopoulos, E. 1970. Pellicular microtubules in the family Trypanosomatidae. *J Protozool*. 17:39-51.

Ansley, S.J., J.L. Badano, O.E. Blacque, J. Hill, B.E. Hoskins, C.C. Leitch, J.C. Kim, A.J. Ross, E.R. Eichers, T.M. Teslovich, A.K. Mah, R.C. Johnsen, J.C. Cavender, R.A. Lewis, M.R. Leroux, P.L. Beales, and N. Katsanis. 2003. Basal body dysfunction is a likely cause of pleiotropic Bardet-Biedl syndrome. *Nature*. 425:628-633.

Avidor-Reiss, T., A.M. Maer, E. Koundakjian, A. Polyanovsky, T. Keil, S. Subramaniam, and C.S. Zuker. 2004. Decoding cilia function: defining specialized genes required for compartmentalized cilia biogenesis. *Cell*. 117:527-539.

Badano, J.L., J.C. Kim, B.E. Hoskins, R.A. Lewis, S.J. Ansley, D.J. Cutler, C. Castellan, P.L. Beales, M.R. Leroux, and N. Katsanis. 2003. Heterozygous mutations in BBS1, BBS2 and BBS6 have a potential epistatic effect on Bardet-Biedl patients with two mutations at a second BBS locus. *American Journal of Human Genetics*. 73:518-518.

Baron, D.M., K.S. Ralston, Z.P. Kabututu, and K.L. Hill. 2007. Functional genomics in Trypanosoma brucei identifies evolutionarily conserved components of motile flagella. *J Cell Sci*. 120:478-491.

Barr, M.M., J. DeModena, D. Braun, C.Q. Nguyen, D.H. Hall, and P.W. Sternberg. 2001. The Caenorhabditis elegans autosomal dominant polycystic kidney disease gene homologs lov-1 and pkd-2 act in the same pathway. *Curr Biol*. 11:1341-1346.

Bastin, P., Z. Bagherzadeh, K.R. Matthews, and K. Gull. 1996a. A novel epitope tag system to study protein targeting and organelle biogenesis in Trypanosoma brucei. *Mol Biochem Parasitol*. 77:235-239.

Bastin, P., T.H. MacRae, S.B. Francis, K.R. Matthews, and K. Gull. 1999a. Flagellar morphogenesis: protein targeting and assembly in the paraflagellar rod of trypanosomes. *Mol Cell Biol*. 19:8191-8200.

Bastin, P., K.R. Matthews, and K. Gull. 1996b. The paraflagellar rod of kinetoplastida: solved and unsolved questions. *Parasitol Today*. 12:302-307.

Bastin, P., T.J. Pullen, T. Sherwin, and K. Gull. 1999b. Protein transport and flagellum assembly dynamics revealed by analysis of the paralysed trypanosome mutant snl-1. *J Cell Sci*. 112 (Pt 21):3769-3777.

Bastin, P., T. Sherwin, and K. Gull. 1998. Paraflagellar rod is vital for trypanosome motility. *Nature*. 391:548.

Berbari, N.F., A.D. Johnson, J.S. Lewis, C.C. Askwith, and K. Mykytyn. 2008a. Identification of ciliary localization sequences within the third intracellular loop of G protein-coupled receptors. *Mol Biol Cell*. 19:1540-1547.

Berbari, N.F., J.S. Lewis, G.A. Bishop, C.C. Askwith, and K. Mykytyn. 2008b. Bardet-Biedl syndrome proteins are required for the localization of G protein-coupled receptors to primary cilia. *Proc Natl Acad Sci U S A*. 105:4242-4246.

Berger, L., A.D. Hyatt, R. Speare, and J.E. Longcore. 2005. Life cycle stages of the amphibian chytrid Batrachochytrium dendrobatidis. *Dis Aquat Organ*. 68:51-63.

Besse, L., M. Neti, I. Anselme, U. Ruther, C. Laclef, and S. Schneider-maunoury. 2009. Cilia-dependent olfactory bulb morphogenesis. *Mech Develop*. 126:S264-S264.

Bielas, S.L., J.L. Silhavy, F. Brancati, M.V. Kisseleva, L. Al-Gazali, L. Sztriha, R.A. Bayoumi, M.S. Zaki, A. Abdel-Aleem, R.O. Rosti, H. Kayserili, D. Swistun, L.C. Scott, E. Bertini, E. Boltshauser, E. Fazzi, L. Travaglini, S.J. Field, S. Gayral, M. Jacoby, S. Schurmans, B. Dallapiccola, P.W. Majerus, E.M. Valente, and J.G. Gleeson. 2009. Mutations in INPP5E, encoding inositol polyphosphate-5-phosphatase E, link phosphatidyl inositol signaling to the ciliopathies. *Nat Genet*. 41:1032-1036.

Blacque, O.E., M.J. Reardon, C. Li, J. McCarthy, M.R. Mahjoub, S.J. Ansley, J.L. Badano, A.K. Mah, P.L. Beales, W.S. Davidson, R.C. Johnsen, M. Audeh, R.H. Plasterk, D.L. Baillie, N. Katsanis, L.M. Quarmby, S.R. Wicks, and M.R. Leroux. 2004. Loss of C. elegans BBS-7 and BBS-8 protein function results in cilia defects and compromised intraflagellar transport. *Genes Dev*. 18:1630-1642.

Boisvieux-Ulrich, E., M.C. Laine, and D. Sandoz. 1989. In vitro effects of taxol on ciliogenesis in quail oviduct. *J Cell Sci*. 92 (Pt 1):9-20.

Bonhivers, M., S. Nowacki, N. Landrein, and D.R. Robinson. 2008. Biogenesis of the trypanosome endo-exocytotic organelle is cytoskeleton mediated. *PLoS Biol*. 6:e105.

Branche, C., L. Kohl, G. Toutirais, J. Buisson, J. Cosson, and P. Bastin. 2006. Conserved and specific functions of axoneme components in trypanosome motility. *Journal of Cell Science*. 119:3443-3455.

Briggs, L.J., J.A. Davidge, B. Wickstead, M.L. Ginger, and K. Gull. 2004. More than one way to build a flagellum: comparative genomics of parasitic protozoa. *Curr Biol*. 14:R611-R612.

Broadhead, R., H.R. Dawe, H. Farr, S. Griffiths, S.R. Hart, N. Portman, M.K. Shaw, M.L. Ginger, S.J. Gaskell, P.G. McKean, and K. Gull. 2006. Flagellar motility is required for the viability of the bloodstream trypanosome. *Nature*. 440:224-227.

Brose, N., K. Hofmann, Y. Hata, and T.C. Sudhof. 1995. Mammalian homologues of Caenorhabditis elegans unc-13 gene define novel family of C2-domain proteins. *J Biol Chem*. 270:25273-25280.

Brun, R., J. Blum, F. Chappuis, and C. Burri. 2010. Human African trypanosomiasis. *Lancet*. 375:148-159.

Brun, R., and L. Jenni. 1977. A new semi-defined medium for Trypanosoma brucei sspp. *Acta Trop*. 34:21-33.

Carvalho-Santos, Z., J. Azimzadeh, J.B. Pereira-Leal, and M. Bettencourt-Dias. 2011. Evolution: Tracing the origins of centrioles, cilia, and flagella. *J Cell Biol*. 194:165-175.

Chen, J., N. Smaoui, M.B. Hammer, X. Jiao, S.A. Riazuddin, S. Harper, N. Katsanis, S. Riazuddin, H. Chaabouni, E.L. Berson, and J.F. Hejtmancik. 2011. Molecular analysis of Bardet-Biedl syndrome families: report of 21 novel mutations in 10 genes. *Invest Ophthalmol Vis Sci*. 52:5317-5324.

Chen, W.M., M.R. Erdos, A.U. Jackson, R. Saxena, S. Sanna, K.D. Silver, N.J. Timpson, T. Hansen, M. Orru, M. Grazia Piras, L.L. Bonnycastle, C.J. Willer, V. Lyssenko, H. Shen, J. Kuusisto, S. Ebrahim, N. Sestu, W.L. Duren, M.C. Spada, H.M. Stringham, L.J. Scott, N. Olla, A.J. Swift, S. Najjar, B.D. Mitchell, D.A. Lawlor, G.D. Smith, Y. Ben-Shlomo, G. Andersen, K. Borch-Johnsen, T. Jorgensen, J. Saramies, T.T. Valle, T.A. Buchanan, A.R. Shuldiner, E. Lakatta, R.N. Bergman, M. Uda, J. Tuomilehto, O. Pedersen, A. Cao, L. Groop, K.L. Mohlke, M. Laakso, D. Schlessinger, F.S. Collins, D. Altshuler, G.R. Abecasis, M. Boehnke, A. Scuteri, and R.M. Watanabe. 2008. Variations in the G6PC2/ABCB11 genomic region are associated with fasting glucose levels. *J Clin Invest*. 118:2620-2628.

Chiang, A.P., D. Nishimura, C. Searby, K. Elbedour, R. Carmi, A.L. Ferguson, J. Secrist, T. Braun, T. Casavant, E.M. Stone, and V.C. Sheffield. 2004. Comparative genomic analysis identifies an ADP-ribosylation factor-like gene as the cause of Bardet-Biedl syndrome (BBS3). *Am J Hum Genet*. 75:475-484.

Christensen, S.T., C.F. Guerra, A. Awan, D.N. Wheatley, and P. Satir. 2003. Insulin receptor-like proteins in Tetrahymena thermophila ciliary membranes. *Curr Biol*. 13:R50-52.

Christensen, S.T., L.B. Pedersen, L. Schneider, and P. Satir. 2007. Sensory cilia and integration of signal transduction in human health and disease. *Traffic*. 8:97-109.

Christensen, S.T., S.F. Pedersen, P. Satir, T.R. Veland, and L. Schneider. 2008. The Primary Cilium Coordinates Signaling Pathways in Cell Cycle Control and Migration during Development and Tissue Repair. *Ciliary Function in Mammalian Development*. 85:261-301.

Clayton, C.E. 1999. Genetic manipulation of kinetoplastida. *Parasitol Today*. 15:372-378.

Cole, D.G. 2003. The intraflagellar transport machinery of Chlamydomonas reinhardtii. *Traffic*. 4:435-442.

Cole, D.G., S.W. Chinn, K.P. Wedaman, K. Hall, T. Vuong, and J.M. Scholey. 1993. Novel heterotrimeric kinesin-related protein purified from sea urchin eggs. *Nature*. 366:268-270.

Cole, D.G., D.R. Diener, A.L. Himelblau, P.L. Beech, J.C. Fuster, and J.L. Rosenbaum. 1998. Chlamydomonas kinesin-II-dependent intraflagellar transport (IFT): IFT particles contain proteins required for ciliary assembly in Caenorhabditis elegans sensory neurons. *J Cell Biol*. 141:993-1008.

Craige, B., C.C. Tsao, D.R. Diener, Y. Hou, K.F. Lechtreck, J.L. Rosenbaum, and G.B. Witman. 2010. CEP290 tethers flagellar transition zone microtubules to the membrane and regulates flagellar protein content. *J Cell Biol*. 190:927-940.

Cross, G.A. 1977. Antigenic variation in trypanosomes. *Am J Trop Med Hyg*. 26:240-244.

Cullen, P.J., G.E. Cozier, G. Banting, and H. Mellor. 2001. Modular phosphoinositide-binding domains--their role in signalling and membrane trafficking. *Curr Biol*. 11:R882-893.

Czarnecki, P.G., and J.V. Shah. 2012. The ciliary transition zone: from morphology and molecules to medicine. *Trends Cell Biol*. 22:201-210.

D'Andrea, L.D., and L. Regan. 2003. TPR proteins: the versatile helix. *Trends Biochem Sci*. 28:655-662.

Dawe, H.R., H. Farr, N. Portman, M.K. Shaw, and K. Gull. 2005. The Parkin co-regulated gene product, PACRG, is an evolutionarily conserved axonemal protein that functions in outer-doublet microtubule morphogenesis. *Journal of Cell Science*. 118:5421-5430.

Dawe, H.R., M.K. Shaw, H. Farr, and K. Gull. 2007. The hydrocephalus inducing gene product, Hydin, positions axonemal central pair microtubules. *BMC Biol*. 5:33.

Dean, S., R. Marchetti, K. Kirk, and K.R. Matthews. 2009. A surface transporter family conveys the trypanosome differentiation signal. *Nature*. 459:213-217.

Deane, J.A., D.G. Cole, E.S. Seeley, D.R. Diener, and J.L. Rosenbaum. 2001. Localization of intraflagellar transport protein IFT52 identifies basal body transitional fibers as the docking site for IFT particles. *Curr Biol*. 11:1586-1590.

Deretic, D., S. Schmerl, P.A. Hargrave, A. Arendt, and J.H. McDowell. 1998. Regulation of sorting and post-Golgi trafficking of rhodopsin by its C-terminal sequence QVS(A)PA. *Proc Natl Acad Sci U S A*. 95:10620-10625.

DiBella, L.M., and S.M. King. 2001. Dynein motors of the Chlamydomonas flagellum. *Int Rev Cytol*. 210:227-268.

Domire, J.S., J.A. Green, K.G. Lee, A.D. Johnson, C.C. Askwith, and K. Mykytyn. 2011. Dopamine receptor 1 localizes to neuronal cilia in a dynamic process that requires the Bardet-Biedl syndrome proteins. *Cell Mol Life Sci*. 68:2951-2960.

Eisenbach, M., and L.C. Giojalas. 2006. Sperm guidance in mammals - an unpaved road to the egg. *Nat Rev Mol Cell Biol*. 7:276-285.

Emmer, B.T., D. Maric, and D.M. Engman. 2010. Molecular mechanisms of protein and lipid targeting to ciliary membranes. *J Cell Sci*. 123:529-536.

Emmer, B.T., C. Souther, K.M. Toriello, C.L. Olson, C.L. Epting, and D.M. Engman. 2009. Identification of a palmitoyl acyltransferase required for protein sorting to the flagellar membrane. *J Cell Sci*. 122:867-874.

Engstler, M., L. Thilo, F. Weise, C.G. Grunfelder, H. Schwarz, M. Boshart, and P. Overath. 2004. Kinetics of endocytosis and recycling of the GPI-anchored variant surface glycoprotein in Trypanosoma brucei. (vol 117, pg 1105, 2004). *Journal of Cell Science*. 117:3703-3703.

Fan, Y., M.A. Esmail, S.J. Ansley, O.E. Blacque, K. Boroevich, A.J. Ross, S.J. Moore, J.L. Badano, H. May-Simera, D.S. Compton, J.S. Green, R.A. Lewis, M.M. van Haelst, P.S. Parfrey, D.L. Baillie, P.L. Beales, N. Katsanis, W.S. Davidson, and M.R. Leroux. 2004. Mutations in a member of the Ras superfamily of small GTP-binding proteins causes Bardet-Biedl syndrome. *Nat Genet*. 36:989-993.

Fauser, S., M. Munz, and D. Besch. 2003. Further support for digenic inheritance in Bardet-Biedl syndrome. *J Med Genet*. 40:e104.

Frearson, J.A., P.G. Wyatt, I.H. Gilbert, and A.H. Fairlamb. 2007. Target assessment for antiparasitic drug discovery. *Trends Parasitol*. 23:589-595.

Gadelha, C., S. Rothery, M. Morphew, J.R. McIntosh, N.J. Severs, and K. Gull. 2009. Membrane domains and flagellar pocket boundaries are influenced by the cytoskeleton in African trypanosomes. *P Natl Acad Sci USA*. 106:17425-17430.

Garcia-Gonzalo, F.R., K.C. Corbit, M.S. Sirerol-Piquer, G. Ramaswami, E.A. Otto, T.R. Noriega, A.D. Seol, J.F. Robinson, C.L. Bennett, D.J. Josifova, J.M. Garcia-Verdugo, N. Katsanis, F. Hildebrandt, and J.F. Reiter. 2011. A transition zone complex regulates mammalian ciliogenesis and ciliary membrane composition. *Nat Genet*. 43:776-784.

Geng, L., D. Okuhara, Z. Yu, X. Tian, Y. Cai, S. Shibazaki, and S. Somlo. 2006. Polycystin-2 traffics to cilia independently of polycystin-1 by using an N-terminal RVxP motif. *J Cell Sci*. 119:1383-1395.

Gibbons, I.R., and A.V. Grimstone. 1960. On flagellar structure in certain flagellates. *J Biophys Biochem Cytol*. 7:697-716.

Gibson, T.J., M. Hyvonen, A. Musacchio, M. Saraste, and E. Birney. 1994. PH domain: the first anniversary. *Trends Biochem Sci*. 19:349-353.

Gilula, N.B., and P. Satir. 1972. The ciliary necklace. A ciliary membrane specialization. *J Cell Biol*. 53:494-509.

Ginger, M.L., E.S. Ngazoa, C.A. Pereira, T.J. Pullen, M. Kabiri, K. Becker, K. Gull, and D. Steverding. 2005. Intracellular positioning of isoforms explains an unusually large adenylate kinase gene family in the parasite Trypanosoma brucei. *J Biol Chem*. 280:11781-11789.

Godsel, L.M., and D.M. Engman. 1999. Flagellar protein localization mediated by a calcium-myristoyl/palmitoyl switch mechanism. *Embo J*. 18:2057-2065.

Grunfelder, C.G., M. Engstler, F. Weise, H. Schwarz, Y.D. Stierhof, G.W. Morgan, M.C. Field, and P. Overath. 2003. Endocytosis of a glycosylphosphatidylinositol-anchored protein via clathrin-coated vesicles, sorting by default in endosomes, and exocytosis via RAB11-positive carriers. *Mol Biol Cell*. 14:2029-2040.

Gunay-Aygun, M. 2009. Liver and kidney disease in ciliopathies. *Am J Med Genet C Semin Med Genet*. 151C:296-306.

Hammarton, T.C., M. Engstler, and J.C. Mottram. 2004. The Trypanosoma brucei cyclin, CYC2, is required for cell cycle progression through G1 phase and for maintenance of procyclic form cell morphology. *J Biol Chem*. 279:24757-24764.

Harlan, J.E., P.J. Hajduk, H.S. Yoon, and S.W. Fesik. 1994. Pleckstrin homology domains bind to phosphatidylinositol-4,5-bisphosphate. *Nature*. 371:168-170.

Hendriks, E.F., and K.R. Matthews. 2005. Disruption of the developmental programme of Trypanosoma brucei by genetic ablation of TbZFP1, a differentiation-enriched CCCH protein. *Mol Microbiol*. 57:706-716.

Henley, G.L., C.M. Lee, and A. Takeuchi. 1978. Electron microscopy observations on Trypanosoma brucei: freeze-cleaving and thin-sectioning study of the apical part of the flagellar pocket. *Z Parasitenkd*. 55:181-187.

Hildebrandt, F., M. Attanasio, and E. Otto. 2009. Nephronophthisis: disease mechanisms of a ciliopathy. *J Am Soc Nephrol*. 20:23-35.

Hirumi, H., and K. Hirumi. 1989. Continuous cultivation of Trypanosoma brucei blood stream forms in a medium containing a low concentration of serum protein without feeder cell layers. *J Parasitol*. 75:985-989.

Hjortshoj, T.D., K. Gronskov, A.R. Philp, D.Y. Nishimura, A. Adeyemo, C.N. Rotimi, V.C. Sheffield, T. Rosenberg, and K. Brondum-Nielsen. 2008. Novel mutations in BBS5 highlight the importance of this gene in non-Caucasian Bardet-Biedl syndrome patients. *Am J Med Genet A*. 146A:517-520.

Hodges, M.E., N. Scheumann, B. Wickstead, J.A. Langdale, and K. Gull. 2010. Reconstructing the evolutionary history of the centriole from protein components. *J Cell Sci*. 123:1407-1413.

Hu, Q., L. Milenkovic, H. Jin, M.P. Scott, M.V. Nachury, E.T. Spiliotis, and W.J. Nelson. 2010. A septin diffusion barrier at the base of the primary cilium maintains ciliary membrane protein distribution. *Science*. 329:436-439.

Hu, Q.C., and W.J. Nelson. 2011. Ciliary Diffusion Barrier: The Gatekeeper for the Primary Cilium Compartment. *Cytoskeleton*. 68:313-324.

Hung, C.H., X. Qiao, P.T. Lee, and M.G. Lee. 2004. Clathrin-dependent targeting of receptors to the flagellar pocket of procyclic-form Trypanosoma brucei. *Eukaryot Cell*. 3:1004-1014.

Hutchings, N.R., J.E. Donelson, and K.L. Hill. 2002. Trypanin is a cytoskeletal linker protein and is required for cell motility in African trypanosomes. *J Cell Biol*. 156:867-877.

Inglis, P.N., K.A. Boroevich, and M.R. Leroux. 2006. Piecing together a ciliome. *Trends Genet*. 22:491-500.

Jacoby, M., J.J. Cox, S. Gayral, D.J. Hampshire, M. Ayub, M. Blockmans, E. Pernot, M.V. Kisseleva, P. Compere, S.N. Schiffmann, F. Gergely, J.H. Riley, D. Perez-Morga, C.G. Woods, and S. Schurmans. 2009. INPP5E mutations cause primary cilium signaling defects, ciliary instability and ciliopathies in human and mouse. *Nat Genet*. 41:1027-1031.

Jauregui, A.R., K.C. Nguyen, D.H. Hall, and M.M. Barr. 2008. The Caenorhabditis elegans nephrocystins act as global modifiers of cilium structure. *J Cell Biol*. 180:973-988.

Jekely, G., and D. Arendt. 2006. Evolution of intraflagellar transport from coated vesicles and autogenous origin of the eukaryotic cilium. *Bioessays*. 28:191-198.

Jin, H., S.R. White, T. Shida, S. Schulz, M. Aguiar, S.P. Gygi, J.F. Bazan, and M.V. Nachury. 2010. The Conserved Bardet-Biedl Syndrome Proteins Assemble a Coat that Traffics Membrane Proteins to Cilia. *Cell*. 141:1208-U1198.

Johnson, M.L., and R. Speare. 2003. Survival of Batrachochytrium dendrobatidis in water: Quarantine and disease control implications. *Emerging Infectious Diseases*. 9:922-925.

Katsanis, N., S.J. Ansley, J.L. Badano, E.R. Eichers, R.A. Lewis, B.E. Hoskins, P.J. Scambler, W.S. Davidson, P.L. Beales, and J.R. Lupski. 2001. Triallelic inheritance in Bardet-Biedl syndrome, a Mendelian recessive disorder. *Science*. 293:2256-2259.

Katsanis, N., E.R. Eichers, S.J. Ansley, R.A. Lewis, H. Kayserili, B.E. Hoskins, P.J. Scambler, P.L. Beales, and J.R. Lupski. 2002. BBS4 is a minor contributor to Bardet-Biedl syndrome and may also participate in triallelic inheritance. *Am J Hum Genet*. 71:22-29.

Keller, L.C., E.P. Romijn, I.P. Zamora, J.R. Yates, and W.F. Marshall. 2006. Dissecting the centriole proteome. *Faseb Journal*. 20:A493-A493.

Kelly, S., J. Reed, S. Kramer, L. Ellis, H. Webb, J. Sunter, J. Salje, N. Marinsek, K. Gull, B. Wickstead, and M. Carrington. 2007. Functional genomics in Trypanosoma brucei: a collection of vectors for the expression of tagged proteins from endogenous and ectopic gene loci. *Mol Biochem Parasitol*. 154:103-109.

Kilmartin, J.V., B. Wright, and C. Milstein. 1982. Rat Monoclonal Antitubulin Antibodies Derived by Using a New Non-Secreting Rat-Cell Line. *Journal of Cell Biology*. 93:576-582.

Kirkham, M., T. Muller-Reichert, K. Oegema, S. Grill, and A.A. Hyman. 2003. SAS-4 is a C. elegans centriolar protein that controls centrosome size. *Cell*. 112:575-587.

Kohl, L., D. Robinson, and P. Bastin. 2003. Novel roles for the flagellum in cell morphogenesis and cytokinesis of trypanosomes. *Embo J*. 22:5336-5346.

Kozminski, K.G., K.A. Johnson, P. Forscher, and J.L. Rosenbaum. 1993. A motility in the eukaryotic flagellum unrelated to flagellar beating. *Proc Natl Acad Sci U S A*. 90:5519-5523.

Kramer-Zucker, A.G., F. Olale, C.J. Haycraft, B.K. Yoder, A.F. Schier, and I.A. Drummond. 2005. Cilia-driven fluid flow in the zebrafish pronephros, brain and Kupffer's vesicle is required for normal organogenesis. *Development*. 132:1907-1921.

Kulaga, H.M., C.C. Leitch, E.R. Eichers, J.L. Badano, A. Lesemann, B.E. Hoskins, J.R. Lupski, P.L. Beales, R.R. Reed, and N. Katsanis. 2004. Loss of BBS proteins causes anosmia in humans and defects in olfactory cilia structure and function in the mouse. *Nature Genetics*. 36:994-998.

Lacomble, S., S. Vaughan, C. Gadelha, M.K. Morphew, M.K. Shaw, J.R. McIntosh, and K. Gull. 2009. Three-dimensional cellular architecture of the flagellar pocket and associated cytoskeleton in trypanosomes revealed by electron microscope tomography. *J Cell Sci*. 122:1081-1090.

Lechtreck, K.F., E.C. Johnson, T. Sakai, D. Cochran, B.A. Ballif, J. Rush, G.J. Pazour, M. Ikebe, and G.B. Witman. 2009. The Chlamydomonas reinhardtii BBSome is an IFT cargo required for export of specific signaling proteins from flagella. *J Cell Biol*. 187:1117-1132.

Lee, L. 2011. Mechanisms of mammalian ciliary motility: Insights from primary ciliary dyskinesia genetics. *Gene*. 473:57-66.

Leidel, S., and P. Gonczy. 2003. SAS-4 is essential for centrosome duplication in C elegans and is recruited to daughter centrioles once per cell cycle. *Developmental cell*. 4:431-439.

Leitch, C.C., N.A. Zaghloul, E.E. Davis, C. Stoetzel, A. Diaz-Font, S. Rix, M. Alfadhel, R.A. Lewis, W. Eyaid, E. Banin, H. Dollfus, P.L. Beales, J.L. Badano, and N. Katsanis. 2008. Hypomorphic mutations in syndromic encephalocele genes are associated with Bardet-Biedl syndrome. *Nat Genet*. 40:443-448.

Lemmon, M.A., and K.M. Ferguson. 2001. Molecular determinants in pleckstrin homology domains that allow specific recognition of phosphoinositides. *Biochem Soc Trans*. 29:377-384.

Lucker, B.F., R.H. Behal, H.M. Qin, L.C. Siron, W.D. Taggart, J.L. Rosenbaum, and D.G. Cole. 2005. Characterization of the intraflagellar transport complex B core - Direct interaction of the IFT81 AND IFT74/72 subunits. *Journal of Biological Chemistry*. 280:27688-27696.

Maffucci, T., and M. Falasca. 2001. Specificity in pleckstrin homology (PH) domain membrane targeting: a role for a phosphoinositide-protein co-operative mechanism. *Febs Letters*. 506:173-179.

Maga, J.A., T. Sherwin, S. Francis, K. Gull, and J.H. LeBowitz. 1999. Genetic dissection of the Leishmania paraflagellar rod, a unique flagellar cytoskeleton structure. *J Cell Sci*. 112 (Pt 16):2753-2763.

Mak, H.Y., L.S. Nelson, M. Basson, C.D. Johnson, and G. Ruvkun. 2006. Polygenic control of Caenorhabditis elegans fat storage. *Nat Genet*. 38:363-368.

Marshall, W.F. 2008. The cell biological basis of ciliary disease. *J Cell Biol*. 180:17-21.

Marshall, W.F., and J.L. Rosenbaum. 2001. Intraflagellar transport balances continuous turnover of outer doublet microtubules: implications for flagellar length control. *J Cell Biol*. 155:405-414.

Marszalek, J.R., P. Ruiz-Lozano, E. Roberts, K.R. Chien, and L.S. Goldstein. 1999. Situs inversus and embryonic ciliary morphogenesis defects in mouse mutants lacking the KIF3A subunit of kinesin-II. *Proc Natl Acad Sci U S A*. 96:5043-5048.

Matthews, K.R. 2005. The developmental cell biology of Trypanosoma brucei (vol 118, pg 283, 2005). *Journal of Cell Science*. 118:2078-2078.

Matthews, K.R., T. Sherwin, and K. Gull. 1995. Mitochondrial Genome Repositioning during the Differentiation of the African Trypanosome between Life-Cycle Forms Is Microtubule Mediated. *Journal of Cell Science*. 108:2231-2239.

Mayer, B.J., R. Ren, K.L. Clark, and D. Baltimore. 1993. A putative modular domain present in diverse signaling proteins. *Cell*. 73:629-630.

Mazelova, J., L. Astuto-Gribble, H. Inoue, B.M. Tam, E. Schonteich, R. Prekeris, O.L. Moritz, P.A. Randazzo, and D. Deretic. 2009. Ciliary targeting motif VxPx directs assembly of a trafficking module through Arf4. *EMBO J*. 28:183-192.

Menco, B.P. 1994. Ultrastructural aspects of olfactory transduction and perireceptor events. *Semin Cell Biol*. 5:11-24.

Merchant, S.S., S.E. Prochnik, O. Vallon, E.H. Harris, S.J. Karpowicz, G.B. Witman, A. Terry, A. Salamov, L.K. Fritz-Laylin, L. Marechal-Drouard, W.F. Marshall, L.H. Qu, D.R. Nelson, A.A. Sanderfoot, M.H. Spalding, V.V. Kapitonov, Q. Ren, P. Ferris, E. Lindquist, H. Shapiro, S.M. Lucas, J. Grimwood, J. Schmutz, P. Cardol, H. Cerutti, G. Chanfreau, C.L. Chen, V. Cognat, M.T. Croft, R. Dent, S. Dutcher, E. Fernandez, H. Fukuzawa, D. Gonzalez-Ballester, D. Gonzalez-Halphen, A. Hallmann, M. Hanikenne, M. Hippler, W. Inwood, K. Jabbari, M. Kalanon, R. Kuras, P.A. Lefebvre, S.D. Lemaire, A.V. Lobanov, M. Lohr, A. Manuell, I. Meier, L. Mets, M. Mittag, T. Mittelmeier, J.V. Moroney, J. Moseley, C. Napoli, A.M. Nedelcu, K. Niyogi, S.V. Novoselov, I.T. Paulsen, G. Pazour, S. Purton, J.P. Ral, D.M. Riano-Pachon, W. Riekhof, L. Rymarquis, M. Schroda, D. Stern, J. Umen, R. Willows, N. Wilson, S.L. Zimmer, J. Allmer, J. Balk, K. Bisova, C.J. Chen, M. Elias, K. Gendler, C. Hauser, M.R. Lamb, H. Ledford, J.C. Long, J. Minagawa, M.D. Page, J. Pan, W. Pootakham, S. Roje, A. Rose, E. Stahlberg, A.M. Terauchi, P. Yang, S. Ball, C. Bowler, C.L. Dieckmann, V.N. Gladyshev, P. Green, R. Jorgensen, S. Mayfield, B. Mueller-Roeber, S. Rajamani, R.T. Sayre, P. Brokstein, et al. 2007. The Chlamydomonas genome reveals the evolution of key animal and plant functions. *Science*. 318:245-250.

Mitchell, D.R. 2004. Speculations on the evolution of 9+2 organelles and the role of central pair microtubules. *Biol Cell*. 96:691-696.

Molla-Herman, A., R. Ghossoub, T. Blisnick, A. Meunier, C. Serres, F. Silbermann, C. Emmerson, K. Romeo, P. Bourdoncle, A. Schmitt, S. Saunier, N. Spassky, P. Bastin, and A. Benmerah. 2010. The ciliary pocket: an endocytic membrane domain at the base of primary and motile cilia. *Journal of Cell Science*. 123:1785-1795.

Mollet, G., F. Silbermann, M. Delous, R. Salomon, C. Antignac, and S. Saunier. 2005. Characterization of the nephrocystin/nephrocystin-4 complex and subcellular localization of nephrocystin-4 to primary cilia and centrosomes. *Hum Mol Genet*. 14:645-656.

Morris, J.C., Z. Wang, M.E. Drew, and P.T. Englund. 2002. Glycolysis modulates trypanosome glycoprotein expression as revealed by an RNAi library. *EMBO J*. 21:4429-4438.

Musgrave, A., P. Dewildt, I. Vanetten, H. Pijst, C. Scholma, R. Kooyman, W. Homan, and H. Vandenende. 1986. Evidence for a Functional Membrane Barrier in the Transition Zone between the Flagellum and Cell Body of Chlamydomonas-Eugametos Gametes. *Planta*. 167:544-553.

Mussmann, R., M. Engstler, H. Gerrits, R. Kieft, C.B. Toaldo, J. Onderwater, H. Koerten, H.G. van Luenen, and P. Borst. 2004. Factors affecting the level and localization of the transferrin receptor in Trypanosoma brucei. *J Biol Chem*. 279:40690-40698.

Mykytyn, K., R.F. Mullins, M. Andrews, A.P. Chiang, R.E. Swiderski, B.L. Yang, T. Braun, T. Casavant, E.M. Stone, and V.C. Sheffield. 2004. Bardet-Biedl syndrome type 4 (BBS4)-null mice implicate Bbs4 in flagella formation but not global cilia assembly. *P Natl Acad Sci USA*. 101:8664-8669.

Mykytyn, K., D.Y. Nishimura, C.C. Searby, G. Beck, K. Bugge, H.L. Haines, A.S. Cornier, G.F. Cox, A.B. Fulton, R. Carmi, A. Iannaccone, S.G. Jacobson, R.G. Weleber, A.F. Wright, R. Riise, R.C. Hennekam, G. Luleci, S. Berker-Karauzum, L.G. Biesecker, E.M. Stone, and V.C. Sheffield. 2003. Evaluation of complex inheritance involving the most common Bardet-Biedl syndrome locus (BBS1). *Am J Hum Genet*. 72:429-437.

Mykytyn, K., D.Y. Nishimura, C.C. Searby, M. Shastri, H.J. Yen, J.S. Beck, T. Braun, L.M. Streb, A.S. Cornier, G.F. Cox, A.B. Fulton, R. Carmi, G. Luleci, S.C. Chandrasekharappa, F.S. Collins, S.G. Jacobson, J.R. Heckenlively, R.G. Weleber, E.M. Stone, and V.C. Sheffield. 2002. Identification of the gene (BBS1) most commonly involved in Bardet-Biedl syndrome, a complex human obesity syndrome. *Nature Genetics*. 31:435-438.

Nachury, M.V., A.V. Loktev, Q. Zhang, C.J. Westlake, J. Peranen, A. Merdes, D.C. Slusarski, R.H. Scheller, J.F. Bazan, V.C. Sheffield, and P.K. Jackson. 2007. A core complex of BBS proteins cooperates with the GTPase Rab8 to promote ciliary membrane biogenesis. *Cell*. 129:1201-1213.

Nagamune, K., T. Nozaki, Y. Maeda, K. Ohishi, T. Fukuma, T. Hara, R.T. Schwarz, C. Sutterlin, R. Brun, H. Riezman, and T. Kinoshita. 2000. Critical roles of glycosylphosphatidylinositol for Trypanosoma brucei. *P Natl Acad Sci USA*. 97:10336-10341.

Nalefski, E.A., and J.J. Falke. 1996. The C2 domain calcium-binding motif: structural and functional diversity. *Protein Sci*. 5:2375-2390.

Nishimura, D.Y., C.C. Searby, R. Carmi, K. Elbedour, L. Van Maldergem, A.B. Fulton, B.L. Lam, B.R. Powell, R.E. Swiderski, K.E. Bugge, N.B. Haider, A.E. Kwitek-Black, L. Ying, D.M. Duhl, S.W. Gorman, E. Heon, A. Iannaccone, D. Bonneau, L.G. Biesecker, S.G. Jacobson, E.M. Stone, and V.C. Sheffield. 2001. Positional cloning of a novel gene on chromosome 16q causing Bardet-Biedl syndrome (BBS2). *Hum Mol Genet*. 10:865-874.

Nojima, D., R.W. Linck, and E.H. Egelman. 1995. At Least One of the Protofilaments in Flagellar Microtubules Is Not Composed of Tubulin. *Current Biology*. 5:158-167.

Nonaka, S., Y. Tanaka, Y. Okada, S. Takeda, A. Harada, Y. Kanai, M. Kido, and N. Hirokawa. 1998. Randomization of left-right asymmetry due to loss of nodal cilia generating leftward flow of extraembryonic fluid in mice lacking KIF3B motor protein. *Cell*. 95:829-837.

Ogbadoyi, E.O., D.R. Robinson, and K. Gull. 2003. A high-order trans-membrane structural linkage is responsible for mitochondrial genome positioning and segregation by flagellar basal bodies in trypanosomes. *Molecular Biology of the Cell*. 14:1769-1779.

Olego-Fernandez, S., S. Vaughan, M.K. Shaw, K. Gull, and M.L. Ginger. 2009. Cell morphogenesis of Trypanosoma brucei requires the paralogous, differentially expressed calpain-related proteins CAP5.5 and CAP5.5V. *Protist*. 160:576-590.

Otto, E.A., B. Loeys, H. Khanna, J. Hellemans, R. Sudbrak, S. Fan, U. Muerb, J.F. O'Toole, J. Helou, M. Attanasio, B. Utsch, J.A. Sayer, C. Lillo, D. Jimeno, P. Coucke, A. De Paepe, R. Reinhardt, S. Klages, M. Tsuda, I. Kawakami, T. Kusakabe, H. Omran, A. Imm, M. Tippens, P.A. Raymond, J. Hill, P. Beales, S. He, A. Kispert, B. Margolis, D.S. Williams, A. Swaroop, and F. Hildebrandt. 2005. Nephrocystin-5, a ciliary IQ domain protein, is mutated in Senior-Loken syndrome and interacts with RPGR and calmodulin. *Nat Genet*. 37:282-288.

Otto, E.A., B. Schermer, T. Obara, J.F. O'Toole, K.S. Hiller, A.M. Mueller, R.G. Ruf, J. Hoefele, F. Beekmann, D. Landau, J.W. Foreman, J.A. Goodship, T. Strachan, A. Kispert, M.T. Wolf, M.F. Gagnadoux, H. Nivet, C. Antignac, G. Walz, I.A. Drummond, T. Benzing, and F. Hildebrandt. 2003. Mutations in INVS encoding inversin cause nephronophthisis type 2, linking renal cystic disease to the function of primary cilia and left-right axis determination. *Nat Genet*. 34:413-420.

Ou, G., M. Koga, O.E. Blacque, T. Murayama, Y. Ohshima, J.C. Schafer, C.M. Li, B.K. Yoder, M.R. Leroux, and J.M. Scholey. 2007. Sensory ciliogenesis in Caenorhabditis elegans: Assignment of IFT components into distinct modules based on transport and phenotypic profiles. *Molecular Biology of the Cell*. 18:1554-1569.

Oubrie, A., H.J. Rozeboom, K.H. Kalk, E.G. Huizinga, and B.W. Dijkstra. 2002. Crystal structure of quinohemoprotein alcohol dehydrogenase from Comamonas testosteroni: structural basis for substrate oxidation and electron transfer. *J Biol Chem*. 277:3727-3732.

Overath, P., and M. Engstler. 2004. Endocytosis, membrane recycling and sorting of GPI-anchored proteins: Trypanosoma brucei as a model system. *Mol Microbiol*. 53:735-744.

Paindavoine, P., S. Rolin, S. Van Assel, M. Geuskens, J.C. Jauniaux, C. Dinsart, G. Huet, and E. Pays. 1992. A gene from the variant surface glycoprotein expression site encodes one of several transmembrane adenylate cyclases located on the flagellum of Trypanosoma brucei. *Mol Cell Biol*. 12:1218-1225.

Pan, J., Q. Wang, and W.J. Snell. 2005. Cilium-generated signaling and cilia-related disorders. *Lab Invest*. 85:452-463.

Patel, A., and E. Honore. 2010. Polycystins and renovascular mechanosensory transduction. *Nat Rev Nephrol*. 6:530-538.

Pazour, G.J., N. Agrin, J. Leszyk, and G.B. Witman. 2005. Proteomic analysis of a eukaryotic cilium. *J Cell Biol*. 170:103-113.

Pazour, G.J., and G.B. Witman. 2003. The vertebrate primary cilium is a sensory organelle. *Curr Opin Cell Biol*. 15:105-110.

Pedersen, L.B., S. Geimer, and J.L. Rosenbaum. 2006. Dissecting the molecular mechanisms of intraflagellar transport in chlamydomonas. *Curr Biol*. 16:450-459.

Perrone, C.A., D. Tritschler, P. Taulman, R. Bower, B.K. Yoder, and M.E. Porter. 2003. A novel dynein light intermediate chain colocalizes with the retrograde motor for intraflagellar transport at sites of axoneme assembly in chlamydomonas and Mammalian cells. *Mol Biol Cell*. 14:2041-2056.

Piperno, G., and K. Mead. 1997. Transport of a novel complex in the cytoplasmic matrix of Chlamydomonas flagella. *Proc Natl Acad Sci U S A*. 94:4457-4462.

Piperno, G., E. Siuda, S. Henderson, M. Segil, H. Vaananen, and M. Sassaroli. 1998. Distinct mutants of retrograde intraflagellar transport (IFT) share similar morphological and molecular defects. *J Cell Biol*. 143:1591-1601.

Poon, S.K., L. Peacock, W. Gibson, K. Gull, and S. Kelly. 2012. A modular and optimized single marker system for generating Trypanosoma brucei cell lines expressing T7 RNA polymerase and the tetracycline repressor. *Open Biol*. 2:110037.

Price, H.P., M.R. Hodgkinson, M.H. Wright, E.W. Tate, B.A. Smith, M. Carrington, M. Stark, and D.F. Smith. 2012. A role for the vesicle-associated tubulin binding protein ARL6 (BBS3) in flagellum extension in Trypanosoma brucei. *Biochim Biophys Acta*. 1823:1178-1191.

Qiao, X., B.F. Chuang, Y. Jin, M. Muranjan, C.H. Hung, P.T. Lee, and M.G. Lee. 2006. Sorting signals required for trafficking of the cysteine-rich acidic repetitive transmembrane protein in Trypanosoma brucei. *Eukaryot Cell*. 5:1229-1242.

Rachel, R.A., H.L. May-Simera, S. Veleri, N. Gotoh, B.Y. Choi, C. Murga-Zamalloa, J.C. McIntyre, J. Marek, I. Lopez, A.N. Hackett, M. Brooks, A.I. den Hollander, P.L. Beales, T. Li, S.G. Jacobson, R. Sood, J.R. Martens, P. Liu, T.B. Friedman, H. Khanna, R.K. Koenekoop, M.W. Kelley, and A. Swaroop. 2012. Combining Cep290 and Mkks ciliopathy alleles in mice rescues sensory defects and restores ciliogenesis. *J Clin Invest*. 122:1233-1245.

Ralston, K.S., and K.L. Hill. 2006. Trypanin, a component of the flagellar dynein regulatory complex, is essential in bloodstream form African trypanosomes. *Plos Pathogens*. 2:873-882.

Ralston, K.S., and K.L. Hill. 2008. The flagellum of Trypanosoma brucei: new tricks from an old dog. *Int J Parasitol*. 38:869-884.

Ralston, K.S., A.G. Lerner, D.R. Diener, and K.L. Hill. 2006. Flagellar motility contributes to cytokinesis in Trypanosoma brucei and is modulated by an evolutionarily conserved dynein regulatory system. *Eukaryotic cell*. 5:696-711.

Ramoino, P., P. Fronte, F. Beltrame, A. Diaspro, M. Fato, L. Raiteri, S. Stigliani, and C. Usai. 2003. Swimming behavior regulation by GABAB receptors in Paramecium. *Experimental cell research*. 291:398-405.

Reed, R.R., A.L.D. Tadenev, H.M. Kulaga, H.L. May-Simera, M.W. Kelley, and N. Katsanis. 2011. Loss of Bardet-Biedl syndrome protein-8 (BBS8) perturbs olfactory function, protein localization, and axon targeting. *P Natl Acad Sci USA*. 108:10320-10325.

Reiter, J.F., O.E. Blacque, and M.R. Leroux. 2012. The base of the cilium: roles for transition fibres and the transition zone in ciliary formation, maintenance and compartmentalization. *EMBO Rep*. 13:608-618.

Ridgley, E., P. Webster, C. Patton, and L. Ruben. 2000. Calmodulin-binding properties of the paraflagellar rod complex from Trypanosoma brucei. *Mol Biochem Parasitol*. 109:195-201.

Robinson, D.R., and K. Gull. 1991. Basal body movements as a mechanism for mitochondrial genome segregation in the trypanosome cell cycle. *Nature*. 352:731-733.

Robinson, D.R., T. Sherwin, A. Ploubidou, E.H. Byard, and K. Gull. 1995. Microtubule polarity and dynamics in the control of organelle positioning, segregation, and cytokinesis in the trypanosome cell cycle. *J Cell Biol*. 128:1163-1172.

Roditi, I., and M. Liniger. 2002. Dressed for success: the surface coats of insect-borne protozoan parasites. *Trends Microbiol*. 10:128-134.

Rohatgi, R., and W.J. Snell. 2010. The ciliary membrane. *Curr Opin Cell Biol*. 22:541-546.

Rohlich, P. 1975. The sensory cilium of retinal rods is analogous to the transitional zone of motile cilia. *Cell Tissue Res*. 161:421-430.

Rosenbaum, J.L., and G.B. Witman. 2002. Intraflagellar transport. *Nat Rev Mol Cell Biol*. 3:813-825.

Salathe, M. 2007. Regulation of mammalian ciliary beating. *Annu Rev Physiol*. 69:401-422.

Sang, L., J.J. Miller, K.C. Corbit, R.H. Giles, M.J. Brauer, E.A. Otto, L.M. Baye, X. Wen, S.J. Scales, M. Kwong, E.G. Huntzicker, M.K. Sfakianos, W. Sandoval, J.F. Bazan, P. Kulkarni, F.R. Garcia-Gonzalo, A.D. Seol, J.F. O'Toole, S. Held, H.M. Reutter, W.S. Lane, M.A. Rafiq, A. Noor, M. Ansar, A.R. Devi, V.C. Sheffield, D.C. Slusarski, J.B. Vincent, D.A. Doherty, F. Hildebrandt, J.F. Reiter, and P.K. Jackson. 2011. Mapping the NPHP-JBTS-MKS protein network reveals ciliopathy disease genes and pathways. *Cell*. 145:513-528.

Santagata, S., T.J. Boggon, C.L. Baird, C.A. Gomez, J. Zhao, W.S. Shan, D.G. Myszka, and L. Shapiro. 2001. G-protein signaling through tubby proteins. *Science*. 292:2041-2050.

Satir, P. 1998. Mechanisms of ciliary motility: an update. *Eur J Protistol*. 34:267-272.

Schafer, J.C., C.J. Haycraft, J.H. Thomas, B.K. Yoder, and P. Swoboda. 2003. XBX-1 encodes a dynein light intermediate chain required for retrograde intraflagellar transport and cilia assembly in Caenorhabditis elegans. *Mol Biol Cell*. 14:2057-2070.

Schlaeppi, K., J. Deflorin, and T. Seebeck. 1989. The major component of the paraflagellar rod of Trypanosoma brucei is a helical protein that is encoded by two identical, tandemly linked genes. *J Cell Biol*. 109:1695-1709.

Seo, S., L.M. Baye, N.P. Schulz, J.S. Beck, Q. Zhang, D.C. Slusarski, and V.C. Sheffield. 2010. BBS6, BBS10, and BBS12 form a complex with CCT/TRiC family chaperonins and mediate BBSome assembly. *Proc Natl Acad Sci U S A*. 107:1488-1493.

Seo, S., Q. Zhang, K. Bugge, D.K. Breslow, C.C. Searby, M.V. Nachury, and V.C. Sheffield. 2011. A novel protein LZTFL1 regulates ciliary trafficking of the BBSome and Smoothened. *Plos Genet*. 7:e1002358.

Shah, A.S., S.L. Farmen, T.O. Moninger, T.R. Businga, M.P. Andrews, K. Bugge, C.C. Searby, D. Nishimura, K.A. Brogden, J.N. Kline, V.C. Sheffield, and M.J. Welsh. 2008. Loss of Bardet-Biedl syndrome proteins alters the morphology and function of motile cilia in airway epithelia. *Proc Natl Acad Sci U S A*. 105:3380-3385.

Sharma, R., L. Peacock, E. Gluenz, K. Gull, W. Gibson, and M. Carrington. 2008. Asymmetric cell division as a route to reduction in cell length and change in cell morphology in trypanosomes. *Protist*. 159:137-151.

Sherwin, T., and K. Gull. 1989a. The cell division cycle of Trypanosoma brucei brucei: timing of event markers and cytoskeletal modulations. *Philos Trans R Soc Lond B Biol Sci*. 323:573-588.

Sherwin, T., and K. Gull. 1989b. Visualization of detyrosination along single microtubules reveals novel mechanisms of assembly during cytoskeletal duplication in trypanosomes. *Cell*. 57:211-221.

Sinden, R.E., E.U. Canning, R.S. Bray, and M.E. Smalley. 1978. Gametocyte and gamete development in Plasmodium falciparum. *Proc R Soc Lond B Biol Sci*. 201:375-399.

Sinden, R.E., E.U. Canning, and B. Spain. 1976. Gametogenesis and fertilization in Plasmodium yoelii nigeriensis: a transmission electron microscope study. *Proc R Soc Lond B Biol Sci*. 193:55-76.

Singla, V., and J.F. Reiter. 2006. The primary cilium as the cell's antenna: Signaling at a sensory organelle. *Science*. 313:629-633.

Smith, E.F. 2007. Hydin seek: finding a function in ciliary motility. *J Cell Biol*. 176:403-404.

Sorokin, S. 1962. Centrioles and the formation of rudimentary cilia by fibroblasts and smooth muscle cells. *J Cell Biol*. 15:363-377.

Stephan, A., S. Vaughan, M.K. Shaw, K. Gull, and P.G. McKean. 2007. An essential quality control mechanism at the eukaryotic basal body prior to intraflagellar transport. *Traffic*. 8:1323-1330.

Timm, D., K. Salim, I. Gout, L. Guruprasad, M. Waterfield, and T. Blundell. 1994. Crystal structure of the pleckstrin homology domain from dynamin. *Nat Struct Biol*. 1:782-788.

Tobin, J.L., and P.L. Beales. 2007. Bardet-Biedl syndrome: beyond the cilium. *Pediatr Nephrol*. 22:926-936.

van Reeuwijk, J., H.H. Arts, and R. Roepman. 2011. Scrutinizing ciliopathies by unraveling ciliary interaction networks. *Hum Mol Genet*. 20:R149-157.

Vassella, E., B. Reuner, B. Yutzy, and M. Boshart. 1997. Differentiation of African trypanosomes is controlled by a density sensing mechanism which signals cell cycle arrest via the cAMP pathway. *Journal of Cell Science*. 110:2661-2671.

Veland, I.R., A. Awan, L.B. Pedersen, B.K. Yoder, and S.T. Christensen. 2009. Primary Cilia and Signaling Pathways in Mammalian Development, Health and Disease. *Nephron Physiol*. 111:39-53.

Ventura, M.P., R.N. Vianna, H.P. Solari, J.P. Filho, and M.N. Burnier. 2006. Bardet-Biedl syndrome associated with glaucoma. *Eye (Lond)*. 20:114-116.

Vickerman, K. 1969. On the surface coat and flagellar adhesion in trypanosomes. *J Cell Sci*. 5:163-193.

Vickerman, K. 1985. Developmental cycles and biology of pathogenic trypanosomes. *Br Med Bull*. 41:105-114.

Vickerman, K., L. Tetley, K.A. Hendry, and C.M. Turner. 1988. Biology of African trypanosomes in the tsetse fly. *Biol Cell*. 64:109-119.

Vieira, O.V., K. Gaus, P. Verkade, J. Fullekrug, W.L. Vaz, and K. Simons. 2006. FAPP2, cilium formation, and compartmentalization of the apical membrane in polarized Madin-Darby canine kidney (MDCK) cells. *Proc Natl Acad Sci U S A*. 103:18556-18561.

Waters, A.M., and P.L. Beales. 2011. Ciliopathies: an expanding disease spectrum. *Pediatr Nephrol*. 26:1039-1056.

Wedaman, K.P., D.W. Meyer, D.J. Rashid, D.G. Cole, and J.M. Scholey. 1996. Sequence and submolecular localization of the 115-kD accessory subunit of the heterotrimeric kinesin-II (KRP85/95) complex. *J Cell Biol*. 132:371-380.

West, A.B., P.J. Lockhart, C. O'Farell, and M.J. Farrer. 2003. Identification of a novel gene linked to parkin via a bi-directional promoter. *Journal of molecular biology*. 326:11-19.

Wheatley, D.N., A.M. Wang, and G.E. Strugnell. 1996. Expression of primary cilia in mammalian cells. *Cell Biol Int*. 20:73-81.

Wickstead, B., K. Ersfeld, and K. Gull. 2002. Targeting of a tetracycline-inducible expression system to the transcriptionally silent minichromosomes of Trypanosoma brucei. *Mol Biochem Parasitol*. 125:211-216.

Wickstead, B., and K. Gull. 2007. Dyneins across eukaryotes: a comparative genomic analysis. *Traffic*. 8:1708-1721.

Williams, C.L., C. Li, K. Kida, P.N. Inglis, S. Mohan, L. Semenec, N.J. Bialas, R.M. Stupay, N. Chen, O.E. Blacque, B.K. Yoder, and M.R. Leroux. 2011. MKS and NPHP modules cooperate to establish basal body/transition zone membrane associations and ciliary gate function during ciliogenesis. *J Cell Biol*. 192:1023-1041.

Wirtz, E., S. Leal, C. Ochatt, and G.A. Cross. 1999. A tightly regulated inducible expression system for conditional gene knock-outs and dominant-negative genetics in Trypanosoma brucei. *Mol Biochem Parasitol*. 99:89-101.

Wolf, M.T.F., J. Lee, F. Panther, E.A. Otto, K.L. Guan, and F. Hildebrandt. 2005. Expression and phenotype analysis of the nephrocystin-1 and nephrocystin-4 homologs in Caenorhabditis elegans. *J Am Soc Nephrol*. 16:676-687.

Wu, Y., N.G. Haghighat, and L. Ruben. 1992. The predominant calcimedins from Trypanosoma brucei comprise a family of flagellar EF-hand calcium-binding proteins. *Biochem J*. 287 (Pt 1):187-193.

Xu, C., and J. Min. 2011. Structure and function of WD40 domain proteins. *Protein Cell*. 2:202-214.

Yang, P.F., D.R. Diener, C. Yang, T. Kohno, G.J. Pazour, J.M. Dienes, N.S. Agrin, S.M. King, W.S. Sale, R. Kamiya, J.L. Rosenbaum, and G.B. Witman. 2006. Radial spoke proteins of Chlamydomonas flagella. *Journal of cell science*. 119:1165-1174.

Yoder, B.K. 2007. Role of primary cilia in the pathogenesis of polycystic kidney disease. *J Am Soc Nephrol*. 18:1381-1388.

Yoder, B.K., X. Hou, and L.M. Guay-Woodford. 2002. The polycystic kidney disease proteins, polycystin-1, polycystin-2, polaris, and cystin, are co-localized in renal cilia. *J Am Soc Nephrol*. 13:2508-2516.

Zhang, Q., D. Yu, S. Seo, E.M. Stone, and V.C. Sheffield. 2012. Intrinsic protein-protein interaction-mediated and chaperonin-assisted sequential assembly of stable bardet-biedl syndrome protein complex, the BBSome. *J Biol Chem*. 287:20625-20635.

Zhang, Y., and W.J. Snell. 1994. Flagellar adhesion-dependent regulation of Chlamydomonas adenylyl cyclase in vitro: a possible role for protein kinases in sexual signaling. *J Cell Biol*. 125:617-624.